TID/SNA--305

SUPPLEMENT TO

s110-XCE01-W181

RADIATION EFFECTS ON ELECTRONICS

PRELIMINARY GUIDELINES FOR DESIGNING ELECTRONICS FOR OPERATION IN A RADIATION ENVIRONMENT

FILE COPY
NRO
Technical Document Center

DISTRIBUTION OF THIS DOCUMENT UNLIMITED

TECHNICAL DOCUMENT CENTER
Nuclear Rocket Operations

DOC. NO. N-2285
AGCS 0120-48

DISCLAIMER

This report was prepared as an account of work sponsored by an agency of the United States Government. Neither the United States Government nor any agency Thereof, nor any of their employees, makes any warranty, express or implied, or assumes any legal liability or responsibility for the accuracy, completeness, or usefulness of any information, apparatus, product, or process disclosed, or represents that its use would not infringe privately owned rights. Reference herein to any specific commercial product, process, or service by trade name, trademark, manufacturer, or otherwise does not necessarily constitute or imply its endorsement, recommendation, or favoring by the United States Government or any agency thereof. The views and opinions of authors expressed herein do not necessarily state or reflect those of the United States Government or any agency thereof.

DISCLAIMER

Portions of this document may be illegible in electronic image products. Images are produced from the best available original document.

CONTENTS

Radiation Hardening of Electronic Systems

Neutron Damage Constant for Bipolar Transistors

Radiation Effects on Semiconductor Devices

Circuits and Systems Analysis

NOTICE

This report was prepared as an account of work sponsored by the United States Government. Neither the United States nor the United States Energy Research and Development Administration, nor any of their employees, nor any of their contractors, subcontractors, or their employees, makes any warranty, express or implied, or assumes any legal liability or responsibility for the accuracy, completeness or usefulness of any information, apparatus, product or process disclosed, or represents that its use would not infringe privately owned rights.

DISTRIBUTION OF THIS DOCUMENT UNLIMITED

RADIATION HARDENING OF ELECTRONIC SYSTEMS

1 July 1969
Revised
1 October 1969

By

G. C. Messenger
Consultant, Autonetics

Prepared for

1969 IEEE Annual Conference
Nuclear and Space Radiation Effects
University Park, Pennsylvania
7-11 July 1969

Autonetics
North American Rockwell

3370 Miraloma Avenue, Anaheim California 92803

CONTENTS

		Page
I.	Introduction	1-1
II.	Neutron Considerations	2-1
III.	Photon Considerations	3-1
IV.	Total Dose Effects	4-1
V.	Circuit Analysis Considerations	5-1
VI.	Buildup Screening	6-1
VII.	Statistical Considerations	7-1
VIII.	Conclusion	8-1
References		R-1

ILLUSTRATIONS

Figure		Page
1	Example of Congruence Between Predicted and Measured Common-Mode Output Voltage Offset for a General-Purpose Amplifier Microcircuit	5-2
2	Application of SCAN/TRAC to a Voltage Regulator	5-3
3	Computer-Aided Design and Analysis	5-4

TABLES

Table		Page
1	Typical Preliminary System Failure Budget for Nuclear Radiation	1-2
2	Buildup Screening - Typical System	6-1
3	Partition of Failure Responsibility	6-2
4	Determination of Statistical Significance Levels for Functional Specifications and Analyses From System Specifications Analysis Levels	7-2

I. INTRODUCTION

Military systems have traditionally been designed to operate over a wide range of environmental conditions; recently, the environment in the vicinity of a nuclear explosion has been added. Several aspects of the radiation hardening problem are relatively unique, such as the high cost and extreme engineering difficulties encountered in subsystem or system level proof tests. Another specific characteristic of nuclear environments is the multiplicity of kill mechanisms. Neutrons produce degradation in device characteristics; photon pulses produce both current transients and catastrophic failures; and the ionizing dose deposited by the total radiation environment produces device surface degradation modes.

Many systems, such as communication satellites, must also operate in the space radiation environment. Here, the total ionizing dose accumulated over long mission times may be the dominant vulnerability to internal electronics. Most satellite electronic systems are powered by solar cells which must be exposed to external radiation with very limited shielding. This makes hardening of solar cells a very important problem for space systems. This presentation will not fully discuss the special problem of space environment, but will emphasize the hardening problems associated with nuclear weapons.

A tractable engineering approach to system hardening necessarily involves a substantial degree of overdesign. This has the net effect of reducing the large number of potential failure modes to a much smaller number of significant failure modes. Furthermore, system level testing can be success oriented, and survival of the system to radiation levels substantially in excess of the required level can be reinter reted in terms of high survival confidence at the required level. This is analogous to the use of overstress techniques in reliability engineering.

The degree of overdesign which is appropriate depends on specification level and system complexity. For example, at 10^{12} n/cm^2,* an overdesign factor of 20 is reasonable, and at 10^{13} n/cm^3, an overdesign factor of 5 is reasonable; whereas, at 5 X 10^{14} n/cm^2, it is difficult to obtain any overdesign factor for safety margin. Generally speaking, the desired overdesign factor increases with system complexity. Fortunately, systems requiring tolerance to very high radiation levels often contain relatively few parts, and hardening design can be accomplished with relatively small overdesign factors.

Radiation specification levels can be qualitatively scoped by a careful survey of the unclassified literature. [1] Scoping radiation levels in terms of neutrons/cm^2, the lower end of the range of interest is about 10^{11} n/cm^2 where some of the most sensitive semiconductor components begin to show radiation effects. The upper end of the range is about 10^{15} n/cm^2 which is currently a practical limit for semiconductor electronics.

---

*Neutron fluence in this report is n/cm^2 (E > 10 Kev, 1 MEV Equivalent Damage (Si)) and is approximately equal to n/cm^2 (E > 10 Kev, TRIGA).

Many systems are manned, and the dose required to kill a man is in the 300 to 500 Rad range. For these systems the radiation specification will be toward the lower end of the range. Furthermore, mechanical, operational, and structural characteristics of many systems dictate radiation specification at the lower end of the range. This is readily deduced by comparing the range-overpressure and range-neutron curves in Glasstone.[1]

One can certainly conceive of special applications, such as operation of electronic instrumentation near the core of a reactor for extended time periods, which would require radiation specifications near the upper limit of our range of interest.

This discussion will concentrate on the lower end of the range of interest which contains the majority of system requirements. This eliminates the requirement for special new hardened devices or circuits, and concentrates the discussion on proper application of current technology to fulfill hardened systems requirements.

The nuclear radiation environment consists of a pulse of photons, X-rays, and γ rays, followed by a pulse of neutrons. System hardening must accommodate the individual radiation effects, plus any synergistic effects. A set of compatible radiation levels, not necessarily balanced, are defined in the radiation specification. A simple statement of radiation levels defines a design goal; the addition of minimum system failure probabilities and associated confidence levels quantify the required degree of hardening. A preliminary failure budget, Table 1, is then allocated, based on a preliminary system evaluation, and functional specifications are derived for subsystems. This logically continues to the delineation of circuit and, finally, component level radiation specifications.

The preliminary failure budget is best approached by reviewing the electronic circuits and semiconductor devices against the specification requirements using the data in a concise summary document such as the TREE Handbook.[2]

Table 1. Typical Preliminary System Failure Budget for Nuclear Radiation

Specific Radiation Failure Mode	Maximum Failure Probability
Neutron Failure Probability	0.04
Photon Failure Probability (Dose Rate)	
Noncatastrophic	0.02
Catastrophic	0.06
Total Dose Failure Probability (Neutron + Photon)	0.08
Maximum System Failure Probability	0.20

The main elements of a hardening device approach are:

1. Shielding at the system or black box level to limit radiation levels in the electronic circuits.

2. Special circuit design techniques to minimize circuit functional response characteristics to radiation effects.

3. Use of hardened semiconductor components.

Shielding can be effectively used to reduce X-ray flux, but because of severe weight and size penalties, shielding is usually ruled out as a means of reducing γ or neutron flux; ground installations are an exception and can be effectively shielded against γ and neutron flux.

Discussions of circuit design techniques and component hardening techniques can be found in the TREE Handbook and will not be discussed further here. The system aspects of component hardness will be treated in Sections II, III, and IV, and the system aspects of circuit hardness will be discussed in Section V.

Electronic systems can be effectively hardened following this approach. It will probably be necessary to revise the failure budget several times as anticipated problems fail to materialize with expected severity and as unanticipated problems become identified by analysis, testing at simulation facilities, or by system level proof tests.

Hardened components are the solid foundation for a survivable system. Recent advances in semiconductor device technology have produced high gain bandwidth, dielectrically isolated, integrated circuits with thin-film passive components optimal for use in radiation environments. Computer-aided design and analysis has been made possible by the development of codes like SCEPTRE, CIRCUS, NET, PREDICT, and TRAC, which utilize large signal radiation equivalent circuits for semiconductor components. The disciplines of reliability engineering and quality control have evolved new techniques for minimizing weak bonds. think overlay patterns, and other structural defects that might limit radiation performance.

II. NEUTRON CONSIDERATIONS

Establishment of a failure budget will determine some maximum failure probability due to neutron effects that will serve as a basis for neutron hardening design decisions. The most important failure mechanism due to neutrons is the degradation of semiconductor device operating characteristics. The core of this problem is β degradation.

Expansion of the expression for $1/\beta$ has been accomplished [3,4] to explain this failure mode, with the result that each of the radiation dependent terms is proportional to base width or base width squared. At low current levels, recombination in the emitter-base field region dominates; [5] at high current levels, recombination in the base, including its expansion into the collector junction, [6] dominates. Therefore, control of base width is mandatory to control degradation in the neutron environment. Usually, it is more convenient to directly control gain bandwidth product, f_t, ($f_t \propto 1/W^2$), and thereby indirectly control base width. Under high current level operation conditions,

$$(1)\Delta\frac{1}{\beta} = \frac{0.16}{f_t K}$$

Selection of an f_t value which ensures the largest overdesign factor consistent with current state-of-the-art and market availability is now made for small signal devices. This might be 200 MHz, for example, which ensures a maximum $\Delta 1/\beta$ of 0.08 at 10^{14} n/cm^2. Problem devices, such as power transistors, are next. The highest practical value of f_t should be obtained; although, this might be as low as 25 MHz. Overdesign must now be enhanced by circuit design techniques that minimize the dependence of circuit functional parameters on the gain of the power transistor.

Devices such as SCR's and unijunction transistors should not be used unless a verified source of hardened devices has been established. Microcircuits, including PNP transistors, should be avoided if possible due to the difficulty of controlling base width in such structures.

Finally, critical circuits, as identified by worst-case analysis in the normal environment, should be carefully reviewed from the neutron damage stand-point. Obviously, these circuits will have the smallest performance margin in the neutron environment.

At this point, identification of the most important neutron vulnerabilities can be summarized. They will consist of circuits that were required to accommodate low gain bandwidth product transistors and circuits that are marginal in the normal environment. A rough estimate of system failure probability as a function of neutron fluence can now be made by computer-aided analysis of these circuits (TRAC), and a computer-aided analysis (SECURE)[13] can be made of the effects of radiation degradation in these circuits on system performance. This failure probability will hopefully be within the failure budget, and some reallocation of failure budget may be possible and desirable. If this failure probability is unacceptable, the major contributors will be obvious from the analysis, and a redesign program can be effectively planned to produce the required hardness.

The entire system should now be exposed in a simulation facility (e.g., TRIGA Reactor) and exposed in steps until failure occurs. A well-designed test program will enable identification of most of the important failure modes by continuing the test past first failure and subsequently determining degradation in the critical circuits by electrical tests.

The analytical predictions and the experimental results will be different; therefore, any substantial or significant differences must be resolved by an engineering program specifically designed to force congruence.

III. PHOTON CONSIDERATIONS

Current transients resulting from photons create noise pulses, change of state in digital circuits, and other transient phenomena that do not involve catastrophic failure of components but which can produce system failure. In addition, large magnitude current pulses can produce catastrophic device failure. Both of these failure modes must be assigned maximum allowed probabilities in the preliminary failure budget.

Intrinsic hardening of devices is impractical for dealing with current transients and, therefore, the system must be designed to tolerate the transient currents. A transient current pulse in linear or analog circuitry is almost never limiting in an overall system sense; most systems must be able to tolerate such pulses since they can also arise from signal channel switching, power supply transients, lightning discharges, and many other normal occurrences. Even for digital circuitry, such current transients are usually just an annoyance that can be corrected by activating a reset button or closing a circuit breaker. In the few cases where such an interruption is intolerable, a circumvention subsystem can be used that senses the radiation pulse, shuts the system down for a very brief period, and automatically restarts the system electronics. The probability of proper functioning of reset or circumvention circuitry can be statistically analyzed using appropriate circuit models and a system analysis computer code. This source of system failure should be a very small part of the error budget in a well designed system.

Catastrophic failure, burnout, can also result from photocurrents. One important failure mode arises when junction photocurrents short circuit a pow r supply to ground, or a positive power supply to a negative power supply. This pitfall can usually be avoided by addition of appropriate current limiting resistors. Another important failure mode is latchup in junction-isolated microcircuitry. This can be avoided by using DIIC's; it is less desirable but possible to use specially hardened JIIC's.

A subtle failure mode occurs primarily in integrated circuits. The thin overlay pattern, usually aluminum or gold, which is used to interconnect the integrated circuit elements, has a relatively low current-handling capacity. Further, defects such as scratches or thin regions above oxide steps can seriously reduce surge current capabilities. For short pulses of radiation, typical of LINAC's and FXR's, the burnout depends primarily on the energy ($\sim I^2 Rt$) dissipated in a portion of the overlay pattern. Usually a well-designed overlay pattern will support the expected photocurrent surges with substantial design margin. The problem then reduces to a very difficult quality control problem, making sure that the probability of finding a defect anywhere in the overlay patterns in any of the devices in the system is within the assigned failure budget. This problem is much easier to manage in DIIC's than in JIIC's because the photocurrents are much lower. The system engineer must allocate a generous portion of the radiation failure budget to this failure mode and demand a very thorough set of process and quality controls from the device manufacturer.

IV. TOTAL DOSE EFFECTS

Both neutrons and photons contribute to total dose in the weapon environment. Surface properties of semiconductor devices are substantially changed by ionizing dose. Silicon devices with good oxide passivation on the surface suffer an increase in positive charge density near the oxide silicon interface, resulting in a change in surface potential, surface conductance, and surface recombination velocity.[8] These changes are relatively large; however, they tend to saturate with increasing dose. Furthermore, the operating parameters of most transistors and microcircuits are relatively independent of changes in surface properties. The net result of these considerations is that most modern diodes, transistors, and microcircuits can be used up to total dose levels of 10^6 Rads (Si) with tolerable changes in operating parameters.

The surface of the oxide can also accumulate charged ions (Telstar effect).[9] In a well-passivated device, this will have a negligible effect on device operation, but this accumulation can cause catastrophic changes such as formation of surface channels in unpassivated devices or in passivated devices with defective passivation.

Surface field effect transistors, e.g., MOSFET's, suffer large changes in turn-on voltage due to total dose effects and have thresholds as low as 5,000 Rads (Si)[10]. They should, therefore, be avoided in radiation hardened systems. Research is currently in progress at several laboratories to develop a hardened surface field effect transistor; and this represents one of the most fruitful contributions device development engineers could currently make to the system hardness problem.

Some degree of control over this failure mechanism can be achieved by imposing stringent control specification limits on junction leakage currents, since defective passivation in most cases also leads to increased saturation currents. This failure mode is generic to some device types,[11] so that a literature check of experimental data is useful for eliminating some failure-prone device types.

Again, the system engineer must be generous in allocating a substantial portion of the failure budget to surface dose effects, and demand a high degree of process and quality control from the device manufacturer.

V. CIRCUIT ANALYSIS CONSIDERATIONS

Analysis and design of electronics in the radiation environment requires the ability to quantitatively describe the electrical effects of radiation on semi-conductor devices. There are a number of models available, but the Ebers and Moll Model is probably the simplest large signal model that can be readily modified to include radiation effects. The first step is to characterize all of the devices which are used in the system and make a prediction, nominal and worst case, of the device response in the neutron and photon environment. Then the devices must be measured in radiation simulation facilities. The predicted and measured responses should then be compared and any significant differences resolved; most probably, congruence will be effected by second-order corrections to the basic device model. A typical example[12] of comparison of measured and predicted response for a general-purpose amplifier microcircuit is shown in Figure 1. Prediction and experimentation must cover all of the current and voltage regions that the devices encounter in the system. This is more difficult for transistors than microcircuits, because microcircuits are usually used at the same specific voltages and currents throughout the system; whereas, transistors are used at various operating biases. In no case should circuit analysis be attempted until satisfactory device models are defined.

Next analysis of circuits can be accomplished, and it is probably cost effective in most cases to use computer codes. One should not overlook the possibility of using simplified hand analysis where it is appropriate and sufficient. Again, nominal and worst-case predictions should be made, some comparison experiments should be conducted and congruence should be effected between predicted and measured results; a typical example of analysis and prediction is shown for a regulated power s pply in Figure 2. After suitable circuit models have evolved, subsystem or system analysis can be started using a computer program such as SECURE[13]. To avoid computer overloading, SECURE allows the analyst to represent the relatively insensitive circuits by functional blocks and to represent the radiation sensitive circuits by detailed equivalent circuits as was done at the circuit level. Results of the circuit runs allow the analyst to decide which circuits show sufficient sensitivity to require detailed modeling.

The results of the SECURE runs allow system operating parameters to be predicted as a function of radiation exposure. Proof tests on the system at radiation simulation facilities can now be made and compared with the SECURE prediction. Agreement between predicted and measured results will provide confidence in the hardened design, and will result in much reduced requirement for statistical testing to reach a specified confidence level.

Figure 3 is a flow chart for computer-aided analysis showing the buildup in complexity from parts to system level, including the important cogruence steps to assure one-to-one correspondence between analysis and test results.

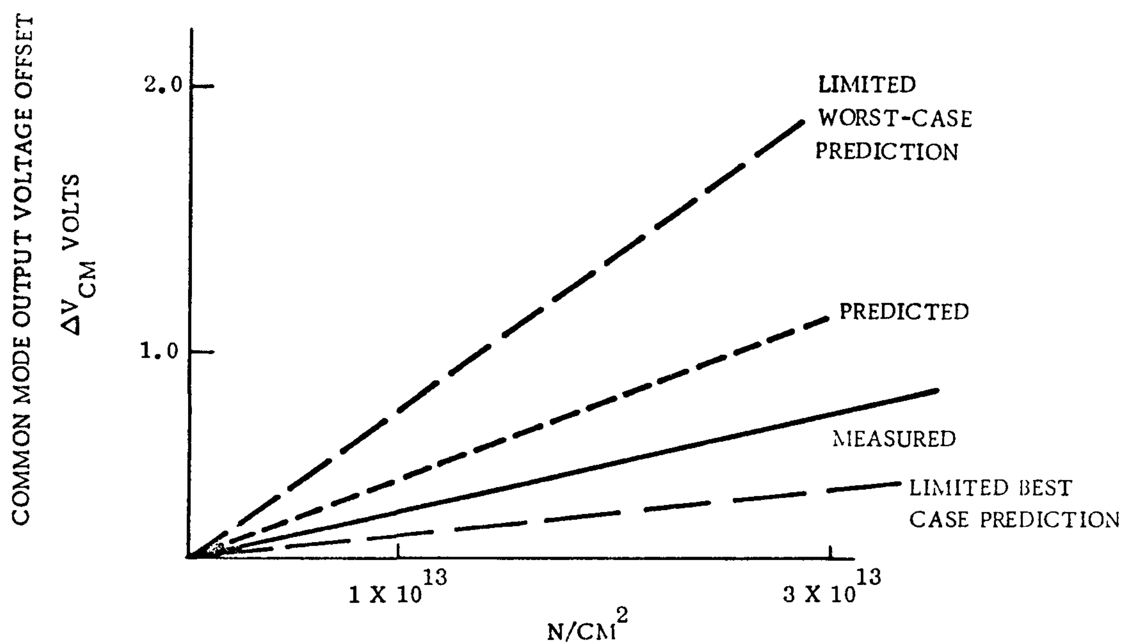

Figure 1. Example of Congruence Between Predicted and Measured Common-Mode Output Voltage Offset for a General-Purpose Amplifier Microcircuit

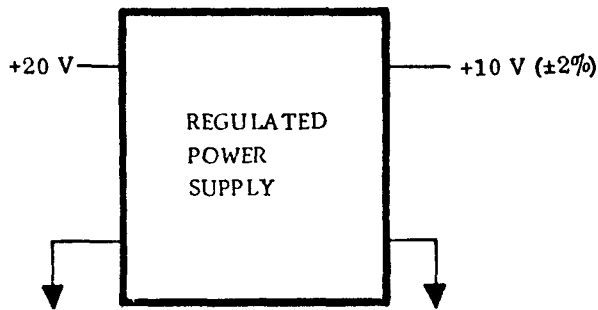

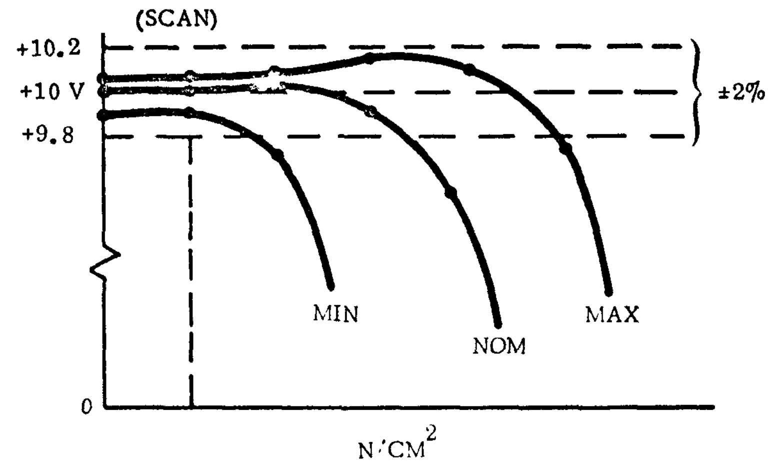

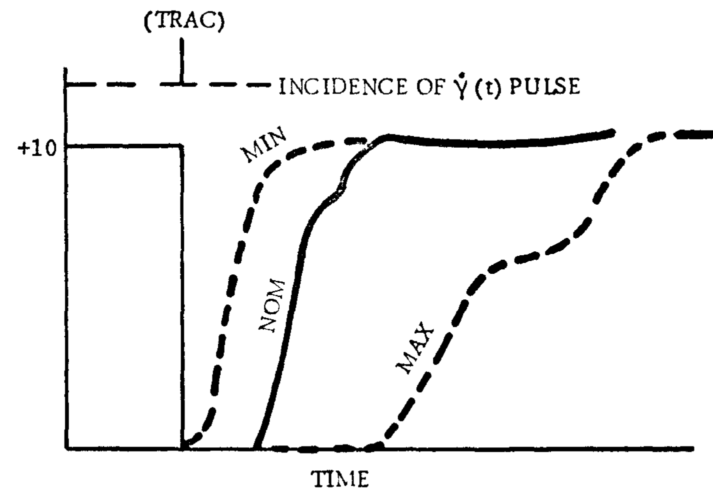

- SCAN USED FOR NEUTRON DEGRADATION
- TRAC USED FOR IONIZATION (TRANSIENT) EFFECT

Figure 2. Application of SCAN/TRAC to a Voltage Regulator

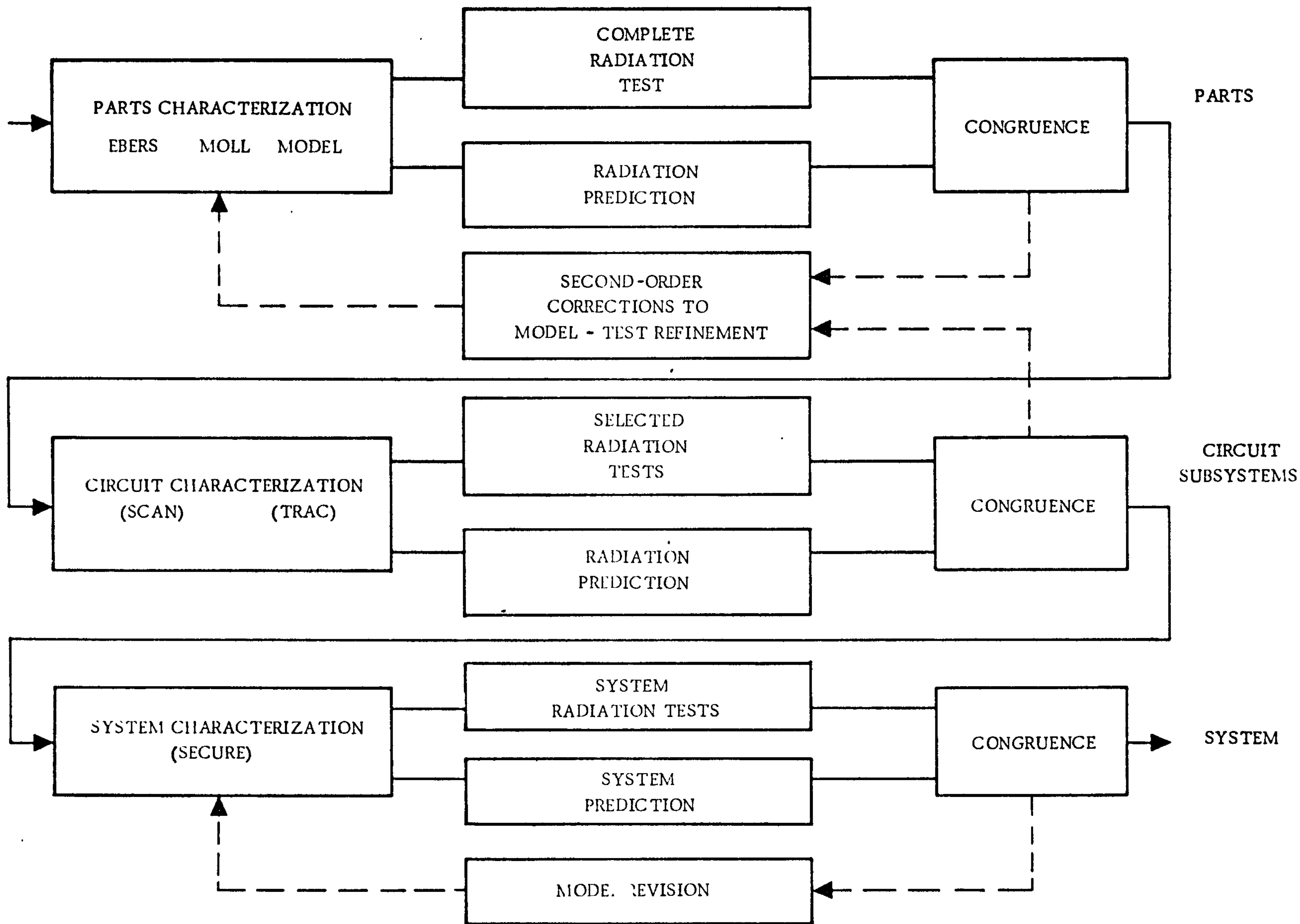

Figure 3. Computer-Aided Design and Analysis

VI. BUILDUP SCREENING

Electronic parts in the finished system must have a failure probability in the range $10^{-8} < P_f < 10^{-5}$, depending on system complexity and requirements. What failure probability should be demanded from the piece part manufacturer? If the system is blindly assembled without any testing or screening or rework cycle by the system manufacturer, the device manufacturer must bear the entire burden and supply parts in the 10^{-5} to 10^{-8} failure probability range. However, if the system manufacturer inserts a practical number of tests, screens, and rework cycles, discrepant devices will be weeded out as the system progresses through various stages of assembly. A hypothetical case shows this process through various stages of assembly in Table 2.

It is possible to demand a failure probability in the 10^{-3} to 10^{-4} range from the device manufacturer and to improve this by about two orders of magnitude using suitable in-process testing and screening during system assembly. This leads to a system failure probability between 10^{-5} and 10^{-8}. This division of failure probability responsibility between device and system manufacturers leads to a practical and cost effective system design. Device manufacturers can and are realizing failure probabilities in the 10^{-3} and 10^{-4} range, and system manufacturers can and are upgrading this to the 10^{-5} to 10^{-8} range by suitable manufacturing processes. Table 3 documents this partition of failure responsibilities.

Table 2. Buildup Screening — Typical System

Manufacturing Level		All Failures (Percent)	Catastrophics (Percent)
Board Mounting	Complete Electrical	1.0	0.1
System	Electrical Confidence	0.1	0.01
	Vibration 5 Gs 3 Axes 5- 3000 cps	0.05	0.002
	Complete Functional Test		
	Burn In	0.001	--
	Temp Cycle (-40 to 150 F)	0.02	0.001
	Electrical Stress Voltage Steps Current Steps Power Steps	0.002	--
Field Returns on per annum basis		0.01	0.004

Table 3. Partition of Failure Responsibility

	Range	Target
Device Manufacturer	10^{-2} - 10^{-3}	10^{-4}
System Manufacturer	10^{-2} - 10^{-3}	10^{-4}
Resulting System Failure Probability	10^{-4} - 10^{-6}	10^{-8}
Requires absolute elimination of device "cancer" by process controls.		

The hard and fast requirement for making the buildup screening work is that the devices must not contain any "cancer." This is best illustrated by recalling the gold-aluminum intermetallics problem (purple plague) that semiconductor manufacturers struggled with and finally conquered. Any condition, such as an incomplete chemical reaction, formation of intermetallic components, impurities sealed in the can, etc., could lead to progressive device deterioration.

On well-controlled, high-reliability lines, several device manufacturers have proven themselves capable of producing high quality devices free of any "cancer" condition. Strict and continuing process control by the device manufacturer is required, of course, to obtain these high quality devices.

These concepts were established by engineers solving the problem of fabricating high reliability systems containing tens of thousands of parts. These same concepts can be very profitably applied to the design of hardened systems. The carryover is quite direct, since radiation introduces stresses similar to those introduced by the various environments the reliability engineer has previously mastered. Further, it is the discrepant device that produces the problem in the radiation environment just as in other stress environments. Specifically, a scratched overlay pattern on an IC will be quite likely to fail due to electrical stress produced by starting the system or by an overvoltage transient in the power supply, and it is also quite likely to fail due to the current overstress produced by a radiation pulse.

The catastrophic failure modes, such as I^2Rt burnout, can be controlled by electrical stress tests used by the device manufacturer, and the resulting failure probability reduced manyfold by further electrical stress tests at various levels of system assembly. The surface degradation mode due to ionizing dose can be controlled by temperature and burn-in screens by the device manufacturer, and the resultant failure probability reduced by suitable burn-in and temperature stress at various levels of system assembly.

VII. STATISTICAL CONSIDERATIONS

Table 1 shows a typical system failure budget for the radiation environment designed to reduce system failure probabilities below 20 percent.

For neutron degradation, sufficient statistical data is available in the literature to make overstress testing feasible. Devices can be tested to failure in incremental steps and a plot of percent failure versus neutron fluence constructed. This can then be extrapolated down in fluence, based on a normal distribution to the specified fluence level. On this basis, one or two device types, and one of two critical circuits will determine the system failure probability due to neutron displacement effects.

The noncatastrophic photocurrent problems can be assessed by testing the several reset or circumvention circuits in a simulation facility. The total number of tests must be consistent with the failure budget and confidence requirements placed on the system.

The catastrophic photocurrent problems and the total dose problems require brute force testing programs in simulation facilities. Practically speaking, overstress testing can be used to increase confidence, but present state of the art does not support quantitative extrapolations.

It is imperative that the system engineer accumulate and document all radiation test data taken on the system, including part characterization data, part sampling data, circuit level data, subsystem level data, and system proof test data. All go no-go type data should be accumulated and documented. An experienced statistician can utilize all of these data sources to increase confidence in the ability of the system to meet radiation specifications.

Worst-case analysis involves setting device or circuit parameters at a worst-case level and determining the effect on some higher level system or subsystem function. What is worst case? Is it one chance in ten? Or one chance in a hundred? Or perhaps one chance in a thousand? This depends on the complexity level. When describing the system in terms of perhaps three to ten subsystems, worst case is something like one chance in ten, and one should work at roughly 1σ levels. The system, however, contains several hundred circuits, a fraction of which (maybe one-third) have important radiation responses. Now worst case should be like one chance in a hundred, and one should work at roughly a 2σ level. There are usually several thousand devices and, therefore, one should work at roughly the 3σ level for worst-case device analysis. The important point is to be sure that the worst-case definition used for the analysis bears a reasonable mathematical relationship to the required system failure probability. This is illustrated in Table 4.

Table 4. Determination of Statistical Significance Levels for Functional Specifications and Analyses From System Specifications Analysis Levels

Statistical Significance Levels			
System Level Statistics		~1σ	~84%
Subsystem, Critical Circuit	Statistics	~2σ	~98%
Component Level Statistics		~3σ	~99.9%

Circuit analysis codes are available that enable the system engineer to determine functional specifications for subsystems, circuits, and components from an overall system specification. Heavy emphasis on process and quality control is required of the device manufacturer, because radiation excites some failure modes that are not important in other environments and other failure modes that are not easily correlated with electrical measurements.

VIII. CONCLUSION

Electronic systems can be effectively hardened against nuclear radiation environments. A combination of shielding, special circuit design techniques, and use of hardened components is required. The difficulty and cost involved in proof testing is reduced by using a substantial degree of overdesign, allowing the proof tests to be success oriented. Overstress techniques can be used to estimate system failure probability; this is very effective for neutron degradation failure modes and very useful, although not completely reliable, for surface dose and photocurrent catastrophic failure modes.

REFERENCES

1. Glasstone, S., "The Effects of Nuclear Weapons," U.S. Government Printing Office, 1964.

2. TREE Handbook, Battelle Memorial Institute, Columbus, Ohio 1968. (DASA Approval Need-To-Know required.)

3. Messenger, G., and Spratt, J., "The Effects of Neutron Irradiation on Germanium and Silicon," Proc. IRE, June 1958, pp 1036-1044.

4. Larin, F., Radiation Effects in Semiconductor Devices, John Wiley. 1968.

5. Goben, C. A., "A Study of the Neutron Induced Base Current Component in Silicon Transistors," IEEE Transactions on Nuclear Science, October 1965, pp 134-146.

6. Gwyn, C. W., et al, "The Analysis of Radiation Effects in Semiconductor Junction Devices," IEEE Transactions on Nuclear Science, December 1967, pp 153-169.

7. Messenger, G. C., and Steele, E. L., "Statistical Modeling of Semiconductor Device for the TREE Environment," IEEE Trans. NS-15, No. 1, pp 133-139.

8. Snow, E. H., et al, "Effects of Ionizing Radiation on Oxidized Silicon Surfaces and Planer Devices," Proc. IEEE, Vol. 55, No. 7, July 1967, pp 1118-1185.

9. Peck, D.S., et al, "Surface Effects of Radiation on Transistors," Bell System Tech. J., Vol. 42, January 1963, pp 95-129.

10. Bary, A.L., and Page, D.F., "Radiation Hardening of MOS Transistors for Low Ionizing Dose Levels," IEEE Trans., Vol. N5-13, December 1966, pp. 255-261.

11. Spratt, J.P., et al, "The Impact of Technology on Radiation - Hardened Integrated Circuits," IEEE 1969, International Solid State Circuits Conference, Philadelphia, Penn.

12. Private Communication from Ron Reeder and R. R. Miltenberger, Autonetics Anaheim.

13. SECURE is a special computer code developed by Autonetics for systems analysis in the radiation environment, and is not currently generally available. However, systems analysis codes similar to SECURE are expected to become available in the near future.

NEUTRON DAMAGE CONSTANT FOR BIPOLAR TRANSISTORS

1 July 1969

C. R. Viswanathan

Department of Electrical Sciences and Engineering

School of Engineering and Applied Science

University of California

Los Angeles

G. C. Messenger,

D. H. Alexander, J. E. Cooper,

E. C. Heaton, and R. N. Lane

Autonetics, Minuteman Division

Anaheim, California

Autonetics
North American Rockwell

3370 Miraloma Avenue, Anaheim, California 92803

NEUTRON DAMAGE CONSTANT FOR BIPOLAR TRANSISTORS

C. R. Viswanathan, Department of Electrical Sciences and Engineering,
School of Engineering and Applied Science,
University of California, Los Angeles

and

G. C. Messenger, D. H. Alexander, J. E. Cooper, E. C. Heaton, and R. N. Land
Autonetics (Minuteman Division), Anaheim, California

ABSTRACT

An exact expression for the neutron damage constant, K, has been derived in terms of the rate of degradation of current gain with neutron fluence in bipolar transistors. It is shown that this expression reduces to the simple form,

$$K = 0.16 / \left(f_T \frac{\partial \frac{1}{\beta}}{\partial \phi} \right) ,$$

for the entire range of damage where the damaged transistor is still a useful device. The effect of neutron irradiation on minority carrier distribution and also on transit time in the base of a bipolar transistor is discussed. It is shown that the gain-bandwidth product remains constant under neutron irradiation unless the transistor is damaged beyond its useful limit. An empirical function for the depender 'e of damage constant on emitter current is obtained from experimental results.

INTRODUCTION

Neutron radiation causes reduction in the minority carrier lifetime by creating defects in the crystal lattice. In a bipolar transistor, minority carrier flow across the base region is the dominant "gain determining" mechanism. Consequently, the current gain of a bipolar transistor is reduced under neutron irradiation due to displacement damage in the base region. The degradation of lifetime under neutron irradiation of fluence, ϕ, is given by

$$\frac{1}{\tau} = \frac{1}{\tau_i} + \frac{\phi}{K} \tag{1}$$

where K is the damage constant, τ_i is the initial (preirradiated) value of lifetime, and τ is the post-irradiated value of lifetime. This expression giving a linear relationship between reciprocal lifetime and neutron fluence has been verified to be valid over a wide range of neutron fluences: therefore, the damage constant, K, is a useful parameter to predict the reduction in current gain for any neutron fluence. In this paper, we report a general solution to the continuity equation in the base of a bipolar transistor, and from this derive an expression for common emitter current gain in terms of the ratio ($k = L_h/w$) of the minority carrier diffusion length to the width of the base and the drift field parameter, η. Using the relationship between diffusion length and lifetime of minority carriers, an expression for damage constant, K, is

derived in terms of the preirradiated gain bandwidth product, f_T, the slope of reciprocal current gain, β, with respect to neutron fluence, ϕ, and η. This expression is shown to be reducible to a simpler form similar to an earlier one[1] over the range of neutron fluence at which the transistor is still a useful device.

The effect of neutron radiation on the distribution of minority carriers in the base region, as well as on the base transit time, is discussed in this paper. Preliminary results of the effect of neutron radiation on gain bandwidth product are also discussed. Finally, the functional dependence of measured damage constant on emitter current is given and is shown to agree with experimental values.

NEUTRON DAMAGE CONSTANT, K

The continuity equation for the base region of a transistor is given by

$$\frac{\partial \Delta p}{\partial t} = D_h \frac{\partial^2 \Delta p}{\partial x^2} - \frac{\eta}{w} D_h \frac{\partial \Delta p}{\partial x} - \frac{\Delta p}{\tau_h}, \qquad (2)$$

where we have assumed a one-dimensional p-n-p transistor with a drift field parameter, η, and

where

D_h = diffusion constant for the holes in the base

w = width of the base

τ_h = lifetime of holes in the base

Δp = excess hole density in the base.

The steady state solution to Equation (2) gives the equilibrium hole distribution in the base region and is equal to

$$\frac{\Delta p}{\Delta p_o} = \frac{1}{1 - e^{w\sqrt{}}} e^{\left(\frac{\eta}{2w} + \frac{1}{2}\sqrt{}\right)x} + \frac{1}{1 - e^{-w\sqrt{}}} e^{\left(\frac{\eta}{2w} - \frac{1}{2}\sqrt{}\right)x} \qquad (3)$$

where Δp_o = excess hole density at the boundary of emitter-base junction, i.e., at x = 0

$$\sqrt{} = \sqrt{\frac{\eta^2}{w^2} + \frac{4}{D_h \tau_h}} = \sqrt{\frac{\eta^2}{w^2} + \frac{4}{L_h^2}} \tag{4}$$

and L_h = diffusion length of holes in the base. From this we can calculate the conductance matrix elements σ_{11} and σ_{21}, and they are

$$\sigma_{11} = \frac{e^2 A}{kT} D_h \Delta p_o \left(\frac{1}{2}\sqrt{} \coth\left(\frac{w}{2}\sqrt{}\right) + \frac{\eta}{2w}\right) \tag{5}$$

and

$$\sigma_{21} = \frac{e^2 A}{kT} D_h \Delta p_o \frac{1}{2} \left(e^{\eta/2}\sqrt{} \operatorname{csch}\left(\frac{w}{2}\sqrt{}\right)\right), \tag{6}$$

where A is the area of cross section of the base region.

The base transport factor, b, is given by

$$b = \sigma_{21}/\sigma_{11}$$

The current gain, β, in the common emitter mode, neglecting all other mechanisms except the base transport process, is then

$$\frac{1}{\beta} = \frac{1}{b} - 1 = \frac{\sigma_{11}}{\sigma_{21}} - 1.$$

Therefore,

$$\frac{1}{\beta} = \frac{\eta}{w\sqrt{}} e^{-\eta/2} \sinh\left(\frac{w}{2}\sqrt{}\right) + e^{-\eta/2} \cosh\left(\frac{w}{2}\sqrt{}\right) -1. \tag{7}$$

If we define k as the ratio of diffusion length, L_h, to base width we can rewrite Equation (7) as

$$\frac{1}{\beta} = \frac{\eta}{2\sqrt{\frac{\eta^2}{4} + \frac{1}{k^2}}} e^{-\eta/2} \sinh\sqrt{\frac{\eta^2}{4} + \frac{1}{k^2}} + e^{-\eta/2} \cosh\sqrt{\frac{\eta^2}{4} + \frac{1}{k^2}} - 1. \tag{8}$$

The expression for β in Equation (7) shows the functional dependence of β on τ_h since

$$\sqrt{} = \sqrt{\frac{\eta^2}{w^2} + \frac{4}{D_h \tau_h}} \; .$$

The degradation of τ_h under neutron irradiation is given by Equation (1) as discussed earlier. Under the assumption that D_h is essentially unchanged under neutron irradiation, the change in β under neutron irradiation is brought about only by the degradation in lifetime.

Therefore,

$$\frac{\partial \frac{1}{\beta}}{\partial \phi} = \frac{\partial \frac{1}{\beta}}{\partial \frac{1}{\tau}} \quad \frac{\partial \frac{1}{\tau}}{\partial \phi} \; . \tag{9}$$

From Equation (1), we know that

$$\frac{\partial \frac{1}{\tau}}{\partial \phi} = \frac{1}{K} \; . \tag{10}$$

We can evaluate $\partial(1/\beta)/\partial\phi$ from Equation (7), and substituting this expression as well as Equation (10) in Equation (9), we obtain

$$\frac{\partial \frac{1}{\beta}}{\partial \phi} = \frac{w^2}{D_h} \frac{1}{K} \left[- \frac{\eta}{4e^{\eta/2}} \frac{\sinh \sqrt{\frac{\eta^2}{4} + \frac{1}{k^2}}}{\left(\frac{\eta^2}{4} + \frac{1}{k^2} \right)^{3/2}} + \frac{\eta}{4e^{\eta/2}} \frac{\cosh \sqrt{\frac{\eta^2}{4} + \frac{1}{k^2}}}{\left(\frac{\eta^2}{4} + \frac{1}{k^2} \right)} + \frac{1}{2e^{\eta/2}} \frac{\sinh \sqrt{\frac{\eta^2}{4} + \frac{1}{k^2}}}{\sqrt{\frac{\eta^2}{4} + \frac{1}{k^2}}} \right] \; . \tag{11}$$

The term w^2/D_h is related to the preirradiated gain bandwidth product f_T as

$$\frac{1}{\omega_T} = \frac{w^2}{D_h} \frac{e^{-\eta} + \eta - 1}{\eta^2} ,$$

where

$$\omega_T = 2\pi f_T .$$

Therefore,

$$\frac{\partial \frac{1}{\beta}}{\partial \phi} = \frac{1}{2\pi f_T} \frac{1}{K} \quad G(\eta) \approx \frac{0.16}{f_T K} \quad G(\eta), \tag{12}$$

where

$$G(\eta) = \frac{\eta^2}{(e^{-\eta} + \eta - 1)} \left[- \frac{\eta}{4e^{\eta/2}} \frac{\sinh\sqrt{\frac{\eta^2}{4} + \frac{1}{k^2}}}{\left(\frac{\eta^2}{4} + \frac{1}{k^2}\right)^{3/2}} \right.$$

$$+ \frac{\eta}{4e^{\eta/2}} \frac{\cosh\sqrt{\frac{\eta^2}{4} + \frac{1}{k^2}}}{\left(\frac{\eta^2}{4} + \frac{1}{k^2}\right)}$$

$$\left. + \frac{1}{2e^{\eta/2}} \frac{\sinh\sqrt{\frac{\eta^2}{4} + \frac{1}{k^2}}}{\sqrt{\frac{\eta^2}{4} + \frac{1}{k^2}}} \right] . \tag{13}$$

The function, $G(\eta)$, is dependent on η and k, where $\eta = \ln N_{DE}/N_{DB}$ and where N_{DE} and N_{DB} are the donor concentrations in the base region near the emitter and collector junctions, respectively.

In Figures 1A and 1B, we have plotted $G(\eta)$ as a function of η for both positive and negative values of η and for various values of the parameter, k. If $G(\eta)$ does not change with k, over a certain range of k's, then over that range

$$\partial \frac{1}{\beta} / \partial \phi$$

will be a constant, i.e., $1/\beta$ will increase linearly with ϕ, as can be seen from Equation (12). From Figure 1A, it can be seen that at high value of η, $G(\eta)$ is essentially close to unity for value of $k \geq 1$. However in homogeneous transistors, $(\eta = 0)$, $G(\eta)$ varies appreciably with k for values of k less than 2. Over the range of neutron fluence where the experimentally-measured value of $1/\beta$ varies linearly with ϕ, we can therefore take $G(\eta)$ essentially as constant and equal to unity. Then, from this linear slope

$$\partial \frac{1}{\beta} / \partial \phi,$$

we can determine the damage constant, K, as equal to

$$K \approx \frac{0.16}{f_T \frac{\partial \frac{1}{\beta}}{\partial \phi}} \quad . \tag{14}$$

We have plotted in Figure 2 the value of β from Equation (8) as a function of k with η as the parameter. From this figure it can be seen that in drift transistors with $\eta = 8$, β goes to a value less than 2 for values of k less than 0.5 while in homogeneous transistors β becomes less than 2 for values of k less than 1. Since, in any circuit operation, the circuit will almost certainly fail for values of β as low as 2, we can therefore assume that if a transistor is so badly damaged that $k = 0.5$, there is complete failure. The range of neutron fluence, over which k never deteriorates to less than 0.5, is seen from Figure 1A to be the range over which $G(\eta)$ is essentially unity.

If we consider the function, $G(\eta)$, it is seen that for values of $k \geq 1$, $G(\eta)$ is essentially constant with η. However, in a badly damaged transistor, $G(\eta)$ varies with η and for example for the case, $k = 0.5$, $G(\eta)$ reaches a maximum value of 1.9 at $\eta \approx -3$. In Figures 1A and 1B, the corresponding β values are marked in different regions of the curve for ease of reference.

In Figure 3, we give the experimentally-measured value of $1/\beta$, plotted as a function of ϕ, for a typical transistor. It can be seen that this plot is essentially linear with a slope of $\partial \frac{1}{\beta} / \partial \phi$ equal to 1.83×10^{-15} per n/cm^2. From the linearity, it can be deduced that in this region of neutron fluence, $G(\eta)$ is essentially unity. We

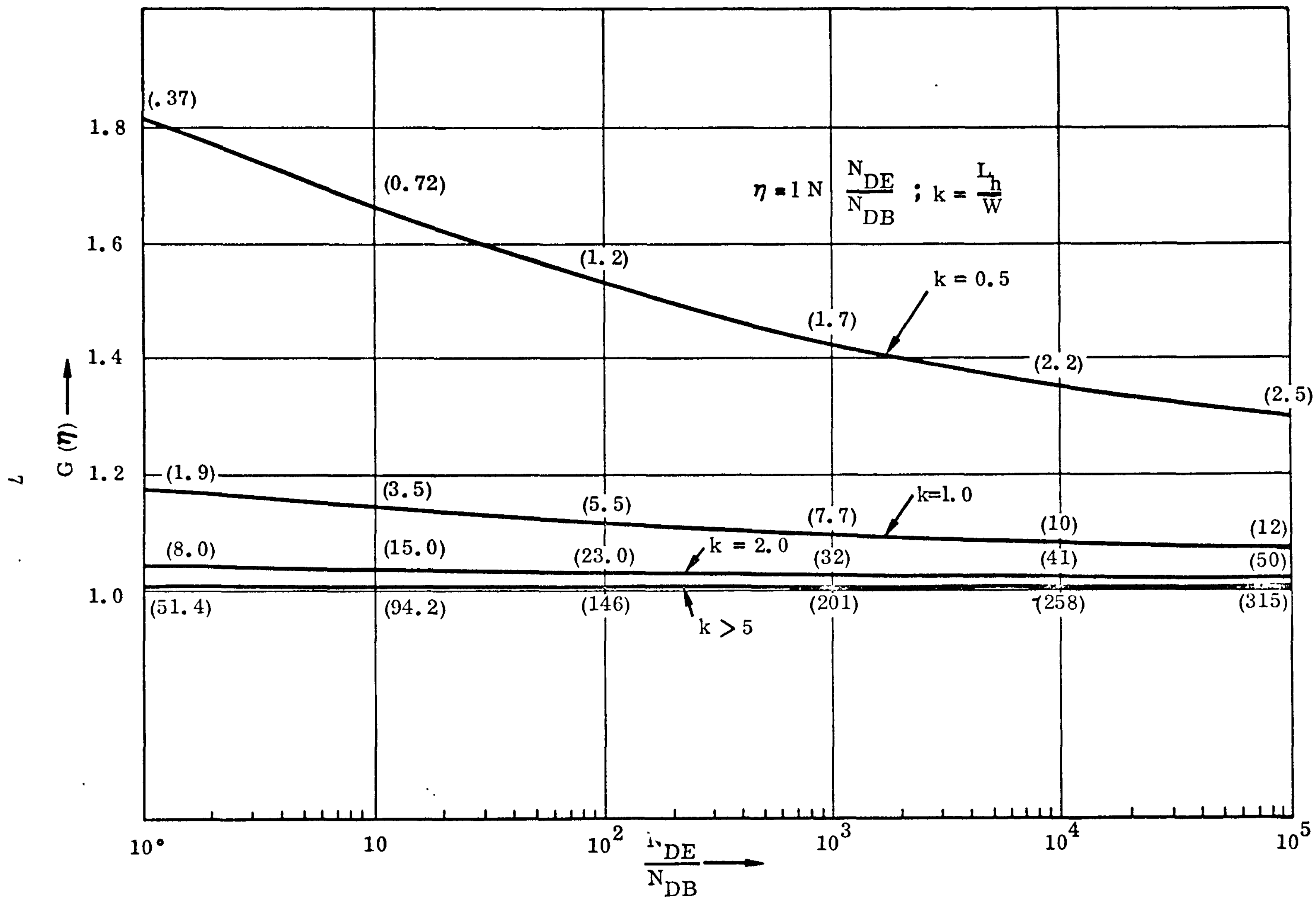

Figure 1A. Plot of G(η) in Forward Mode [Numbers within Parentheses, ( ), Denote β Values due to Transport Alone]

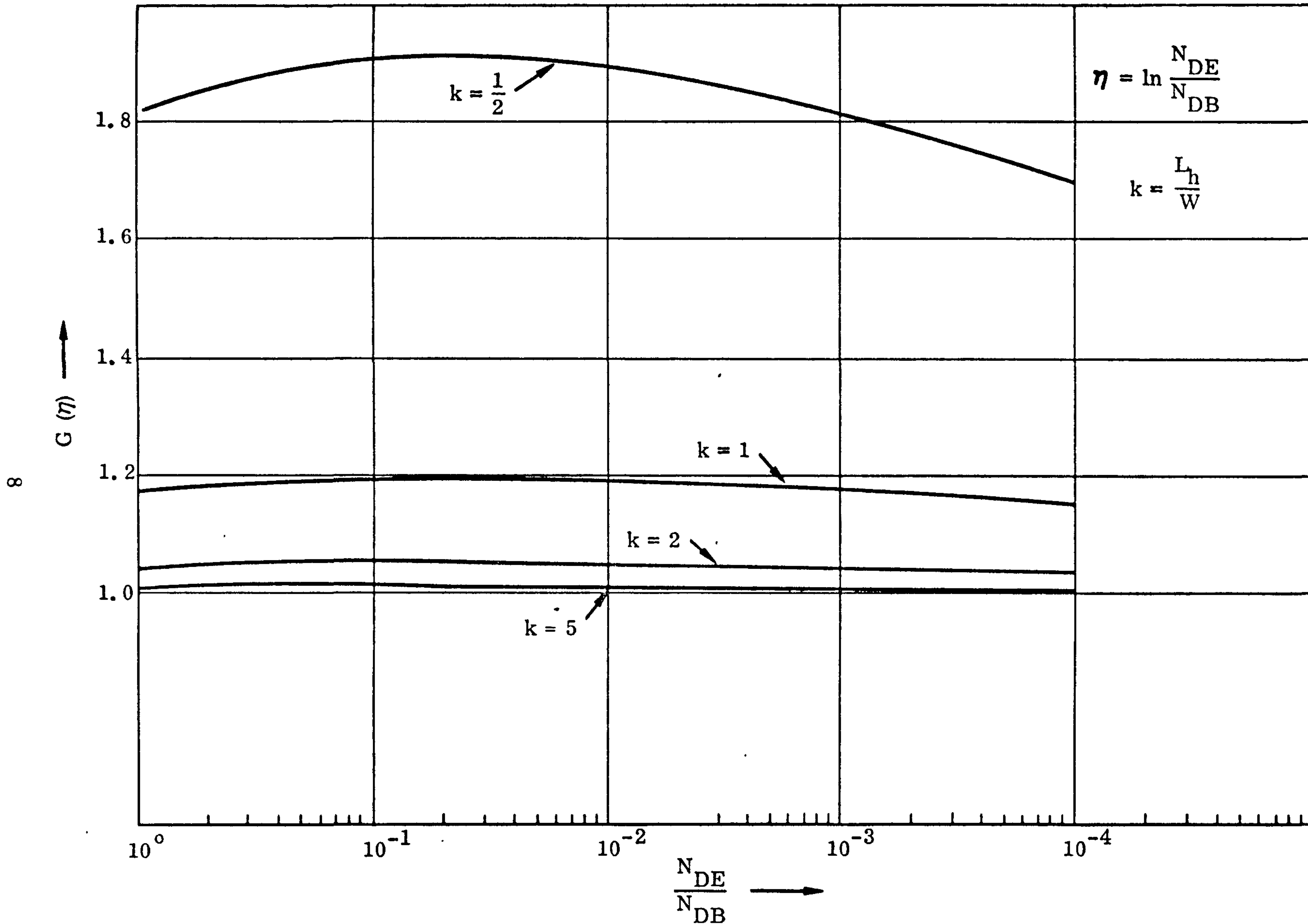

Figure 1B. Plot of G(η) in Inverse Mode

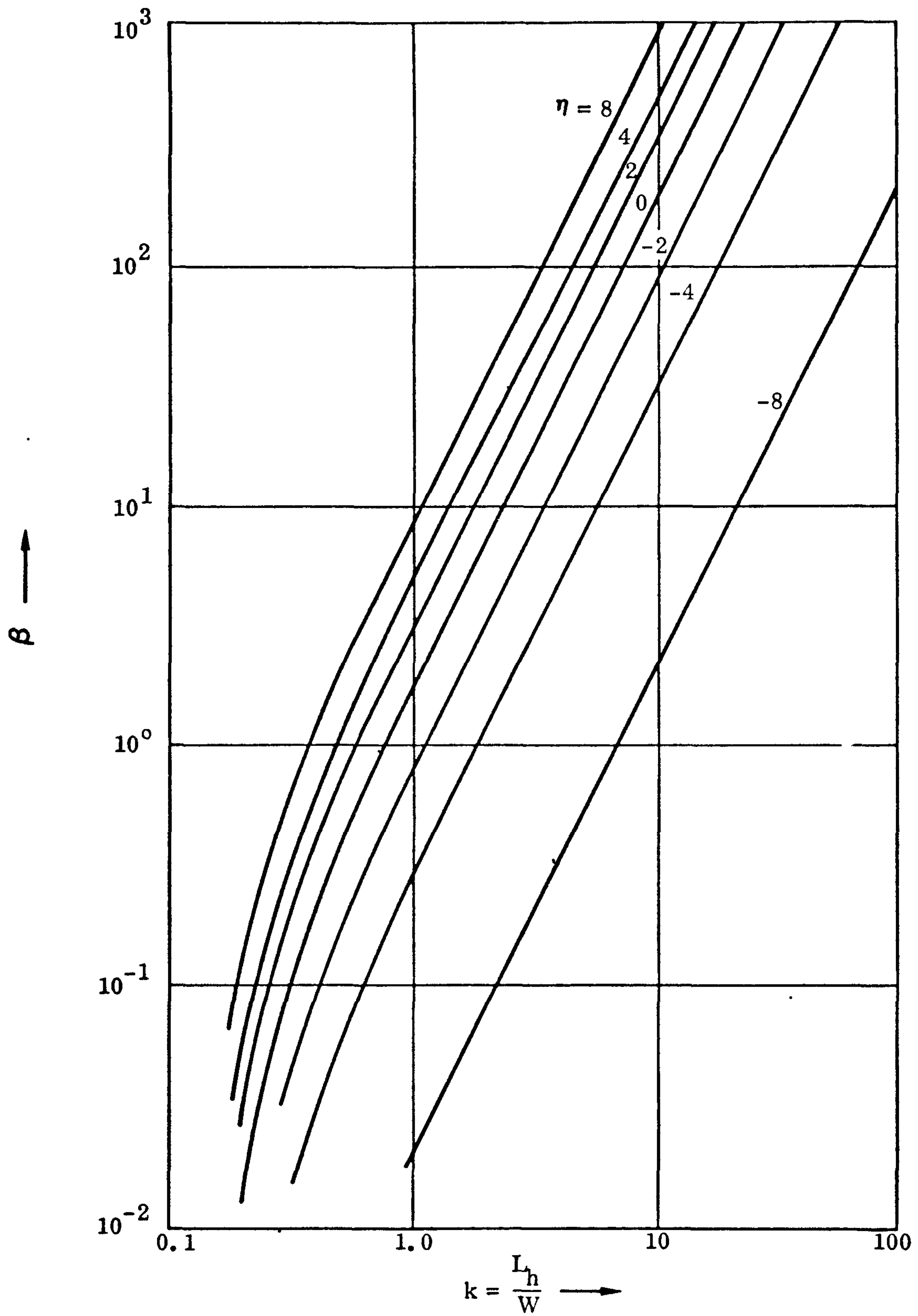

Figure 2. Plot of β Against k

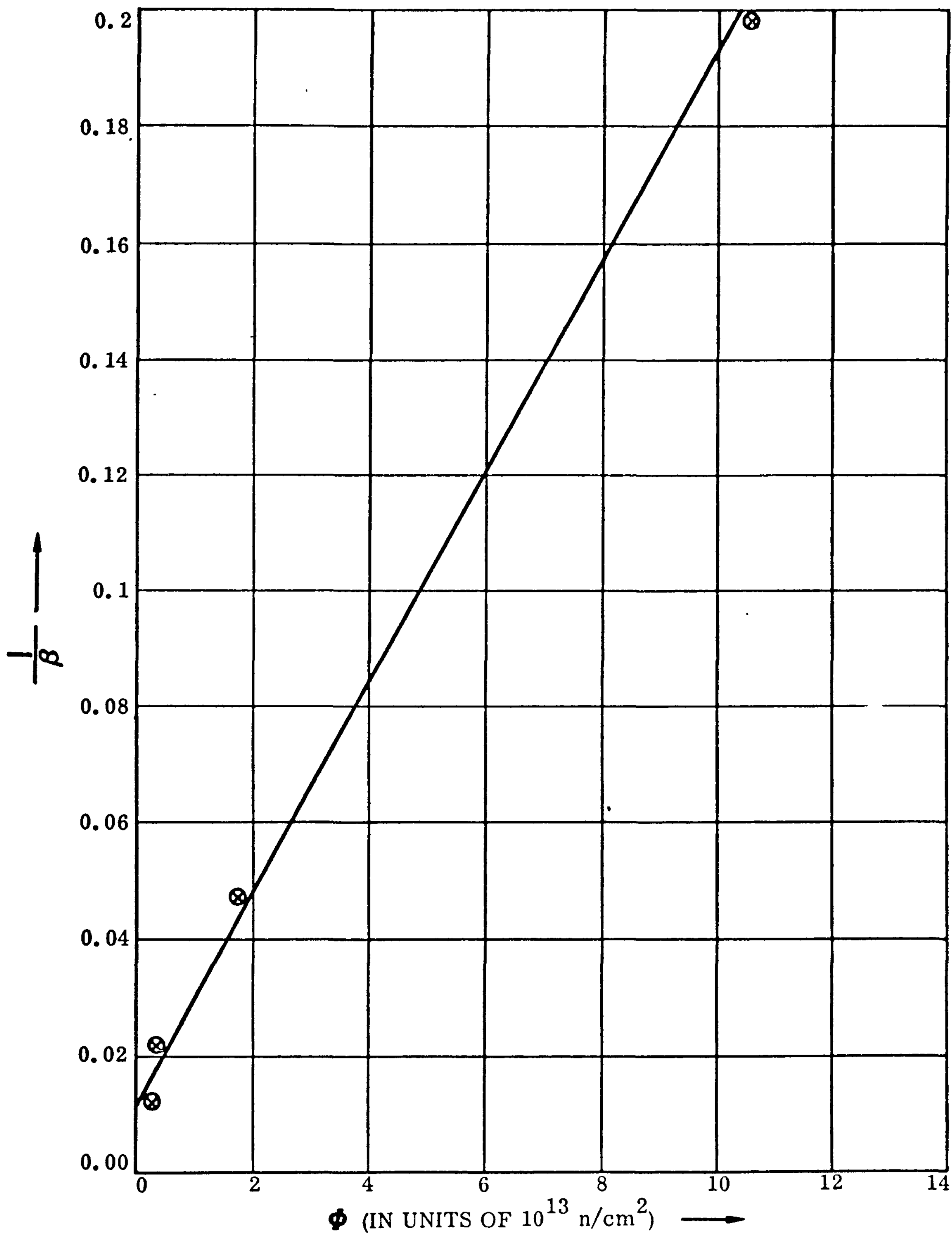

Figure 3. Plot of $1/\beta$ vs ϕ Measured in a Typical Transistor

can verify this as follows. For this transistor, η was measured by the methods decribed later to be ≈ 8 ie ($N_{DE}/N_{DB} \approx 3000$). From Figure 3, we find the lowest measured β to be 5, and using Figure 2, we find this corresponds to $k = 2.5$. In Figure 1A, $G(\eta)$ for $k = 2.5$ and $N_{DE}/N_{DB} \approx 3000$, is very close to unity. Therefore, the use of Equation (14) is justified in this case. Intrinsic f_T was measured for this transistor to be ≈ 85 Mc/s. Using this value in Equation (14), we obtain the damage constant,

$$K = 1.03 \times 10^6 \ \frac{\text{n-sec}}{\text{cm}^2}.$$

BASE-TRANSIT TIME, τ_B

The base transit time, τ_B, which is defined as the average time taken by a minority carrier to traverse the base region, is given by the following integral:

$$\tau_B = \int_{x=0}^{w} \frac{dx}{v_h} = \int_{x=0}^{w} \frac{eA\Delta p}{I_h} \, dx \tag{15}$$

where A is the area of cross section of the base region. Equation (15) can be transformed into

$$\tau_B = \frac{1}{D_h} \int_0^w \frac{dx}{-\frac{1}{\Delta p}\frac{d\Delta p}{dx} + \frac{\eta}{w}} \tag{16}$$

by writting I_h explicitly as the sum of diffusion and drift components. Substituting for Δp from Equation (3) in equation (16) and integrating, we obtain

$$\tau_B = \frac{L_h^2}{D_h}\left(\sqrt{\frac{\eta^2}{4} + \frac{1}{k^2}} - \frac{\eta}{2}\right)$$

$$+ \frac{L_h^2}{D_h}\left[\ln\left(\frac{\frac{\eta}{2} + \sqrt{\frac{\eta^2}{4} + \frac{1}{k^2}} - e^{-\sqrt{\frac{\eta^2}{4} + \frac{1}{k^2}}}\left(\frac{\eta}{2} - \sqrt{\frac{\eta^2}{4} + \frac{1}{k^2}}\right)}{\sqrt{\frac{\eta^2}{4} + \frac{1}{k^2}}} \right)\right], \tag{17}$$

where

$$k = \frac{L_h}{w}.$$

It can be seen that when we consider the limit, $k \gg 1$ (i.e., $L_h \gg w$), Equation (17) reduces to the familiar form,

$$\tau_{B_\infty} = \frac{w^2}{D_h} \; \frac{\eta - + e^{-\eta}}{\eta^2} ,$$

which is the base transit time when there is no recombination in the base region (the subscript, ∞, in τ_{B_∞} is used to denote that $L_h \gg w$). Dividing Equation (17) by τ_{B_∞}, we obtain

$$\frac{\tau_B}{\tau_{B_\infty}} = k^2 \frac{\eta^2}{\eta - 1 + e^{-\eta}} \left[\left(\sqrt{\frac{\eta^2}{4} + \frac{1}{k^2}} - \frac{\eta}{2} \right) + \ln \left(\frac{\frac{\eta}{2} + \sqrt{\frac{\eta^2}{4} + \frac{1}{k^2}} - e^{-\sqrt{\frac{\eta^2}{4} + \frac{1}{k^2}}} \left(\frac{\eta}{2} - \sqrt{\frac{\eta^2}{4} + \frac{1}{k^2}} \right)}{\sqrt{\frac{\eta^2}{4} + \frac{1}{k^2}}} \right) \right] . \quad (18)$$

Since neutron irradiation reduces the value of k, the change in τ_B under neutro' irradiation is brought about by its dependence on k as given in Equation (18). In Figure (4), τ_B/τ_{B_∞} is plotted as a function of k for $\eta = 8$ (forward mode in a drift transistor), $\eta = 0$ (homogeneous transistor), and for $\eta = -8$ (inverse mode in a drift transistor). It can be seen that in a drift transistor, little change takes place in τ_B until k is reduced to less than 0.5 (useful operating limit from the point of view of gain) in the forward mode. However, in a homogeneous transistor and to a larger extent in a drift transistor in the inverse mode, the base transit time is reduced appreciably even when k is as large as 5.

MINORITY CARRIER DISTRIBUTION

The expression for excess minority carrier density in Equation (3) can be rewritten as

$$\frac{\Delta p}{\Delta p_o} = \frac{1}{\left(1 - e^{\sqrt{\frac{\eta^2}{4} + \frac{1}{k^2}}}\right)} e^{\left(\frac{\eta}{2} + \frac{1}{2}\sqrt{\frac{\eta^2}{4} + \frac{1}{k^2}}\right)\frac{x}{w}} +$$

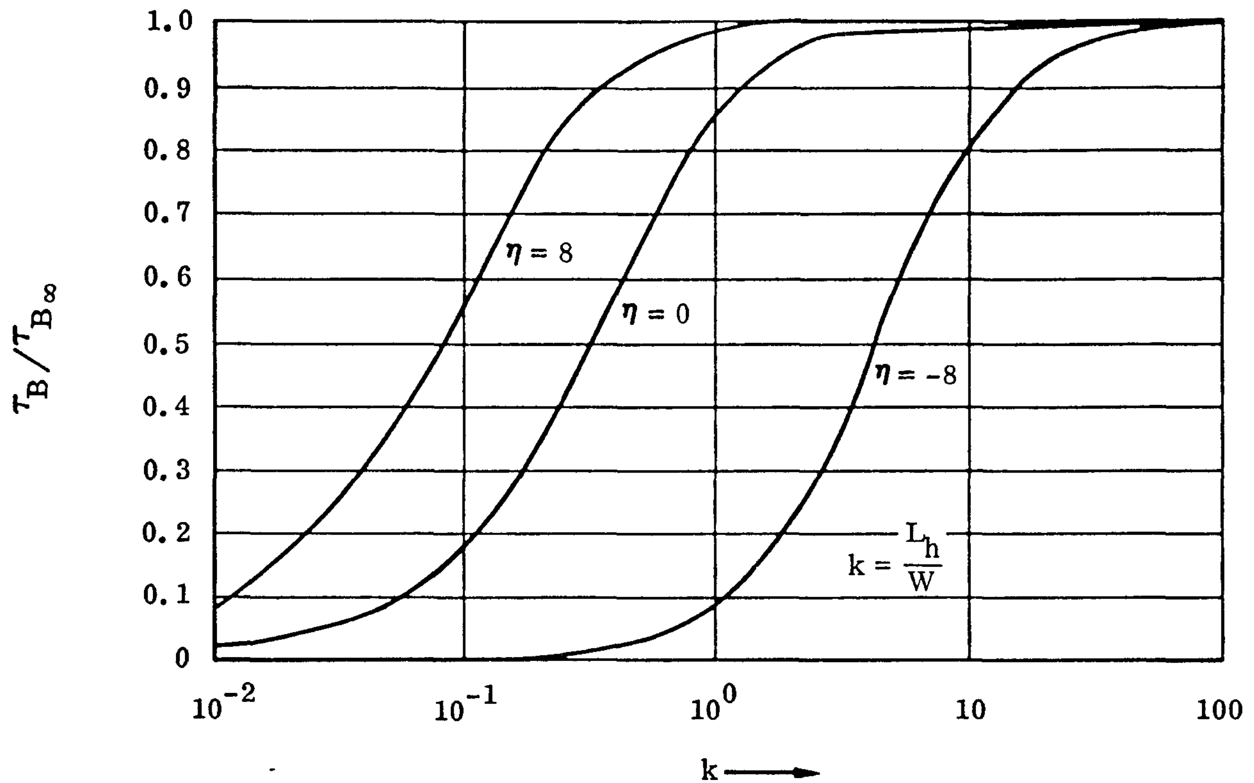

Figure 4. Plot of Base Transit Time as a Function of k

$$+ \frac{1}{\left(1 - e^{-\sqrt{\frac{\eta^2}{4} + \frac{1}{k^2}}}\right)} e^{\left(\frac{\eta}{2} - \frac{1}{2}\sqrt{\frac{\eta^2}{4} + \frac{1}{k^2}}\right)\frac{x}{w}} \quad . \tag{19}$$

Values of $\Delta p/\Delta p_o$ are plotted as a function of x/w for k = 10, 1, and 0.1 for a drift transistor with $\eta = 8$ in Figure 5A and for a homogeneous transistor in Figure 5B. It can be seen that unless k is reduced to less than 1, the minority carrier distribution is essentially the same as the unirradiated case. This agrees with our earlier discussion on β degradation with k.

DETERMINATION OF η

Our discussion so far has shown that the value of η is required to predict the degradation of transistor performance under neutron irradiation. We describe below three methods by which η was determined for a particular transistor and it was found that all three methods yield η values close to each other within 10 percent.

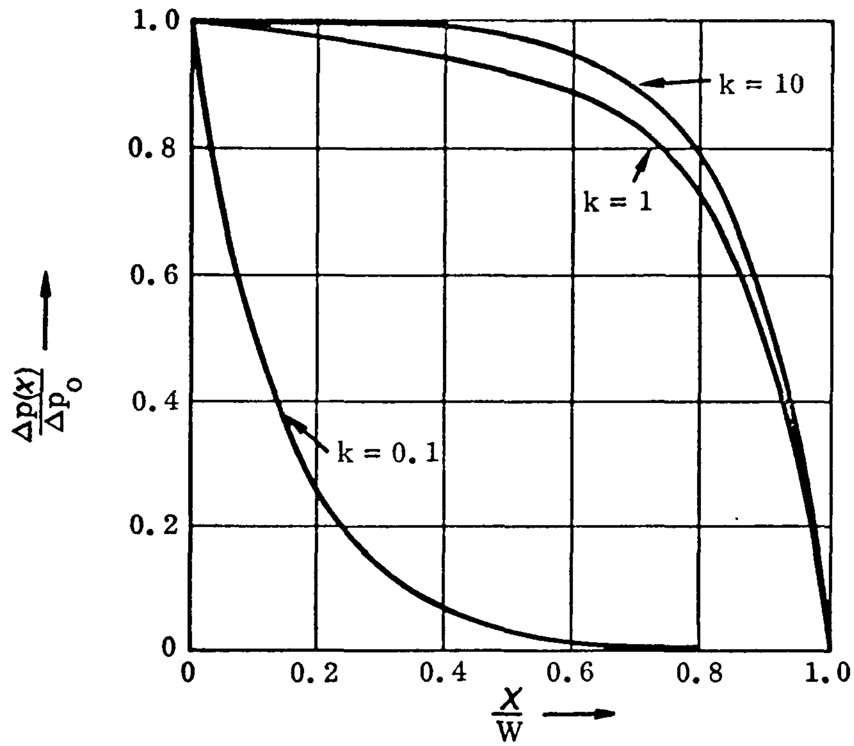

Figure 5A. Minority Carrier Distribution in the Base of a Drift Transistor ($\eta = 8$)

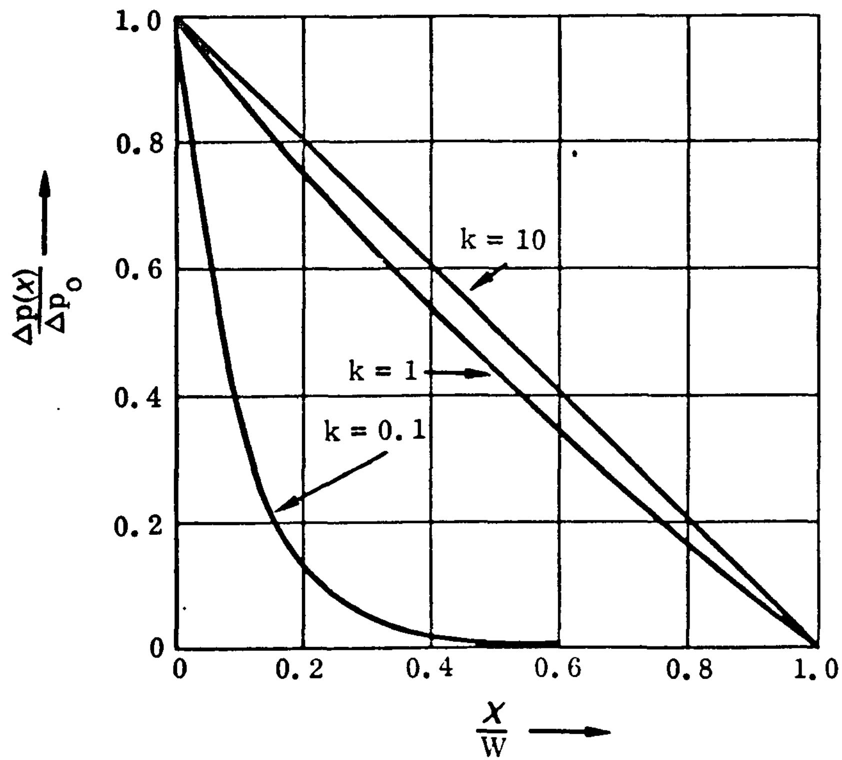

Figure 5B. Minority Carrier Distribution in the Base of a Homogeneous Transistor

In the first method, diffusion profiles of impurity distribution were obtained from the device manufacturer and approximating this distribution by an exponential as discussed by Lindmayer and Wrigley[2], η was determined to be 8.5.

If the fringe field effects in the base region arising due to differences in emitter and collector junction areas are neglected, then the ratio, f_{T_N}/f_{T_I}, is given by

$$\frac{f_{T_N}}{f_{T_I}} = \frac{e^{\eta} - \eta - 1}{e^{-\eta} + \eta - 1}, \tag{20}$$

where f_{T_N} and f_{T_I} are the gain bandwidth product in the normal and inverse modes, respectively. This expression is plotted in Figure 6 as a function of η. If f_{T_N}/f_{T_I} is known, η can be determined from this plot. For the transistor referred to in the previous paragraph, f_{T_N} and f_{T_I} were measured and an average value of η was obtained as 8.4.

It is also possible to obtain gain bandwidth product from small signal transient measurements. The time constant for the small signal transient response is $\beta_o \tau_B$, where τ_B is base transit time and β_o is the d.c. beta. Therefore, the ratio τ_{B_I}/τ_{B_N} can be obtained by performing small signal transient measurements in the forward and inverse mode, and since

$$\tau_{B_I}/\tau_{B_N} = f_{T_N}/f_{T_I},$$

Figure (6) can be used to obtain η from the ratio, τ_{B_I}/τ_{B_N}. For the reference transistor an average value of 8.1 for η was obtained.

Thus, we see that the average values obtained for η by all three methods are close to each other. It must be mentioned that individual values varied by larger amounts and the maximum deviation, i.e., the difference between the highest and lowest value, occurred in the transient method and this was of the order of 10 percent.

f_T VARIATION WITH NEUTRON IRRADIATION

If we assume in Equation (2) that the injected excess carrier density consists of a DC component and a superimposed small signal AC component at an angular velocity of w, we can write the high frequency β as

$$\frac{1}{\beta} = \frac{\eta}{2\sigma w} \frac{1}{e^{\eta/2}} \sinh(\sigma w) + \frac{1}{e^{\eta/2}} \cosh(\sigma w) - 1, \tag{21}$$

where

$$\sigma w = \sqrt{\frac{\eta^2}{4} + \frac{1}{k^2} (1 + i\omega\tau_h)} .$$

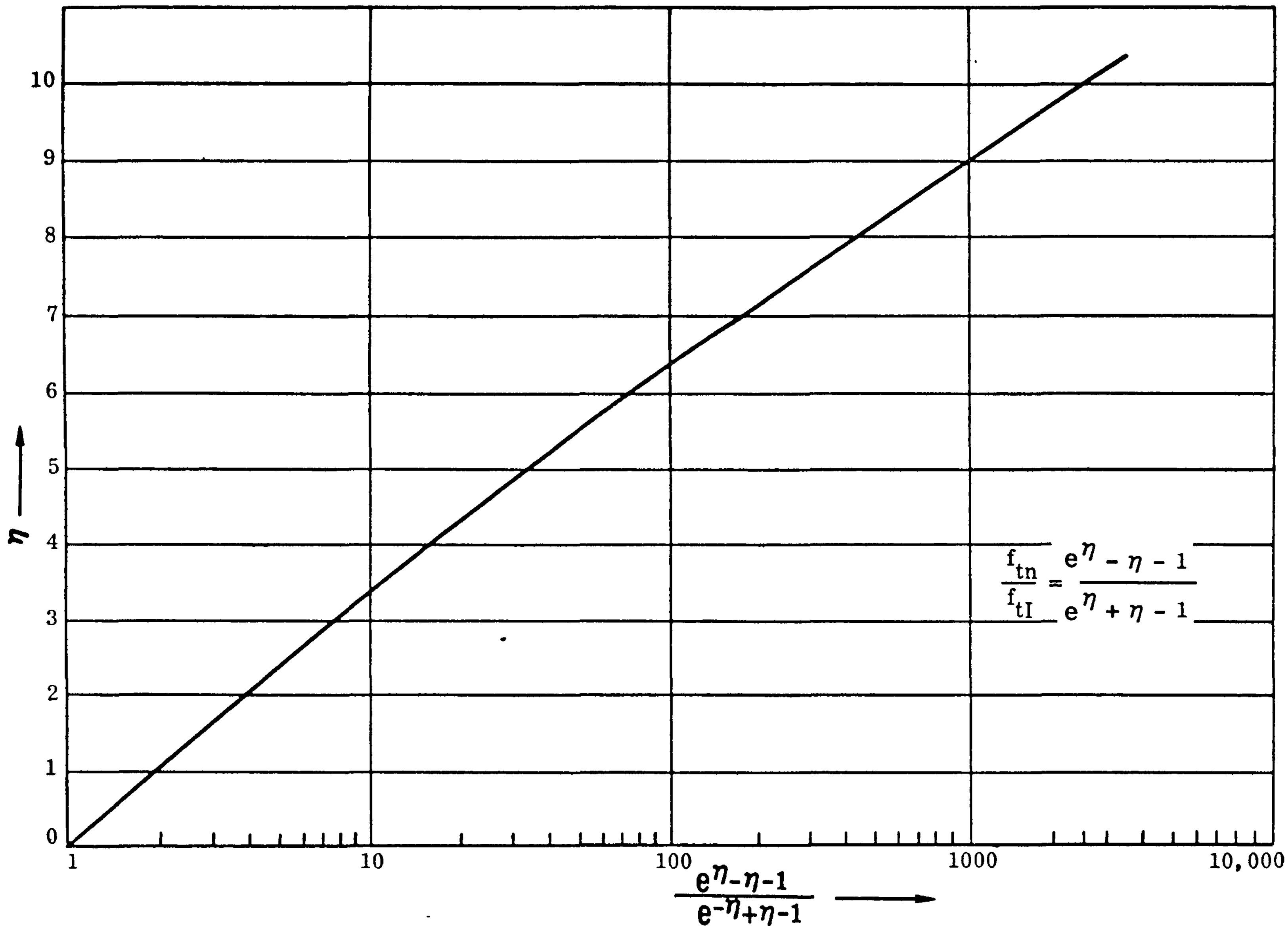

Figure 6. Plot of η vs $\frac{e^{\eta} - \eta - 1}{e^{-\eta} + \eta - 1}$

From Equation (21), complex β can be evaluated. A digital computer was used to calculate β and in Figure 7A, $|\beta|/\beta_o$ was plotted as a function of $M = \omega\tau_h$ for $k = 5$, $k = 1$ and $k = 0.5$ for a homogeneous transistor where β_o is the DC Beta. It is seen that the 6 db-per-octave approximation is valid for $k > 1$. In Figure 7B, we plotted $|\beta|/\beta_o$ as a function of $M = \omega\tau_h$ for $k = 1$ and $k = 0.5$ and $k = 0.1$ for a drift transistor with $\eta = 8$. It can be seen in this case that for $k > 0.5$, the 6 db-per-octave approximation is valid for the fall off in $|\beta|$.

We notice in Figures 7A and 7B that in the region where we have 6 db/octave fall off,

$$\frac{M|\beta|}{\beta_o} = 1.0.$$

However,

$$\omega_T = \frac{M|\beta|}{\tau_h}$$

$$= \frac{M|\beta|}{\beta_o}\frac{\beta_o}{\tau_h} \approx \frac{\beta_o}{\tau_h}, \tag{22}$$

where $\omega_T = 2\pi \times$ gain bandwidth product

But

$$\frac{1}{\tau_h} = \frac{1}{\tau_i} + \frac{\phi}{K} \approx \frac{\phi}{K} \tag{23}$$

$$\therefore \omega_T = \frac{1}{K}\beta_o\phi. \tag{24}$$

In the region where

$$\frac{\partial\frac{1}{\beta}}{\partial\phi} = \text{constant},$$

$$\beta_o\phi = \text{constant}.$$

Therefore, ω_T should essentially remain constant in the usable range of the transistor. When a transistor is very badly damaged, the gain bandwidth product will change. In fact, from Figures 7A and 7B, we can see it is not meaningful to talk of ω_T since we do not obtain a 6 db/octave roll-off in a badly damaged transistor.

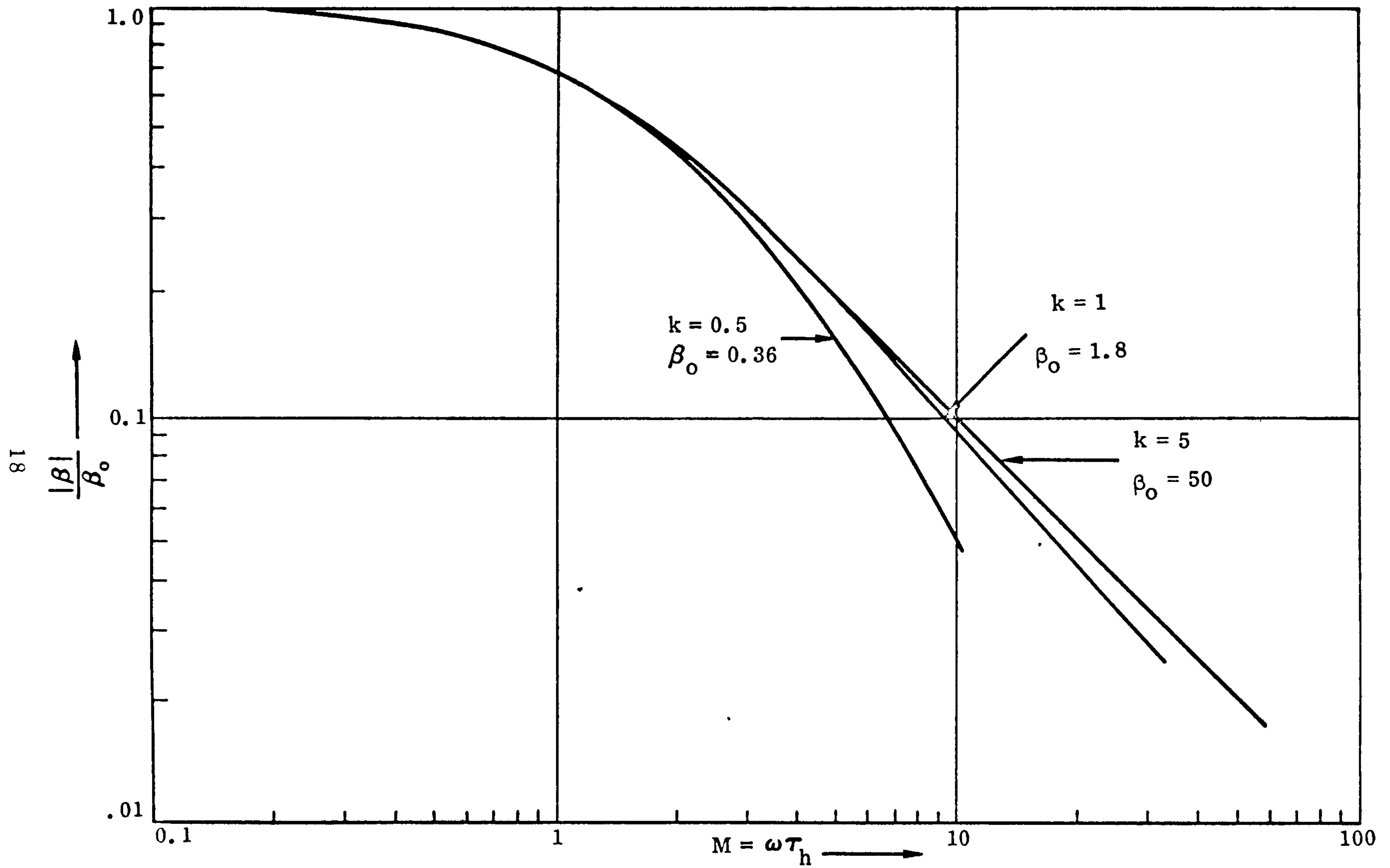

Figure 7A. Plot of $|\beta|/\beta_o$ for a Homogeneous Transistor

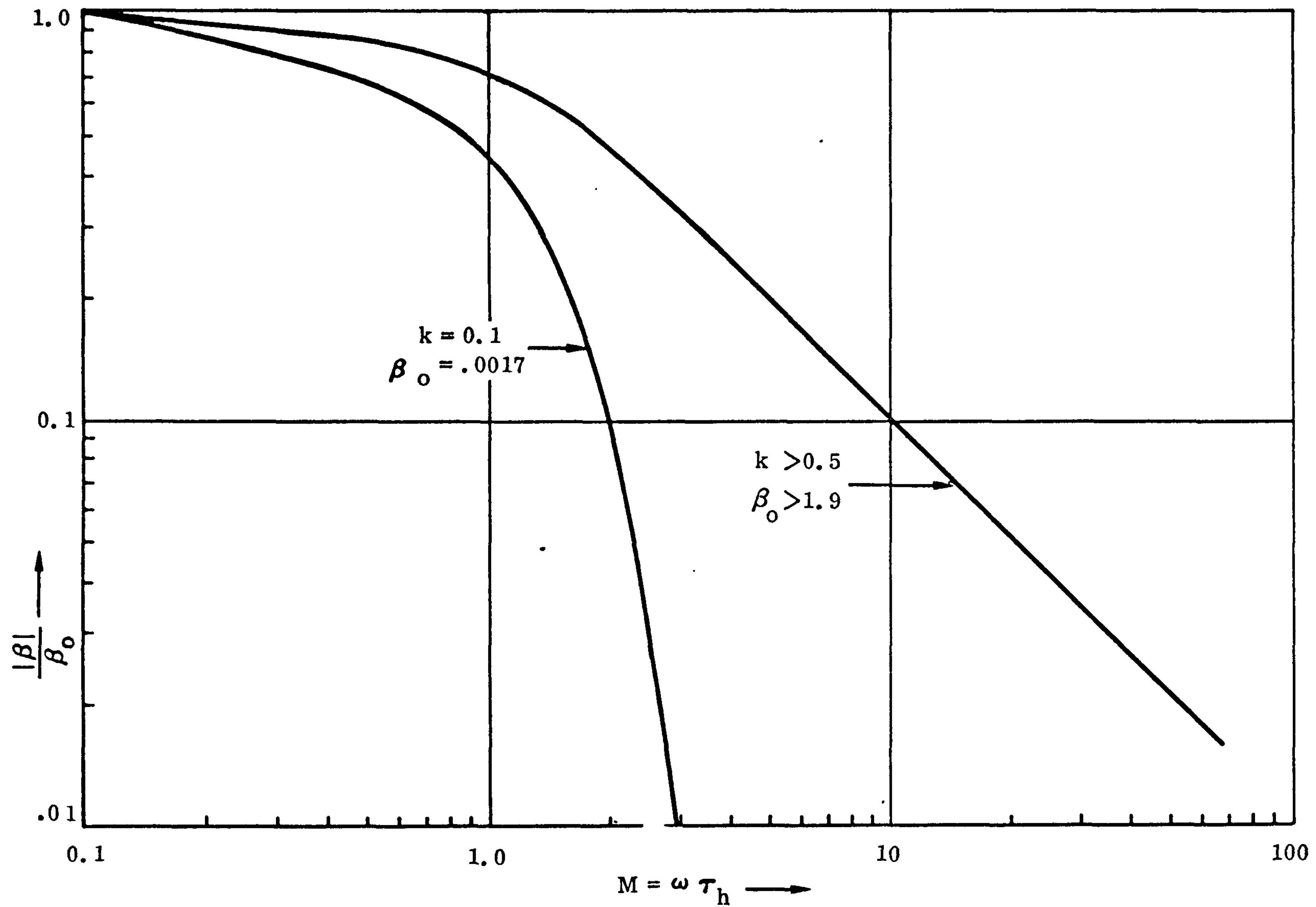

Figure 7B. Plot of $|\beta|/\beta_o$ for a Drift Transistor ($\eta = 8$)

Experimentally-measured values of ω_T for various transistors in the normal mode for neutron fluences up to 10^{14} n/cm^2 do not show any significant variation from the preirradiated value.

CURRENT DEPENDENCE OF DAMAGE CONSTANT

The measured damage constant, K, is strongly dependent upon the emitter current density flowing in the transistor during measurement. This dependence arises since the lifetime of a minority carrier depends upon the injection level. The lifetime deterioration under neutron irradiation arises because of the increase in recombination centers due to displacement damage. Shockley and Read[3] derived an expression for the lifetime in the presence of one recombination center. However, it is known[4] that several recombination centers are produced typically under neutron irradiation. Messenger[5] proposed a two-level model in which all the recombination centers in the upper half of the band gap are lumped into one recombination level and all the centers in the lower half are lumped into a second level. Assuming the two levels to be acting independently, the reciprocal lifetime due to both centers can be added to yield a reciprocal of damage constant, K, as

$$\frac{1}{K} = \frac{n_o + p_o + \Delta p}{\dfrac{(p_o + p_1 + \Delta p)}{r_{c_1} R_1} + \dfrac{(n_o + n_1 + \Delta p)}{r_{v_1} R_1}} + \frac{n_o + p_o + \Delta p}{\dfrac{(p_o + p_2 + \Delta p)}{r_{c_2} R_2} + \dfrac{(n_o + n_2 + \Delta p)}{r_{v_2} R_2}} \quad (25)$$

where R_1 and R_2 are the recombination centers produced per unit neutron fluence at levels 1 and 2, respectively, r_c and r_v with appropriate subscripts are the recombination rate constants, Δp is the excess carrier density, n_o and p_o are the carrier densities in thermal equilibrium and n_1 and p_1 and n_2 and p_2 are the concentrations of electrons and holes if the Fermi level were to be at levels 1 and 2 respectively. The expression for K can be rearranged as

$$\frac{1}{K} = \frac{C_1 \Delta p^2 + C_2 \Delta p + C_3}{C_4 \Delta p^2 + C_5 \Delta p + C_6} . \quad (26)$$

These coefficients, C_1 through C_6, are related to the various parameters of Equation (25). For example,

$$C_1 = \frac{1}{r_{c2}R_2} + \frac{1}{r_{v2}R_2} + \frac{1}{r_{c1}R_1} + \frac{1}{r_{c2}R_2} .$$

The expressions for the constants. C_1 through C_6. can be simplified appreciably if the facts that the base region is extrinsic and that level 1 is above the intrinsic Fermi level, and level 2 is below the intrinsic Fermi level are considered. From Equation (26), we see that $1/K$ is a function of the injected carrier density, Δp. Under low level injection,

$$\Delta p_o = \frac{I_h W}{eA\ D_h}$$

for a homogeneous transistor, where Δp_o = excess carrier density at $x = 0$ (at the boundary of emitter junction) at low injection. For brevity, let us write $\Delta p_o = \delta\ I_h$, where $\delta = w/eA\ D_h$. Under high injection, the excess carrier density at $x = 0$ is no longer equal to $\delta\ I_h$, but an empirical relation of the following form is approximately valid:

$$\Delta p_{Eo} = \Delta p_o \frac{1 + \theta \dfrac{\Delta p_o}{N_{DE}}}{1 + 2\theta \dfrac{\Delta p_o}{N_{DE}}}, \tag{27}$$

where

θ = constant approximately equal to 0.3 for homogeneous transistor

N_{DE} = donor density in the base region, and

Δp_{EO} = excess carrier density at $x = 0$ for any level of injection.

Equation (27) can be written in terms of I_h as

$$\Delta p_{EO} = \frac{\dfrac{\delta^2 I_h^2 \theta}{N_{DE}} + \delta\ I_h}{\dfrac{2\delta\ I_h\ \theta}{N_{DE}} + 1}. \tag{28}$$

Although Equation (28) gives the relationship between the excess carrier density at $x = 0$ and the emitter current, it is reasonable to assume that the excess carrier density to be used in Equation (26) can be approximated by a similar functional relationship as

$$\Delta p = \frac{M_1\ J_E^2 + M_2\ J_E}{M_3\ J_E + 1}, \tag{29}$$

where J_E is the emitter current density in amps/cm2. Substituting Equation (29) in Equation (26), multiplying both numerator and denominator by $(M_3 J_E + 1)^2$ and rearranging terms, we obtain

$$K = \frac{AJ_E^4 + BJ_E^3 + CJ_E^2 + DJ_E + H_1}{J_E^4 + EJ_E^3 + FJ_E^2 + GJ_E + H_2} \quad . \tag{30}$$

The constants in Equation (30) can be obtained by fitting the experimentally-obtained plot of K vs J_E. For this purpose, the curve given in Larin[6] for the measured composite damage constant, 1/K, for 20 n-p-n transistors as a function of emitter current density was taken and plotted in Figure 8. The ratio of the constants, H_1/H_2, was obtained by plotting K vs J_E on a linear graph and extrapolating the linear value for $J_E = 0$ to obtain $H_1/H_2 \approx 0.15$. Then H_2 was set equal to 1 and $H_1 = 0.15$. Seven points were chosen on the measured curve and seven simultaneous equations were set up. The seven constants, A through G, were then obtained by solving these simultaneous equations. The values of the constants are:

A = 1.68

B = 332

C = 2850

D = 420

E = 313

F = 6280

G = 3410

Using these constants, values of K were calculated for other points on the curve and it was found that the error was less than 3 percent. It may be questioned why the coefficient of J_E^4 was set equal to unity while H_2 also was set equal to unity in the denominator in Equation (30). The correct procedure would have been to introduce one more constant but it should be noticed in the range of J_E plotted in Figure 8, K is not very sensitive to H_1/H_2 and as such to reduce labor, H_2 was taken as unity. As a matter of fact, H_1 and H_2 each can be even set equal to zero and the resulting expression for K will be a cubic in I_E divided by a cubic in I_E, as given below

$$K = \frac{AJ_E^3 + BJ_E^2 + CJ_E + D}{J_E^3 + EJ_E^2 + FJ_E + G} \quad . \tag{31}$$

This expression also gives a good agreement with the experimental curve.

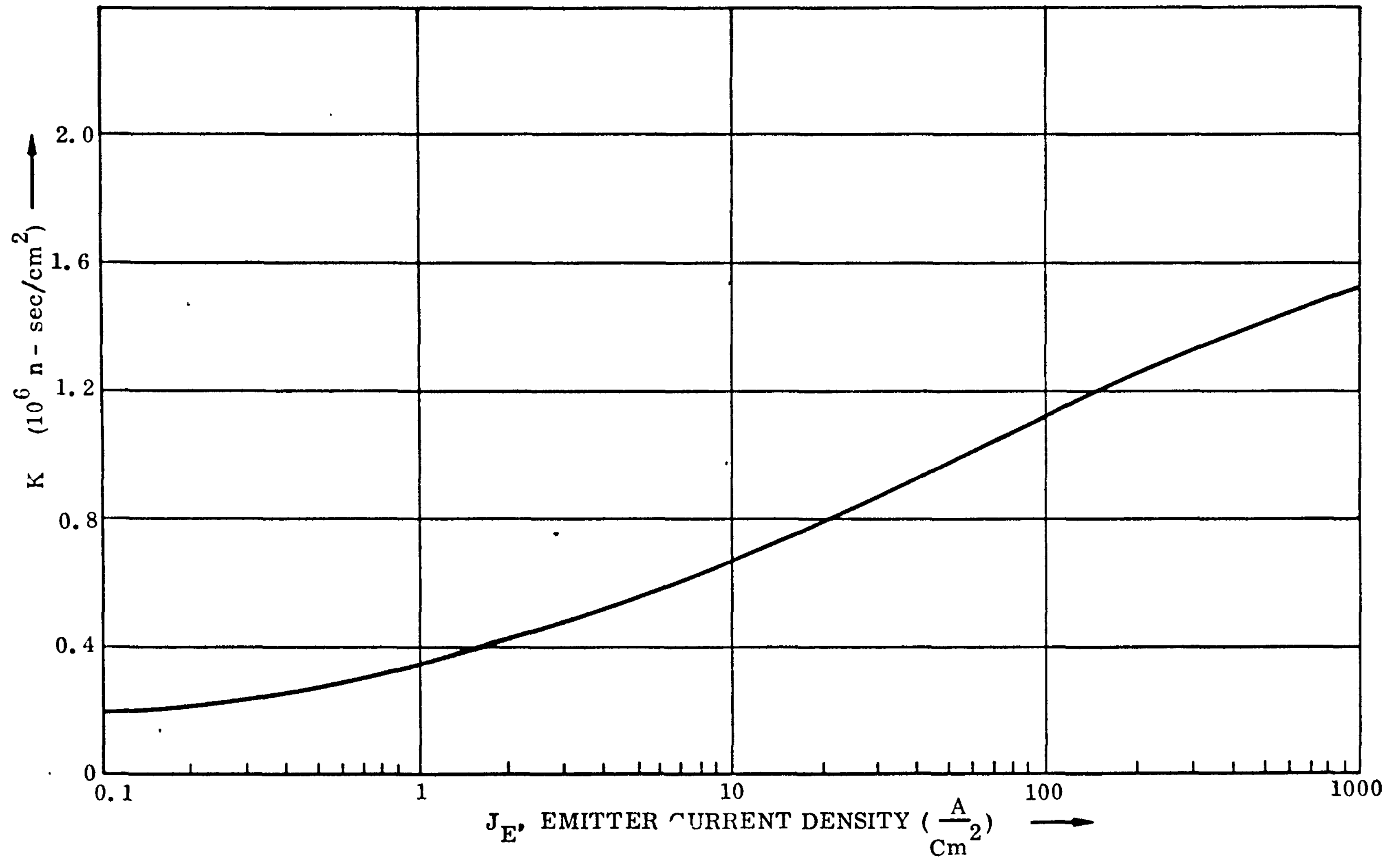

Figure 8. Plot of Measured k

CONCLUSION

In the above discussions, an exact expression has been derived for the damage constant and it is approximated by a simpler expression over the range of neutron fluence where the transistor is still a useful device. Effect of neutron irradiation on base transit time, minority carrier distribution, and gain-bandwidth product are discussed.

The base transit time in a drift transistor is shown to be the same as the pre-irradiated value, over the range of neutron fluence where the transistor is still a useful device. However, in homogeneous transistors and in the inverse mode operation of drift transistors, the base transit time is reduced even over the useful range of the device. The gain bandwidth product is shown to be essentially constant unless the device is damaged beyond its useful range. Finally, the emitter current dependence of the damage constant is obtained by fitting an empirical relationship to an experimental curve.

REFERENCES

1. Messenger, G. C., IEEE Proc, 55, 413 (1967).
2. Lindmayer, J. and Wrigley, C. Y., Fundamentals of Semiconductor Devices, p 143. Van Nostrand Co.
3. Shockley, W. and Read, W. J., Phys. Rev. 87, 835 (1952).
4. Konopleva, R. F., et al, Soviet Phys. Solid State 8, 264 (1966).
5. Messenger, G. C., IEEE Trans. on Nuclr. Sc., NS-14 (1967).
6. Larin, F., Radiation Effects in Semiconductor Devices p 161, John Wiley and Sons.

RADIATION EFFECTS ON SEMICONDUCTOR DEVICES

15 August 1968

by

George C. Messenger

Prepared for UCLA Short Course
Radiation Effects on Semiconductors

Autonetics Division of North American Rockwell Corporation
3370 Miraloma Avenue, Anaheim, California 92803

CONTENTS

	Page
Introduction	1
Basic Semiconductor Effects	2
Characterization of Transistors in a Neutron Environment	3
Surface Recombination Velocity	6
Recombination in the Base Emitter Field Region	6
Emitter Efficiency	6
High Injection Levels	7
Current Gain Cut-Off Frequency	7
Displacement Damage Process	7
Dependence on Incident Neutron Energy	9
Dependence of Damage Constant on Resistivity and Injection Level	11
Silicon	12
Germanium	13
References	18
Recommended Supplementary Reading	19
Appendix 1. "Statistical Modeling of Semiconductor Devices for the TREE Environment"	1-1
Appendix 2. "A Two Level Model for Lifetime Reduction Processes in Neutron Irradiation Silicon and Germanium	2-1
Appendix 3. "Radiation Effects on Microcircuits"	3-1

ILLUSTRATIONS

Figure		Page
1	F(n) as a Function of k	5
2	A Plot of $1/f_t$ vs the Inverse of the Emitter Current	8
3	Energy Going into Atomic Processes and Normalized Reciprocal Lifetime Damage Constant as a Function of Incident Neutron Energy	10
4	Silicon Lifetime Damage Constants K_n and K_p as a Function of Reciprocal Temperatures for Various Values of Resistivity and Injection Level, $x = \frac{\delta n}{n_o}$	14
5	Lifetime Damage Constant as a Function of Base Resistivity for Germanium pnp Transistors	15
6	Damage Constant vs Injection Ratio for Solar Cells	17

TABLES

Number		Page
1	Functions of the Conductance Matrix Elements Applicable to Both Homogeneous Base and Graded Base Transistors	5
2	Particle-Type Displacement Equivalences, $\Delta(h_{FE}^{-1})$	11

RADIATION EFFECTS ON SEMICONDUCTOR DEVICES

INTRODUCTION

Numerous transistor applications involve actual or potential exposure to a fast neutron environment. The use of transistors in reactor control circuits - especially in the space program - involves continuous exposure to a low flux rate of fast neutrons; over an extended mission, the neutron fluence will degrade transistor performance. Modern military systems designers must consider the neutron pulse from a nuclear weapon, and specifications defining transistor vulnerability to neutron fluence must also be considered. Solar cell applications in space systems also involve exposure to damaging electron and proton radiation. Furthermore, if the vehicle skin is very thin, transistors within the system are also exposed to proton and electron radiation.

Lifetime degradation is the dominant failure mechanism found in almost every design problem. It causes a decrease in power output in solar cells; in transistors, it decreases the common emitter current gain. Other effects, such as decreased storage time or output impedance, can usually be expressed in terms of decreased current gain or related directly to lifetime degradation.

There are several secondary radiation effects which may cause device changes. These include increases in surface charge density resulting from ionizing radiation, changes in majority carrier density, and decreases in carrier mobility. Radiation effects on semiconductor devices are best explained by obtaining general admittance matrix equations containing all of the basic semiconductor properties which undergo changes in the radiation environment. The functional dependence of the semi-conductor properties on radiation is then added, resulting in a radiation-dependant matrix equation. The admittance matrix is derived under ordinary operating conditions. When required, however, modifications may be introduced to compensate for extraordinary conditions such as very high or very low operating current levels.

It is necessary to obtain the functional dependence of basic semiconductor properties on radiation fluence. Neutron effects are very different from both proton and electron effects due to the uncharged nature of the neutron compared to the charged nature of protons and electrons. Neutrons undergo hard sphere scattering, whereas charged particles undergo Rutherford scattering. Electron and proton effects also differ greatly due to the difference in mass. Radiation effects are also dependent upon the energy of the incident radiation.

Fast neutrons create cluster defects in semiconductor material. The defects thus produced in transistor bases act as recombination centers, by reducing minority carrier lifetime (in the base region), and, consequently, by reducing transistor current gain. The cluster defect is a small volume of semiconductor material containing several hundred atoms which have been displaced from their proper lattice sites as a result of the collision process. Following the collision process, the cluster rapidly assumes a quasi-equilibrium state. Short term annealing is associated with this process, which lasts less than a second. However, further annealing of transistors may be effected by storing them at elevated temperatures.

The amount of damage produced above the damage threshold increases with the energy of the incident neutrons, linearly at low incident neutron energies, then shows a saturating characteristic at incident neutron energies above 1 MeV. The environment usually encountered is a moderated fission spectrum. For purposes of standardization, the data in this lecture have been normalized to a reactor spectrum of average energy of 1.6 MeV; only neutrons with energy greater than 10 keV are counted.

The effectiveness of recombination centers associated with cluster defects depends upon the position of the Fermi level. This behavior may be quantitatively described by using Hall-Schockley Read statistics, resulting in dependence of transistor current gain degradation on base resistivity, injection level, and temperature.

BASIC SEMICONDUCTOR EFFECTS

The dependence of basic semiconductor properties upon radiation fluence is a necessary building block for understanding device behavior in radiation environments. The most important property is minority carrier lifetime, followed by majority carrier density, majority carrier mobility, and three interrelated surface properties; (a) surface charge density, (b) surface potential and, (c) surface recombination velocity.

The basic factor for relating minority carrier lifetime, τ, to radiation fluence, Φ, is:[1]

$$\frac{1}{\tau} = \frac{1}{\tau_i} + \frac{\Phi}{K(\rho_o, E_n)} \tag{1}$$

Where K is the lifetime damage constant which has the properties of a radiation lifetime,* K is a function of the energy and type of radiation, the base resistance and injection level of the semiconductor, and, to some extent, the impurities in the semiconductor. This relationship has been found to apply accurately from $10^9 n/cm^2$ to $10^{16} n/cm^2$.

Majority carrier density is related to radiation fluence as follows[2]:

$$n = n_o \pm \Phi \frac{dn}{d\Phi} \tag{2}$$

Values for $dn/d\Phi$ depend upon base resistance and type and energy of incident radiation.

For silicon, both n- and p-types tend toward intrinsic resistivity with increasing fluence; germanium tends toward low-resistivity p-type.

Carrier mobility decreases with the introduction of defects in that they act as scattering centers. Cluster defects remove a volume of semiconductors, which contain the cores of the cluster and the surrounding field region from the conduction path, thereby causing an effective decrease in mobility. Mobility can be characterized by[2]:

$$\mu = \mu_o - \Phi d\mu/d\phi \tag{3}$$

*Some experimenters use $1/\tau = 1/\tau_i + \alpha\Phi$ and speak of α as a damage constant.

All forms of radiation contribute to ionization processes. One effect of ionization is an increase in surface charge density[3]. This is a non-linear effect which saturates at values of fluence substantially lower than those which cause bulk effects. The resulting change in surface potential causes either an increase or decrease in surface recombination velocity[4].

CHARACTERIZATION OF TRANSISTORS IN A NEUTRON ENVIRONMENT

Transistor operation is described in terms of an admittance matrix, including all semiconductor properties subject to change in the neutron environment in admittance matrix elements. A number of basic semiconductor properties such as carrier densities, carrier mobilities, and carrier lifetime are changed by neutron irradiation. However, minority carrier lifetime degradation in the base region is the dominant mechanism, and this degradation is principally determined by cluster defects in the bulk base material; changes in surface recombination velocity are relatively unimportant. Another factor which sometimes becomes noticeable in very high frequency transistors is a decrease in emitter efficiency due to minority carrier degradation in the emitter region.

The small signal, low frequency admittance matrix will be accurately developed for the intrinsic transistor[5]. Various extensions, including very low and very high injection levels, will then be developed. Precautions necessary in using current gain cut-off frequency to determine the ratio of diffusion constant to the square of the base width will also be discussed.

At low frequencies the intrinsic transistor is described by:

$$\begin{aligned} I_E &= a_{11}\,\psi_E - a_{12}\,\psi_C \\ I_C &= -a_{21}\,\psi_E + a_{22}\,\psi_C \end{aligned} \qquad (4)$$

where

$$\psi_{E,C} = e^{\frac{qV_{E,C}}{kT}} - 1$$

$I_{E,C}$ are emitter and collector currents, $V_{E,C}$ are emitter and collector voltages, and the a's are admittance matrix parameters. The matrix parameters are shown in Table 1.

In Table 1,

$$\sigma = 1/2\sqrt{\left(\frac{n}{W}\right)^2 + \left(\frac{4}{L_p}\right)^2}, \quad k = \frac{N_{DE}}{N_{DC}},$$

$$n = \ln k, \quad L_p = \sqrt{D_p \tau},$$

W is transistor base width, N_{DE} is donor density in the base near the emitter, N_{DC} is donor density in the base near the collector, L_p is hole diffusion length in the base, D_p is hole diffusion constant in the base, and τ is lifetime in the base.

Current gain $a = -\frac{a_{21}}{a_{11}} = \frac{\beta}{1+\beta}$. Using the expressions in Table 1, an expression for $1/\beta$ can be obtained,

$$\frac{1}{\beta} = \left[\frac{1}{\sqrt{k}}\left(1+\frac{n^2}{8}+\frac{W^2}{2L_p^2}\right) + \frac{n}{2\sqrt{k}}\left(1+\frac{n^2}{24}+\frac{W^2}{6L_p^2}\right)\right] - 1 \tag{5}$$

This expression applies for homogeneous base transistors ($k = 1$, $n = 0$) and graded base transistors ($k \approx 10$, $n \approx 2.3$).

For a transistor whose base lifetime has been substantially degraded by displacement damage, $\tau = K/\Phi$, where K is lifetime damage constant and Φ is radiation fluence. Now,

$$\frac{\beta^{-1} - \beta_i^{-1}}{\Phi} = \left(\frac{W^2}{2D_pK}\right)\left(\frac{1}{\sqrt{k}} + \frac{n}{6\sqrt{k}}\right) \tag{6}$$

Usually, $W^2/2D_p$ is calculated using a measured value of current gain cut-off frequency, f_a. An expression[7] applicable to both homogeneous and graded base transistors is:

$$\frac{W^2}{2D_p} = \frac{0.2\left[1+\left(\frac{n}{2}\right)^{\frac{4}{3}}\right]}{f_a} \tag{7}$$

Therefore, for both homogeneous and graded base transistors, lifetime damage constant is given by:

$$K = \frac{0.2\left(\frac{1}{\sqrt{k}} + \frac{n}{6\sqrt{k}}\right)\left[1+\left(\frac{n}{2}\right)^{\frac{4}{3}}\right]\Phi}{f_a\left(\beta^{-1} - \beta_i^{-1}\right)} = \frac{0.2\ F(n)\Phi}{f_a\left(\beta^{-1} - \beta_i^{-1}\right)} \tag{8}$$

The function, F(n), is unity for homogeneous base transistors, as expected. The variation of F(n) with K is shown in Figure 1. Notice that F(n) is approximately unity for values of k up to 10 and has only dropped to 0.72 for k = 100.

Table 1. Functions of the Conductance Matrix Elements Applicable to Both Homogeneous Base and Graded Base Transistors

Matrix Element Function	Exact Form	Approximate Form
$\frac{a_{11}}{AD_p q\, p_n^o}$	$\sigma \coth \sigma W + \frac{n}{2W}$	$\frac{1 + \frac{W^2}{2L_p^2} + \frac{n}{2} + \frac{n^2}{8}}{W}$
$\frac{a_{12}}{AD_p q\, P_n^W}$	$\frac{\sigma \operatorname{csch} \sigma W}{\sqrt{k}}$	$\frac{1}{w\sqrt{k}}\left(1 + \frac{W^2}{6L_p^2} + \frac{n^2}{24}\right)$
$\frac{a_{21}}{AD_p q\, P_n^o}$	$\sqrt{k}\, \sigma \operatorname{csch} \sigma W$	$\frac{\sqrt{k}}{w}\left(1 + \frac{W^2}{6L_p^2} + \frac{n^2}{24}\right)$
$\frac{a_{22}}{AD_p q\, P_n^W}$	$\sigma \coth \sigma W - \frac{n}{2W}$	$\frac{1 + \frac{W^2}{2L_p^2} - \frac{n}{2} + \frac{n^2}{8}}{W}$

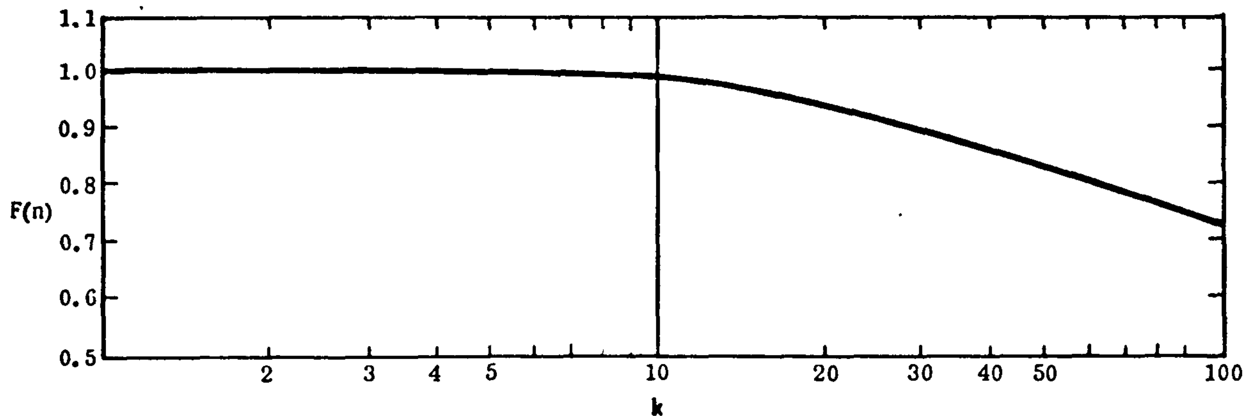

Figure 1. F(n) as a Function of k

The dependence of transistor parameters upon radiation flux has been quantitatively expressed in terms of a damage constant, K, by replacing base lifetime by K/ϕ in the parameters of the admittance matrix. The dependence of K upon neutron energy spectrum, base resistivity, injection level, and temperature will be developed. First, however, several extensions of the admittance matrix should be discussed.

SURFACE RECOMBINATION VELOCITY

It is possible for a small percentage of minority carriers, injected into the base, to return to the surface around the emitter periphery. This surface recombination current is proportional to surface recombination velocity and provides a contribution to $1/\beta$ approximated by the following expression:

$$1/\beta_s = \frac{SWAs}{2D_pA_e\ (1 + n)} \tag{9}$$

In the radiation environment, small but measurable changes may take place in surface recombination velocity at lower values of flux than those required to cause the onset of current gain reduction due to bulk processes. Such changes have been observed in both directions and cause both anomalous increases and decreases of current gain preceding the normal degradation in current gain[7]. Most transistors do not exhibit this effect. Even in susceptible transistors, the effect is usually small in the neutron environment. The resulting effect is much more important in the space environment.where the radiation environment is protons and electrons. This effect is caused by an increase in surface change density resulting from ionizing radiation and is not a displacement effect.

RECOMBINATION IN THE BASE EMITTER FIELD REGION

At very low values of emitter current, recombination centers in the base emitter field region are very effective, resulting in a contribution to $1/\beta$; however, this correction $1/\beta R_F$, is inversely proportional to the square root of emitter current and, therefore, decreases rapidly in importance as the emitter bias current is increased. The level of emitter current at which this effect ceases to be of importance varies greatly from transistor to transistor. It is an effect exclusively associated with silicon and is nearly always present in the microampere range while almost never present in the milliampere range. There is relatively little known about the effect of radiation on this recombination process.

EMITTER EFFICIENCY

For some transistor structures, the majority carrier current in the base depends upon minority carrier lifetime in the emitter. A reduction of emitter region minority carrier lifetime will cause increased majority carrier current flow across the base emitter junction which is equivalent to a reduction in emitter efficiency. This effect is probably limited to very high frequency germanium transistors in which it causes some additional current gain degradation[8].

HIGH INJECTION LEVELS

At very high values of emitter current, base conductivity increases in order to maintain charge neutrality. This condition causes a proportional reduction in emitter efficiency. In graded base transistors, conductivity modulation reduces the effectiveness of the built-in field.

Further, a transverse field, due to the base current, usually appears in the base region, and is accompanied by non-uniform current density through the emitter. A general modification to include these effects in the admittance matrix has not been accomplished, although several good approximations have been made. It will be shown later that high-injection levels minimize radiation-induced current gain degradation; however, this effect saturates with increasing injection level, and most of the benefit is obtained if the transistor is operated at injection ratios from one to three.

CURRENT GAIN CUT-OFF FREQUENCY

In Equation 4, $W^2/2D_p$ of the intrinsic transistor was expressed as a function of the current gain cut-off frequency of the intrinsic transistor. In a practical measurement technique, the cut-off frequency of the transistor, including input and output time constant, is measured. Furthermore, it is common practice to measure the current gain bandwidth product, f_t. Therefore, the required process is one which measures the intrinsic f_t by correcting for the effect of the input and output time constants. Next, with the intrinsic f_t known, a relationship is necessary to obtain the intrinsic f_a. Gain bandwidth product is first measured as a function of emitter bias current[6], then the plot of $1/f_t$ vs $1/I_E$ is constructed, resulting in a straight line; the extrapolation to infinite current yields the intrinsic value of $1/f_t$, as shown in Figure 2.

The relationship between f_t and f_a is rather complex, but it is a slowly varying function of the field in the base region.

$$f_t = a_o K_\theta f_a \tag{10}$$

K_θ varies from 0.6 for steeply graded transistors to 0.87 for homogeneous base transistors and up to 0.95 for some transistors containing a retarding field.

DISPLACEMENT DAMAGE PROCESS

The defect structure in a lattice disordered by high energy radiation may be very complex[9]. The initiating collision between the incident radiation and the lattice atom results in Frenkel defects. Subsequently, diffusion of interstitials and vacancies occurs to form defects which are stable at room temperature. The resulting defect scheme will depend upon many factors, including (a) the type of incident radiation and its energy spectrum, (b) the characteristics of the semiconductor lattice, including dopants, dislocations, and trace impurities, and (c) the temperature at which the irradiation takes place.

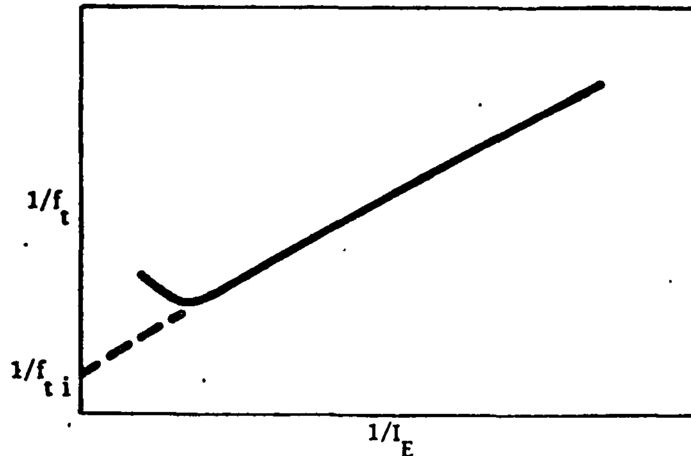

Figure 2. A Plot of $1/f_t$ vs the Inverse of the Emitter Current Results in a Straight Line at Low Currents (Extrapolation to Infinite Current Yields Reciprocal of Intrinsic Current Gain Bandwidth Product)

Electrons and protons undergo Rutherford scattering in semiconductors. This process is characterized by a relatively small average energy imparted to the atoms in the lattice. Thus, the first stage of the damage process is a uniform distribution of simple Frenkel defects. Subsequent vacancy diffusion results in formation of recombination centers which has been well documented in silicon by electron paramagnetic resonance studies(10) and had been extended to germanium, partly by analogy, and partly by other experiments(10). When the vacancy interacts with an oxgyen impurity atom in silicon, the A center is formed. It lies 0.18 eV below the conduction band and is a very effective recombination center. The vacancy may also interact with a donor atom, such as arsenic or phosphorous, thus producing the E center. This interaction has been observed 0.40 eV below the conduction band in oxygen-free silicon, and is also an effective recombination center. Vacancies may pair up, forming divacancies, which produces a recombination level 0.30 eV above the valence band.

Neutrons undergo hard sphere scattering in semiconductors resulting in a relatively large value of average energy imparted to the primary atom, $\bar{E}p = Epmax/2$. This atom then collides with neighboring atoms in a cascade process until all of the atoms involved are reduced to energies below the displacement threshold. The mean free path of the high energy lattice atoms is small so that all of this energy is released in a small volume of the crystal lattice. Since several hundred atoms are usually involved, a damage cluster is created. The cluster contains a large number of vacancies in its core and is initially surrounded by a large number of interstitials. Some annealing of the initial damage occurs almost immediately at room temperature and the cluster assumes a stable form. Some of the vacancies diffuse away from the cluster and form point defects of the variety produced by electrons and protons.

Experimental evidence indicates that the clusters act as recombination centers and dominate the recombination process at room temperature. Annealing at higher temperatures increases the importance of the point defects peripheral to the cluster at the expense of the cluster.

The cluster contains many levels in the forbidden band, some of which should act as effective recombination centers. The effect of the cluster, acting as a recombination center, can be approximated by two "average" recombination levels, one in the upper and the other in the lower half of the band.

In addition to introducing recombination centers, neutron radiation also introduces trapping centers. These centers remove majority carriers so that the resistivity of both n- and p-type silicon increases toward intrinsic, with increasing neutron fluence. The effect on resistance is quite different in germanium; both n- and p-type germanium tends toward low-resistivity p-type as neutron fluence increases.

DEPENDENCE ON INCIDENT NEUTRON ENERGY

At very low incident neutron energies, the energy transferred to a lattice atom is insufficient to cause displacement. Above ~200 eV, ~30 eV can be imparted to the silicon atom and a displacement will result. As the incident neutron energy increases from about 200 eV to 1 MeV, the amount of displacement damage increases linearly. For incident neutron energies above 1 MeV, the initial displaced atom has so much energy that a rapidly increasing amount is dissipated in producing ionization rather than atomic displacements. The amount of displacement damage, reflected by recombination measurements, increases by a factor of ~3 as incident neutron energy from ~1 MeV to 14 MeV.

Figure 3 shows the energy going into atomic processes, which results in lifetime degradation as a function of incident neutron energy for silicon. The irregular curve accurately reflects various neutron resonances; the smoothed curve follows the relationship.

$$\sigma = aE_n(1 - e^{-A/E_n}) \qquad \begin{aligned} a &= 1.02/\text{MeV} \\ A &= 3.1/\text{MeV} \end{aligned} \tag{11}$$

and is more suitable for analytical work with various neutron spectra. Here, En is incident neutron energy and $\sigma = K^{-1}$ is the reciprocal of lifetime damage constant. The damage constant, K, can be determined for any spectrum in the normal range of interest, $0 < En < 15$ MeV, by an integration process,

$$K^{-1} = \sigma = \frac{\int_{0.01\ \text{MeV}}^{\infty} \sigma(E)N(E)dE}{\int_{0.01\ \text{MeV}}^{\infty} N(E)dE} \tag{12}$$

Damage constant is normally reported for a standard reactor spectrum of average energy, ~1.6 MeV, counting all neutrons with energy greater than 10 keV (fast neutrons). Equation (9) may be used to accurately assess the relative damage of different neutron spectra on silicon. Experimental results for germanium. based on carrier removal, suggest that displacement damage increases linearly with neutron energy up to ~0.5 MeV, and then begins to saturate. For germanium, 14-MeV neutrons are ~1.5 times more effective than 1-MeV neutrons[9].

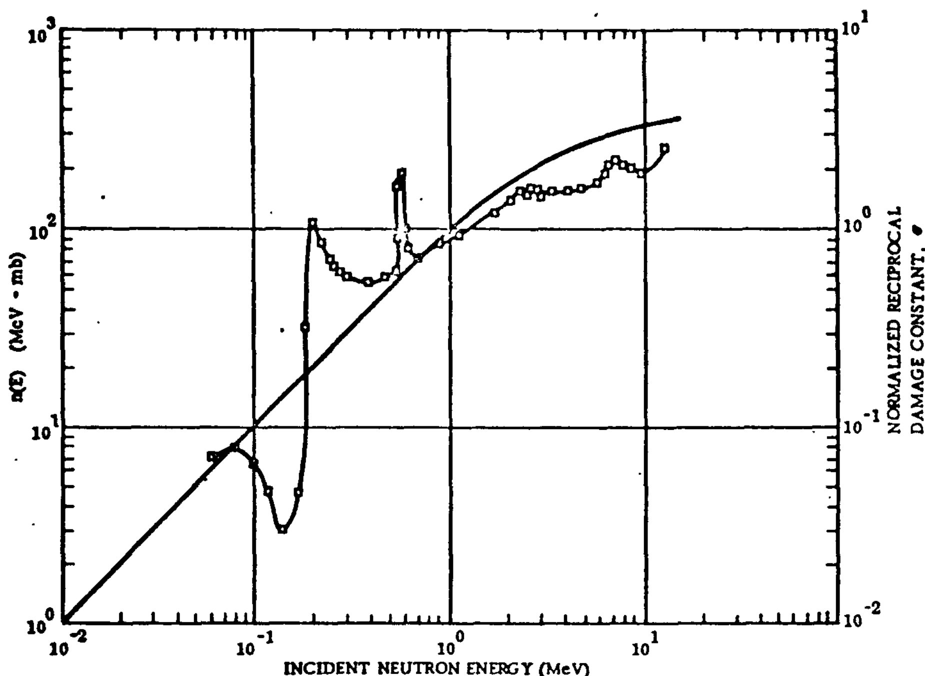

Figure 3. Energy Going into Atomic Processes and Normalized Reciprocal Lifetime Damage Constant as a Function of Incident Neutron Energy

Protons are charged particles having approximately the same mass as neutrons. They undergo Rutherford scattering in the silicon lattice, resulting in a relatively small average energy imparted to the target atom. Ep = Ed ln Epmax/Ed. The resulting defects are substantially all point defects, although on rare occasions, some cluster-type defects may be found. The lower energy ranges (<1 MeV) are screened out by the device package; the higher energy ranges become relatively unimportant due to the I/E dependence of the differential cross section. Furthermore, in the space environment, the number of protons/MeV decreases rapidly with increasing energy. This combination of factors makes the one-to-ten-MeV range of maximum practical importance for semiconductor devices.

Electrons are extremely light, charged particles and must attain relativistic velocities in order to produce displacement damage. Consequently, the differential cross section becomes relatively constant at high energies. Again, package shielding, combined with the decreasing number of electrons/MeV at high energies encountered in the space environment, combine to focus attention in the 5-MeV range.

Gamma radiation produces displacements indirectly, usually by generating Compton electrons; therefore, gamma radiation effects may be treated by utilizing the discussion presented for electrons and combining this with the statistics relevant to the Compton scattering process.

Table 2 allows a displacement damage equivalence comparison between various commonly encountered radiations, usually on the basis of change in reciprocal grounded emitter current gain[12].

Table 2. Particle-Type Displacement Equivalences, $\Delta(h_{FE}^{-1})$

Particle Type and Energy	Alpha Particle (5 MeV)	Proton (1 MeV)	Neutron (Reactor Spectrum)	Electron (1 MeV)	Gamma Ray (Co^{60})
Alpha Particle (5 MeV)	1	3.5	1.4×10^2	*7×10^3	1.5×10^5
Proton (1 MeV)	2.9×10^{-1}	1	4×10^1	*2×10^3	4.3×10^4
Neutron (Reactor)	7.1×10^{-3}	2.5×10^{-2}	1	*5×10^1	1.1×10^3
Electron (1 MeV)	*1.4×10^{-4}	*5×10^{-4}	*2.0×10^{-2}	1	*2.2×10^1
Gamma Ray (Co^{60})	6.7×10^{-6}	2.3×10^{-5}	9.1×10^{-4}	*4.5×10^{-2}	1

*Transistor caps of 0.17 gm cm^{-2}

DEPENDENCE OF DAMAGE CONSTANT ON RESISTIVITY AND INJECTION LEVEL

Recombination processes in semiconductor increase linearly with neutron fluence over a very wide range in semiconductors; therefore, the following basic relationship is generally applicable to transistors.

$$\frac{1}{\tau} = \frac{1}{\tau_i} + \frac{\phi}{K} \tag{13}$$

For a substantially-damaged sample, $\tau = K/\Phi$. The lifetime damage constant, K, has the properties of semiconductor lifetime. When the density of recombination centers is small compared to majority carrier concentration, the following Hall-Schockley-Read statistics apply:

$$\tau = \tau_{P_o}\left(\frac{n_o + n_1 + \delta_n}{n_o + P_o + \delta_n}\right) + \tau_{n_o}\left(\frac{P_o + P_1 + \delta_n}{n_o + P_o + \delta_n}\right) \tag{14}$$

The properties of the recombination center are implicit in τ_{p_o}, the low level hole lifetime, τ_{n_o}, the low level electron lifetime, and n_1 and P_1, the electron and hole density resulting when the Fermi level coincides with the energy level of the recombination center. The effect of semiconductor resistivity is implicit to n_o and P_o, the equilibrium electron and hole concentration. The effects of injection level are included by δ_n ($= \delta_p$), the injected carrier density.

SILICON

The variation of low-level lifetime damage constant with resistivity for both p- and n-type silicon has been carefully measured. There is no dependence upon doping material or oxygen concentration supporting the belief that defect clusters dominate the recombination process. For p-type material, a good fit to the low-level data is obtained by using a level 0.19 eV below the conductance band with $\tau_{n_o} / \tau_{p_o} = 45$ and $RC_{p_o} = 1.8 \times 10^{-6}$.

Here, RC_{po} is the product of the introduction rate and capture rate of the 0.19 eV level. The explanation of these data in terms of one level is at variance with damage constant vs injection level taken on transistors. The low-level data for n-type silicon cannot be adequately explained by a single level.

If one assumes that two levels are operating simultaneously in an independent fashion, so that reciprocal lifetimes are additive, one obtains

$$\frac{1}{K} = \frac{1}{\frac{1}{C_{p_1} R_1}\left(\frac{n_o + n_1 + \delta_n}{n_o + p_o + \delta_n}\right) + \frac{1}{C_{n_1} R_1}\left(\frac{p_o + p_1 + \delta_n}{n_o + p_o + \delta_n}\right)} + \frac{1}{\frac{1}{C_{p_2} R_2}\left(\frac{n_o + n_2 + \delta_n}{n_o + p_o + \delta_n}\right) + \frac{1}{C_{n_2} R_2}\,\frac{p_o + p_2 + \delta_n}{n_o + p_o + \delta_n}} \tag{15}$$

All of the experimental data can now be fit (within a factor of about two) using the following constants:

$n_1 = 2.0 \times 10^{14}$ cm^3, $R_1 C_{p_1} = 0.37 \times 10^{-6}$ (nvt-sec)$^{-1}$,

$R_1 C_{n_1} = 0.40 \times 10^{-5}$ (nvt-sec)$^{-1}$, $P_2 = 1.3 \times 10^{13}$ cm^{-3},

$R_2 C_{n_2} = 0.76 \times 10^{-6}$ (nvt-sec)$^{-1}$, $R_2 C_{p_2} = 0.68 \times 10^{-5}$

(nvt-sec)$^{-1}$

This implies a level of 0.31 eV below the conductance band and a level 0.35 eV above the valence band.

The complicated nature of the equation precludes easy visualization of the functional dependences. Therefore, a computer run was made varying the parameters over the range of interest for transistors and the results then put in graphical form. Appendix 1, Figure 4, (1-4), shows the variation of K with resistivity and injection level for both p- and n-type silicon. Figure 4 shows the variation of K with temperature for several values of resistivity. Several experimental observations are readily understood from this model. P-type silicon has been found to be more radiation resistant than n-type silicon. The low resistivity, low injection level form of Equation 12 shows

$$K_p = \frac{1}{C_{n_1} R_1 + C_{n_2} R_2} \qquad (16)$$

$$K_n = \frac{1}{C_{p_1} R_1 + C_{n_2} R_2}$$

(Low resistivity low injection level approximation).

Thus, the electron capture cross sections determine the damage constant in p-type material and the hole capture cross sections in n-type material. Although the difference between n- and p-type material becomes smaller as injection level increases, most experimenters have found some differences in favor of p-type material, even at high injection levels. Experimenters determining damage constant from measurements on bulk material have consistently reported much lower values than experimenters working with transistors. Bulk measurements have been made at very low injection ratios whereas transistor measurements have been made at injection ratios ≈ 1. Figure 1-4 shows that damage constant measurements made at an injection ratio of one should be about five times greater than those made at an injection ratio approaching a zero.

GERMANIUM

Most experimenters agree that the recombination center about 0.18 eV below the conduction band dominates recombination processes in neutron-irradiated germanium. Thus, the low level damage constant relationships become

$$K_n = \frac{1}{C_{p_o} R_o}\left(1 + \frac{n_1}{n_o}\right) \qquad (17)$$

$$K_p = \frac{1}{C_{p_o} R_1}\left(\frac{n_1}{p_o} + \frac{\tau_{n_o}}{\tau_{p_o}}\right)$$

Experimental data (13) verifying this general behaviour have been reported and are shown in Figure 5. For transistors having an injection ratio of ≈ 1, assuming $n_1 \approx 4 \times 10^{15}$,

$K_n = 3.3 \times 10^6 \ (1 + 2.3p)$, and $K_p = 3.3 \times 10^6 \ (1 + 1.1p)$.

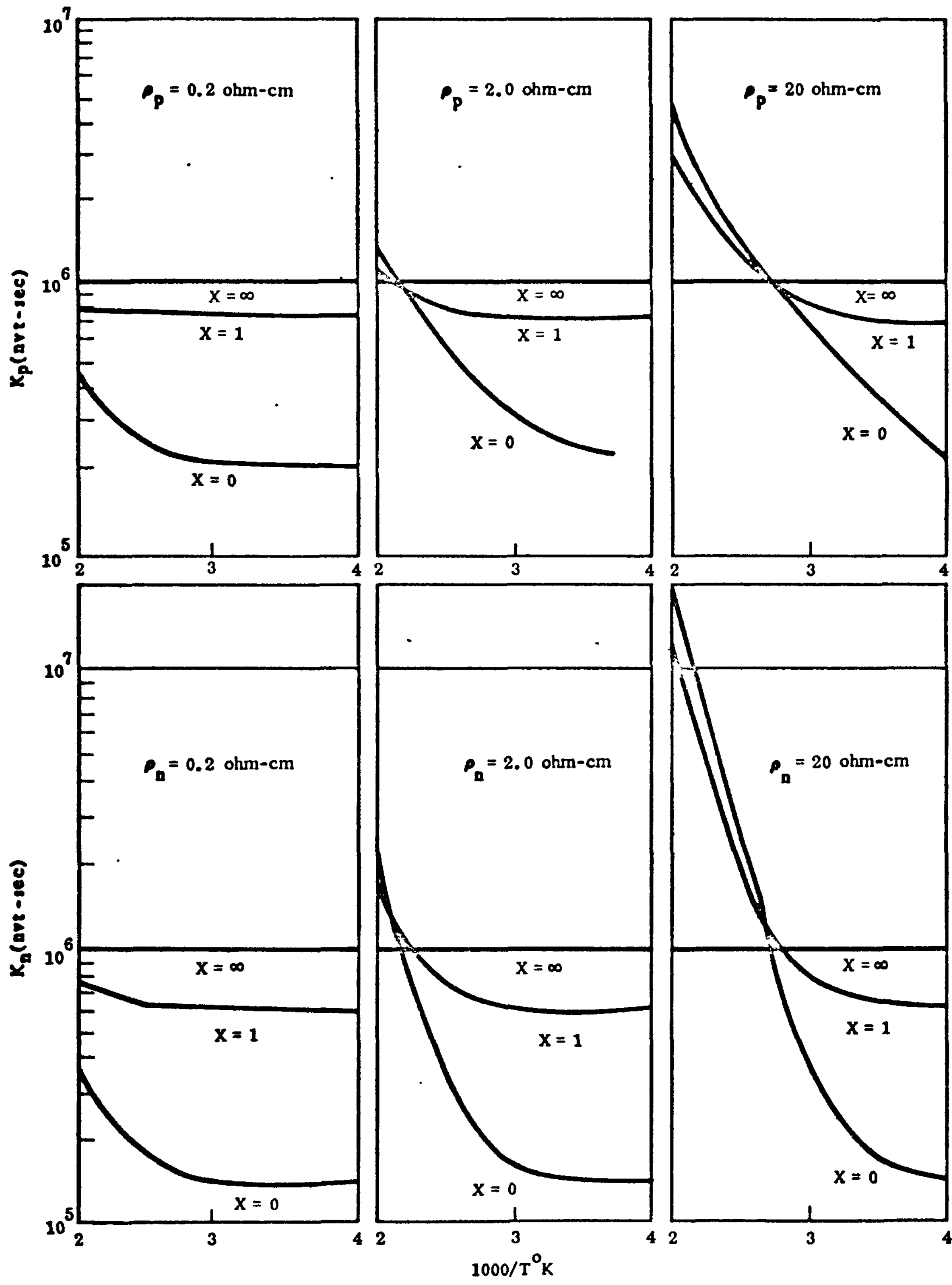

Figure 4. Silicon Lifetime Damage Constants K_n and K_p as a Function of Reciprocal Temperatures for Various Values of Resistivity and Injection Level, $x = \frac{\delta n}{n_o}$

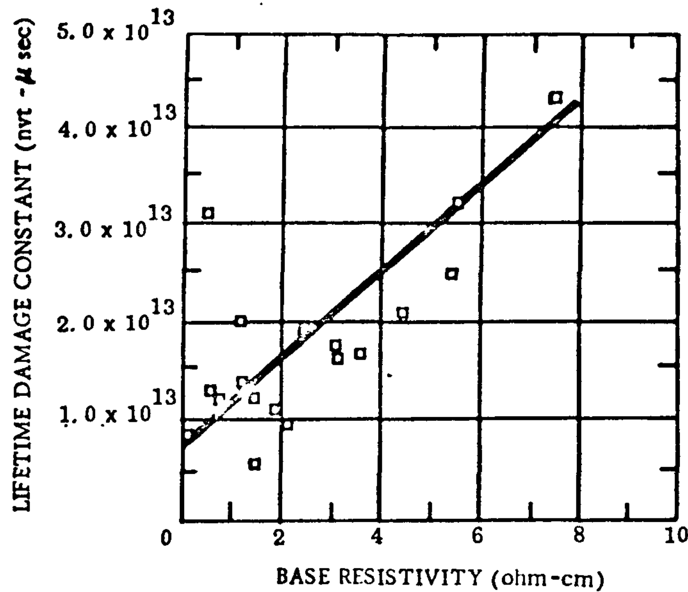

Figure 5. Lifetime Damage Constant as a Function of Base Resistivity for Germanium pnp Transistors

It has also been shown that a mid-band level is important at very low injection levels on the basis of injection level measurements on n-type material[14]. Equation 17, therefore, will not extend to variations with injection level. A model encompassing all of the data can be formulated on a two-level basis. The appropriate constants are:

$$n_1 = 5.0 \times 10^{14}, \; P_2 = 5.0 \times 10^{13}$$

$$C_{p1}R_1 = 4. \times 10^{-8}, \; C_{n1}R_1 = 35 \times 10^{-8}$$

$$C_{p2}R_2 = 92 \times 10^{-8}, \; C_{n2}R_2 = 0.92 \times 10^{-8}$$

These constants may be substituted directly into Equation 15 and the variation of K with resistivity, injection level, and temperature then results.

It is instructive to review some experimental data to appreciate the practical implication of the previous discussions. The Motorola MC 201 Gate has been thoroughly evaluated in a fast neutron environment. Grounded emitter current gain degradation is the dominant effect; characterized by a damage constant of approximately 1.4×10^6 n sec/cm and a grounded emitter current gain cut-off frequency of

approximately 7 megahertz. Appendix 2, Figure 4, (2-4) shows the equivalent circuit, Figure 2-5 the reduction in current gain, Figure 2-6 the resulting reduction in fan out capability, Figure 2-7 the transfer function, Figure 2-8 the threshold and saturation voltages, and Figure 2-9 the leakage currents.

The SE 124 Flip Flop, Appendix 2, Figure 10 (2-10) has also been studied in the past neutron environment. Figure 2-11 shows the saturation voltage, off voltage, and minimum voltage required to switch.

THe MC 1525 is a differential amplifier characteristic of linear circuits. Appendix 2, Figure 12 (2-12) shows the schematic, Figure 2-13 the transfer function, and Figure 2-14 the current gain degradation.

Gregory[15] has measured solar cells in the past neutron environment. Figure 6 shows his results and calculated values using Equation 15.

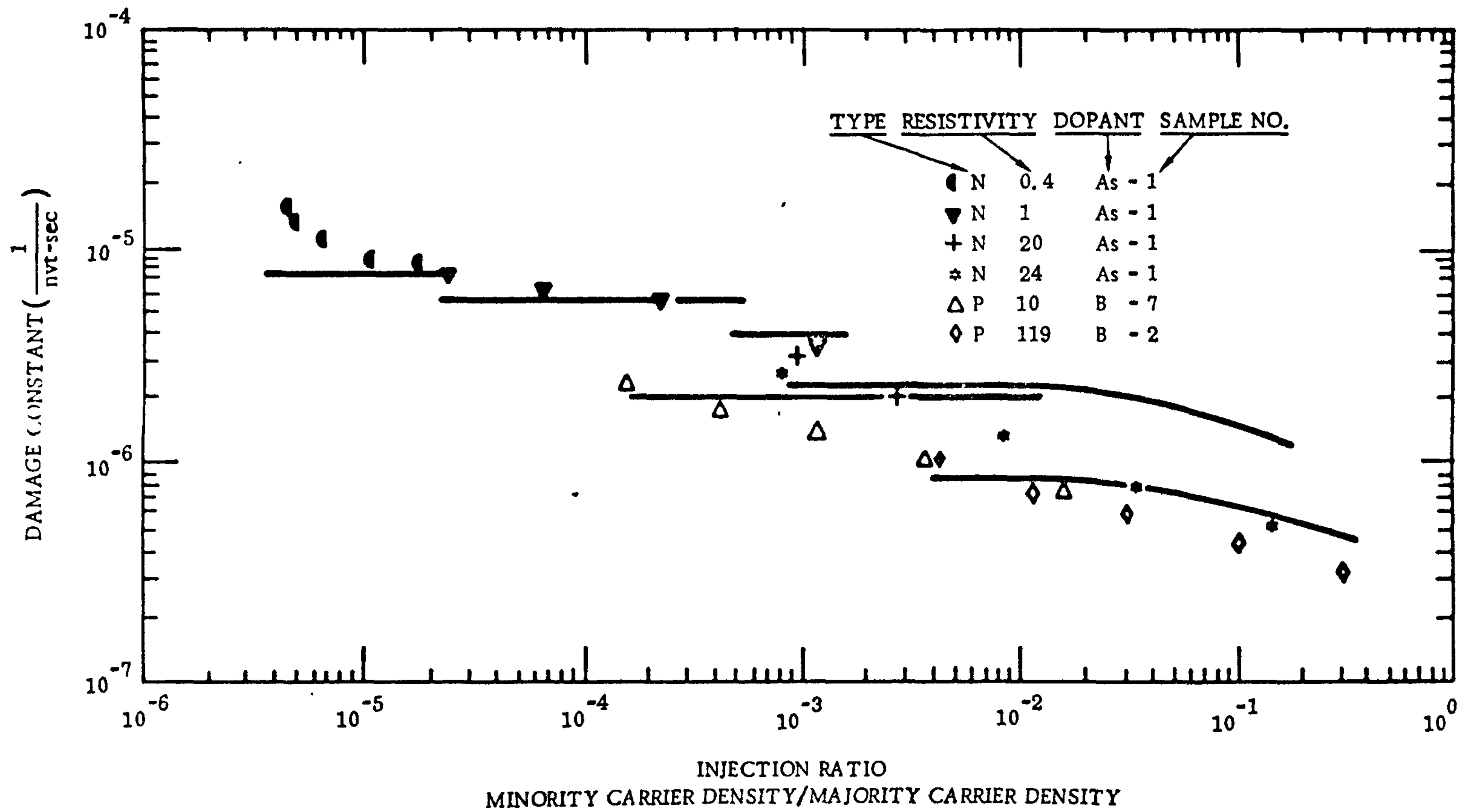

Figure 6. Damage Constant vs Injection Ratio for Solar Cells

REFERENCES

1. TREE Handbook, Battelle Memorial Institute, Section E, (July 1966).

2. Billington and Crawford, Radiation Damage to Solids, Chap. 7, Princeton Univ. Press (1961).

3. Mitchell, J. and Wilson, K., "Surface Effects of Radiation on Semiconductor Devices," pp 1-80, (Jan 1967).

4. Goldstein, M., et al, Semiconductor Surfaces, John Wiley & Sons (1965).

5. Messenger, G.C., "Current Gain Degradation Due to Displacement Damage for Graded-Base Transistors," Proc. IEEE, 55, No. 3, (March 1967).

6. Lindmayer, J. and Wrigley, C., Fundamentals of Semiconductor Devices, D. Van Nostrand (1965).

7. Messenger, G.C., IEEE Trans. on Nuc. Sci., NS-12, 2, p 53 (1965).

8. Early, J.N. and Dooley, J.A., J. Appl. Phys., 31, p 1024 (1960).

9. Billington, D.S., (ed.), Radiation Damage in Solids, Academic (1962).

10. Dunod, "Radiation Damage in Semiconductors," Proc. 7th Int. Conf. Phys. of Semicond., Vol II, p 401 (1962).

11. Curtis, O.L., Jr., Cleland, J.W., and Crawford, J.H., Jr., "Radiation-Induced Recombination Centers in Germanium," J. Appl. Phys., 29, p 1722, (Dec 1958).

12. Brown, R., "Energy Dependence ..... Semiconductor Devices," Conf. on Radiation Effects on Semiconductor Devices, Toulouse, France, (7-10 Mar. 1967).

13. Messenger, G.C., "The Effects of Neutron Irradiation on Transistors," Proc. Int. Solid State Conference, Brussels (Jan 1958).

14. Germano, C.A. and Curtis, O.L., Jr., "Effect of Injection Level on Carrier Lifetime in Neutron-Irradiated Germanium," IEEE Trans. on Nuc. Sci. NS-13, 6, pp 47-52, (Dec 1966).

15. Gregory, B.L. and Sander, H.H., "Injection Dependence of Transient Annealing in Neutron Irradiated Silicon Devices," IEEE Radiation Effects Conf., Columbus, Ohio (July 1967).

RECOMMENDED SUPPLEMENTARY READING

"Integrated Circuits" R. Warner and J. Fordemwalt, McGraw Hill, 1965 pp 88

Motorola Integrated Circuit Course (1964) Vol II, Chapter 19 and pp 19-6

"Electronics and Holes in Semiconductors" W. Shockley, Van Nostrand Co., Aug.1956, Chapter 12

"Statistics of the Recombination of Holes and Electrons" W. Shockley and W. Read, Phys.Rev., Vol 87, No. 5, Sept.1952, pp 835 - 842

"Silicon Semiconductor Technology" W. Runyan, McGraw Hill, 1965, pp 177

"Transistor Engineering" A. Phillips, McGraw Hill, 1962, Chapter 10

"Carrier Generation and Recombination in P-N Junctions" C. Sah and R. Noyce, Proc.IRE, Sept 1957, pp 1228-1243

"Fundamentals of Semiconductor Devices" Lindmayer and Wrigley, D. Van Nostrand Co. 1966, p 241 and Chapter 7 Section 3

"The Effects of Neutron Irradiation on Germanium and Silicon" G. Messenger and J. Spratt, Proc.IRE June 1958, pp 1038-1044

"Radiation Effects on Microcircuits" G.C. Messenger, IEEE Trans.on Nucl.Sci., NS-13, No. 6, pp 141-159

"Displacement Damage in MOS Transistors" G.C. Messenger and E.J. Steele, IEEE Trans.on Nucl.Sci., NS-12, No. 5, Oct 1965, pp 78-82

"Radiation Damage in Solids" Billington and Crawford Princeton Univ. Press, 1961, Section 9.9 pp 344-348

"Fundamentals of Semiconductor Devices" Lindmayer and Wrigley, D. Van Nostrand Co., 1966, pp 178

"Disordered Regions in Semiconductors .... Neutrons" B. Gossick, JAP 30 p 1214 (1959)

"Correlation of Radiation Damage ..... " S. Brucker Conf.on Radiation Effects on Semiconductor Devices, Toulouse, France, Mar. 7-10, 1967

"Transient Annealing ..... " H. Sander and B. Gregory. IEEE Trans on Nuc.Sci., NS-13, No. 6, pp 53-62

"A Two Level Model ..... " G.C. Messenger, Conf.on Radiation Effects on Semiconductor Devices, Toulouse, France, Mar. 7-10, 1967

Gossick, B.R., J. Appl.Phys.30, 1214 (1959)

STATISTICAL MODELING OF SEMICONDUCTOR DEVICES FOR THE TREE ENVIRONMENT

by

George C. Messenger, Consultant, and Earl L. Steele, Staff Scientist

July 15, 1968

Presented at

IEEE/G-NS Annual Conference on Nuclear and Space Effects

University of Montana
Missoula, Montana

AUTONETICS, Division of North American Rockwell
3370 Miraloma Avenue
Anaheim, California

Introduction and Summary

The modeling of semiconductor devices for use with circuit analysis computer codes is a very important endeavor. The accuracy of the model ultimately will determine the accuracy of the analysis and its relation to actual circuit operation. The transistor model used in the Autonetics Transient Radiation Analysis by Computer (TRAC) code is discussed. Particular emphasis is placed on the simulation of radiation-induced photocurrent in the p-n junctions. The photocurrent generator is first derived for a single junction. The result is then extended to the transistor model by appropriately combining two junctions which interact. The interaction is accomplished by including a current transport factor at each junction, as in the Ebers and Moll[1] formulation. The photocurrents are then examined in terms of defining equations which lead to the criterion for measuring the photocurrent parameters which, in turn, are related to the conventionally defined primary photocurrents in the devices.

A statistical analysis for treating the change in current gain factor with neutrons is also presented. Histograms of actual device measurements are shown to permit the determination of the damage constants. The resulting damage constant for silicon devices is given for neutron radiation. The primary photocurrent generator model is also evaluated in terms of statistical measurements on silicon devices.

Photocurrent Generation in a Single Junction

Radiation incident upon a semiconductor material generates photocurrent in p-n junctions present. The resulting current across a p-n junction in the presence of radiation can be derived from the basic continuity equation. Consider a p-n junction located at $x = 0$ in a semiconductor where holes are the prime injected charge carriers contributing to the current. The equation describing the injected hole density, (p), is

$$\frac{\partial p}{\partial t} = D \frac{\partial^2 p}{\partial x^2} - \frac{(p - p_n)}{\tau} + G \qquad (1)$$

where (τ) is the hole lifetime, (D) the diffusion constant, and (p_n) the equilibrium hole density concentration with no injecting bias. Radiation incident upon the semiconductor now generates hole-electron pairs at a rate, (G), per unit volume. We will now evaluate the resulting hole density under equilibrium conditions.

Thus, assume $[\partial p/\partial t = 0]$ and defining the diffusion length as (L),

$$L^2 = D\tau \qquad (2)$$

we see the above equation becomes.

$$L^2 \frac{\partial^2 p}{\partial x^2} - (p - p_n) + G\tau = 0 \qquad (3)$$

Assuming that the boundary conditions of a semi-infinite sample are $p = p_o$ at $x = 0$ and that p(x) remains finite as we go to large distances away from the junction, we obtain the solution for hole density versus position, (x), away from the junction as the following.

$$p(x) = p_n + (p_o - p_n - G\tau)e^{-x/L} = G\tau \qquad (4)$$

The resulting current due to holes diffusing across an area, (A), is given by

$$I(x) = -qDA \frac{\partial p}{\partial x}$$

$$= + \frac{qDA}{L} (p_o - p_n - G\tau) e^{-x/L} \qquad (5)$$

and at the junction, $(x = 0)$, the resulting current is

$$I = \frac{qDA}{L} (p_o - p_n - G\tau) \qquad (6)$$

Recall that the injected hole density at the junction, (p_o), is related exponentially to the applied bias voltage (V), then

$$p_o = p_n e^{qV/kT} = p_n e^{V/M\theta} \qquad (7)$$

where $\theta = kT/q$ and $M = 1$ for a perfectly well behaved

junction. Then, the current/voltage relation of a junction under radiation conditions is given by:

$$I = \frac{qDA}{L}\left[p_n(e^{V/M\theta} - 1) - G\tau\right]$$

$$= \frac{qDA}{L} p_n(e^{V/M\theta} - 1) - qGAL \quad (8)$$

$$= I_D - I_p$$

where:

$$I_D = \frac{qDA}{L} p_n (e^{V/M\theta} - 1) = I_S(e^{V/M\theta} - 1) = I_S\psi$$

$$I_p = qGAL = qGA\sqrt{D\tau} \quad (9)$$

Thus, it develops that the presence of the radiation-generated carriers adds a component of current, (I_p), in addition to the normal diode current, (I_D). Furthermore, it is in the same direction as the diode reverse saturation current and, in essence, adds to it. The photocurrent is expressed in terms of the generation rate, (G), and the "effective volume" occupied by the injected carriers.

The equivalent circuit model of this p-n junction can then be given as shown in Figure 1.

Transistor Model Including Photocurrent Generator

The model of the transistor behavior in a radiation environment is now formulated by combining two single junction models, plus interaction terms. The transistor model is shown schematically in Figure 2 in which two additional current generator terms are added to account for the additional current term at one junction due to the presence of the adjacent junction. The additional currents are expressed in terms of the current transport factors, α_N and α_I. The Ebers and Moll[1] formulation of the current/voltage relations for a transistor follows immediately from this model with the additional feature of current terms arising from radiation effects. Thus, the total emitter current, (I_E) and collector current, (I_C), can be written:

$$I_E = I_{ED} - \alpha_I I_{CD} - I_{pE}$$

$$= I_{ES}\psi_{EB} - \alpha_I I_{CS}\psi_{CB} - I_{pE} \quad (10a)$$

$$I_C = I_{CD} - \alpha_N I_{ED} - I_{pC}$$

$$= I_{CS}\psi_{CB} - \alpha_N I_{ES}\psi_{EB} - I_{pC} \quad (10b)$$

where we have defined:

$$I_{ED} = I_{ES}\left[\exp(V_{EB}/M_E\theta) - 1\right] = \left(\frac{I_{EO}}{1 - \alpha_N\alpha_I}\right)\psi_{EB} \quad (11a)$$

$$I_{CD} = I_{CS}\left[\exp(V_{CB}/M_C\theta) - 1\right] = \left(\frac{I_{CO}}{1 - \alpha_N\alpha_I}\right)\psi_{CB} \quad (11b)$$

with

$$\psi_{EB} = \exp\left[(V_{EB}/M_E\theta) - 1\right]$$

$$\psi_{CB} = \exp\left[(V_{CB}/M_C\theta) - 1\right]$$

and V_{EB} and V_{CB} being the emitter and collector bias voltages, respectively; I_{CO} and I_{EO} are the conventional junction saturation currents of the transistor.

The radiation current generators are modeled in this form in the Autonetics TRAC code. It should be noted that the radiation current generators described here, (I_{pE} and I_{pC}), are not the primary photocurrents as usually defined. The relation between these TRAC radiation current generators and the primary photocurrents will be established later.

Using this transistor model, the radiation current generator for the emitter, (I_{pE}), or collector, (I_{pC}), can be measured by setting zero bias on both emitter and collector and recording the value of the pertinent current when the transistor is irradiated. Thus, under this condition:

$$V_{EB} = V_{CB} = 0$$

$$\psi_{EB} = \psi_{CB} = 0$$

$$I_E = -I_{pE}$$

$$I_C = -I_{pC} \quad (12)$$

More realistically, the junctions would be reverse biased in order to eliminate effects due to internal resistances, but since

$$I_{ES} \ll I_{pE} \text{ and } I_{CS} \ll I_{pC}$$

the variation from a valid measure of the radiation current generator will be insignificant.

Primary Photocurrent for Transistor

The traditional definition of primary photocurrent in a transistor junction[2] due to radiation is to reverse bias the pertinent junction and leave the other junction floating, that is, carrying zero current. Thus, the primary collector photocurrent, (I_{ppc}), is defined as the collector current obtained when $V_{CB} \ll 0$ and $I_E = 0$ in Equation (10):

$$I_E = 0 = I_{ES}\psi_{EB} + \alpha_I I_{CS} - I_{pE}$$

$$I_C = -I_{ppc} = -I_{CS} - \alpha_N I_{ES}\psi_{EB} - I_{pC} \quad (13)$$

Eliminating $I_{ES}\psi_{EB}$ leads to the following where we also recognize that $I_{pC} \gg I_{CS}$

$$I_{ppc} = \alpha_N I_{pE} + I_{pC} \quad (14)$$

Similarly, the primary emitter photocurrent, (I_{ppe}), is defined as the observed emitter current in a

radiation environment when the emitter is reverse biased and the collector is floating; then $V_{EB} << 0$ and $I_C = 0$. From Equation (10) we then write:

$$I_E = -I_{ppe} - -I_{ES} - \alpha_I I_{CS} \psi_{CB} - I_{pE}$$

$$I_C = 0 = I_{CS} \psi_{CB} + \alpha_N I_{ES} - I_{pC} \quad (15)$$

Eliminating ($I_{CS} \psi_{CB}$) then leads to the following where we again recognize that $I_{pE} >> I_{ES}$:

$$I_{ppe} = \alpha_I I_{pC} + I_{pE} \quad (16)$$

By combining Equations (14) and (16) we may write the radiation current generators of the transistor model of Figure 2 in terms of the primary photocurrents. This relationship is:

$$I_{pE} = \frac{\left[I_{ppe} - \alpha_I I_{ppc}\right]}{1 - \alpha_N \alpha_I} \quad (17a)$$

$$I_{pC} = \frac{\left[I_{ppc} - \alpha_N I_{ppe}\right]}{1 - \alpha_N \alpha_I} \quad (17b)$$

Using the primary photocurrent expressions as current generators we may reformulate the Ebers-Moll model described in Equation (10) by substituting Equation (17) with the following result:

$$I_E = \frac{(I_{EO} \psi_{EB} - I_{ppe})}{1 - \alpha_N \alpha_I} - \alpha_I \frac{(I_{CO} \psi_{CB} - I_{ppc})}{1 - \alpha_N \alpha_I} \quad (18a)$$

$$I_C = \frac{(I_{CO} \psi_{CB} - I_{ppc})}{1 - \alpha_N \alpha_I} - \alpha_N \frac{(I_{EO} \psi_{EB} - I_{ppe})}{1 - \alpha_N \alpha_I} \quad (18b)$$

The conclusion to be drawn is that care must be exercised in using radiation current generators in the mathematical models when computer analyses are performed. The modeling takes a different form when primary photocurrents are used than when a straight parallel current generator is introduced, as in Figure 2. The formulation, using the primary photocurrents, in effect, simply adds a term onto the reverse saturation current of the appropriate junction. However, the parallel formulation expressed mathematically by Equations (10) and shown in Figure 2 makes the implementation of the actual model in a computer program simpler to employ.

The following material describes changes in the current gain factors, (α_N, α_I), due to neutron irradiation. These factors enter the modeling equations as defined in Equation (10), however, the more useful current gain factors are the common emitter current gain factor, (β_N, β_I), and are related to the common base factors as follows:

$$\beta_N = \frac{\alpha_N}{1 - \alpha_N} \quad (19a)$$

$$\beta_I = \frac{\alpha_I}{1 - \alpha_I} \quad (19b)$$

The neutron effects are described in terms of the β factors.

Neutron Damage Constant Statistics

The most important neutron effect is the decrease of current gain with fluence. This is included in the Ebers and Moll model by making both the forward current gain, α_N, and the inverse current gain, α_I, functions of fluence. Current gain is a function of operating conditions so that the most accurate statistical description is obtained by specifying the operating conditions and measuring the damage constant, K_D, for a statistically-significant sample of a particular device type. This leads to a K_D distribution function closely reflecting the f_α distribution function of the sample. The factor, K, for a typical group of 15 2N1613 devices under bias conditions of $V_{CE} = 5$ volts and $I_E = 30$ ma had an average value of 0.91×10^6 nsec/cm^2.[3] The appropriate device equation is:[4]

$$\Delta \frac{1}{\beta} = \frac{0.2 \, \Phi \, F(n)}{K f_\alpha} = K_D \Phi \quad (20)$$

Here, Φ is the neutron fluence greater than 10 Kev, K is the lifetime damage constant, f_α is the intrinsic current gain cutoff frequency, and F(n) is a function of the electric field in a graded base device; it is assumed equal to one for the devices studied here. Note that f_α depends on collector bias voltage and emitter current; K is a function of the silicon resistivity, the neutron energy, and the emitter current. K_D is the β damage constant for a specific device type.

A large system will typically contain many different device types and a significant testing economy can be realized if Equation (20) can be used to define a universal damage constant so that test data from each device type can be statistically combined for analytical and control purposes. This has been done with considerable success, although it is obvious from the distributions to be presented that the spread in damage constant is considerably greater than that which is obtainable for a single device. Neutron energy has been normalized to a reactor spectrum which produces 1 Mev equivalent Si damage. The variation with resistivity has been neglected since the totality of base resistivities encountered is below 5 Ω cm; Curtis[5] has shown that lifetime damage constant is independent of resistivity in this region. V_C has been set at 6.0 volts. This is typical of usage, i.e., high enough to prevent substantial collector region recombination and low enough to prevent collector multiplication. I_E has been set at approximately the current level where β, as a function of I_E, maximizes; this occurs at a current density of approximately 100 A/cm^2 for most devices. K is then measured as a function of I_E from approximately 10 A/cm^2 to 100 A/cm^2. K_∞ is obtained by extrapolation from $K = K_\infty + A/I_E$. K_∞ is approximately 20 percent larger than K measured at the value of I_E where β peaks.

Data were supplied from several cooperating laboratories to provide a larger data base and to assure that the distribution reflected dosimetry differences, etc., representative of several good laboratories.

Data supplied by the Air Force Weapons Laboratory (AFWL) used the intrinsic value of f_α, appropriate corrections for the input time constant having been made. The data from Northrop, TRW, and Autonetics utilized uncorrected f_α measurements. The use of uncorrected f_α data is expected to result in skewing the distribution on the high K side of the distribution. This is acceptable for control purposes and generally the cost of measuring f_α intrinsic for values less than 300 Mc is not justified. Further, f_t was usually measured and f_α was assumed equal to f_t.*

Damage constants for both forward and inverse current gain were available from the Autonetics data, and it was determined that Equation (20) accurately described the damage process in the inverse direction. There is usually a much greater correction required to obtain intrinsic f_α from measured f_α because the collector time constant, rather than the emitter time constant, must be removed.

Figure 3 shows a K_∞ histrogram which is comprised of 344 data points. The subset of AFWL data is shown heavily shaded to illustrate how the correction to f_α intrinsic tends to remove the skewness toward the high K end of the distribution. The small block of values around K = 5.0 came from inverse damage constants on a group of power transistors, again using uncorrected frequency data.

The histogram is important from a parts control standpoint. Neutron testing is partially destructive and can thus be used only on a lot sampling basis.** A non-destructive electrical 100 percent test is desired to control performance in a neutron environment. If Equation (20) is used, and f_α (or f_t) is used as a control test, Figure 3 shows that there is one chance in 344 of K_∞ being less than 1.0×10^6 nsec/cm^2 and 0 chance in 344 of K_∞ being less than 0.8×10^6 nsec/cm^2. If a value of 100 MHz is set as a 100 percent control minimum, then the maximum value (1 chance in 344) of $\Delta(1/\beta)$ will be 0.2 at 10^{14} n/cm^2, 0.02 at 10^{13} n/cm^2, and 0.002 at 10^{12} n/cm^2. Obviously, control of gain bandwidth product will prove useful for many applications.

The possibility of a maverick, i.e., a transistor which does not follow Equation (20), must be faced. This possibility can be reduced by accumulating more data, hopefully to the point where maverick probability becomes extremely small. Surface and emitter field region recombination effects are not directly and totally controllable by using f_α measurements. In this sense, f_α control is necessary but, perhaps, not sufficient. For the 147 units in the Autonetics test, the values of M_E and M_C were monitored as a function of fluence. When these values "track," or change in the same direction, the base recombination dominates as described by Equation (20); when M_E increases with fluence more rapidly than M_C, then surface and emitter field region recombination is dominant. For all devices, surface and emitter region recombination decrease in importance relative to base region recombination as the emitter current increases. For the devices tested in the Autonetics program this transition occurred at approximately 100 μamps. It therefore seems proper to use f_α control for application above 100 μamps; but to require supplementary controls for applications below 100 μamps.

The value of K_∞ is not used directly in analytical programs. A value of K applicable to the particular current level of interest is obtained from a normalized curve of K vs I_E. [6]

Photocurrent Statistics

The most important parameters for including ionizing effects in the Ebers and Moll model are the primary photocurrents. These have been measured over a wide range of ionizing dose rate for both long and short pulses. The p-n junction photocurrent response to a rectangular pulse of length (t_p) is given by [7]

$$Ippj = qGAj\sqrt{D\tau}\left[\operatorname{erf}\left(\frac{t}{\tau}\right)^{\frac{1}{2}} - \operatorname{erf}\left(\frac{t-tp}{\tau}\right)^{\frac{1}{2}}\right] \quad (21)$$

where $G = g\dot{Y}$ and $g \approx 4.0 \times 10^{13}$ carries/cm^3 per Rad and $\dot{Y}$ is the radiation rate in Rads/sec. Two special cases are important for the maximum photocurrent, Ippm, the short pulse response, $Ippm \approx qGAj\sqrt{Dt_p}$, and the long pulse response, $Ippm \approx qGAj\sqrt{D\tau}$. Short pulse values were obtained using 25 ns and 50 nsec flash X-ray pulses; long pulse values were obtained using a 4.5 μsec LINAC pulse. Three histograms for collector primary photocurrent density are shown in Figure 4. The 25-nsec and 50-nsec pulse widths are in the short pulse regions where I_{ppm} increases with the square root of pulse width. The 4.5-μsec pulse width histogram displays the equilibrium photocurrent density There is evidence of super-linear behavior in some of the devices[8], but the onset as a function of photocurrent is gradual rather than sharp. The emitter primary photocurrents show a much greater incidence of super-linear behavior than the collector primary photocurrents. Some of the spread in the distribution functions is due to this effect.

There is a definite trend in the data for the primary photocurrent density to decrease with increasing area. This suggests a perimeter effect. Possibly there is a narrow region around the periphery which contributes to the photocurrent. This would result in a substantial underestimate of the effective area for the small area devices and would be negligible for the large area device. Assuming that the actual radius of the collector is equal to the measured radius plus a small increment δ which is independent of radius, the spreads in histogram of Figure 4 can be reduced by approximately a factor of two for an optimum $\delta \approx 5 \times 10^{-4}$ cm.

The value of $j_{ppm}/\dot{Y}$ should be 4.0×10^{-9} A/cm^2 per R/sec for a 25-nsec pulse (D $\approx$ 16 cm^2/sec) and

---

* Actually, $f_\alpha = f_t/k\alpha_o$ where $k\alpha_o$ varies from about 0.7 in an ordinary field to 0.85 with zero field to 1.0 in a retarding field. The error introduced by assuming $f_t = f_\alpha$ is approximately equal and opposite to the error introduced by neglecting the correction for input time constant.

** There have been some suggestions of a scheme involving 100 percent test at the slice level followed by annealing. This scheme is not very attractive from cost and other quality control aspects.

5.6×10^9 A/cm^2 per R/sec for a 50-nsec pulse. In both cases the histogram spreads out on the high side of these numbers, as expected, thus indicating some underestimate of the geometrical parameter. In the 4.5 μsec wide pulse environment, the value of j_{ppm}/γ is expected to be 25×10^{-3} A/cm^2 per R/sec based on a 5 μsec collector lifetime, which is typical of the devices measured. This value checks well with the average value observed.

Conclusions

The mathematical model of the transistor for use in the TRAC simulation of radiation effects is discussed. It is shown to be consistent when using a modified Ebers and Moll approach with either parallel radiation current generator or conventional primary photocurrent generators. However, the form of the current/voltage relations and the mathematical formulation depends on the particular method used for photocurrent measurement.

In addition, statistical distributions in the form of histograms of damage constant and primary photocurrent are presented for transistors. These data yield the multiplying constants which will be used in simulating the transistor transient response in computer-aided analysis. The results show satisfactory correlation with the presently formulated theoretical models.

Acknowledgement

Acknowledgement is made to the Air Force Weapons Laboratory, TRW, Boeing, and Northrop Corporation for supplying some of the transistor data.

References

1. Ebers, J. J. and Moll, J. L., "Large Signal Behavior of Junction Transistors;" Proc IRE, 42, 1761-1772 (December 1954).
2. Rosenberg, C., Gage, D. S., Caldwell, R. S., and Hanson, G. H., "Charge-Control Equivalent Circuit for Predicting Transient Radiation Effects in Transistors;" IEEE Trans on Nuclear Science, NS-10, 149-158 (November 1963).
3. Private Communication from AFWL.
4. Messenger, G. C., "Current Gain Degradation due to Displacement Damage for Graded Base Transistors;" Proc IEEE, 55, 413-414 (March 1967).
5. Curtis, O. L., Jr., "Effects of Oxygen and Dopant on Lifetime in Neutron Irradiation Silicon " IEEE Trans on Nuclear Science, NS-13, 33-40 (December 1966).
6. Larin, F., Radiation Effects in Semiconductor Devices; p. 163; John Wiley and Sons (1968).
7. Wirth, J. L. and Rogers, S. C., "The Transient Response of Transistors and Diodes to Ionizing Radiation;" IEEE Trans on Nuclear Science, NS-11; 24-38 (November 1964).
8. Habing, D. H. and Wirth, J. L., "Anomalous Photocurrent Generation in Transistor Structures;" IEEE Trans on Nuclear Science; NS-13; 86-94 (December 1966).

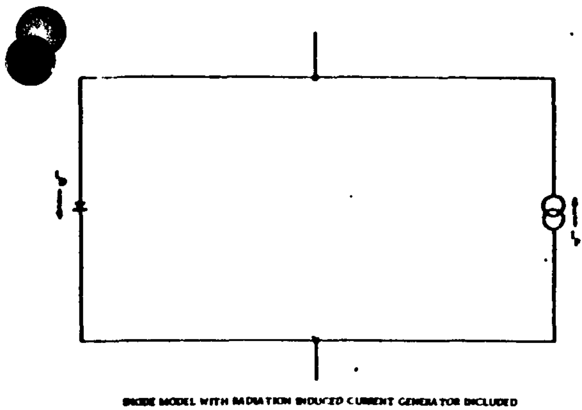

Figure 1. Diode Model with Radiation Induced Current Generator Included

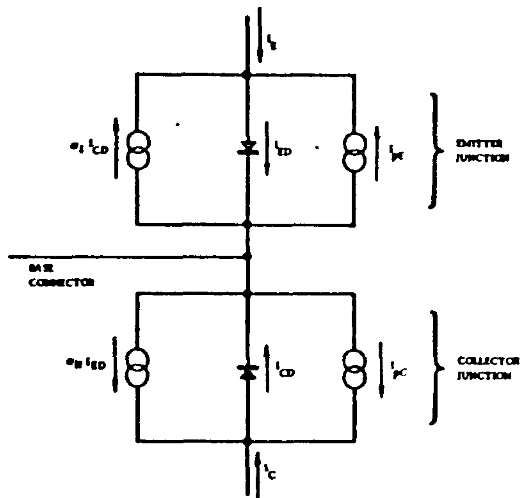

Figure 2. Transistor Model with Two Interacting Junctions and Radiation Current Generators (P-N-P Transistor)

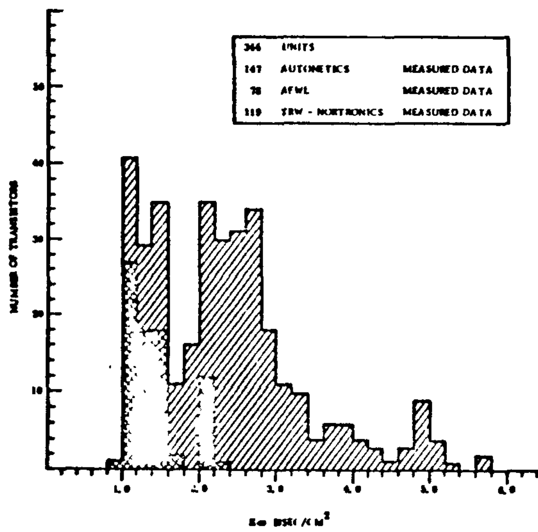

Figure 3. Histogram of Measured Values of $K\alpha$ for 344 Transistors

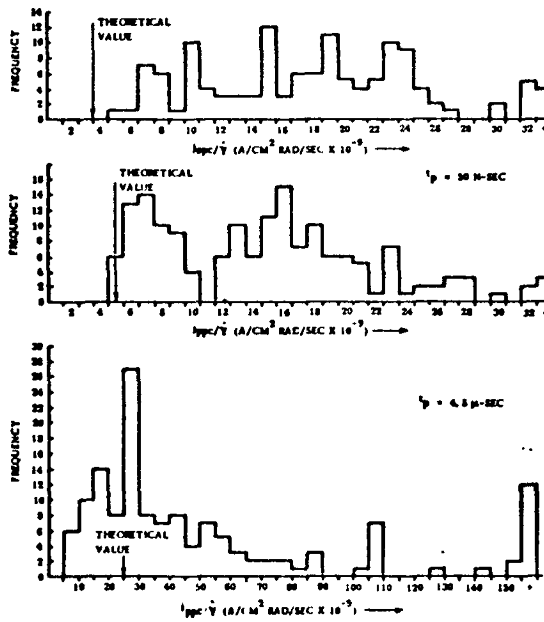

Figure 4. Collector Primary Photocurrent Density Histograms

A TWO LEVEL MODEL FOR LIFETIME REDUCTION PROCESSES IN NEUTRON IRRADIATED SILICON AND GERMANIUM

by

George C. Messenger
Nortronics, A Division of Northrop Corporation
Applied Research Department
Newbury Park, California

Abstract

A two level model for recombination processes in neutron irradiated silicon and germanium is proposed. This model successfully explains published experimental data for lifetime and lifetime damage constant as a function of resistivity, injection level and temperature.

Summary

A two level model for recombination processes in neutron irradiated bulk germanium and silicon and germanium and silicon devices is proposed. This model explains the large body of published experimental data much better than the previously used single level models.

The fact that the resistivity of neutron irradiation silicon tends toward intrinsic shows that donor and acceptor levels are both being introduced simultaneously. Konopleva[1] has indicated that a number of donor and acceptor levels are actually being simultaneously introduced. Swanson[2] has shown that both donors and acceptors are introduced into neutron irradiated germanium. Curtis[3] and Swanson have both used two level models to explain various facets of neutron irradiation on germanium.

Recently, Curtis[4] reported extensive measurements of lifetime damage constant as a function of silicon resistivity, dopants and oxygen concentration. He concluded that recombination was dominated by centers within defect clusters, and that there was no dependence on oxygen concentration or type of defect in n-type material. A very small dependence on dopant was noted in highly doped p-type material. This contrasts with the results reported for silicon and germanium irradiated with electrons or gammas where dopant and oxygen concentration have been shown to substantially affect the rate of introduction of recombination centers.[5,6,7] Curtis further concluded that it was impossible to reconcile all of his experimental data with a single level recombination model. Specifically, the dependence of lifetime damage constant on resistivity for n-type material cannot be explained by a one level model. He suggested a number of effects which might be responsible for the failure of the single level model, (1) dependence of capture probabilities on Fermi level through modulation of the potential wells surrounding primary defect clusters[8], (2) occurrence of two or more recombination levels operating simultaneously, (3) creation of impurity-defect complexes (low resistivity p-type materials only), (4) complication of a multi-level recombination center[9], (5) broadening of energy levels due to defect interaction with the primary defect cluster, (6) Fermi level dependence of stability of recombination centers[10], (7) impurity-defect interactions which are independent of size of dopant atoms.

This paper will show that a two level model adequately explains Curtis' experimental data on silicon material as well as the transistor data previously reported by Messenger[11]. The dependence of lifetime damage constant on resistivity for n-type silicon, which could not be explained by a one level model is readily explained by the two level model. Some of the other alternative explanations mentioned by Curtis, especially items 1, 3 and 5, cannot be ruled out. Items 4 and 6 relate more directly to point defects and their extension to the cluster defect is unlikely.

For germanium, the data on lifetime damage constant as a function of resistivity is not as extensive as for silicon. However, adequate data has been presented by A. E. Walters[12] covering both n and p type germanium at low injection levels. Messenger[13] has reported lifetime damage constant as a function of resistivity at moderate injection levels. A two level model will be developed which adequately explains this data.

It is assumed that the lattice damage is primarily vacancy clusters. Each cluster has two associated "average" recombination centers which can be characterized by discrete energy levels, one in the upper half and the other in the lower half of the forbidden energy band. The recombination centers are "associated" with the clusters. They may be contained within the clusters, or they may be near the cluster as a result of migration of some vacancies from the cluster[1]. In addition, it is possible that the two energy levels associated with the recombination centers are not truly discrete, but are average energies which adequately represent the net effect of a distribution of energy levels associated with the cluster. Previous experimenters have identified energy levels and cross sections derived from experimental data with discrete defect levels in the forbidden band. This analysis may identify a discrete level if the level is truly dominant; otherwise it identifies an average level representative of a number of discrete levels. Further, this discussion is restricted to unannealed damage present at room temperature after neutron irradiation. Any substantial higher temperature annealing will change the characteristic of the recombination centers. The energy levels, capture cross sections and introduction rates of these recombination centers are assumed to be independent of silicon resistivity, dopant type, and oxygen concentration. The two recombination centers are further assumed to act independently so that their reciprocal lifetimes are additive.

Further, the capture cross sections of the recombination centers are assumed to be independent of temperature. Both Van Lint[14] and Galkin[15] have reported temperature dependence of electron capture cross sections for electron irradiated silicon. Galkin finds hole capture cross sections independent of temperature. However, (1) it is not obvious that these arguments can be extended to clusters, (2) preliminary analyses indicate that their data could alternatively be explained by a two level model with temperature independent capture cross sections. For silicon the energy level $E_1 \approx 0.31$ ev is substantially different from the values of $E_1 \approx 0.18$ ev deduced from a one level model analysis by both Curtis[4] and Messenger[11]. It should probably be interpreted as an "average" level. The level $E_2 \approx 0.35$ ev is close to previously reported values[15,16]; it therefore may approximate a dominant recombination level.

For germanium, the donor level at 0.26 ev below the conduction band is deeper than the level usually determined from a one level model[11]. However, the acceptor level 0.30 ev above the value band agrees with previously identified levels. As for silicon, the donor level is probably an average effect from several levels in the upper half of the band, whereas the acceptor level is probably a dominant level.

Using the above assumptions, expressions are developed for the variation of lifetime and lifetime damage constant with resistivity, injection level and temperature. Previously published experimental data on bulk silicon, bulk germanium and silicon and germanium transistors is used to verify the applicability of the two level models and determine the constants which characterize each level.

Development of Two Level Model

The lifetime damage constant K is defined by the post-irradiation life time τ at a neutron fluence Φ[17], assuming that τ is much smaller than the preirradiated lifetime. The lifetime τ is assumed to result from the independent action of two recombination centers characterized by lifetime τ_1 and τ_2.

$$\frac{1}{\tau} = \frac{\Phi}{K} = \frac{1}{\tau_1} + \frac{1}{\tau_2} \qquad (1)$$

A straight forward application of Shockley-Read[18] leads to a general formulation of the damage constant[19].

$$\frac{1}{K} = \frac{1}{\frac{1}{C_{p1}R_1}\left(\frac{n_0+n_1+\delta n}{n_0+p_0+\delta n}\right) + \frac{1}{C_{n1}R_1}\frac{(p_0+p_1+\delta n)}{(n_0+p_0+\delta n)}} + \frac{1}{\frac{1}{C_{p2}R_2}\left(\frac{n_0+n_2+\delta n}{n_0+p_0+\delta n}\right) + \frac{1}{C_{n2}R_2}\frac{(p_0+p_2+\delta n)}{(n_0+p_0+\delta n)}} \qquad (2)$$

Here, n_0 and p_0 are the equilibrium electron and hole densities in the silicon and $\delta n = \delta p$ is the excess carrier density. C_{p1}, C_{n1}, C_{p2}, and C_{n2} are the electron and hole capture rates for the two recombination centers and R_1 and R_2 are the introduction rates of the centers. Notice that the combined effects of injection level, resistivity and temperature are implicitly contained in this expression.

At low values of injection level, Eq. (1) becomes

$$\frac{1}{K_{LN}} = \frac{C_{p1}R_1}{1+\frac{n_1}{n_0}} + \frac{C_{p2}R_2}{1+\frac{C_{p2}}{C_{n2}}\frac{p_2}{n_0}} \qquad (2a)$$

$$\frac{1}{K_{LP}} = \frac{C_{n1}R_1}{1+\frac{C_{n1}}{C_{p1}}\frac{n_1}{p_0}} + \frac{C_{n2}R_2}{1+\frac{p_2}{p_0}} \qquad (2b)$$

At high values of injection level, Eq. (1) becomes

$$\frac{1}{K_H} = \frac{C_{n1}R_1}{\frac{C_{n1}}{C_{p1}}+1} + \frac{C_{p2}R_2}{\frac{C_{p2}}{C_{n2}}+1} \qquad (3)$$

Curtis'[4] experimental data for low level damage constant vs resistivity was fitted using Eq. (2) with one level in each half of the forbidden band[20]. A least squares fit, Fig. 1 and 2, was obtained using a computer program. The fit is excellent, and Eq.(2), using the characteristics of the recombination centers shown in Table Ia may be used to determine K_L for any value of resistivity within the experimental error inherent in the basic experimental data.

The values for capture cross sections can be deduced by using the values of carrier removal rate which were also measured on the samples used in Fig. 1 and 2. This assumes that the carrier removal rate and the introduction rate of recombination centers are approximately equal. The results are given in Table II for comparison with the results of other experiments. The level in the upper half of the band is behaving as a donor and the level in the lower half of the band as an acceptor. Table III shows the room temperature defect level scheme determined by Konopleva[1] and the two level approximation for comparison.

Walters[12] data for low level damage constant vs resistivity was fitted using Eq. (2) with one level in each half of the forbidden band. The resulting fit is shown in Fig. 3, and the constants used are shown in Table Ib. This data is too sparse to justify a least squares curve fitting procedure; consequently the germanium values in Table Ib are not as well determined as the silicon values in Table Ia.

Damage Constant as a Function of Resistivity

The variation of silicon damage constant with resistivity for various values of injection ratio is shown in Fig. 4. Values for $C_{p1}R_1$, $C_{n1}R_1$, $C_{p2}R_2$, and n_1 and p_2 are taken from the least squares fit to Curtis' low level data (Table Ia). Several aspects of Fig. 4 warrant comment.

K always increases monotonically with resistivity. The variation in K is greatest for the low injection level case; at very high injection levels K is independent of resistivity. At low injection levels, K approaches the following asymptotes for very low resistivities.

$$\frac{1}{K^*_{LP}} = C_{n1}R_1 + C_{n2}R_2 \qquad (4a)$$

$$\frac{1}{K^*_{LN}} = C_{p1}R_1 + C_{p2}R_2 \qquad (4b)$$

This behavior is qualitatively similar to the one level model.

Germanium damage constant as a function of resistivity for various values of injection ratio is shown in Figs. 5 and 6. In germanium, devices are made with base resistivities much closer to intrinsic resistivity, relatively speaking, than is the case for silicon. Consequently, it is expected that device verification of a flat or decreasing lifetime damage constant with increasing injection level can be found. The 2N1308 data, to be discussed subsequently, bears this out.

Damage Constant as a Function of Injection Level

Fig. 7 shows the variation of silicon K with injection level for various values of resistivity. For resistivities below 50 ohm-cm[21], K will increase with increasing injection level. For the recombination center constants in Table I, K_p always increase monotonically with injection level; K_N usually increases monotonically with injection level but for some values of resistivity (e.g., ≈ 100 ohm-cm) K_N goes through a maximum as injection level is increased. This behavior has previously been reported for germanium[22].

Figs. 8 and 9 show the variation of germanium K with injection level for various values of resistivity. Notice that a maximum is expected for n type

resistivities in the range of one to [illegible]teen ohm cm.

A one level model can never result in a maximum in the K_N vs injection level curve.

Damage Constant as a Function of Temperature

The temperature dependence of K is explicitly introduced into Eq. (1) through n_1 and p_2: $n_1 = AT^{3/2}\exp-(E_c-E_1)/kT$, $p_2 = BT^{3/2}\exp-(E_2-E_v)/kT$. n_0 and p_0 are assumed independent of temperature, thus limiting this discussion to the temperature range over which the material is extrinsic and the doping centers are fully ionized. The capture cross sections are assumed independent of temperature. The constants A and B are eliminated by normalizing the temperature dependence to T_1 ($\frac{q}{kT_1} = 38.6$ at $T_1 = 300^{\circ}K$). Eq. (1) becomes,

$$\frac{1}{K_P} = \frac{C_{p1}R_1}{\frac{C_{p1}}{C_{n1}} + \frac{\delta n}{p_0 + \delta n} + \left(\frac{p_0}{p_0+\delta n}\right)\left(\frac{n_1}{p_0}\right)_{T_1}\left(\frac{T}{T_1}\right)^{3/2}\exp[38.6(1 - \frac{T_1}{T})\Delta E_1]} + \frac{C_{n2}R_2}{\frac{C_{n2}}{C_{p2}}\left(\frac{\delta n}{p_0+\delta n}\right) + 1 + \left(\frac{p_0}{p_0 + \delta n}\right)\left(\frac{p_2}{p_0}\right)_{T_1}\left(\frac{T}{T_1}\right)^{3/2}\exp[38.6(1 - \frac{T_1}{T})\Delta E_2]} \quad (5a)$$

$$\frac{1}{K_N} = \frac{C_{p1}R_1}{\frac{C_{p1}}{C_{n1}}\left(\frac{\delta n}{n_0 + \delta n}\right) + 1 + \left(\frac{n_0}{n_0+\delta n}\right)\left(\frac{n_1}{n_0}\right)_{T_1}\left(\frac{T}{T_1}\right)^{3/2}\exp[38.6(1 - \frac{T_1}{T})\Delta E_1]} + \frac{C_{n2}R_2}{\frac{C_{n2}}{C_{p2}} + \frac{\delta n}{n_0 + \delta n} + \left(\frac{n_0}{n_0 + \delta n}\right)\left(\frac{p_2}{n_0}\right)_{T_1}\left(\frac{T}{T_1}\right)^{3/2}\exp[38.6(1 - \frac{T_1}{T})\Delta E_2]} \quad (5b)$$

These equations are relatively complicated. Therefore, a computer run was made at a number of different resistivities varying both temperature and injection level. A typical set of curves is shown in Fig. 10 and 11 for one ohm cm silicon material, where K_N, K_P is plotted against $\frac{1000}{T(^{\circ}K)}$ for various values of injection level. Fig. 12 shows K_N for germanium of various resistivities at an injection ratio of unity.

Several important characteristics [illegible] evident in these curves. As the injection level increases the value the K at low temperature increases and the value of K at high temperature decreases. The apparent slope decreases as a function of increasing injection level. Therefore, in experiments where the slope of this line is used to deduce an activation energy, one must be sure to consider the effect of injection level.

Substantially different values of energy levels result when experimental curves are fit to a two level model rather than a one level model even after injection level effects are properly considered.

Previously, data showing relatively constant values of lifetime below room temperature had been attributed to trapping effects. Eq. (5a) and (5b) show that both a finite injection level and a second recombination center can cause this effect. It is instructive to examine the low level asymptote for several approximations[23].

$$\frac{1}{K_n^{**}} = \frac{C_{p1}R_1}{\frac{C_{p1}}{C_{n1}}\left(\frac{\delta n}{n_0 + \delta n}\right)} + \frac{C_{n2}R_2}{\frac{C_{n2}}{C_{p2}} + \frac{\delta n}{n_0 + \delta n}} \quad \text{(no approximations)} \quad (6a)$$

$$\frac{1}{K_n^{**}} = C_{p1}R_1 + C_{p2}R_2 \quad (\frac{\delta n}{n_0} = 0) \qquad (6b)$$

$$\frac{1}{K_n^{**}} = \frac{C}{1 + \frac{C_{p1}}{C_{n1}}(\frac{\delta n}{n_0 + \delta n})} \quad \text{(one level model)} \qquad (6c)$$

$$\frac{1}{K_n^{**}} = C_{p1}R_1 \quad (\text{one level model and } \frac{\delta n}{n_0} = 0) \qquad (6d)$$

Extension to Electron, Proton and Gamma Radiation

The preceding analysis has been developed for the neturon case. It should have a logical extension to the point defects present in semiconductor materials damaged by other radiations such as electrons, protons or gammas, when the defect does not involve a donor atom which would not be present in p-type material[24], or when the characteristics of the defect do not depend on Fermi Level position. Thus, divacancies, A centers, etc., should be expected to contribute to lifetime degradation for both n- and p-type material.

Experimental Results

Lifetime vs temperature measurements were also taken by Curtis. Fig. 13 shows an example of experimental lifetime vs 1000/T data. The solid line represents the fit using Eq. (5b) with the experimental values from Table I. There is excellent agreement. A number of similar data sets have been checked at various resistivity values for both p- and n-type samples. The agreement between the data and Eq. (5a) is usually very good.

A small discrepancy at low temperatures in Fig. 13 is real and appears in most of the data checked. It is probably due to annealing. The constants in Table I used in Eq. (5a) were determined from unannealed data. The data in Fig. 13 were taken after 1/2 hour anneal at each temperature before taking the data at that particular temperature.

Messenger[11] has published data on the variation of current gain with temperature for neutron irradiated silicon transistors. Fig. 14 shows data for a 2N335 transistor. Current gain is related to lifetime damage constant by,

$$\beta = \frac{f_t\ K}{0.2\phi\ F'(Z)} \qquad (7)$$

Using the measured characteristics of the transistor, $f_t/0.2\phi = 4.2 \times 10^{-6}$, and using K from Eq. (5a) with the experimental constants of Table I, the theoretical curve (solid line) for β vs $\frac{1000}{T}$ is obtained. The qualitative fit is very good. The qualtitative discrepancy is well within the expected experimental error and can possibly be attributed to two factors. The data used in obtaining Table I was taken between 10^{10} and 10^{11} n/cm^2; the data of Fig. 8 was taken at 8.6×10^{13} n/cm^2. Thus, it is possible that a dosimetry correction factor is required. The factor $f_t/0.2$ in Eq. (7) contains several approximations and may not be quantitatively correct.

Fig. 14 is representative of a number of analyses which have been run. The experimental data consistently increase at a slightly greater rate than the calculated curve at very high temperatures. The systematic error is probably due to annealing and device overheating. The shape of the curve is also affected by the value of injection ratio calculated from the device equations. For example the shape of the experimental curve in Fig. 8 is even more closely approximated by using an injection ratio of 0.2 in Eq. (5a). The determination of injection ratio on the devices is probably only good to within a factor of two.

The variation of current gain with injection level for irradiated transistors provides another check for the two level model. Fig. 15 shows experimental data for a 2N1655 silicon transistor[11]. The solid curve is calculated from Eq. (1) with the constants of Table I. The relationship between β and K calculated from the device equation is $\beta = 2.9 \times 10^{-6} K_n$.

Fig. 16 shows the variation of lifetime damage constant with injection level for a 2N1308 transistor. Again, the agreement is excellent between the calculated and experimental results. Notice the characteristic is almost flat, the resistivity of 6.3 ohm cm is close to the value for which the theoretical curve is flat, the factor of 1.5 increase observed at low injection levels is due to the increase of the diffusion constant in the base of the transistor as injection level is increased. The fall off at high current

levels is attributed to base conductivity modulation.

The data is representative of a number of transistors both p and n base. The agreement between Eq. (1) and the data at low injection levels was frankly not expected. Rather, it was expected that the recombination process in the base emitter field region which has been discussed by Sah et al,[25] would cause the experimental curve of $1/\beta$ to increase more rapidly with decreasing injection level, at least in the case of silicon. Evidently, lifetime variation with injection level contained in Eq.(1) is sufficient to explain the transistor data, for both silicon and germanium above injection ratios of about 0.01.

Concluding Discussion

An attempt has been made to see how successful a two level model could be in resolving the contradictions inherent in fitting experimental data for neutron irradiated silicon and germanium to the one level models previously used.

As a mathematical formalism the two level model is very successful in predicting the variation of lifetime damage constant with resistivity, temperature, and injection levels.

As a physical reality, the two level model has two substantial deficiencies. First, it is an approximation to a very complicated defect structure which is known to contain many levels[24]. Second, there are several other plausible alternative extensions or modifications to the one level model which might resolve its contradictions with experimental data.

Several important conclusions can be deduced from the two level models. The damage constants reported for experiments on semiconductor materials have always been much lower than those reported for experiments using transistors. The variation of lifetime with temperature reported on silicon material has been larger than the variation of current gain with temperature measured on devices. This is because the material measurements have been made at very low injection ratios, and the device measurements at intermediate to high values of injection ratio. It is characteristic of both the one level and two level models that damage constant will increse substantially with injection level, and that temperature dependence will decrease with increasing injection level.

The tendency of lifetime to asymptote at low temperatures can be caused by a finite injection ratio or the presence of a second recombination center. These effects have probably been at least as important as the trapping effects which have previously been mentioned.

The two level model approximates a very complex physical picture by representing a spectrum of donor levels in the upper half of the forbidden band by a single donor level of appropriate average activation energy and capture cross sections; and by representing a spectrum of acceptor levels in the lower half of the band by a single acceptor level of appropriate average activation energy and capture cross sections. The clusters are in a quasi-equilibrium condition at room temperature; annealing at higher temperatures will result in a reduction of the effect of the clusters at the expense of introducing point defects. Therefore, the characteristics of the two level model are applicable only at room temperature and will change with further annealing.

References

1. Konopleva, R.F., et al, Soviet Phys. Solid State 8, 264 (1966).
2. Swanson, M.L., Can. J. Phys. 44, 2181 (1966).
3. Curtis, O.L., Jr., J. Appl. Phys. 36, 2094 (1965).
4. Curtis, O.L., Jr., "Effects of Oxygen and Dopant on Lifetime in Neutron Irradiated Silicon," IEEE Conf. on Nuclear and Space Radiation Effects, Stanford University, July 1966.
5. Brown, W.L., et al, J. Appl. Phys. 30, 1258 (1959).
6. Watkins, G.D., et al, J. Appl. Phys 30, 1198 (1959).
7. Curtis, O.L., Jr., and Crawford, J. H., Jr., Phys. Rev. 124, 1731 (1961); 122, 1342 (1961).
8. Gossick, B.R., J. Appl. Phys. 30, 1214 (1959).
9. Curtis, O.L., Jr., et al, J. Appl. Phys. 29, 1722 (1958).

10. Mackay, J.W., and Klontz, E., "Low Temperature Irradiation of Semiconductors and Ionizing Effects," Radiation Damage in Semiconductors (Dunod Press, Paris, 1965) p 11.

11. Messenger, G.C., IEEE Trans. on Nuclear Sci. NS-12, 53 (1965).

12. Walters, A.E., "Minority Carrier Lifetime in Neutron Bombarded Germanium," Proc. 2nd Conf. on Radiation Effects on Semiconductor Devices, Materials and Circuits (Cowan Pub., New York 1959) p 35.

13. Messenger, G.C., "The Effect of Fast Neutron Irradiation on Transistors," International Conf. on Solid State Physics, Brussels Conf. June 1958.

14. Van Lint, V.A.J., and Harrity, J.W., "Carrier Lifetime Studies in High Energy Electron Irradiated Silicon," Radiation Damage in Semiconductors (Dunod Press, Paris, 1965) p 417.

15. Galkin, G.N., et al, "Volume Recombination of Current Carriers in n-Type Silicon Containing Radiation-Induced Structural Defects," Sov. Phys. Solid State 2, 1819 (1960).

16. Klein, Claude A., J. Appl. Phys. 30, 1222 (1959).

17. Neutron fluence Φ used in this report refers to a reactor spectrum of average energy 1.6 MeV, counting all neutrons with energies greater than 10 keV.

18. Shockley, W., and Read, W.J., "Statistics of Recombination of Holes and Electrons," Phys. Rev. 87, 835 (1952).

19. The density of recombination centers is assumed very small compared with the density of majority carriers.

20. Assuming both levels either in the upper half or lower half of the band, results in no possible fit to the experimental data.

21. This includes nearly all important semiconductor device applications.

22. Germano, C.A., and Curtis, O.L., Jr., "Effect of Injection Level on Carrier Lifetime in Neutron Irradiated Germanium," IEEE Conf. on Nuclear and Space Radiation Effects, Stanford Univ, July 1966.

23. This will be done for n-type material; the extension to p-type is obvious.

24. A similar argument applies to acceptors.

25. Sah, et al, Proc. Inst. Radio Engrs. 1228 (1957).

26. Ramdas, A.K., and Rao, M.G., Phys. Rev. 142, 451 (1966).

Acknowledgements

The author gratefully acknowledges many helpful discussions with Dr. O. Curtis, Jr. and Dr. Donavon Pretzer. The contributions of Mr. David Lawrence in obtaining the computer calculations is acknowledged.

Table 1a. Parameters for the recomination centers determined by a least square fit to Curtis' low level lifetime damage constant data.

$R_1C_{p1} = 0.37 \times 10^{-6}(\text{sec-n/cm}^2)^{-1}$
$R_1C_{n1} = 0.40 \times 10^{-5}(\text{sec-n/cm}^2)^{-1}$
$R_2C_{p2} = 0.68 \times 10^{-5}(\text{sec-n/cm}^2)^{-1}$
$R_2C_{n2} = 0.76 \times 10^{-6}(\text{sec-n/cm}^2)^{-1}$
$n_1 = 2.0 \times 10^{14}\ \text{cm}^{-3}$
$p_2 = 1.3 \times 10^{13}\ \text{cm}^{-3}$

$$K_{LN} = \left[\frac{1.4 + 8.6\cdot 10^{-2}\rho + 1.2\cdot 10^{-3}\rho^2}{1 + 3.8\cdot 10^{-2}\rho}\right] \times 10^5$$

$$K_{LP} = \left[\frac{2.1 + 0.18\rho + 9.0\cdot 10^{-5}\rho^2}{1 + 1.4\cdot 10^{-2}\rho}\right] \times 10^5$$

Table 1b. Parameters for the recombination centers determined by fitting Equation (2) to Walters[12] experimental data.

$R_1C_{p1} = 4.4 \times 10^{-8}\ (\text{sec-n/cm}^2)^{-1}$
$R_1C_{n1} = 3.5 \times 10^{-8}\ (\text{sec-n/cm}^2)^{-1}$
$R_2C_{p2} = 92 \times 10^{-8}(\text{sec-n/cm}^2)^{-1}$
$R_2C_{n2} = 0.9 \times 10^{-8}\ (\text{sec-n/cm}^2)^{-1}$
$n_1 = 5.0 \times 10^{14}/\text{cm}^2$
$p_2 = 0.5 \times 10^{14}/\text{cm}^2$

Table II. Parameters for the recombination centers determined by a least square fit to Curtis' low level lifetime damage constant data

$$A_{p1} = 1.2 \times 10^{-14}\ cm^2$$
$$A_{p2} = 2.3 \times 10^{-13}\ cm^2$$
$$A_{n1} = 1.0 \times 10^{-13}\ cm^2$$
$$A_{n2} = 1.9 \times 10^{-14}\ cm^2$$

Table III. A comparison of the silicon room temperature defect level scheme due to Konopleva[1] with the two-level approximation

Konopleva[1] Room Temperature Model	Two-Level Approximation
p-Si	
$-E_c - 0.21$	
$-E_c - 0.31$	$-E_c - 0.31$ 'Average' Level
$-E_c - 0.38$	
$-E_c - 0.48$	
$-E_c - 0.50$	
$-E_c - 0.53$	
$-E_v + 0.58$	
$-E_v + 0.55$	
$-E_v + 0.53$	
$-E_v + 0.48$	$-E_v + 0.35$ 'Dominant' Level
$-E_v + 0.31$	

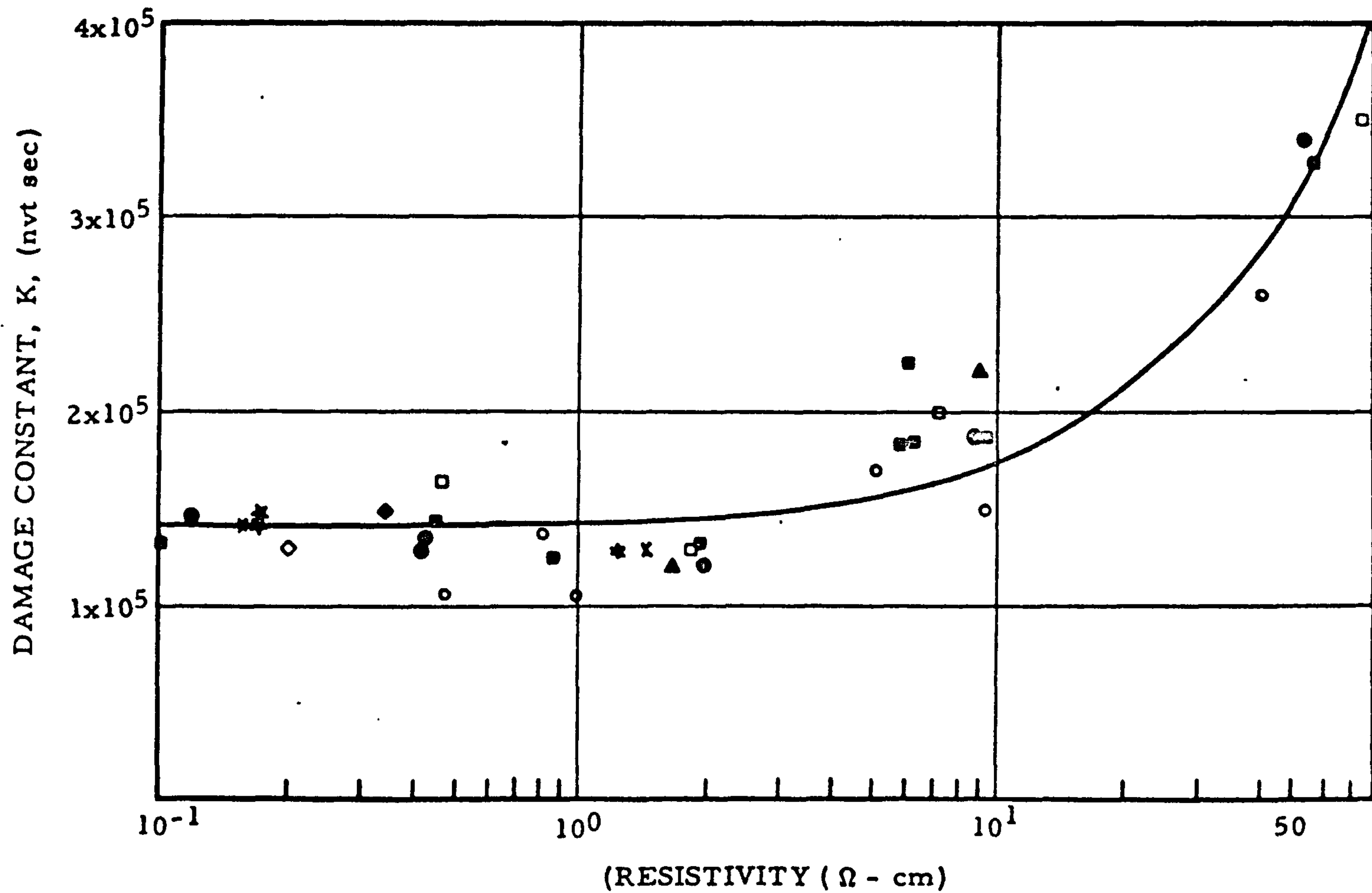

Figure 1. Damage constant vs resistivity for n-type silicon. Curtis' experimental data are given, showing least squares fit to Eq. (1a). Constants determined by the least squares fit are shown in Table Ia.

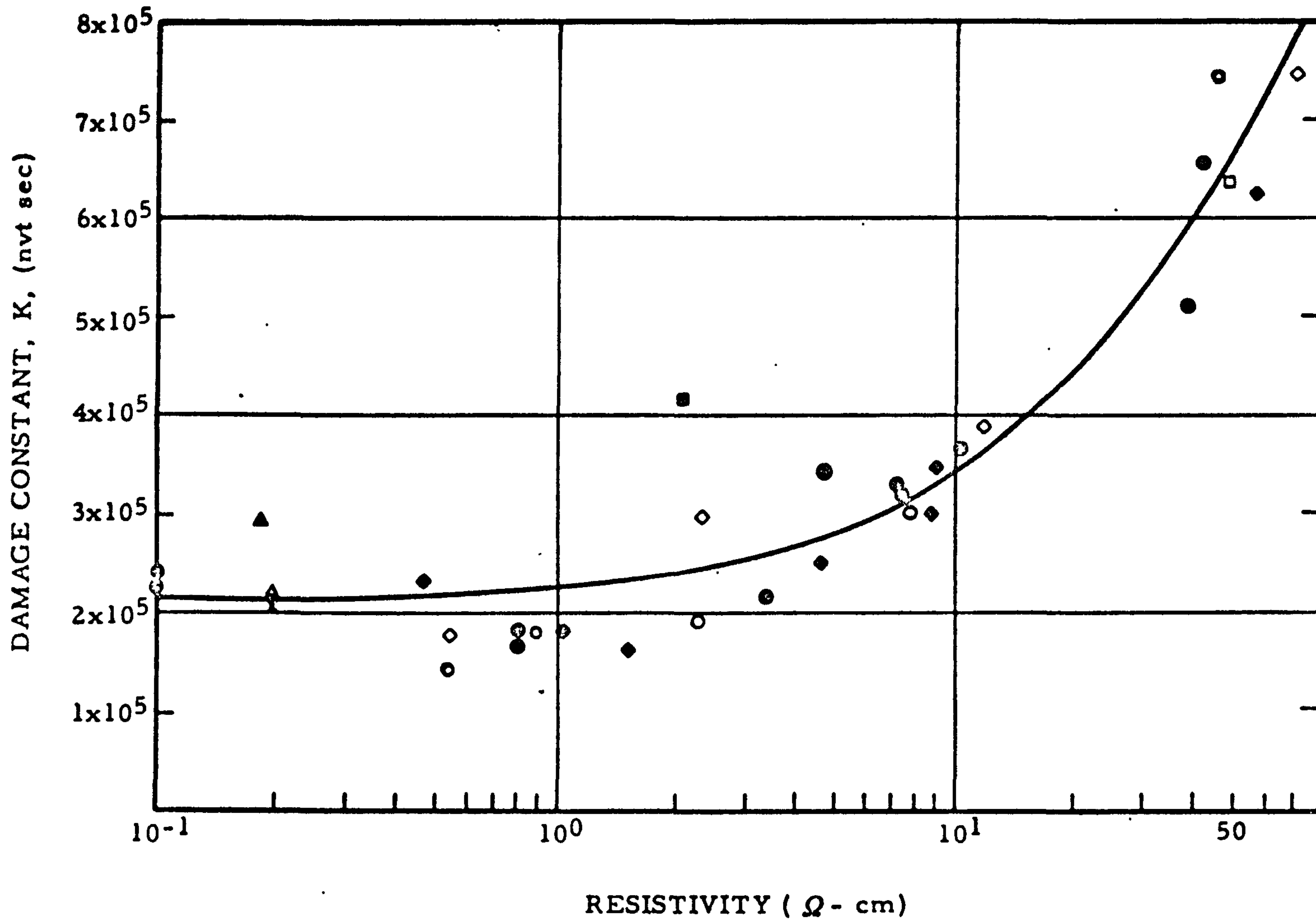

Figure 2. Damage constant vs resistivity for p-type silicon Curtis' data are given, showing least squares fit to Eq. (1b). Constants determined by the least squares fit are shown in Table Ia

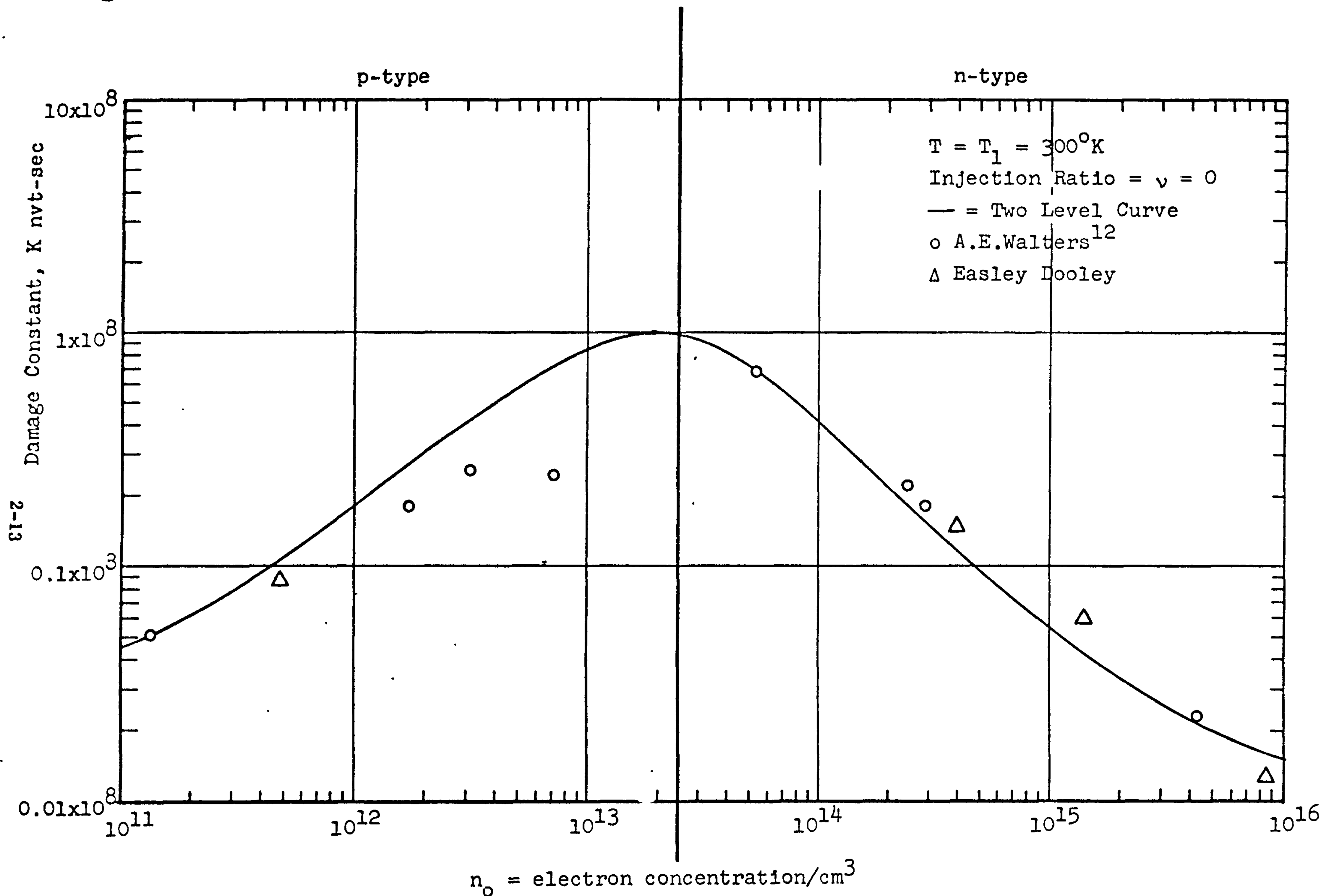

Figure 3. Lifetime damage constant vs equilibrium electron concentration for Germanium. A two level fit is shown for Walters[12] data. Constants are shown in Table Ib.

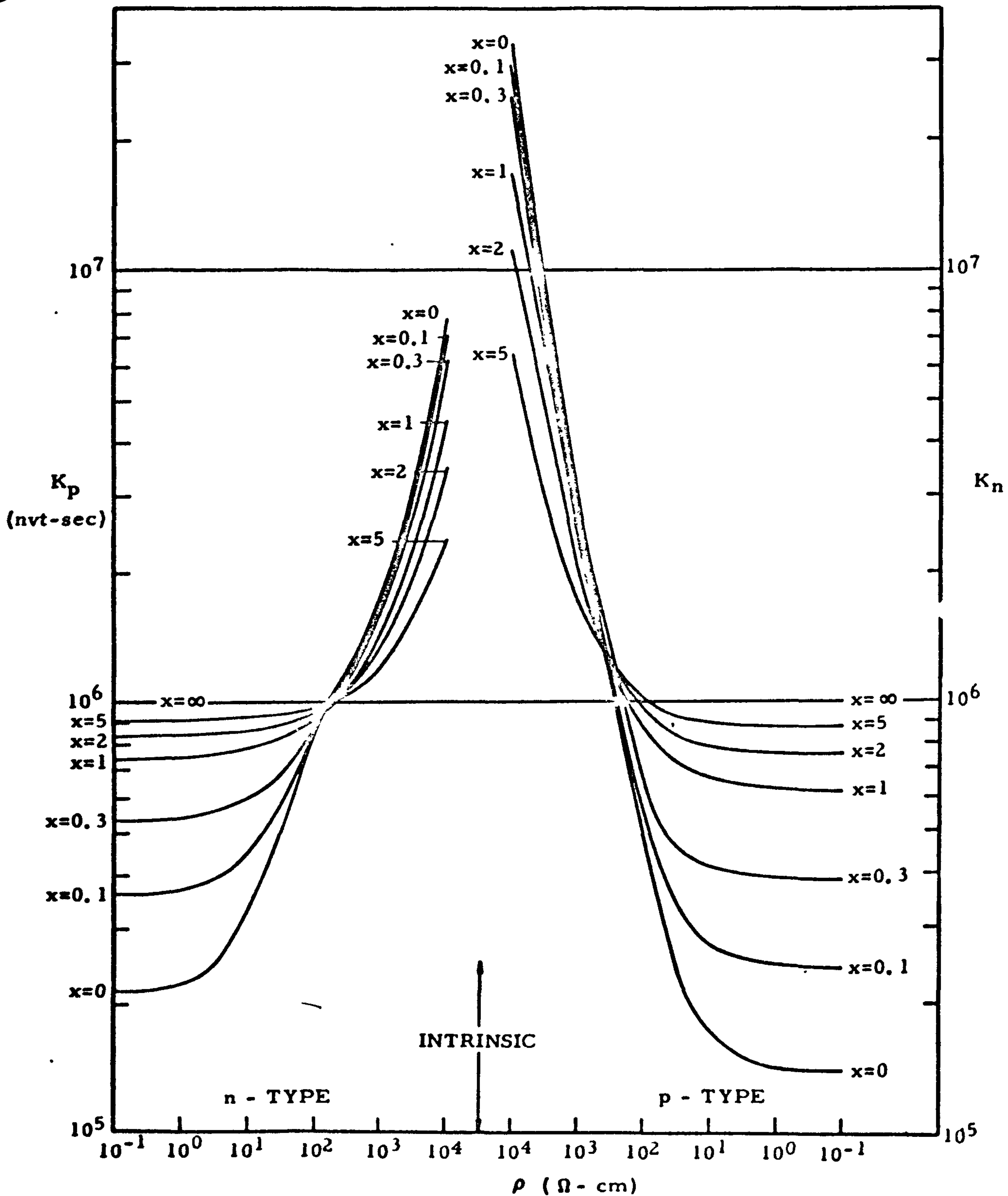

Figure 4. Lifetime damage constant K_n, K_p vs resistivity for various injection ratios, $x = \frac{\delta n}{[illegible]}, \frac{\delta p}{[illegible]}$. Equation (2) is plotted with constants from Table I. $\rho_n = 5.0[illegible] \times 10^{1[illegible]}/n_o$ and $\rho_p = 2.5 \times 10^{1[illegible]}/p_o$.

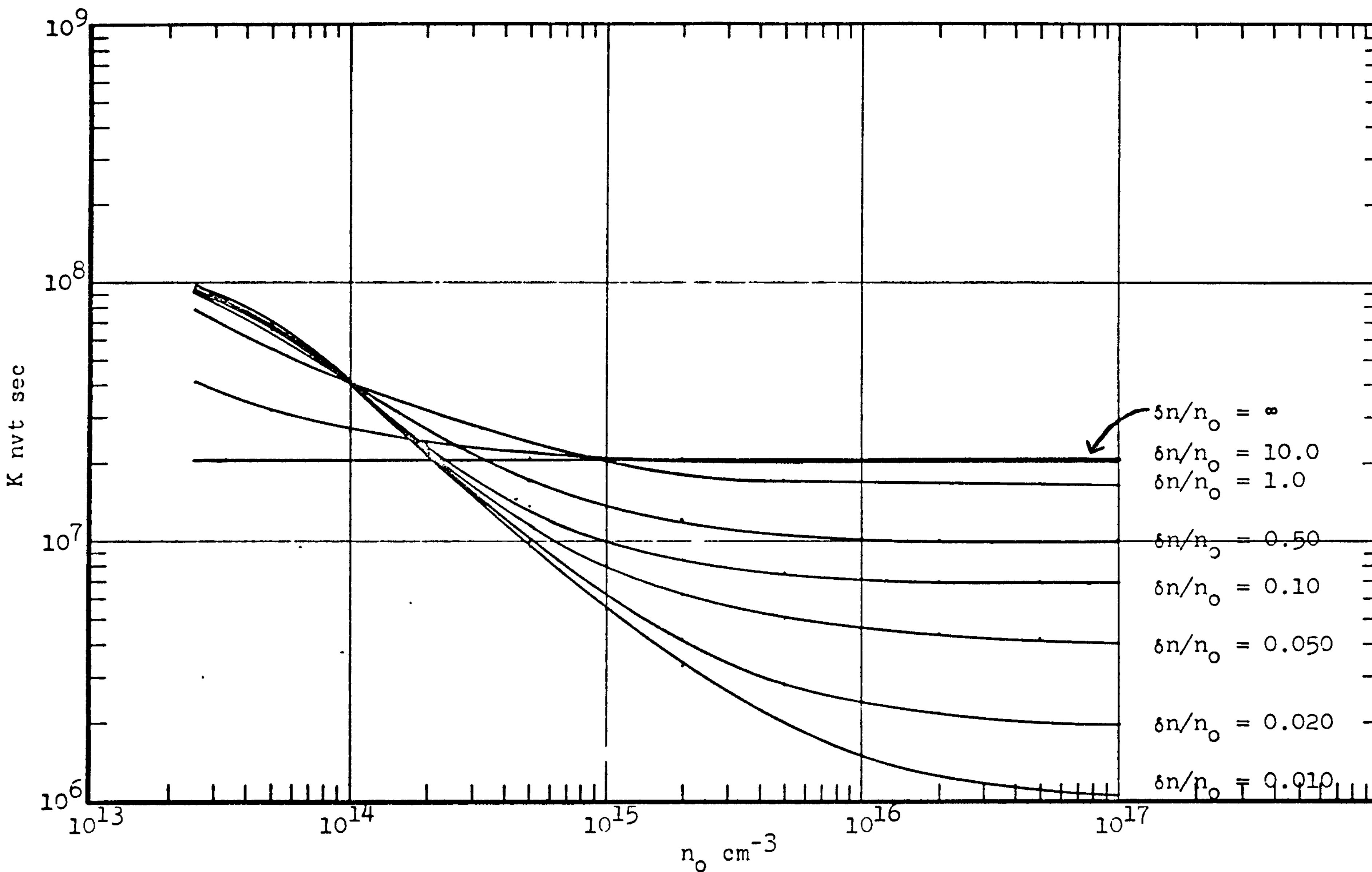

Figure 5. Germanium lifetime damage constant vs equilibrium electron density for various values of injection ratio.

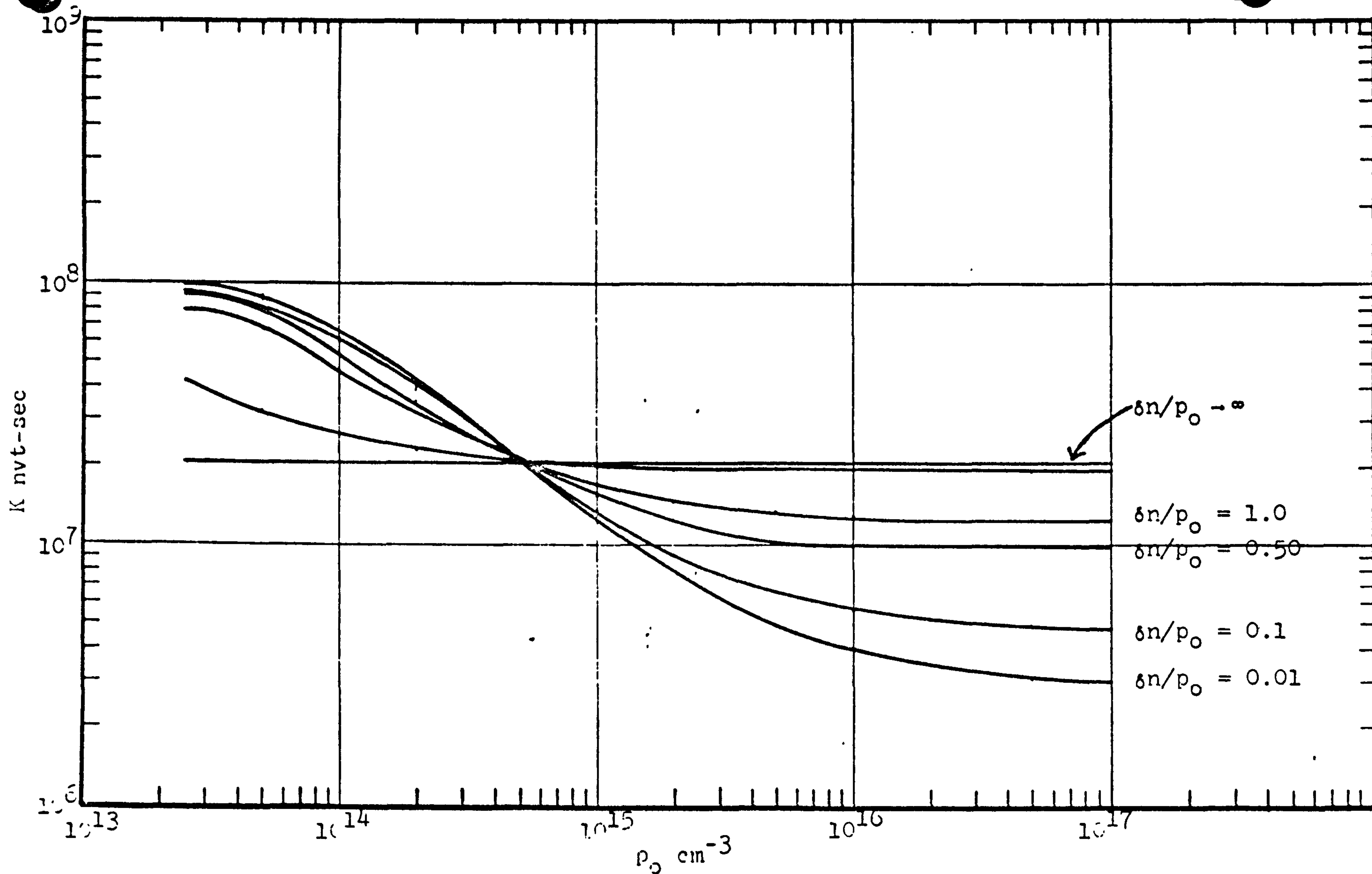

Figure 6. Germanium lifetime damage constant vs equilibrium hole density for various values of injection ratio.

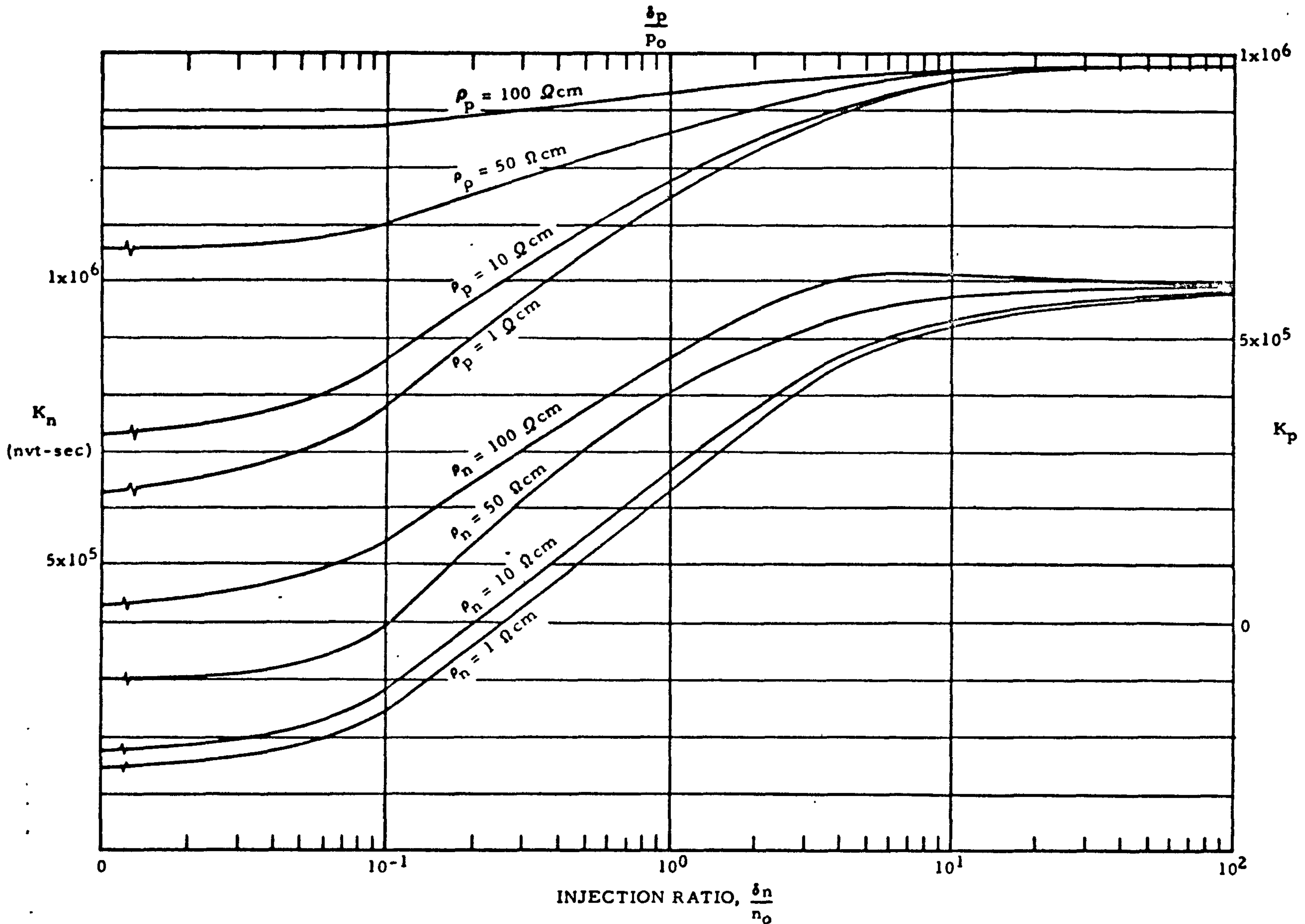

Figure 7. Lifetime damage constant K_n, K_p vs injection level $\frac{\delta n}{n_o}$, $\frac{\delta p}{p_o}$ for various resistivities. Equation (2) is plotted with constants from Table I. $\rho_n = 5.0 \times 10^{15}/n_o$ and $\rho_p = 2.5 \times 10^{16}/p_o$.

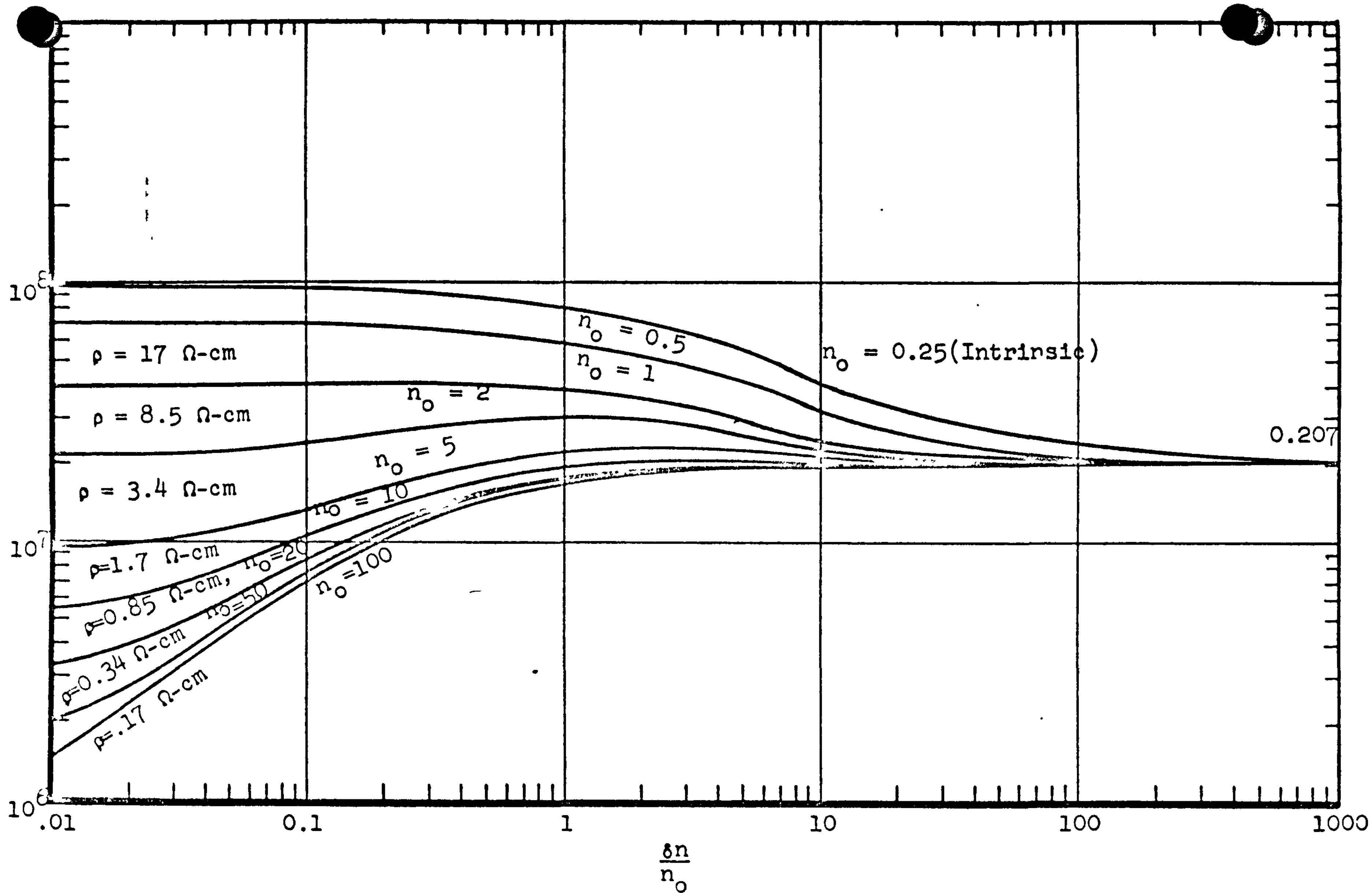

Figure 8. Germanium K_n as a function of injection ratio for various values of resistivity.

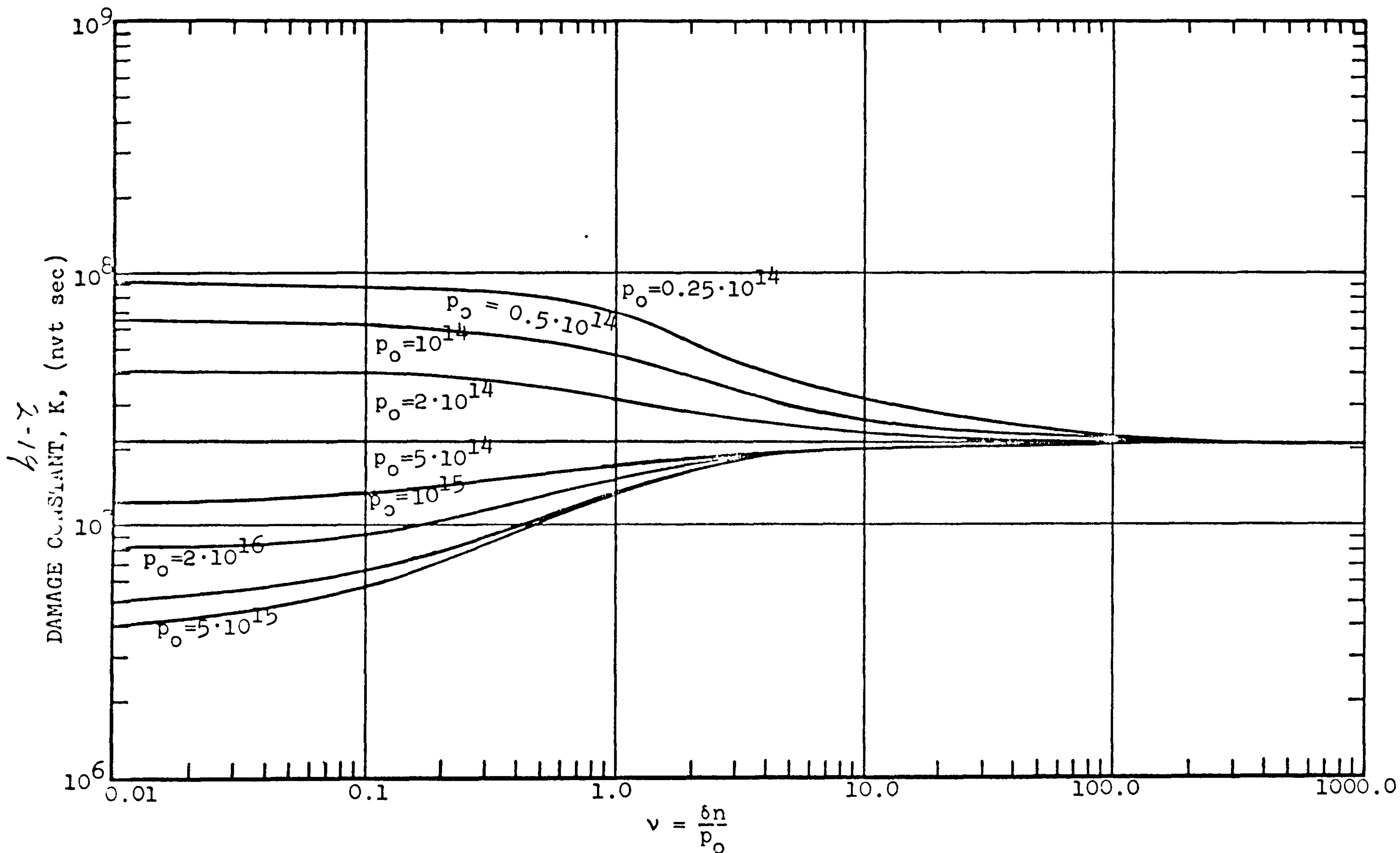

Figure 9. Germanium K_p as a function of injection ratio for various values of equilibrium hole density.

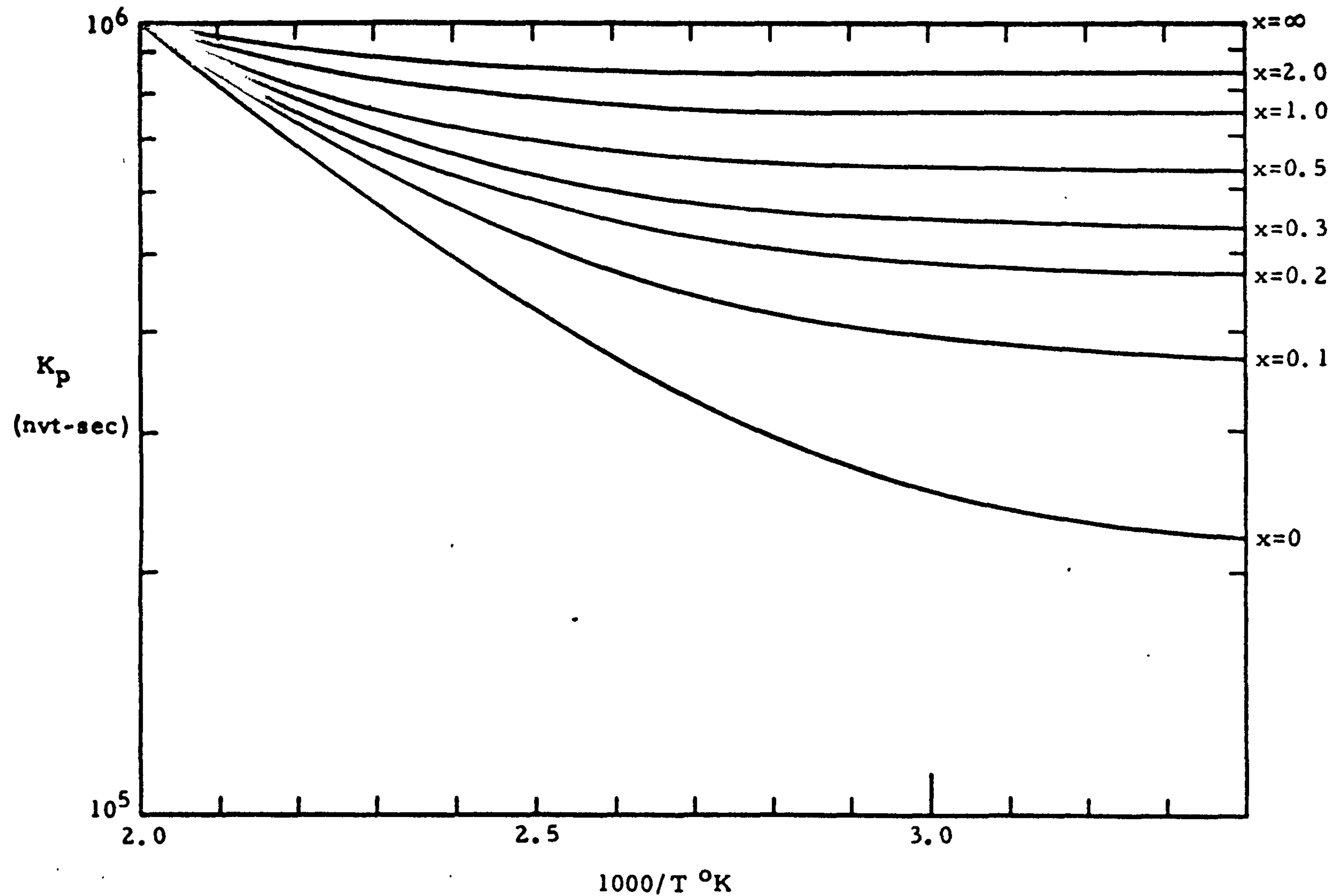

Figure 10. K_p vs $10^3/T^oK$ for $\rho_p = 1$ ohm-cm for various injection ratios, $x = \frac{\delta p}{p_o}$. Equation (5a) is plotted with constants from Table I.

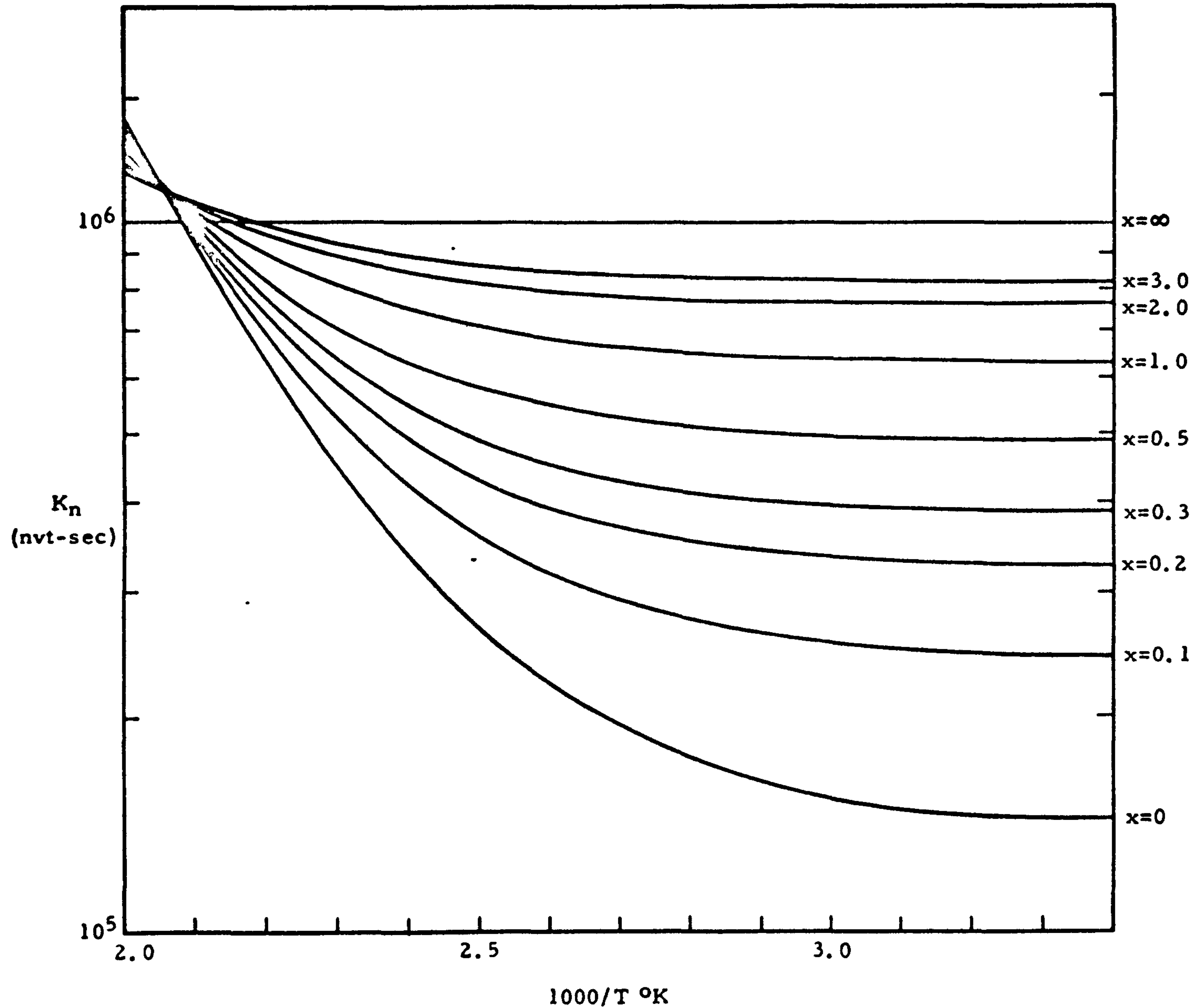

Figure 11. K_n vs $10^3/T\,^{o}K$ for ρ_n = 1 ohm-cm for various injection ratios, $x = \frac{\delta n}{}$. Equation (5b) is plotted with constants from Table I.

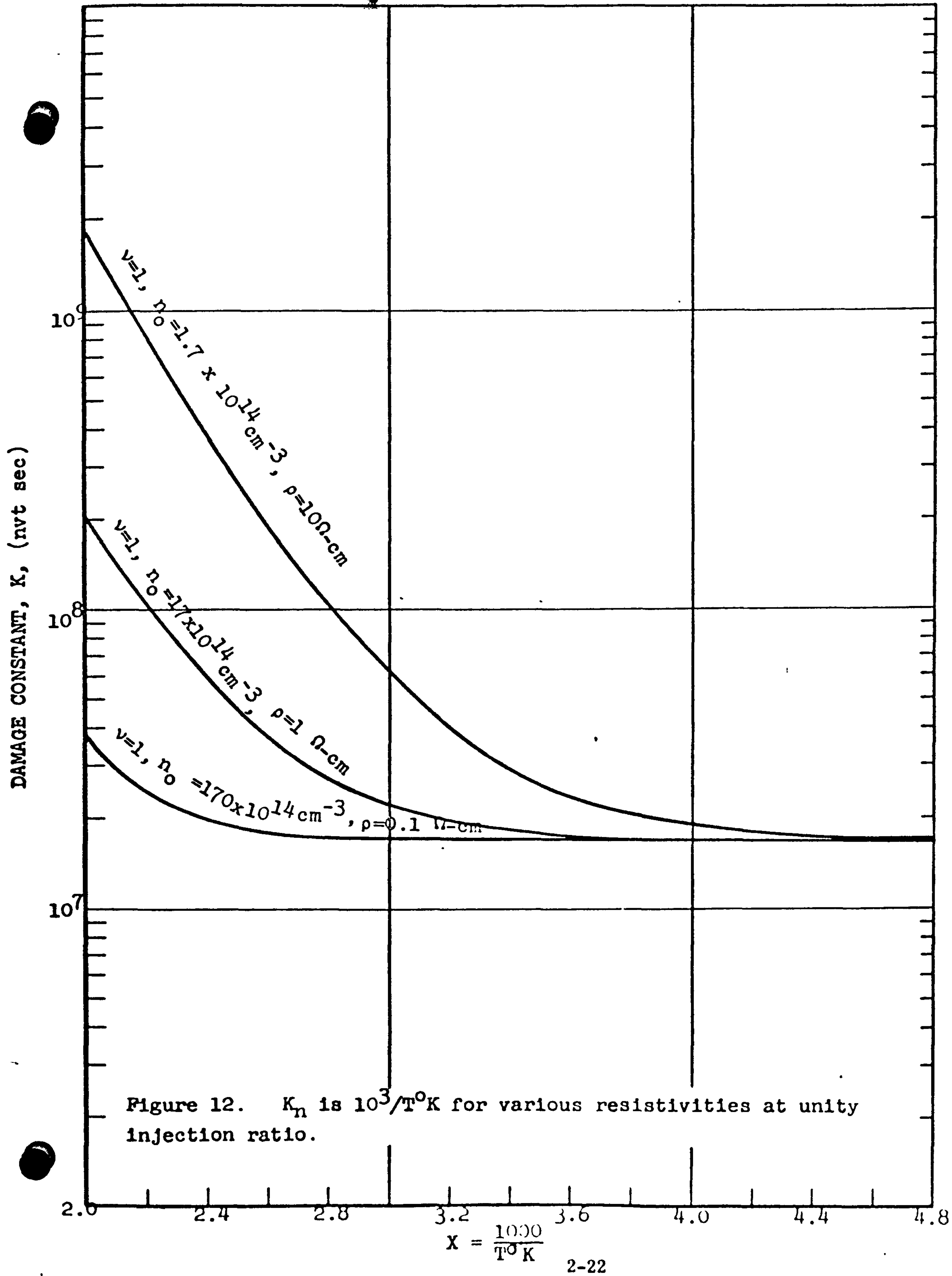

Figure 12. K_n is $10^3/T^oK$ for various resistivities at unity injection ratio.

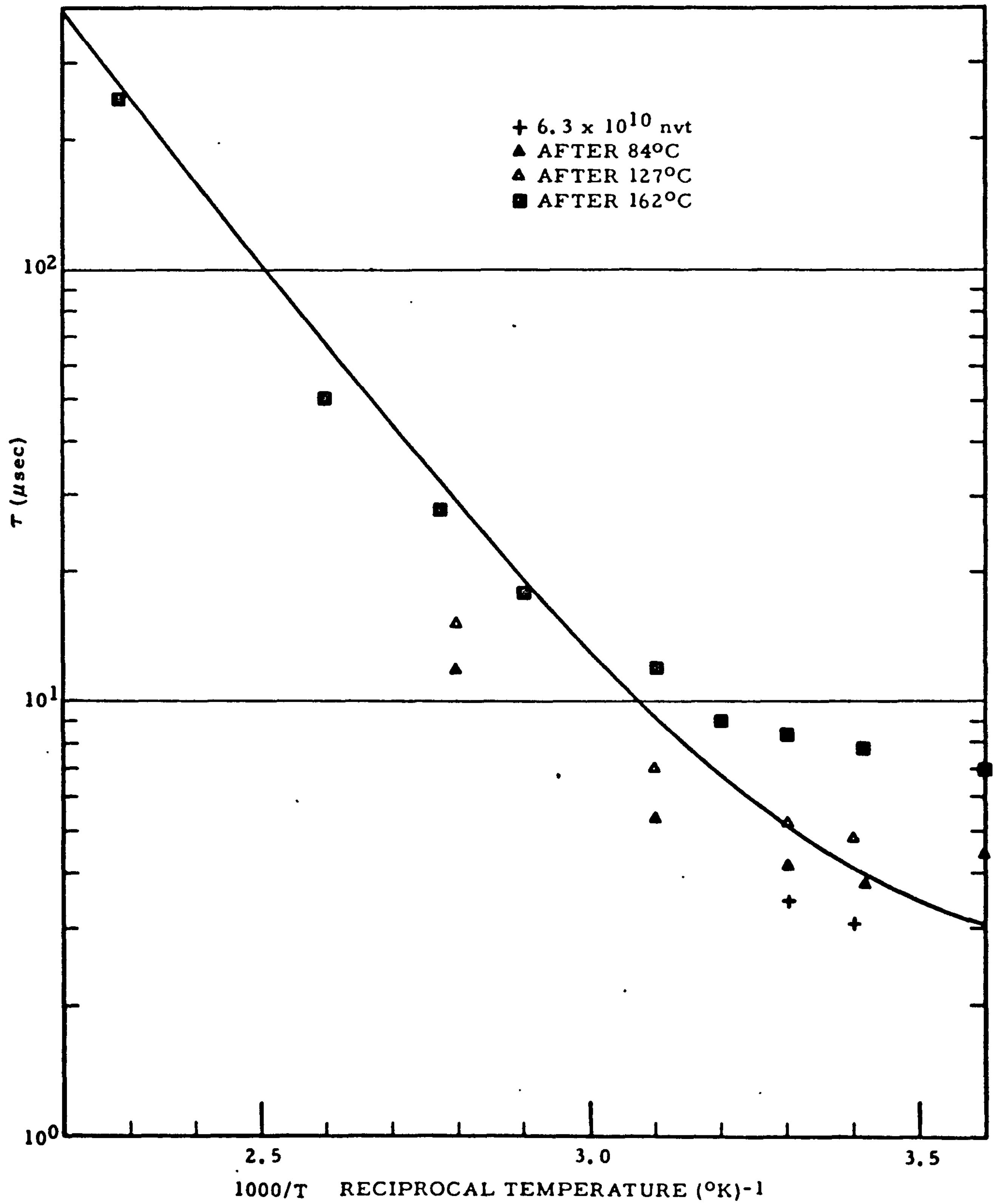

Figure 13. A comparison of Curtis' measured lifetime data with Eq. (5b) using the constants of Table I. $\rho_n = 58$ ohm-cm.

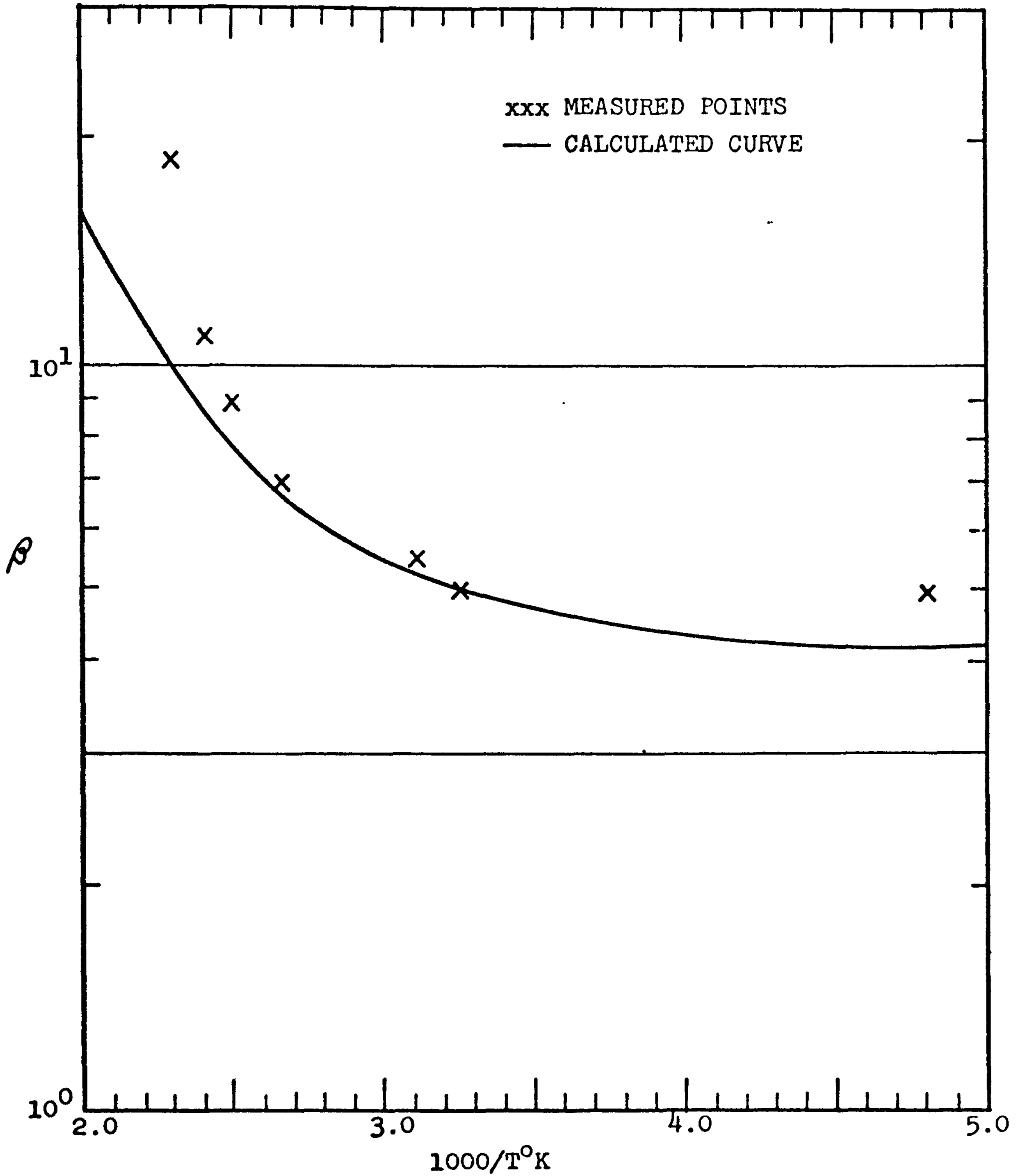

Figure 14. A comparison of Messenger's β vs $10^3/T^oK$ measured data with Eq. (5a) using the constants of Table I and the auxiliary relation [illegible] = 4.2 x 10^{-6}K. Transistor is [illegible]325 npn [illegible] n; [illegible] ~ 0.3, V_{CE} = 2.0 V, [illegible] = 8.0 ma, ϕ = 8.6 x 10^{13} n/cm², and ρ_b ~ [illegible] ohm-cm.

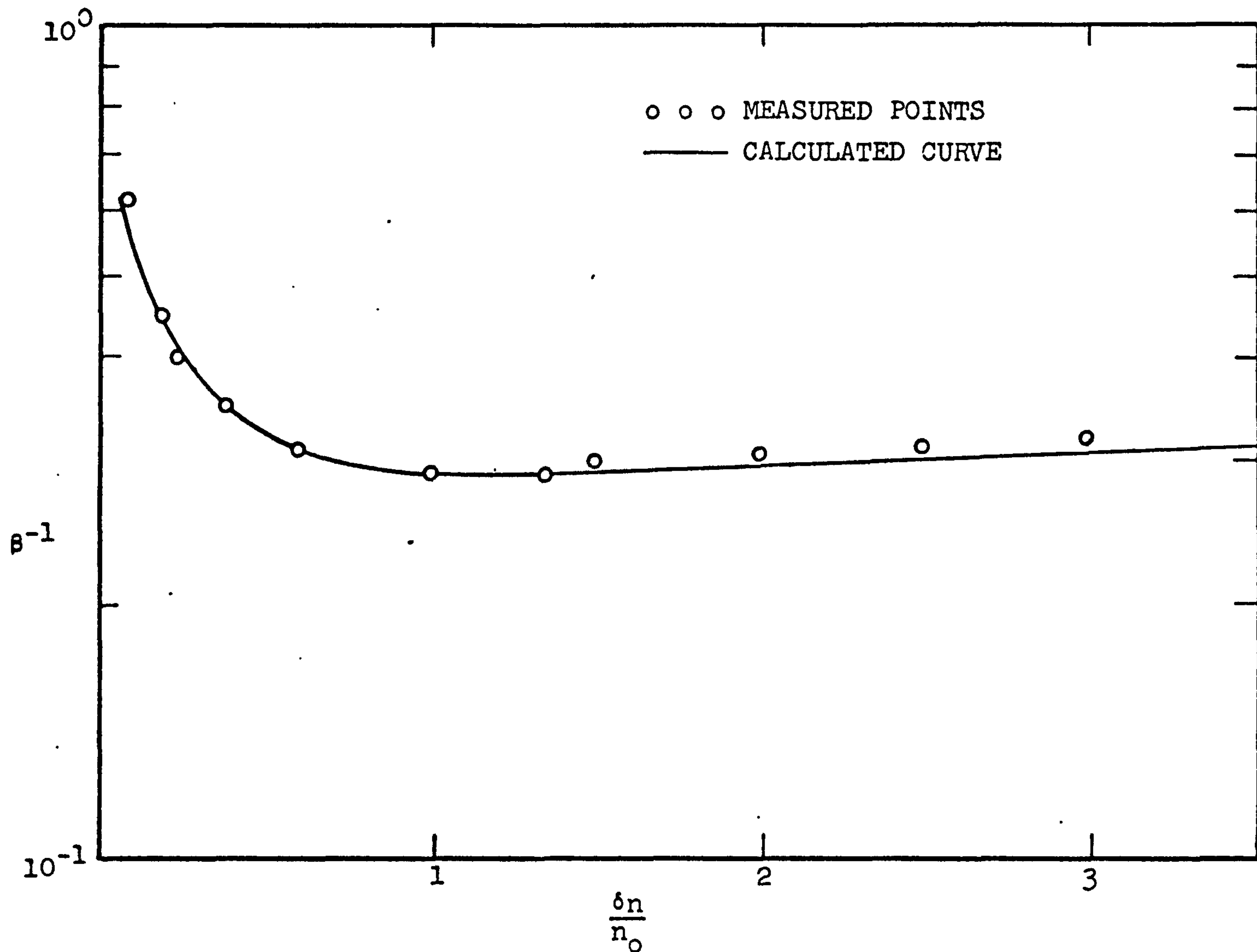

Figure 15. A comparison of Messenger's β^{-1} vs $\delta n/n_o$ data with Eq. (1) using the constants of Table I and the auxiliary relationship $\beta = 2.9 \times 10^{-6}K$. Transistor is 2N1655; $V_{CE} = 2.0$ V, $\phi = 5.0 \times 10^{12}$ n/cm^2, $\rho_b = 9.8$ ohm-cm.

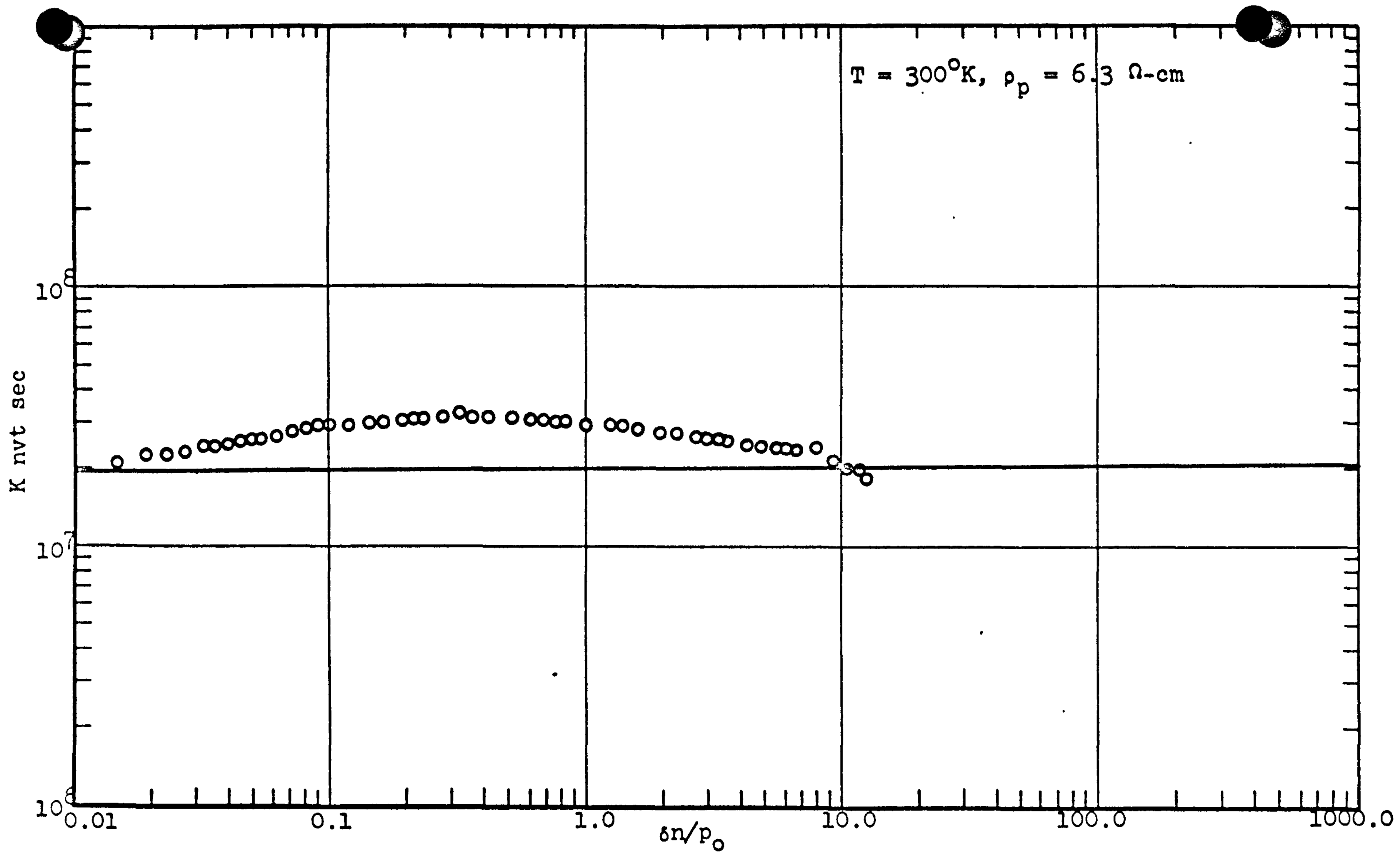

Figure 16. A comparison of K_p vs injection level derived from Messenger β^{-1} vs injection level data for 2N1308 transistor.

RADIATION EFFECTS ON MICROCIRCUITS

George C. Messenger
Nortronics, a Division of Northrop Corporation
Applied Research Department
Newbury Park, California

I Introduction and Summary

Microcircuit response to nuclear radiations has become an increasingly important concern over the past year. This discussion will consider transient radiation effects (TRE); a companion discussion will cover space radiation effects[1]. The interesting effects occur in two areas: displacement effects resulting from fast neutron irradiation, and ionizing effects caused by prompt pulses composed of x-rays and γ-rays. Fast neutron degradation of microcircuit performance is dominated by transistor current gain reduction. Current gain degradation in microcircuit transistor elements follows the same laws as current gain reduction in discrete transistors of similar base region design and geometry.

Ionization effects in monolitic p-n junction isolated microcircuits are usually about an order of magnitude larger than in comparable discrete element circuits. The dominant additional source of photoresponse is the large area substrate junction which gives rise to a very large photocurrent. The substrate junction in combination with the microcircuit p-n junctions close above it gives rise to parasitic diode and transistor elements. Primary and secondary photocurrents in these parasitics tend to dominate the overall response of the microcircuit.

These parasitics and their photocurrents are essentially eliminated by use of dielectric isolation. The problem of minimizing microcircuit transient responses has been considered. Pulse compensation techniques involve balancing photocurrents within the microcircuit, especially within the base region of transistor elements. The use of memory elements to return flip-flops to their pre-pulse condition is suggested. Additional elements in the microcircuits may be effectively used to desensitize critical subcircuits.

II Experimental Program

Test specimens were selected to determine radiation effects on modern microelectronic circuits and included three basic circuit types representing five different fabrication techniques. Circuit types included digital logic gates, flip-flops, and differential or digital sense amplifiers. Fabrication techniques included monolithic p-n junction isolated, monolithic dielectric isolated, multiple chip, thin film compatible, and thin film hybrid. The experimental matrix is shown in Table I.

The devices were tested at the Northrop TRIGA Reactor, at the General Atomic LINAC, at the Physics International Super Flash X-ray and at the Northrop Flash X-ray test facilities.

Experiments designed to determine the displacement damage effects in a reactor environment were generally performed on a "before" and "after" basis. Dynamic tests were performed on selected circuits, however, in an attempt to isolate the effects of the mixed neutron-gamma environment. The results indicated neutrons produce the predominant damaging effect, with only very minor variations due to a reduction in neutron-to-gamma ratio from 1.9 to 0.1. Sulfur-activiation powders were used to determine the integrated fast neutrons with energies greater than 2.9 MeV. The ratio of neutrons with energy greater than 10 keV (plutonium threshold) to neutrons with energy greater than 2.9 MeV (sulfur threshold) has been carefully determined for the Northrop reactor. This factor, 7.65, was used in order to report all data in terms of fast neutrons with the standard 10 keV threshold.

Measurement of the circuit transient response in the ionizing radiation environments required wide-bandpass instrumentation, of moderate gain, with effective x-ray and rf shielding. Several dosimetry techniques were used. The total dose was determined with the use of thermoluminescence powders and colbalt-glass chips. The radiation dose rate was determined from th waveform of a vacuum tube photodiode or a silicon diode and the measurement of total dose. The accuracy of the dosimetry was further checked by means of a correlation experiment with the Boeing Company involving the trade of test specimens and dosimetry.

III Displacement Damage

Fast neutrons degrade microcircuits by producing the same damaging effects which have been extensively studied in discrete devices. However, there are two differences worth comment. Microcircuits exhibit smaller "surface" effects than discrete devices, perhaps due to the carefully controlled protective oxide used on the surface throughout the fabrication process. The β degradation characteristic from microcircuit transistor elements is more uniform from device to device than in similar discrete transistors, reflecting another facet of the carefully controlled microcircuit processing technology.

There has been substantial progress in understanding the degradation produced in semiconductors by fast neutrons. The dependence of damage on incident neutron energy has been satisfactorily explained by Lindhard[2], and an experimental verification of the theory relating to ionization effects in silicon has recently been published[3]. This is directly applicable to displacement and ionization processes produced by fast neutrons in silicon microcircuits.

The current gain reduction in microcircuit transistor elements can be discussed exactly as for regular transistors[4].

$$\frac{1}{\beta} = \frac{1}{\beta_1} + \frac{0.2}{f_t}\left[\frac{\phi}{K(\rho_b,E_n)} + \frac{1}{\tau_1}\right]h(Z) + \frac{dI_{RE}}{dI_E}, \quad (1a)$$

$$\Delta\frac{1}{\beta} \approx \frac{0.2\phi}{f_t K(\rho_b,E_n)}, \quad (1b)$$

where

$$\frac{1}{\tau} = \frac{1}{\tau_1} + \frac{\phi}{K(\rho_b,E_n)} . \quad (1c)$$

Here β is small signal current gain, β_1 initial gain, f_t is gain bandwidth product, ϕ is neutron fluence, τ is transistor base lifetime, τ_1 initial lifetime, ρ_b is transistor base resistivity, E_n is neutron energy, h(Z) is a function of injection level, dI_{RE}/dI_E is a term accounting for recombination in the base emitter field region, and K is the damage constant.

Damage Constant as a Function of Incident Neutron Energy

Equation 1b is the approximation usually valid at the operating biases recommended for microcircuit operation. As indicated K is a function of neutron energy. Several authors have discussed the dependence of displacement damage on neutron energy [4, 5, 6]. Recently Lindhard[2] has used an approach based on energetics which divides the integrated results of neutron interactions into two classes, viz., atomic processes and electronic processes. The total energy E obtained from the incident neutron is assumed to divide between the two processes so that

$$\bar{n}(E) + \bar{\nu}(E) = E, \quad (2)$$

where $\bar{n}$ is the energy lost to electronic processes and $\bar{\nu}$ is the energy lost to atomic processes. A calculation of $\bar{n}(E)/E$ and $\bar{\nu}(E)/E$ as a function of incident neutron energy was then performed. Sattler[3] has obtained experimental verification of the theoretical function $\bar{n}(E)/E$ as a function of incident neutron energy for silicon. Smits[7] has established a ratio of 3 for the lifetime reduction produced by 14-MeV neutrons compared to the lifetime reduction produced by a Godiva fission spectrum. Smith[8] has taken the various energy-dependent neutron cross sections for the important neutron interactions with silicon, multiplied them by the appropriate functions $\bar{n}(E)$ E and $\bar{\nu}(E)$ E[9], summed both the electronic processes and the atomic processes, and has obtained curves of the energy going into atomic processes as a function of incident neutron energy (Figure 1) and a curve of the energy going into electronic processes as a function of incident neutron energy (Figure 17). If one assumes[10] that the number of recombination centers produced in silicon is proportional to the energy going into atomic processes, Smith's curve can be used to determine normalized damage constant as a function of incident neutron energy. Further, the damage produced by various neutron spectra can be compared using an integration technique. Smith's[8] curve can be transposed to a curve of σ vs incident neutron energy by dividing the ordinate by 94 MeV-mb (1 MeV mb = 3.4×10^{-13} rads-cm^2/neutron). Then the value of σ ($\sigma = K^{-1}$) for monoenergetic neutrons normalized to 1 MeV can be read directly from the curve. The effective value of K for a particular neutron spectrum is obtained by an integration process

$$K^{-1} = \sigma = \frac{\int_{0.01\ \mathrm{Mev}}^{\infty} \sigma(E)N(E)dE}{\int_{0.01\ \mathrm{Mev}}^{\infty} N(E)dE} .$$

where N(E) is the differential fluence of the incident neutrons. The lower limit of integration is taken as 0.01 MeV consistent with the accepted definition of fast neutrons; it is important to standardize on such a lower limit when comparing different spectra. The upper limit of integration can easily be made 15 MeV in practice.

Messenger's[4] curve for σ vs E_N is reproduced for comparison. It was obtained by fitting Smits'[7] experimental data to the function

$$\sigma = aE_n(1 - e^{-A/E_n}).$$

Here a = 1.02/MeV and A = 3.6 MeV. A comparison of Smith's curve with Messenger's earlier estimate shows that Messenger's averaging procedure obscured a substantial amount of fine structure in the curve.

Dependence of Lifetime Damage Constant on Resistivity

Curtis[11] has recently measured the dependence of lifetime damage constant on silicon resistivity at low injection levels. The experimental results are shown in Figures 2 and 3.

This behavior is expected for relatively shallow recombination centers near either band edge. Consider a recombination center below the conduction band. At low resistivities the Fermi level will be between the recombination center and the conduction band; consequently the recombination centers will be heavily populated with electrons and very efficient at capturing holes. At high resistivities the Fermi level will be below the recombination center; consequently the recombination centers will be lightly populated with electrons and much less efficient for capturing holes. Thus, one expects the damage constant to increase with resistivity[12]. p-type semiconductor material in the resistivity range 0.1 to 2.0 ohm-cm is normally used in microcircuit transistor bases; Figure 3 shows that K is relatively constant over this range of resistivity so that an average value may be used with confidence. The variation of K with resistivity shown in Figure 3 applies directly to transistors and microcircuits; however, the absolute magnitude will require correction[13]. A good average value

of K for microcircuit transistor elements is 1.5×10^6 nvt-sec. A direct comparison with unpublished electron degradation data obtained by Batelle on similar microcircuits showed that the damage produced by approximately 30 electrons per square centimeter of energy (3 MeV) is equivalent to the damage produced by one fast neutron.

Figures 1, 2, and 3 are the best presently available estimates for the variation of lifetime damage constant with incident neutron energy and transistor base resistivity. Since nearly all microcircuit transistor elements have a p-type base, Figures 1 and 3 will normally suffice for microcircuit application.

Gates

A number of gates (Table I) were evaluated to determine degradation in a fast neutron environment. The MC201G (Figure 4) is typical of the results obtained. Figure 5 shows the normalized small signal common emitter current gain as a function of fast neutron fluence. The uniformity in characteristic response from device to device is typical of microcircuit transistor elements and is several times better than that observed in comparable discrete transistors. Analyzing these results according to (1b) shows that $f_\beta K = 9.8 \times 10^{12} \pm 2.0 \times 10^{12}$ n/cm^2 with $f_\beta (= f_t/\beta) \approx 7 \times 10^6$/sec and $K \approx 1.4 \times 10^6$ nvt-sec.

The current gain decrease degrades gate performance by reducing fanout capability; finally the gain drops below 2.1, the minimum gain required to drive another similar gate (fanout of 1). This is shown in Figure 6. There are several other interesting gate degradation characteristics: transfer function is shown in Figure 7, threshold and saturation voltages are shown in Figure 8, and leakage currents are shown in Figure 9. Consideration of Figures 6, 7, 8, and 9 indicates transistor current gain is the predominant cause of performance degradation in microcircuit gates.

Flip-flops

A group of flip-flops compatible with the gates discussed above were evaluated for neutron degradation. The SE124K, Figure 10, is typical. Analysis of flip-flops was partially frustrated by inability to measure characteristics of individual microcircuit elements due to lack of terminals. One expects the transistors to degrade like those measured for Figure 5. When the closed loop gain in the flip-flop drops below unity, the circuit will not operate. The degradation of "off" voltage, saturation voltage, and minimum pulse amplitude required to switch are shown in Figure 11 for the Q output.

Amplifiers

The amplifiers studied included differential amplifiers, digital buffer amplifiers, and gated sense amplifiers. Transistor current gain decrease was the predominant cause of circuit degradation and failure. The MC1525 (Figure 12) is typical; pre- and post- irradiation transfer characteristics are shown in Figure 13. Current gain degradation is shown as a function of flux in Figure 14. Again note the uniformity from device to device. Microcircuit differential amplifiers maintain their balance during degradation significantly better than differential amplifiers made from discrete devices. This is probably due to the increased uniformity resulting from fabrication of both sides of the amplifier close together on the same chip.

Another typical circuit is the gated sense amplifier (Figure 15) whose transfer characteristics are shown as a function of neutron fluence in Figure 16.

Significant Conclusions

Fast neutron induced microcircuit performance degradation results directly from current gain decrease in the transistor elements. Other changes such as increased leakage currents are not large enough to significantly contribute to circuit malfunctions.

Degradation in microcircuit performance from device to device is more uniform than with similar discrete component circuits.

No significant differences in neutron degradation exist between the five fabrication techniques tested.

IV Ionization Effects in Microcircuits

Experiments to measure ionizing radiation effects necessarily involve short-duration pulses which are inevitably accompanied by rf interference or noise of electromagnetic nature. Therefore, extensive shielding was felt to be mandatory and measures were taken in designing appropriate instrumentation to minimize these effects.

To minimize the rf interference, only the test specimens and their loading circuits were exposed to the radiation beam. The operating controls were enclosed in an aluminum box, with fixtures for additional lead shielding of the cathode follower vacuum tubes, which were the only vulnerable components of the system. To further eliminate rf noise, storage batteries were employed for dc bias supplies and all remote control cabling was decoupled at the entrance of the box.

To minimize charge-scattering and air-ionization effects during irradiation, the test specimens and logic loads were completely enclosed in potting compound (Sylgard), exposing only the pickup connections. The applied biases and output-monitoring pickups were completely shielded from the radiation beam.

Despite these precautions there was evidence of charge scattering effects in the transient response of the test circuits, especially at circuit nodes where the impedance to ground was high.

Basic Effects

High energy radiation produces hole-electron pairs in silicon. These changes move under the influence of concentration gradients and electric fields producing photocurrents. After the radiation pulse, the induced charges recombine at a rate determined by the minority carrier lifetime. Usually, however, microcircuit bias currents remove the radiation-induced charge in a time much shorter than the minority carrier lifetime. In a continuous radiation environment, an equilibrium is established between the carrier generation process, and carrier removal processes which include recombination and bias currents.

The carrier generation rate depends only on the rate of energy absorption through electronic processes and not on the type or spectrum of incident radiation[14].

$$g = k\dot{\gamma} = 4 \times 10^{13}\dot{\gamma} \quad . \qquad (3)$$

Here g is the generation rate-electron hole pairs per cm^3/sec, $\dot{\gamma}$ is the energy absorption rate in rads/sec, and k is 4×10^{13} electron hole pairs per cm^3/per rad for silicon. The short circuit photocurrent in a p-n junction resulting from a radiation pulse has been derived by Wirth[15].

$$i = qgA \left\{ W_{SC} + L \left[\mathrm{erf}\left(\frac{t}{\tau}\right)^{\frac{1}{2}} - \mathrm{erf}\left(\frac{t - t_p}{\tau}\right)^{\frac{1}{2}} \right] \right\} \qquad (4)$$

Here g is electronic charge, A is junction area, W_{SC} is width of p-n junction field region, t is time, τ is minority carrier lifetime, L is minority carrier diffusion length and t_p is the pulse width.

Energy absorbed in silicon from x-rays, γ-rays, electrons and protons goes almost entirely into electronic processes; for transient response calculation, $\dot{\gamma}$ in rads/sec is required from dosimetry measurements. Absorbed energy from neutrons divides between electronic and atomic processes as previously discussed. Figure 17 shows rads/g(Si) per n/cm^2 as a function of incident neutron energy which goes into electronic processes[8]. In a reactor experiment, the neutrons arrive with negligible time of flight for all neutron energies. Assuming a square pulse,

$$\dot{\gamma} = \frac{\int_0^\infty \bar{\nu}(E)N(E)dE}{t_p} \qquad (5)$$

A neutron spectrum produced at a substantial distance from the test specimen requires a further correction due to the dependence of time of flight on neutron energy. If neutron capture processes are important, ionization can also be produced by the resulting nuclear reactions.

For all types of radiation, very short pulses should be characterized by $\int_0^t \gamma dt$ in rads (Si) since charges are created in a time short compared to characteristic time for minority carrier recombination or response time of the circuit.

Isolation Junction and Parasitic Elements

Monolithic microcircuits differ from their discrete element counterparts because of the built-in isolation between circuit elements and between circuit elements and substrate. The monolithic and compatible microcircuits (columns 1 and 3 of Table I) use p-n junction isolation; the monolithic circuits (column 4, Table I) use a silicon dioxide dielectric region for isolation; multiple chip and hybrid microcircuits (columns 2 and 5, Table I) are actually a miniaturized packaging of discrete elements and do not contain isolation regions.

The p-n junction isolation results in very large photocurrents between circuit elements and substrate. The silicon dioxide isolation, however, is almost as good as the isolation between discrete devices. The distributed nature of the devices, interconnects, and parasitic elements in p-n junction isolated microcircuits makes it difficult to devise simple and accurate equivalent circuits. Fortunately, the use of lumped elements is sufficiently accurate for most analysis in the radiation environment. It is now necessary to discuss individual microcircuit elements together with their parasitics.

The most troublesome element is the transistor. Figure 18 shows the transistor element along with the transistor parasitic element. If the gain of the parasitic pnp transistor is sufficiently low, its effect can be represented by a parasitic diode between collector and ground. The holes created in the n-type collector region may flow either into the transistor base region or the substrate region; the amount of current flowing into the transistor base is a function of the current gain of the parasitic transistor. Raymond[16] has analyzed this quantitatively using a Linvill "lumped" model equivalent circuit. His treatment provides analytical expressions for secondary photocurrent in the complex frequency domain. The photocurrent in a microcircuit transistor element is compared with the photocurrent from an equivalent discrete transistor in Figure 19. The substrate is grounded and the comparison is made for the limiting cases of base resistance $R_G \rightarrow 0$ and $R_G \rightarrow \infty$. At low irradiation levels, I_{pp} is proportional to $\dot{\gamma}$ and the difference between the microcircuit transistor and the discrete transistor is due to the substrate photocurrent. For the condition $R_G \rightarrow \infty$ ($R_G \approx 10$ kilohms is sufficient) and at higher levels of $\dot{\gamma}$ in the microcircuit transistor, the parasitic transistor drains some of the hole current originating in the transistor collector region to ground, preventing it from reaching the transistor base. This effectively reduces the secondary photocurrent in the microcircuit transistor. For the condition $R_G \rightarrow \infty$, the microcircuit transistor photocurrent is larger than the discrete transistor photocurrent at low $\dot{\gamma}$ levels, but is substantially lower at higher $\dot{\gamma}$ levels. The ability of the substrate photocurrent to reduce secondary photocurrent in microcircuit transistor elements is very important; a design which carefully balances the

photocurrent into the transistor base against photocurrents out of the transistor base and into the substrate, prevents secondary photocurrent and is very useful for hardening microcircuits.

Figure 20 shows equivalent circuits for diodes commonly used in monolithic microcircuits. Again, the parasitic transistors can often be replaced by parasitic diodes. Figure 21 is a capacitor equivalent circuit and Figure 22 shows two resistor types with the appropriate equivalent circuits. It should be noted that a substantial photocurrent will arise in resistor elements even though dielectric isolation is used since a p-n junction diode is used to isolate the resistor from the underlying semiconductor region. This underlying semiconductor region gives rise to photocurrents which tend to short circuit the resistor even though it is isolated from the rest of the substrate by the silicon dioxide.

The thin film passive elements did not show sufficient photo-response in any of the test circuits to contribute substantially to the observed microcircuit responses.

Photocurrents in Microcircuit Gates

Photocurrents produced in microcircuit gates must be analyzed using the complete equivalent circuit including parasitics; complete equivalent circuits vary in complexity from the MC201 to the A7WA. The MC201 is shown in Figure 23; the A7WA has the same equivalent circuit as shown for the MC201 in Figure 4. A typical set of response curves for the MC201 is shown in Figure 24. With the gate originally off, a turn-on transient appears at the output; this is a net result of photocurrents flowing into the base of the output transistor from its collector and emitter regions and photocurrents flowing out of the base through the pull-down resistor, the offset diodes, and the substrate junction. There is no evidence of secondary photocurrent. With the gate originally on, a turn-off transient appears. The photocurrents flowing out of the base region are larger than the photocurrents flowing into the base and the net effect is a transient reduction in output current. The transient vulnerability is seen to be different in the on state than it is in the off state. The transient at the input is negative. This cannot be understood by considering microcircuit photocurrents alone. Photocurrents from the offset diodes, input diodes, and bias resistor are into node e_1 and the substrate photocurrents are out of node e_1. The net effect should be a positive transient. A possible explanation for the negative transient is scattering of electrons into node e_1 during the pulse. This explanation is supported by experimental evidence using a dummy TO-5 can with an open-circuited transistor inside; here a similar negative pulse was observed. Examination of other gates has frequently shown the expected positive transient at e_1. The preferred explanation is that the net effect of photocurrents and electron scattering at this node are nearly balanced and that small changes in experimental variables may lead either to a positive or negative pulse. This illustrates the difficulty previously discussed of separating the expected microcircuit photocurrent and secondary electron scattering effects.

In general, p-n junction isolated microcircuits showed the greatest transient response, with the other microcircuit fabrication techniques producing transient responses approximately equal to those expected from similar discrete element circuits. This is illustrated by Figure 25. The MC201 shows nearly an order-of-magnitude more response at low radiation levels and reaches saturation nearly an order of magnitude lower in radiation levels than the XC201. This illustrates the reduction in photocurrents resulting from the use of dielectric isolation instead of p-n junction isolation.

Flip-flops

Flip-flops are relatively complex microcircuits; however, the major concern in a radiation environment is whether a change of state occurs.

Experimentally, the changes of state threshold is about 5 rads for a short pulse. Sometimes flip-flops reset in a symmetrical manner. That is, they come out of saturation into either of the two possible states with equal probability independent of the original state. Occasionally, a flip-flop is found which always comes out of saturation in the same state, independent of the original state. Such flip-flops have a built-in assymmetry resulting in a "preferred state." Figure 26 summarizes the experimental results for the SE 124 flip-flop driving an SE115G gate. This is typical of the flip-flops which responded in a symmetrical manner and contains some waveforms which show change of state and other waveforms which show a return to the original state. The duration of saturation is about 0.5 μsec. Table II summarizes the experiments performed with various loads at various radiation levels.

The monolithic p-n junction isolated flip-flops showed larger photocurrent responses and greater change-of-state vulnerability than the dielectric-isolated, multiple-chip, and hybrid units by almost an order of magnitude. This was very similar to the microcircuit gates.

Amplifiers

Amplifiers exhibit a transient response dominated by secondary photocurrent from the transistor elements. These circuits therefore spend an increasing amount of time in saturation as the radiation dose is increased. The PC-12 (Figure 25) illustrates this effect.

At dose rates of less than 5×10^6 rads (Si)/sec the output response of the PC-12 was negligible when the output was in the low voltage state. Above this level beta multiplication of first stage transistor primary photocurrent resulted in a large turn-off response at the output.

The output response with the output in the high voltage state was negative and a function of

photocurrent into the transistor base against photocurrents out of the transistor base and into the substrate, prevents secondary photocurrent and is very useful for hardening microcircuits.

Figure 20 shows equivalent circuits for diodes commonly used in monolithic microcircuits. Again, the parasitic transistors can often be replaced by parasitic diodes. Figure 21 is a capacitor equivalent circuit and Figure 22 shows two resistor types with the appropriate equivalent circuits. It should be noted that a substantial photocurrent will arise in resistor elements even though dielectric isolation is used since a p-n junction diode is used to isolate the resistor from the underlying semiconductor region. This underlying semiconductor region gives rise to photocurrents which tend to short circuit the resistor even though it is isolated from the rest of the substrate by the silicon dioxide.

The thin film passive elements did not show sufficient photo-response in any of the test circuits to contribute substantially to the observed microcircuit responses.

Photocurrents in Microcircuit Gates

Photocurrents produced in microcircuit gates must be analyzed using the complete equivalent circuit including parasitics; complete equivalent circuits vary in complexity from the MC201 to the A7WA. The MC201 is shown in Figure 23; the A7WA has the same equivalent circuit as shown for the MC201 in Figure 4. A typical set of response curves for the MC201 is shown in Figure 24. With the gate originally off, a turn-on transient appears at the output; this is a net result of photocurrents flowing into the base of the output transistor from its collector and emitter regions and photocurrents flowing out of the base through the pull-down resistor, the offset diodes, and the substrate junction. There is no evidence of secondary photocurrent. With the gate originally on, a turn-off transient appears. The photocurrents flowing out of the base region are larger than the photocurrents flowing into the base and the net effect is a transient reduction in output current. The transient vulnerability is seen to be different in the on state than it is in the off state. The transient at the input is negative. This cannot be understood by considering microcircuit photocurrents alone. Photocurrents from the offset diodes, input diodes, and bias resistor are into node e_1 and the substrate photocurrents are out of node e_1. The net effect should be a positive transient. A possible explanation for the negative transient is scattering of electrons into node e_1 during the pulse. This explanation is supported by experimental evidence using a dummy TO-5 can with an open-circuited transistor inside; here a similar negative pulse was observed. Examination of other gates has frequently shown the expected positive transient at e_1. The preferred explanation is that the net effect of photocurrents and electron scattering at this node are nearly balanced and that small changes in experimental variables may lead either to a positive or negative pulse. This illustrates the difficulty previously discussed of separating the expected microcircuit photocurrent and secondary electron scattering effects.

In general, p-n junction isolated microcircuits showed the greatest transient response, with the other microcircuit fabrication techniques producing transient responses approximately equal to those expected from similar discrete element circuits. This is illustrated by Figure 25. The MC201 shows nearly an order-of-magnitude more response at low radiation levels and reaches saturation nearly an order of magnitude lower in radiation levels than the XC201. This illustrates the reduction in photocurrents resulting from the use of dielectric isolation instead of p-n junction isolation.

Flip-flops

Flip-flops are relatively complex microcircuits; however, the major concern in a radiation environment is whether a change of state occurs.

Experimentally, the changes of state threshold is about 5 rads for a short pulse. Sometimes flip-flops reset in a symmetrical manner. That is, they come out of saturation into either of the two possible states with equal probability independent of the original state. Occasionally, a flip-flop is found which always comes out of saturation in the same state, independent of the original state. Such flip-flops have a built-in assymmetry resulting in a "preferred state." Figure 26 summarizes the experimental results for the SE 124 flip-flop driving an SE115G gate. This is typical of the flip-flops which responded in a symmetrical manner and contains some waveforms which show change of state and other waveforms which show a return to the original state. The duration of saturation is about 0.5 μsec. Table II summarizes the experiments performed with various loads at various radiation levels.

The monolithic p-n junction isolated flip-flops showed larger photocurrent responses and greater change-of-state vulnerability than the dielectric-isolated, multiple-chip, and hybrid units by almost an order of magnitude. This was very similar to the microcircuit gates.

Amplifiers

Amplifiers exhibit a transient response dominated by secondary photocurrent from the transistor elements. These circuits therefore spend an increasing amount of time in saturation as the radiation dose is increased. The PC-12 (Figure 25) illustrates this effect.

At dose rates of less than 5×10^6 rads (Si)/sec the output response of the PC-12 was negligible when the output was in the low voltage state. Above this level beta multiplication of first stage transistor primary photocurrent resulted in a large turn-off response at the output.

The output response with the output in the high voltage state was negative and a function of

the primary photocurrent of the output transistor. At a dose rate of 2.8×10^6 rads(Si)/sec the response was less than 0.2 volt negative. At 1×10^8 rads(Si)/sec and higher dose rates the response was greater than 1.5 volts negative. Typical response waveforms are shown in Table III.

To understand the transient response of this device, first consider the high voltage output state in which the second stage transistor is "off" and the first stage transistor is "on". The first stage transistor then presents a low impedance to the base of the second stage transistor preventing secondary photocurrents from occurring. Therefore, the "on" response at the output is due simply to the primary photocurrent generated in the second stage transistor. Assuming the two transistors are identical, this value of primary photocurrent calculated for the second stage transistor with the output high will be valid for the first stage transistor when the output is low since the first stage transistor is now turned "off." The calculated photocurrents and corresponding dose rates are shown in the following table:

Dose Rate [rads(Si)/sec]	Primary Photocurrents			
	Device No.			Average
	3	4	7	
2.8×10^6	76 μa	136 μa	170 μa	127 μa
1.0×10^8	1.6 ma	1.8 ma	2.6 ma	2.0 ma
7.0×10^8	4.0 ma	4.8 ma	4.0 ma	4.3 ma

With the output in the low voltage state the input is grounded. A primary photocurrent of slightly more than 230 μa is required through the 3K input resistor to turn "on" the first stage transistor. This is assuming a 0.7 drop is necessary across the base to emitter junction of the first stage transistor. The photocurrents at the lowest dose rate are not large enough to cause the first stage to turn "on" which accounts for the negligible response at these dose rates. For the two higher dose rates the photocurrents are much greater than the 230 μa necessary to switch the first stage "on," resulting in secondary photocurrents because of beta multiplication in the first stage. The current flowing into the collector of the first stage must come from the base of the second stage as well as the power supply, resulting in the large positive "off" response at the output. This assumes a linear relationship of dose rate to primary photocurrent would require a dose rate of 5×10^6 for 230 μa. At dose rates higher than this the device response is dominated by the large "turn-off" response just described at the output when in the low state.

Latch-up

None of the microcircuits tested under this experimental program showed latch-up. However, the type of latch-up described by Kinoshita[17] has been experimentally produced on a p-n-p-n switch; this means that microcircuits with p-n junction isolation are potentially susceptible to this latch-up phenomenon. One of the virtues of dielectric isolation is that it precludes this type of latch-up.

Prediction

An equivalent circuit such as Figure 23 can be programmed on a computer using a transient analysis code such as NET, PREDICT, or CIRCUS and the transient output produced by a radiation driving function determined. This technique is qualitatively successful, and in some cases, good quantitative results have been obtained[18, 19]. Charge scattering effects, and imperfect equivalent circuit models combine to limit this technique at the preset time.

For many microcircuits, interesting aspects of the radiation response such as the approximate level of radiation required to produce saturation and the approximate length of time the circuit will remain in saturation after a radiation pulse can be calculated directly from the equivalent circuit using appropriate simplifying assumptions[20].

Significant Conclusions

Major differences in response to ionizing radiation exist between p-n junction isolated microcircuits and the other microcircuit fabrication techniques analyzed. Microcircuits fabricated with p-n junction isolation showed almost an order of magnitude greater photocurrents than those fabricated with dielectric isolation or from discrete components. Response of p-n junction isolated microcircuits was usually dominated by photocurrents from the isolation junction whereas the response of the other microcircuits was dominated by the photocurrents arising in the transistor and diodes.

Amplifiers always showed transistor secondary photocurrent effects. This resulted in increased circuit saturation time as the radiation level was increased. Flip-flops and gates usually showed only primary photocurrent responses.

Charge scattering effects are significant and often produce identifiable photoresponses in microcircuits. This results in a dependence of experimental results on the specific geometry of the experimental set-up including the encapsulant used, and limits the effectiveness of present prediction techniques. More work is required in this area.

Microcircuit vulnerability to short pulses occurs in the 1 to 10 rad(Si) region for the circuits tested. Most of the circuits were saturated in the ten to ten thousand rad environment but recovered in less than one microsecond providing transistor secondary photocurrents had not been excited; secondary photocurrents prolonged the saturation up to one hundred microseconds depending on the circuit and radiation level.

V Hardening

It is desirable to reduce the response of microcircuits to pulses of ionizing radiation. The experimental and analytical results obtained provide useful guidance for reducing transient responses. A major step is replacement of p-n junction isolation by dielectric isolation to eliminate large substrate photocurrents.

Pulse compensation techniques can be used to provide photocurrent cancellation especially in the base region of transistor elements where proper balancing can eliminate secondary photocurrents. It is economically more feasible to add specially tailored device elements to accomplish this in microcircuits than in discrete element circuits. This technique is very useful in gates and will be mandatory in amplifiers.

Figure 26 shows the current paths for an "off" gate and the equation and parameters involved in increasing the radiation "hardness" of the circuit by changing the design parameters.

To turn the gate on from the "off" condition, the base of the transistor has to go through a voltage swing of $V_{be_{off}}$ to $V_{be_{on}}$. As soon as V_{be} is larger than or equal to 0.6 volt, the collector photocurrent increases rapidly due to the creation of secondary photocurrent. By preventing V_{be} from reaching 0.6 volt, the secondary photocurrent effect will be minimized.

Referring to the schematic diagram in Figure 26, the transistor will be kept in the "off" condition if,

$$i_{rs}(t) + i_{dn}(t) \geq i_{pp}(t), \qquad (6)$$

where

$i_{rs}(t)$ is the pull-down resistor-substrate photocurrent

$i_{dn}(t)$ is the coupling diode photocurrent and

$i_{pp}(t)$ is the primary photocurrent of the transistor.

In the ideal case, the sum of the coupling diode photocurrent and the pull-down resistor-substrate photocurrent should be equal to the primary photocurrent for both the "on" and "off" conditions. For this condition, photocurrents in the base circuit balance each other and there is no net effect due to radiation if contributions from other parts of the circuit are assumed negligible.

When the sum of the coupling diode photocurrent and the pull-down resistor-substrate photocurrent is larger than the collector photocurrent, there is a net decrease in the normal current flowing in the base circuit. In this operating condition, the transistor will not turn on. However if,

$$i_{pp}(t) > i_{dn}(t) + i_{rs}(t), \qquad (7)$$

part of the i_{pp} flowing through the pull-down resistor will forward bias the base emitter junction and eventually turn on the "off" gate.

To prevent the base emitter junction from reaching a forward bias of 0.6 volt, the following inequality has to be satisfied.

$$i_{pp}(t) \leq \frac{0.6v + V_{dn} - V_{di}}{R_2} + i_{dn}(t) + i_{rs}(t) \qquad (8)$$

Equation 8 explicitly shows which design parameters can be varied to prevent the output transistor from generating large secondary photocurrent.

The curves on the right side of Figure 28 show the effect of the pull-down resistor on the change of collector current versus dose rate. By reducing the pull-down resistance, the threshold for creation of secondary photocurrent versus dose rate is moved from curve (a) to curve (b). A further reduction in pull-down resistance yields curve (c) which represents the normal generation of primary but no secondary photocurrent.

The photocurrent paths of an "on" gate are shown in Figure 29. In the "on" gate, there will be no problem if,

$$i_{pp}(t) \geq i_{dn}(t) + i_{rs}(t) \qquad (9)$$

If eq. 9 is satisfied, the photocurrents in the base circuit are either balanced out or unbalanced in the direction required to drive the already "on" transistor further into saturation. However, if

$$i_{pp}(t) < i_{dn}(t) + i_{rs}(t), \qquad (10)$$

the normal base current has to supply the difference needed to compensate for the photocurrent of the coupling diode and the substrate photocurrent of the pull-down resistor.

To keep the "on" transistor in saturation, the inequality presented in Figure 27 has to be satisfied. A rearrangement of these equations gives

$$i_{pp}(t) \geq \frac{V_1}{\beta R_L} + \frac{V_{dn} + V_{be} - V_1}{R_1} + \frac{V_{be} + V_2}{R_2} + i_{dn}(t) + i_{rs}(t) \qquad (11)$$

where β is common emitter forward current gain of the transistor and V_{be} is the base to emitter voltage which is normally at 0.8 volt. Since $i_{pp}(t)$ in eq. 11 is an undesirable radiation effect that cannot be eliminated, it cannot be considered a variable parameter for improving the vulnerability of the circuit. A logical approach is to select materials and devices with the smallest $i_{pp}(t)$ that the state-of-the-art can provide and then vary the parameters on the right hand side of eq. 11 to improve the radiation

vulnerability of the circuit. It is apparent from . 8 and 11 that a change in a design parameter one direction may decrease the radiation response of the gate in one state but increase it in the other.

Table IV gives some of the design parameters which can be varied to improve the radiation resistance of the circuit. Also included are suggestions on how they should be changed to accomplish this.

As shown in the table, the transistor current gain should be maximized for the "on" state so that the transistor will be driven further into saturation. In the "off" state, especially when the secondary photocurrent is created by radiation, the transistor current gain should be small to minimize the radiation effect. All other parameters in the table should be changed in such a way so as to drive the "on" transistor further into saturation and to prevent the "off" transistor from turning on. Since, in most cases, the gate circuits have different responses in the two different states, the most vulnerable state determines the vulnerability of the circuit. The change of design parameters is often aimed at improving the radiation resistance of one state and accepting the associated increase in sensitivity of the other. A final set of compromise design parameters is obtained so that the circuit has the maximum overall radiation resistance.

It is desirable to add a memory element to flip-flops, directing them to return to their initial state upon emerging from saturation. In the past, magnetic components have been used to accomplish this. The experimental results on some flip-flops have shown a preferred state after irradiation. This leads one to speculate about additional components which would make the preferred state after irradiation always the same as the pre-irradiated state. A voltage dependence capacitor attached from collector to ground on both sides of the flip-flop is one possibility.

VI Conclusions

A review of experimental data in the transient radiation environment available on a variety of contemporary microcircuits of various construction techniques has been presented. It has been demonstrated that the well-known neutron degradation effect on transistor gain can be directly extended to microcircuits. A large photocurrent arising in the p-n isolation junction of monolithic microcircuits has been shown to dominate the transient response of these devices. Microcircuits with dielectric isolation or discrete elements are preferred for use in the ionizing radiation environment. The experimental results have been used as a basis for suggesting hardening techniques for the ionizing radiation environment which include pulse compensation, especially in the transistor base regions and the addition of internal memory elements to flip-flops.

The present understanding of basic mechanisms has been reviewed both for neutron displacement damage processes and the creation of hole electron pairs due to ionizing radiation. Charge scattering has shown up as an important experimental variable, and further work is suggested to understand better this phenomenon in microcircuits.

Acknowledgement

I would like to acknowledge helpful contributions from and discussions with J. Raymond, R. Johnson, W. Chang, and E. Steele. R. Caldwell provided valuable assistance in cross checking dosimetry measurements and circuit responses on microcircuits which we both have studied. Finally, acknowledgment is made of many helpful contributions made by RADC personnel who directly supported most of the work reported under Air Force Contract AF-30(102)3589.

Reference

1. D. Hamman, "Space Radiation Effects," 1966 Radiation Effects Conference

2. O. Lindhard, V. Nielsen, M. Sharff, and P.V. Thompson, Kgl. Danske, Selskab, Nat. Fys. Medd. 33, no. 10, 1963

3. A.R. Sattler, "Ionization Produced by Silicon Atoms Within a Silicon Lattice," Phys. Rev. vol. 135, no. 1A, June 1965

4. G.C. Messenger, "Displacement Damage in Silicon and Germanium Transistors," IEEE Transactions on Nuclear Science, NS-12 no. 2, April 1965

5. G.J. Dienes and G.H. Vineyard, Radiation Effects in Solids, Princeton University Press, 1961

6. D. Billington and J. Crawford, Radiation Damage in Solids, Princeton University Press, 1961

7. F.M. Smits and H.J. Slein, "Energy Dependence of Neutron-Damaged in Silicon Experiments," Bulletin of APS, Series 2, 9, no. 3, p. 289, March meeting

8. E.S. Smith, D. Binder, P.A. Compton, and R.I. Wilson, "Theoretical and Experimental Determination of Neutron Energy Deposition in Silicon," 1966 Radiation Effects Conference

9. Atomic recoil processes; proton and alpha particles give up nearly all their energy to ionization processes

10. This assumption may not be valid over a wide range of incident neutron energies, because the nature of the damage is believed to change from production of simple defects such as vacancy interstitial pairs to clusters as the incident neutron energy increases. Over the energy range from 0.01 to 14 MeV, this assumption is suggested as a reasonable estimate compatible with present

understanding of the processes leading to the formation of recombination centers. Experimental verification of this point requires a measurement of lifetime damage constant as a function of neutron energy for monoenergetic neutrons.

11. O.L. Curtis, Jr., "Effects of Oxygen and Dopant on Lifetime in Neutron Irradiated Silicon," 1966 Radiation Effects Conference

12. A similar argument applies to p-type material. The same behavior is also expected if the recombination center is located near the valence band in n-type material, or near the conduction band in p-type material.

13. Three factors are involved in this correction. The data has been taken at very low relative injection levels whereas transistor elements are normally operated at higher relative injection levels. Lifetime damage constants will increase with relative injection level for much the same reasons that it increases with resistivity. The data has been taken at neutron fluence levels between 10^{10} and 10^{11} n/cm^2; the range of interest for transistor elements is 10^{13} to 10^{15} n/cm^2. Thus it is possible that a dosimetry correction could be required. The numerical factor 0.2 in equation 16 involves the relationship between lifetime and transit time in the base. This relationship varies with the field in the base; the factor 0.2 is correct only for homogeneous bases.

14. R.F. Bass and O.L. Curtis, "The Use of Bulk Semiconductor Material for Absorbed Dose Measurements," IEEE Transactions, NS-12, no. 1, February 1965

15. J.L. Wirth and S.C. Rogers, "The Transient Response of Transistors and Diodes to Ionizing Radiation," IEEE Transactions, NS-11, no. 5, November 1964

16. J.P. Raymond and J. Willis, "Generalized Model Analysis of Ionizing Radiation Effects in Semiconductor Devices," IEEE Transactions, NS-12, no. 5, October 1965

17. G. Kinoshita, et al., "Radiation-Induced Regeneration Through the p-n Junction Isolation in Monolithic 1/C's," IEEE, NS-12, no. 5

18. R. Caldwell, private communication.

19. W.H. Sullivan and J.L. Wirth, "Methods for Measuring and Characterizing Transistor and Diode Large Signal Parameters for Use in Automatic Circuit Analysis Programs," IEEE, NS-12, no. 5

20. E.A. Carr, "Simplified Techniques for Predicting TREE Response," IEEE, NS-12, no. 5

TABLE I DEVICES STUDIED

	Monolithic Diffused Active and Passive Devices. p-n junction isolation.	Multiple Chip Several interconnected chips containing diffused active and passive devices.	Compatible Diffused Active Devices with thin film passive devices. p-n junction isolation.	Monolithic Diffused Active and passive Devices. SiO_2 isolation	Hybrid Diffused Active devices with thin film interconnects and passive devices.
GATES	[1]MC-201G - 8 (units tested) [1]MC-201F - 3 " " [2]SE-115G - 2 " " [3]RC-1031 - 6 " " [4]PF-801T - 2 " " [4]PF-800T - 2 " "	[5]A7WA - 8 (units tested)	[8]A11 - 8 (units tested) [3]RC401 - 8 " "	[1]XC201-G - 8 (units tested) [9]RD111 - 2 (units tested) [8]WX-1 - 1 (unit tested)	[10]M8214 - 8 (units tested)
FLIP FLOPS	[1]MC209G - 2 " " [2]SE124K - 2 " " [3]SE124G - 6 " " [5]SN337A - 2 " "	[7]PC-8 - 8 " "	[8]A16 - 8 " "	Not available	[10]M8107 - 8 (units tested)
AMPLIFIERS	[1]MC1525G - 9 " " [2]SE500K - 2 " " [5]SN3514 - 2 " " [6]NM1024 - 3 " " [6]NM2002 - 2 " "	[7]PC-12 - 8 " "	[1]MC1527-G - 8 (units tested) [6]NM2021 - 8 (units tested)	[6]NM3401 - 8 (units tested)	[10]M8201 - 8 (units tested)

Note: The superscript before the device description refers to the following manufacturer:
[1]Motorola, [2]Signetics, [3]Raytheon, [4]Signetics, [5]Texas Instruments, [6]Norden, [7]General Instruments, [8]CBS, [9]Radiation Incorporated, [10]Vare.

TABLE II SE124 RADIATION RESPONSE

Serial No.	Loading	Original State	Radiation Response (* Induced change of state; o No change)
K-1	Q - 220Ω Ext. R	Q = 1	
	$\bar{Q}$ - 220Ω Ext. R	$\bar{Q}$ = 1	
K-2	Q - MC201G DTL Gate	Q = 1	
	$\bar{Q}$ - 220Ω Ext. R	$\bar{Q}$ = 1	
G-4	$\bar{Q}$ - 1/2 SE115 Dual DTL Gate	Q = 1	
	Q - 1/2 SE115 Dual DTL Gate	$\bar{Q}$ = 1	
G-5	Q - 1000Ω Ext. R	Q = 1	
	$\bar{Q}$ - 220Ω Ext. R	$\bar{Q}$ = 1	
G-6	Q - 1000Ω Ext. R	Q = 1	
	$\bar{Q}$ - 220Ω Ext. R	$\bar{Q}$ = 1	
G-7	Q - 1000Ω Ext. R	Q = 1	
	$\bar{Q}$ - 220Ω Ext. R	$\bar{Q}$ = 1	
G-8	Q - 1000Ω Ext. R	Q = 1	
	$\bar{Q}$ - 220Ω Ext. R	$\bar{Q}$ = 1	

10^7 10^8 10^9 10^{10}

$\dot{\gamma}$ rad(Si)/sec

Note: No radiation-induced transitions were observed at flash x-ray levels [i.e., ~ 2×10^6 rads(Si)/sec]

TABLE III RESPONSE WAVEFORMS

Note: All voltages in volts. All times in microseconds

Radiation Source: Source	Radiation Source: rads (Si)/sec.	Input/Output Configuration	Response: Collector Supply	Response: Output
600 kV Flash X-ray $t_p \approx 200ns$	2.8×10^6	Low	0.12; 0.02; 0.1	Negligible
		High	0.11; 0.023; 0.031; 0.11	0.14; 0.17
Linac 10 MeV Electrons $t_p \approx 40ns$	1×10^8	Low	0.08; 0.92; 1.2; 1.2; 0.04; 0.02	13.0; 0.4
		High	0.15; 0.85; 0.88; 0.11	2.0; 0.16
	7×10^8	Low	0.13; 7.4; 4.0; 0.13	16.0; 6.0
		High	0.14; 7.2; 4.0; 0.14	0.12; 6.5; 4.3; 0.16

TABLE IV
DTL GATE VULNERABILITY PARAMETERS

TRANSISTOR CURRENT GAIN :	MAXIMIZE FOR "ON" STATE MINIMIZE FOR "OFF" STATE
COUPLING DIODE VOLTAGE DROP :	MINIMIZE FOR "ON" STATE MAXIMIZE FOR "OFF" STATE
COUPLING DIODE PHOTOCURRENT :	MINIMIZE FOR "ON" STATE MAXIMIZE FOR "OFF" STATE
PULL DOWN RESISTOR :	MAXIMIZE FOR "ON" STATE MINIMIZE FOR "OFF" STATE
PULL DOWN RESISTOR-SUBSTRATE PHOTOCURRENT :	MINIMIZE FOR "ON" STATE MAXIMIZE FOR "OFF" STATE
COLLECTOR SUPPLY VOLTAGE :	MAXIMIZE FOR "ON" STATE
PULL DOWN SUPPLY VOLTAGE :	MINIMIZE FOR "ON" STATE

PHOTOCURRENTS : IDEALLY, $i_{pp}(t) = i_{dn}(t) + i_{rg}(t)$

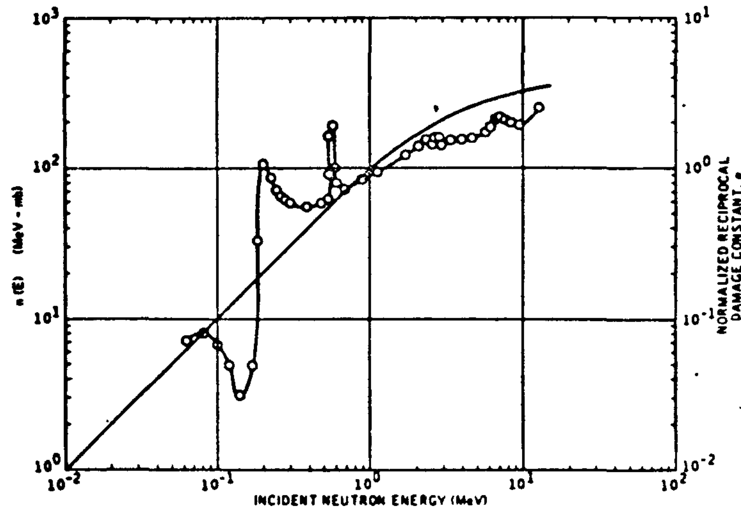

Fig. 1. Energy Going into Atomic Processes and Normalized Reciprocal Lifetime Damage Constant as a Function of Incident Neutron Energy.

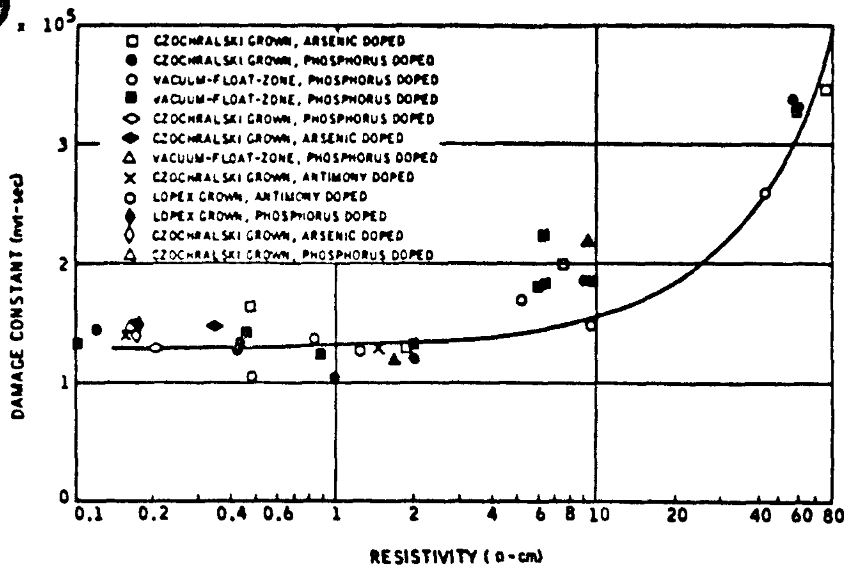

Fig. 2. Lifetime Damage Constant at Low Injection Levels as a Function of Resistivity for n-type Silicon.[11]

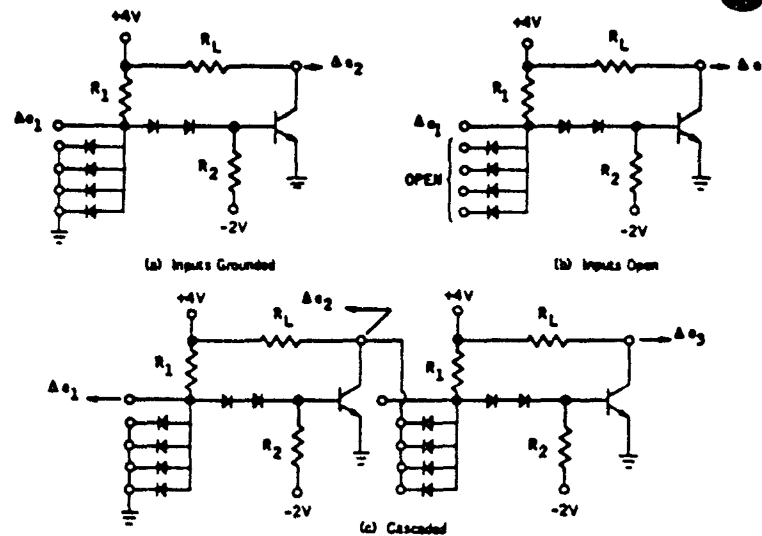

Fig. 4. MC201 Test Circuit Configuration.

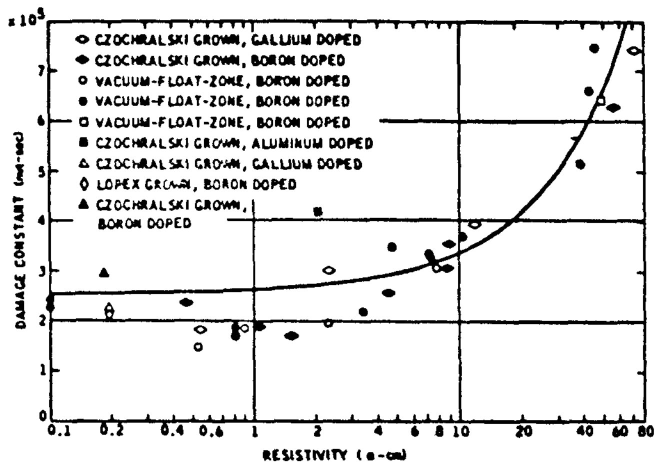

Fig. 3. Damage Constant at Low Injection Level as a Function of Resistivity for p-type Silicon.[11] (Boron is the impurity used in most commercial microcircuits.)

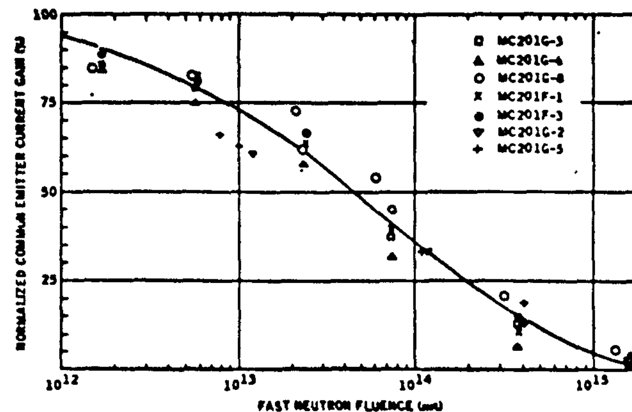

Fig. 5. MC201 Transistor Current Gain Degradation.

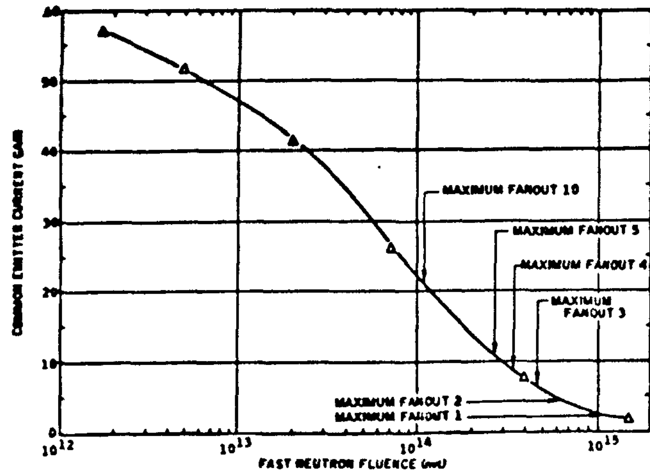

Fig. 6. MC201 Monolithic DTL Gate Circuit Vulnerability.

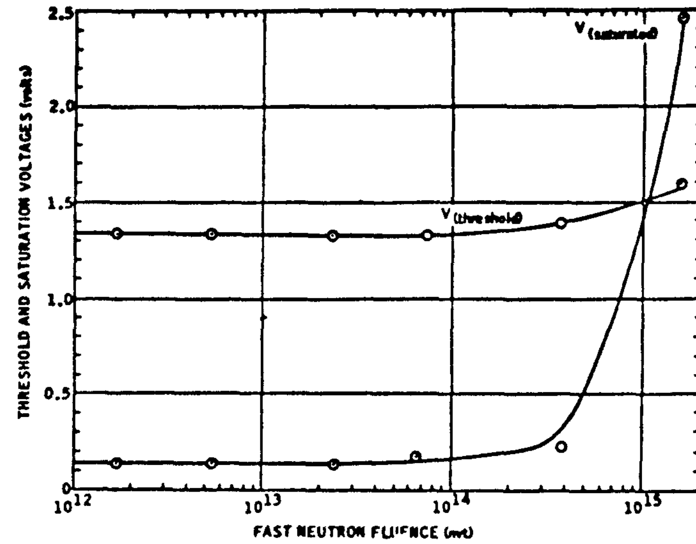

Fig. 8. Neutron Degradation of MC201-3 Threshold and Saturation Voltages.

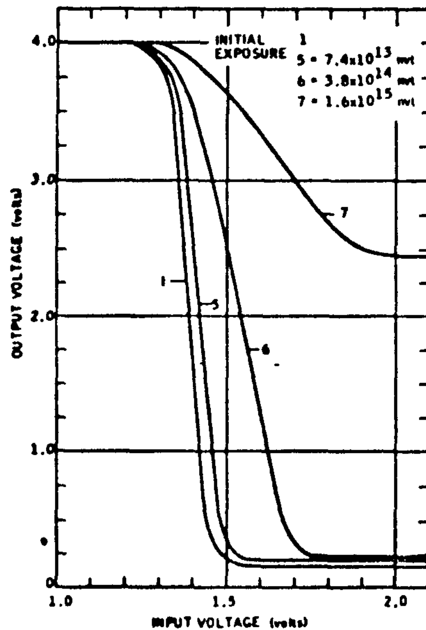

Fig. 7. Neutron Degradation of MC201F-3 Transfer Function.

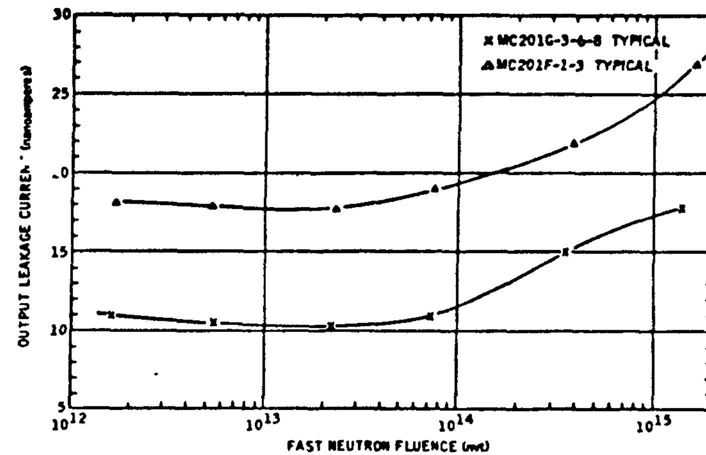

Fig. 9. Neutron Degradation of MC201 Output Leakage Current.

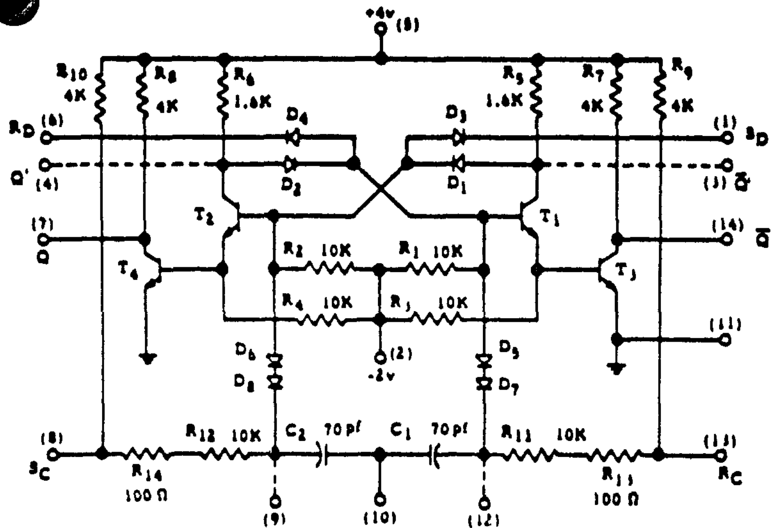

Fig. 10. Signetics SE124 Monolithic Binary Element

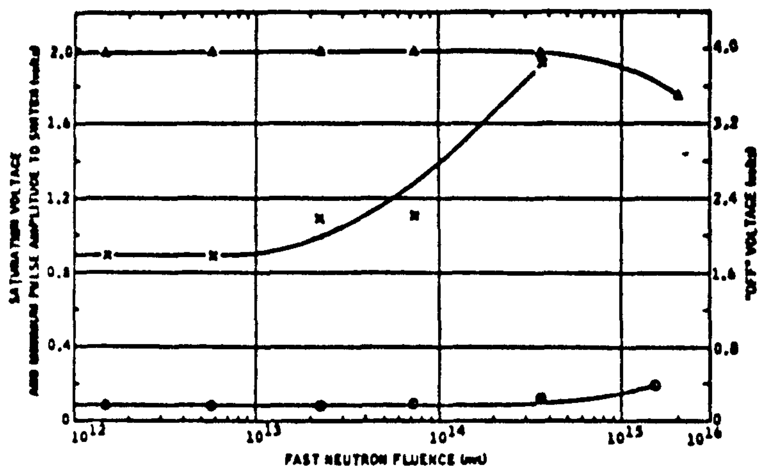

Fig. 11. Neutron Degradation of SE124K-1 "off" Voltage, Saturation Voltage, and Minimum Pulse Amplitude to Switch Q Output.

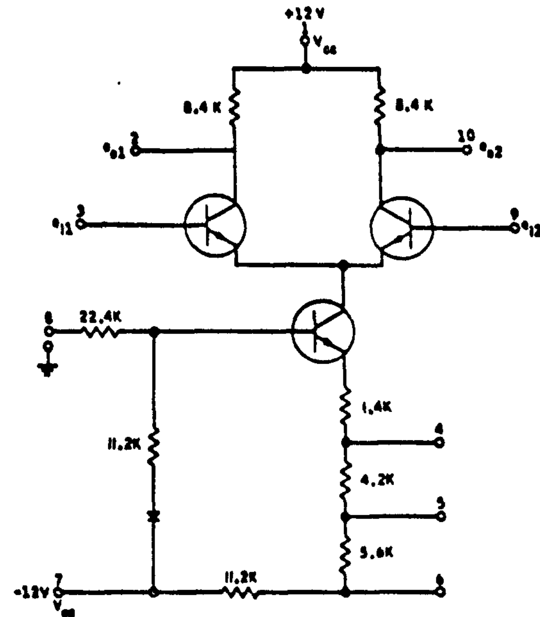

Fig. 12. MC1525 Monolithic Differential Amplifier.

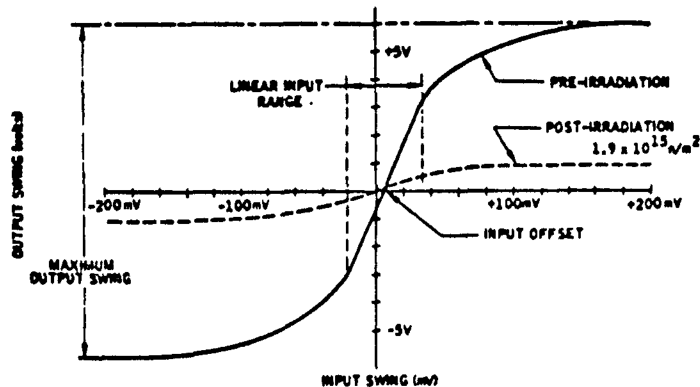

Fig. 13. MC1525 Typical Transfer Characteristics.

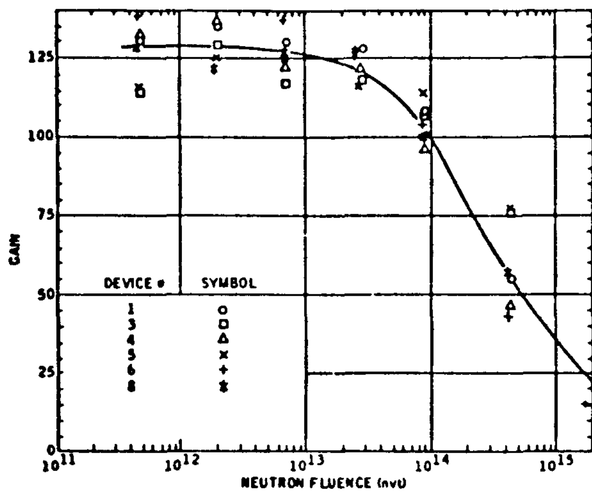

Fig. 14. MC1525 Gain vs Neutron Dose.

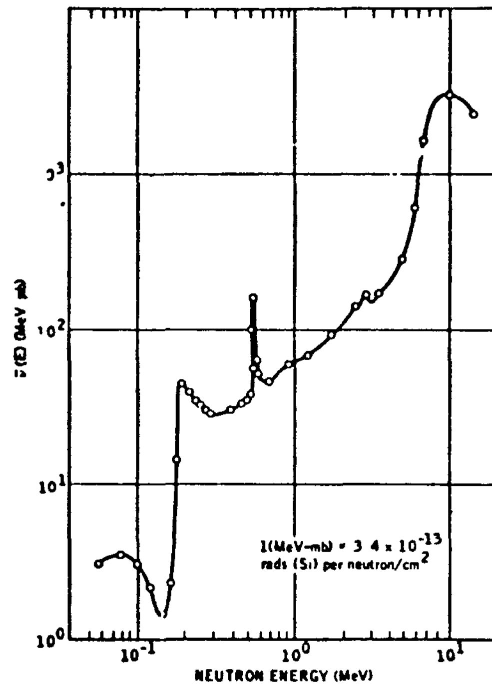

Fig. 17. $\bar{V}$ ($\bar{E}$) vs Neutron Energy[8]

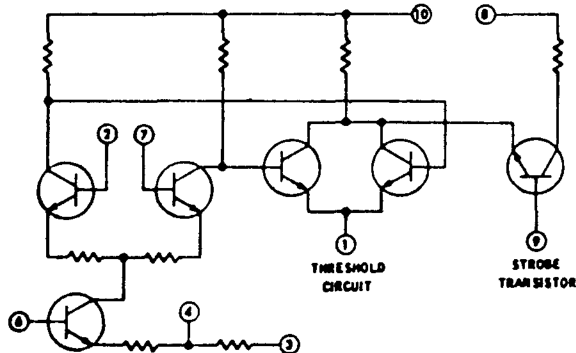

Fig. 15. NM2021 Gated Sense Amplifier.

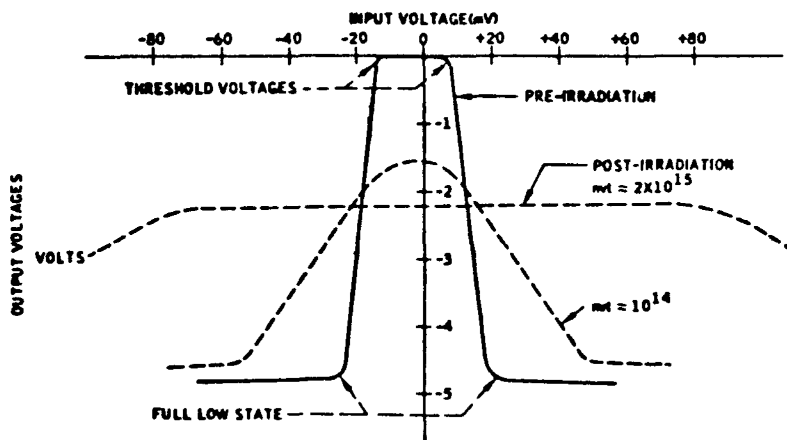

Fig. 16. NM2021 Typical Transfer Characteristics.

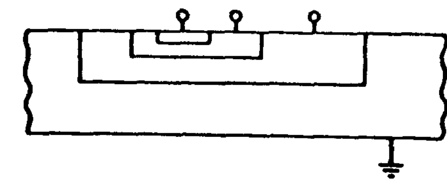

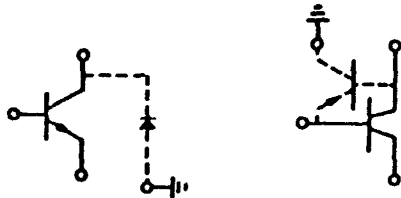

Fig. 18. Monolithic Microcircuit Transistor Element and its Equivalent Circuits.

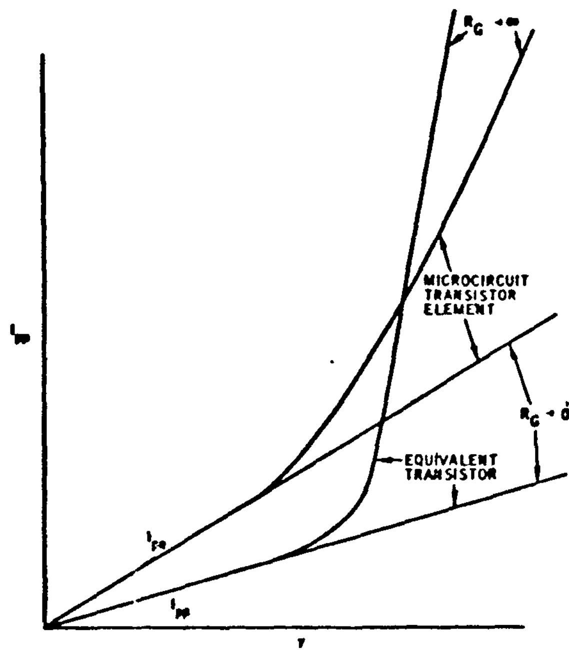

Fig. 19. Comparison of Photocurrents as a Function of Dose Rate in a Microcircuit Transistor Element and an Equivalent Discrete Transistor.

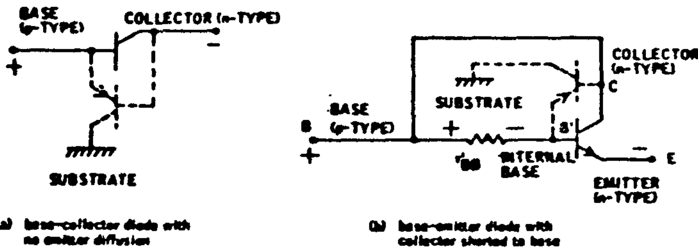

Fig. 20. Equivalent Circuits of Diode Commonly used in Monolithic Integrated Circuits.

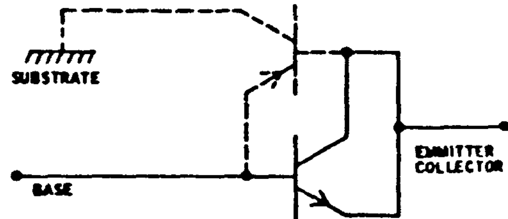

Fig. 21. Capacitor Equivalent Circuit.

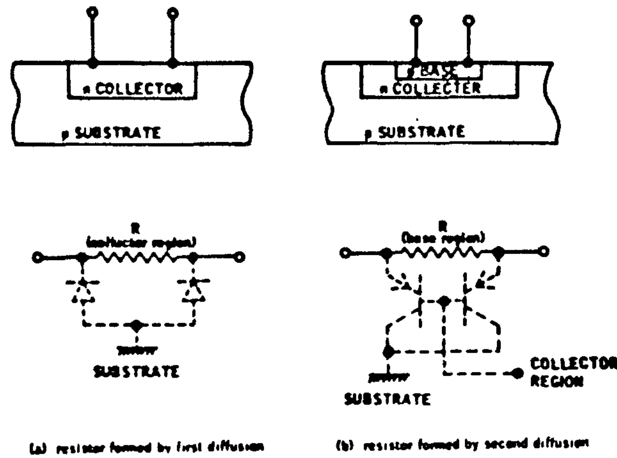

Fig. 22. Equivalent Circuits of Resistors.

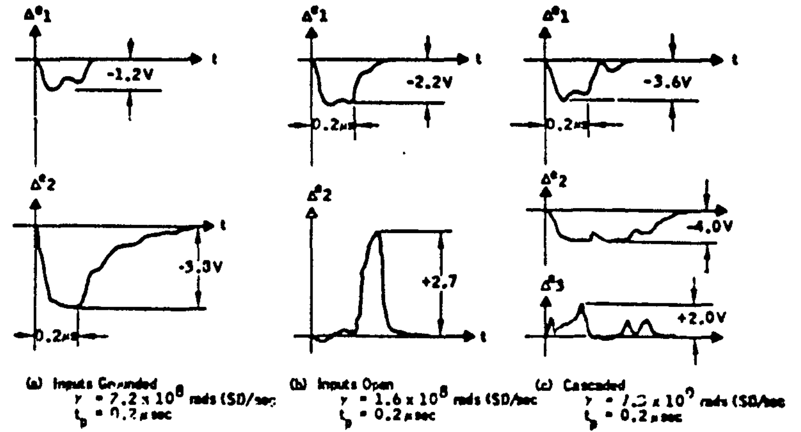

Fig. 24. MC201 Monolithic DTL Gate Transient Responses

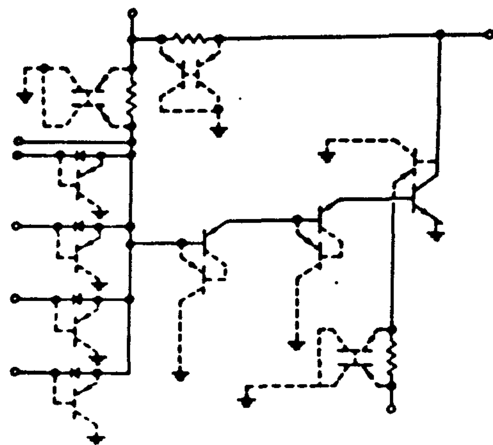

Fig. 23. Radiation Equivalent Circuit for the MC201 Showing Important Parasites.

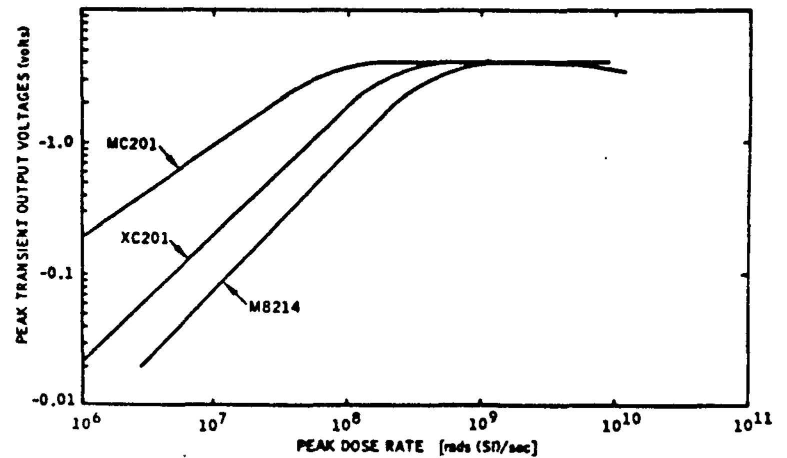

Fig. 25. Peak Transient Output Voltages (Gate Circuit Cascaded).

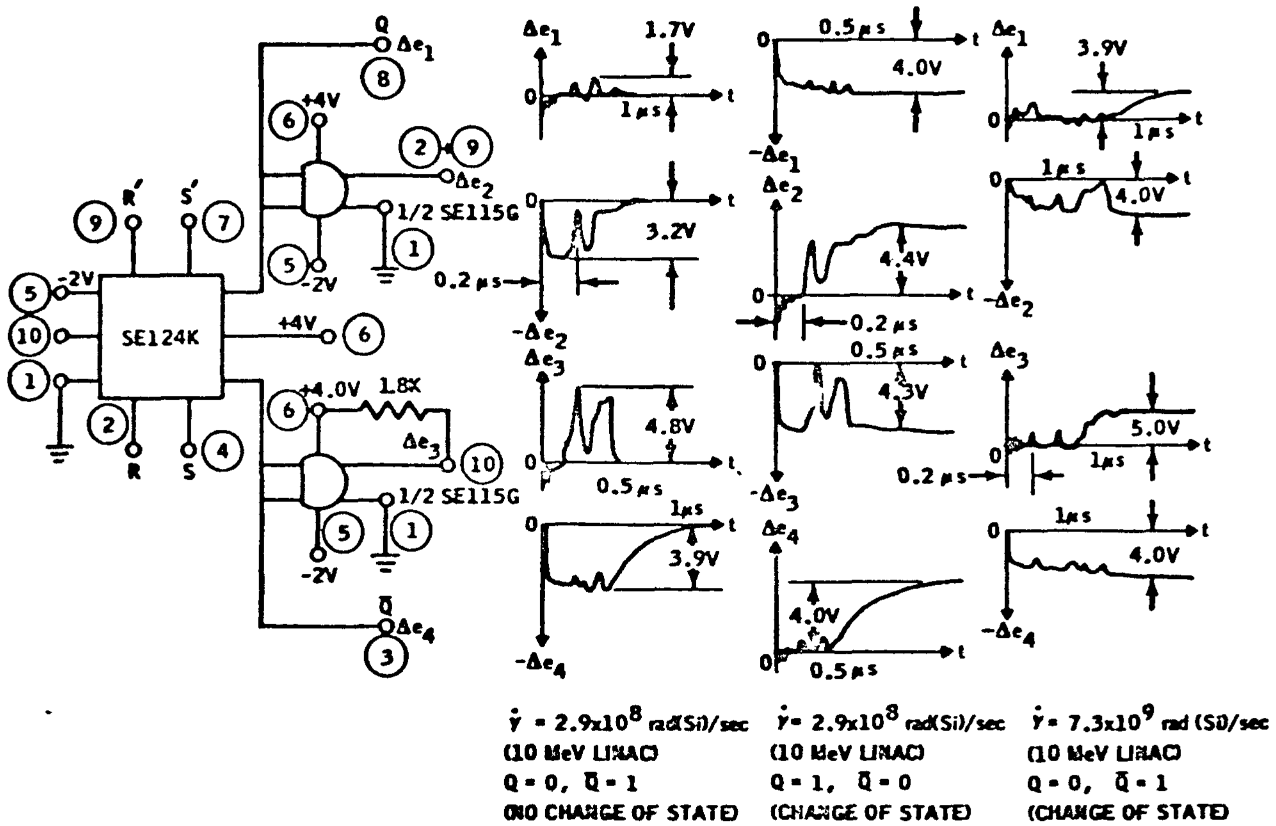

Fig. 26. Test Configuration and Transient Responses (Balanced Gate Loading).

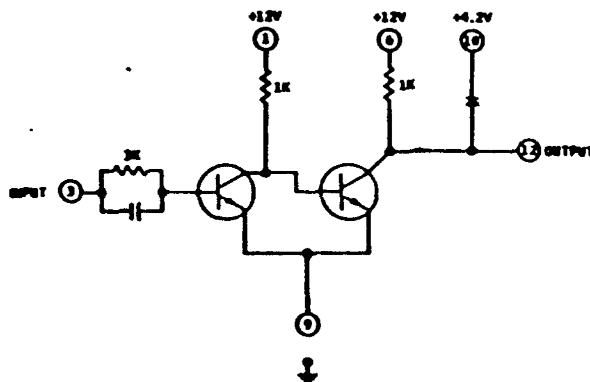

Fig. 27. PC-12 Buffer Amplifier.

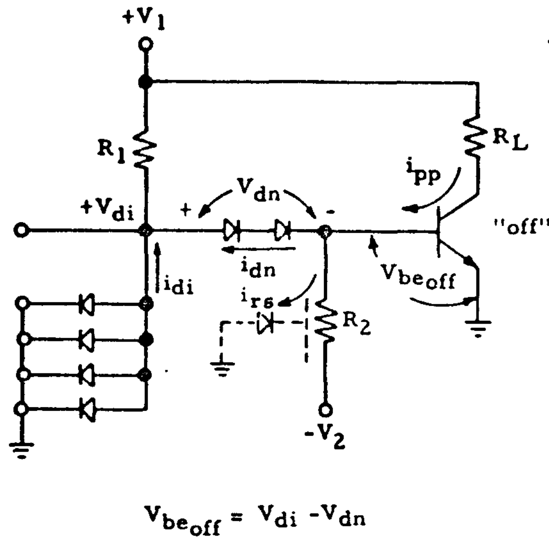

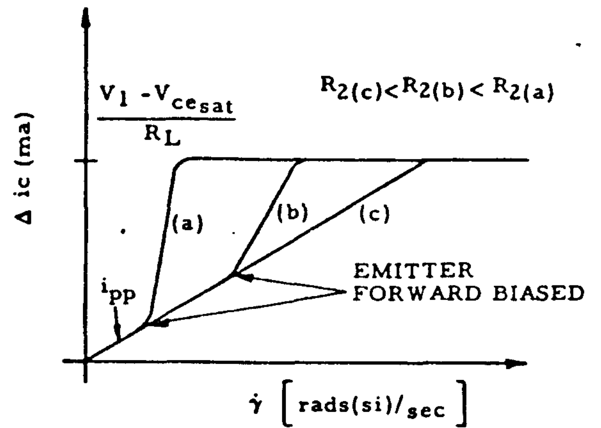

$$V_{be_{off}} = V_{di} - V_{dn}$$

To prevent transistor secondary photocurrent

$$i_{pp} \leqq \frac{0.6v + V_{dn} - V_{di}}{R_2} + i_{dn} + i_{rs}$$

Fig. 28. DTL Gate Vulnerability ("off" State).

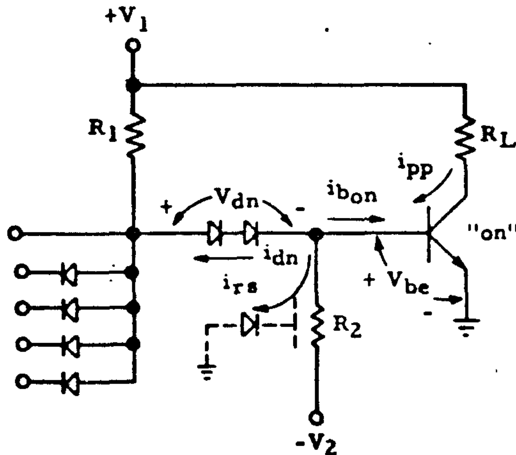

To prevent transistor turn-Off:

$$i_{b_{on}}(t) \geq \frac{V_1}{\beta R_L} - i_{pp}(t)$$

where,

$$i_{b_{on}}(t) = \frac{V_1 - V_{dn} - V_{be}}{R_1} - \frac{V_{be} + V_2}{R_2} - i_{dn}(t) - i_{rs}(t)$$

Fig. 29. DTL Gate Vulnerability ("on" State).

SPACE-RADIATION EFFECTS IN INTEGRATED CIRCUITS

Donald J. Hamman
Battelle Memorial Institute
Columbus, Ohio

This paper* discusses the damage mechanisms in semiconductors from space radiation and the effects on the microcircuit elements and the microcircuit parameters. Some tabular data are presented and a general-effects summary and some design considerations are included.

Introduction

Microelectronic circuitry, and especially monolithic semiconductor circuitry, offers many potential advantages for space-mission applications. Its use in the environment of space, however, must be predicated upon a sound knowledge of the effects of that environment on the microcircuits. The information that has been compiled about the cumulative effects of charged-particle radiation on microcircuits is useful to the system designer for estimates of operating life, selection of the best circuitry, and knowledge of trade-offs involved in this selection. In this paper, the types of microcircuit degradation effects and those parameters that are most critical in determining the radiation tolerance of microcircuits are discussed. The possibilities for minimizing the deleterious effects of space radiation are discussed from the points of view of both the manufacturer and the designer.

Microcircuit Behavior Under Space Radiation

Messenger[1] in this session's companion paper has told you how microcircuits behave in the transient-nuclear-radiation environment. This paper discusses the damage mechanisms in semiconductors from space radiation and the effects on the microcircuit elements and the microcircuit parameters. Some tabular data are presented and a general-effects summary and some design considerations are included.

*The information in this paper is primarily the result of work performed by Battelle Memorial Institute, under Contract No. NAS5-3985, for Goddard Space Flight Center under the technical monitorship of Mr. Frederick Gordon, Jr. A limited amount of the information was derived from the Radiation Effects Information Center at Battelle.

As is well known, the radiation found in space consists primarily of electrons having energies ranging up to several Mev and protons of energies up to several tens or even hundreds of Mev. No further description of the environment is presented here, as the primary purpose of this paper is to discuss the effects rather than the nature of space radiation. Further information on the environment may be found in the writings of Vette.[2,3]

The effects caused in integrated circuits by space radiation are essentially the same as those caused by nuclear radiation. However, the electrons and protons, being charged particles, can cause both ionization as well as bulk damage effects and, also, may produce brehmsstrahlung. The first area of discussion for this paper is damage mechanisms in semiconductors.

Damage Mechanisms

The irradiation of semiconductor crystalline strata with energetic changed particles results in the production of defects in the crystal lattice. These defects (primarily vacancy-interstitial pairs) result in a distorted energy structure for the lattice, and hence, in changes in the physical properties of the material.

Although the precise changes that occur are dependent on the relative position of the defect energy levels with respect to the Fermi level, the overall electrical effects in silicon are manifested by reductions in mobility, effective free-carrier concentration, and minority-carrier lifetime. The changes in the latter two electrical parameters as a function of particle fluence are usually most important for bulk damage and have been approximated by the expressions

$$N = N_o - K_1 \varphi \quad (1)$$

$$\frac{1}{\tau} = \frac{1}{\tau_o} + K_2 \varphi \quad (2)$$

where

τ = effective minority-carrier lifetime

CIRCUIT AND SYSTEMS ANALYSIS

September 1968

by

C. T. Kleiner

Prepared for UCLA Short Course
Radiation Effects on Semiconductors

Autonetics Division of North American Rockwell Corporation

3370 Miraloma Avenue, Anaheim, California 92803

THE USE OF COMPUTERS TO ANALYZE THE EFFECTS OF NUCLEAR RADIATION ON CIRCUITS AND SYSTEMS

INTRODUCTION

In the preceding series of lectures, the effects of nuclear radiation on semiconductor materials and devices have been treated in detail. Likewise, reasonably accurate device mathematical models have been developed to predict displacement and ionization effects on semiconductors. With the proper specification and collection of device parameter data, it is possible to calculate the expected semiconductor performance for ionization/degradation effects caused by a nuclear radiation environment.

When a mathematical model for a semiconductor device is verified by experiment and deemed adequate for the general prediction of device behavior, it is necessary to establish a means of performing these predictions when a multiplicity of such semiconductors (in combination with other devices) are interconnected to form a circuit. Further, it is necessary to establish a means of performing predictions when a multiplicity of circuits is combined to form a system. The total system generally consists of electronic and electromechanical elements, some or both of which can be treated as transfer functions.

At the circuit level, it is possible to establish the effect of nuclear radiation by the use of manual calculations using simplifying assumptions.[1] This method is effective and fairly rapid. The principle difficulty in the manual approach is in the prediction of large circuit response with multiple feedback. This type of circuit is generally found in secondary power subsystems and/or electronic regulator circuits such as digital-to-analog converters. With the advent of large scale computer facilities in the early 1960's, an effort was made to use analog and digital computation for the prediction of circuit response by automated techniques. Some of the initial efforts considered made use of analog computer techniques.[2] Although successful, this method of prediction required estensive equation writing and the usual scaling problems involved with analog computation techniques.

While the analog approach was being developed, digital computer techniques were also being pursued. Special purpose programs were developed by various agencies to calculate critical circuit response. This method was also reasonably successful but required considerable effort and skill with the added disadvantage that a circuit change required reformulation of equations and consequently a new computer program. Various general purpose computer codes were developing during the period 1960 to 1964* among which was the NET-1[3] program developed on the MANIAC computer at Los Alamos by A. Malmberg. Shortly after the development of the NET-1, the Boeing Company modified the basic program and mathematical models to be used in a program termed CIRCUS.[4] In 1965, the Air Force Weapons Laboratory sponsored the development of the PREDICT code, a more general purpose program than NET-1

*The computer programs listed use the same basic Ebers and Moll or the equivalent charge control bipolar transistor model, other programs had been used which employ simplified linear or piece-pulse linear models.

or CIRCUS which allowed for a wide variety of mathematical models to be used in the program. Improvements in the PREDICT code resulted in significant changes and it was renamed SCEPTRE. These general purpose digital computer programs are progressing both in application and in the improved development of computing hardware and software. At this point, the small and large digital computer and associated software is developing at a very rapid pace with attendant lower computing costs. As a result of this overall trend, this form of computation becomes extremely attractive for circuit and system calculations. Since the testing and verification of nuclear radiation effects is generally more costly than determining the electrical performance of the circuits/systems, these prediction codes have become essential for the accurate analysis of circuit behavior in a nuclear environment. At present, there are four computer programs available to universities and industry in the United States as follows:

1. NET-1 - Los Alamos Scientific Laboratory
2. CIRCUS - Boeing Company
3. SCEPTRE - IBM Oswego
4. TRAC - Autonetics

These programs have the following general capabilities:

1. Automatic generation of circuit equations
2. Built-in or user models
3. Automatic initial conditions
4. Transient solution (time history)
5. Restart capability
6. Tabular or graphic output

As an example, the circuit shown in Figure 1 would have various nodal points designated and coded as follows:

R_1 is connected from circuit node 5 to node 1

R_2 is connected from circuit node 1 to ground (circuit node 0)

Etc.

Generally, the value of R_1 and R_2, etc. will be entered with the topological connection. This will be treated in detail later on a specific circuit which has been subjected to radiation. A typical ionization response of node 3 of the circuit illustrated in Figure 1 is shown in Figure 2.

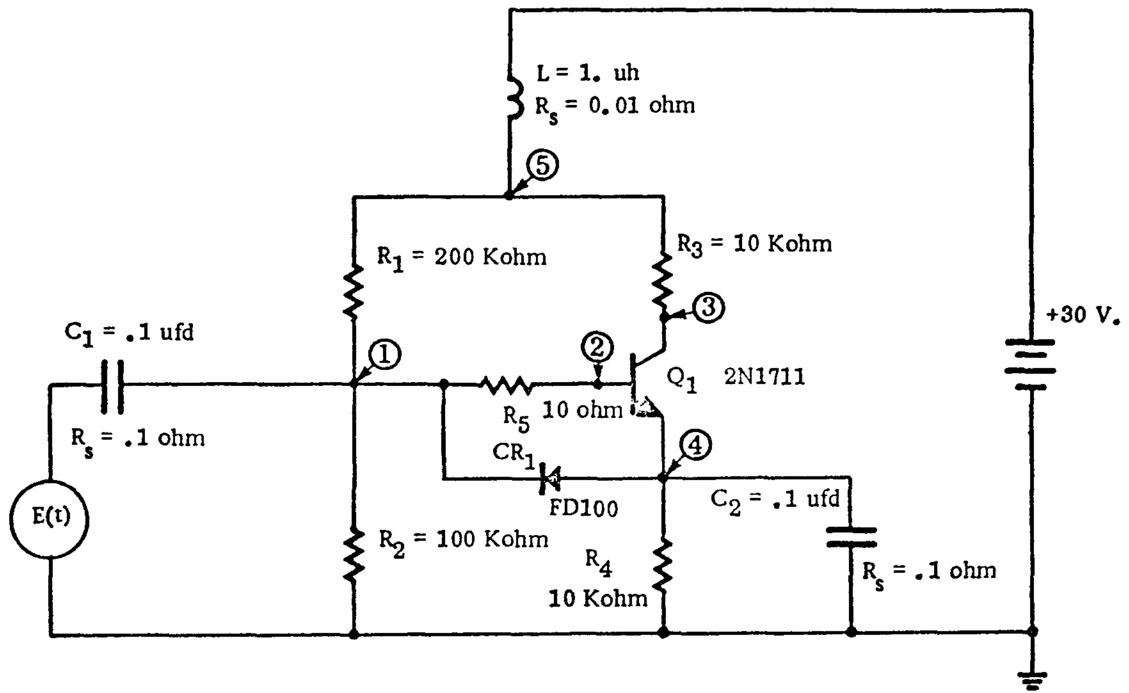

Figure 1. Example of Circuit Prepared for Computer Coding

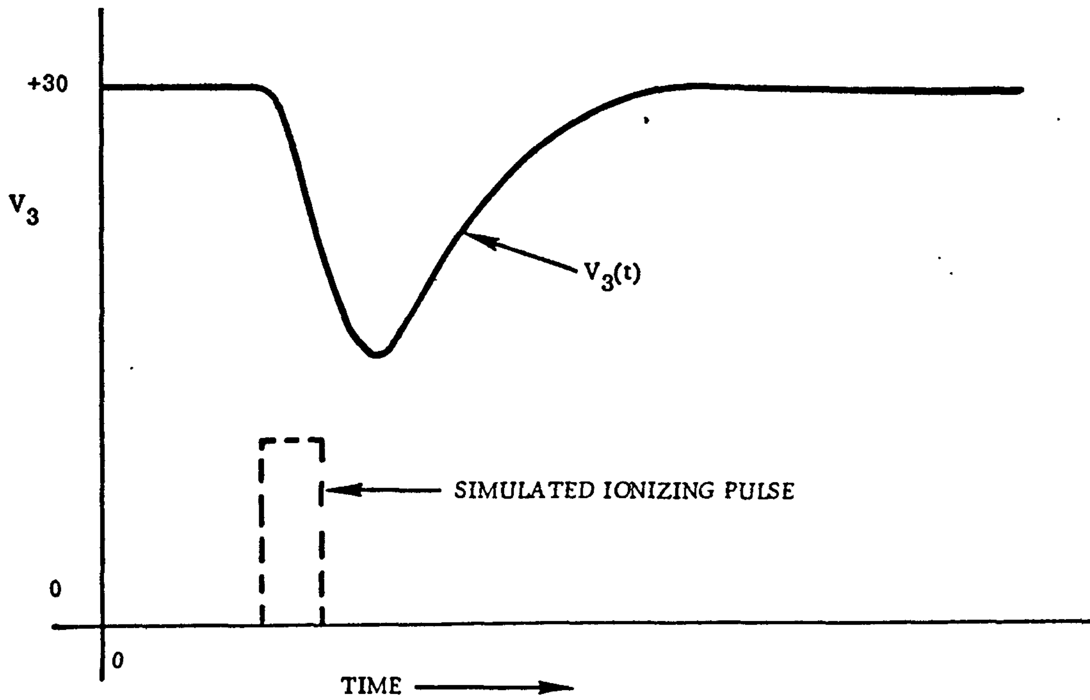

Figure 2. Response of Node 3 to an Ionizing Pulse of Radiation

In general, the computer codes described here are limited to circuits of approximately 70 nodes due largely to the theoretical limits associated with inverting or partitioning matrices. An attempt to solve larger arrays generally results in computational error and excessive computer run time. There is a need for an analytical tool to provide solutions for a multiplicity of circuits (subsystems, systems). One such code SECURE has been developed at Autonetics and presently has the capability of solving for 5000 unknowns by partitioning these in arrays of 50 or less. In addition, functional block models are capable of being combined with detailed circuits to form a complete control loop system simulation. An example of such a system (in very simplified form) is illustrated in Figure 3. A typical response of the control loop system is illustrated in Figure 4.

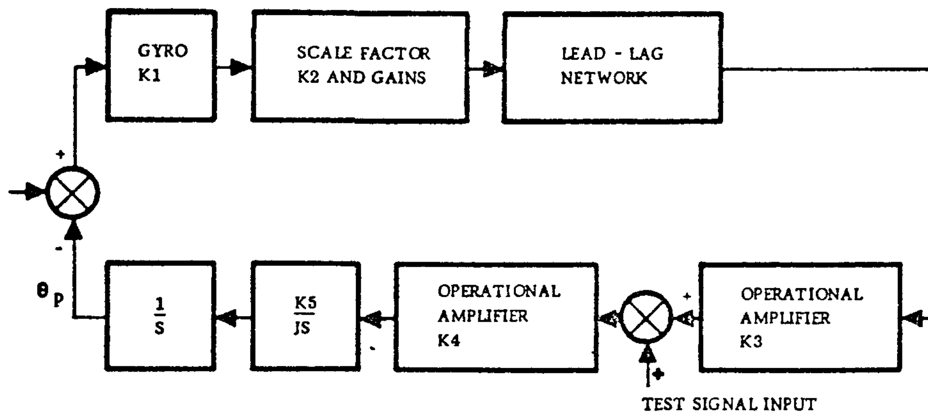

Figure 3. Closed Loop System

The application of the Transient Radiation Analysis by Computer (TRAC) Program will be used as a vehicle to describe the method for the solution of nuclear radiation effects at the circuit level.

APPLICATION OF COMPUTER CODES FOR RADIATION EFFECTS ANALYSIS AT THE CIRCUIT LEVEL

The transient radiation effects on electronics (TREE) at the circuit level are based on the definition and validation of adequate mathematical models of electronic devices and the combination of these models through mathematical techniques with the aid of a digital computer such as IBM 7094, CDC 3600, Burroughs 5000, etc. As a result, these mathematical models are usually represented by an equivalent circuit. Figure 5 illustrates equivalent circuits for passive elements which include radiation effects. Figure 6 illustrates an equivalent circuit for a p-n diode and n-p-n bipolar transistor. Typical response characteristics for the bipolar transistor are illustrated in Figures 7, 8, and 9. Figure 10 illustrates the equation used for neutron degradation effects.

The solution of combinations of these models can be illustrated as follows: Consider the simple resistor network in Figure 11 with associated nodal equations. Note that the current through each element (resistor) is calculated by obtaining the voltage across the element and the resistance (parameter) value. Generally, the resistor is treated as a single "model" and can be generalized as illustrated in Figure 12.

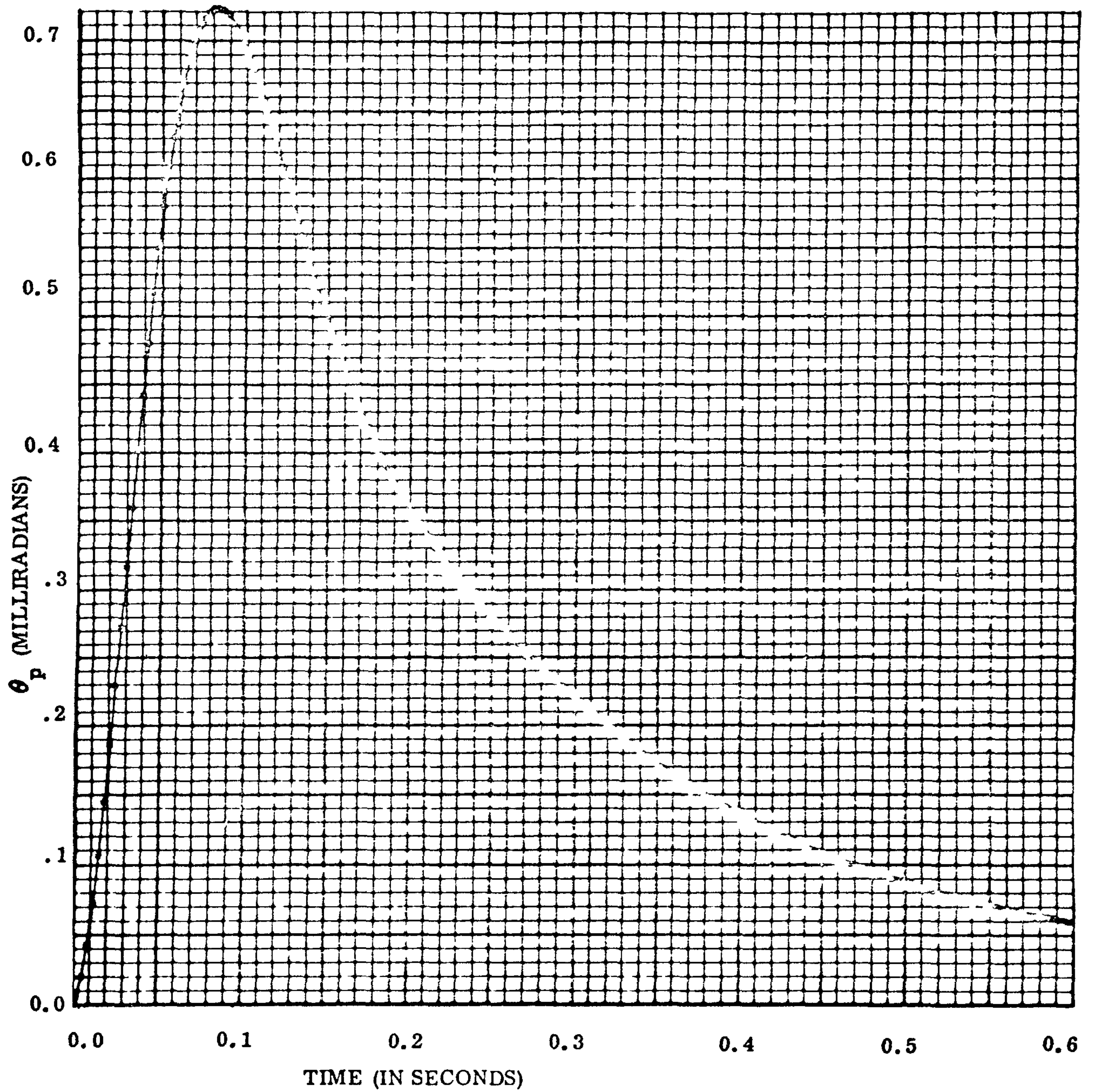

Figure 4. Servo Response to Test Input

ELECTRICAL MODEL 1

RESISTOR

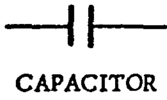
CAPACITOR

IONIZATION MODEL

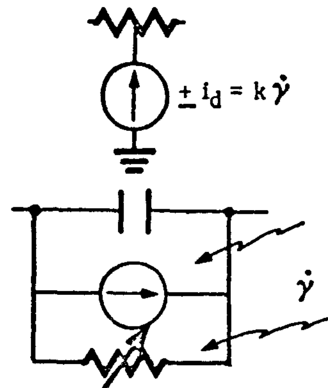

Figure 5. Passive Elements Modified for Ionization Effects

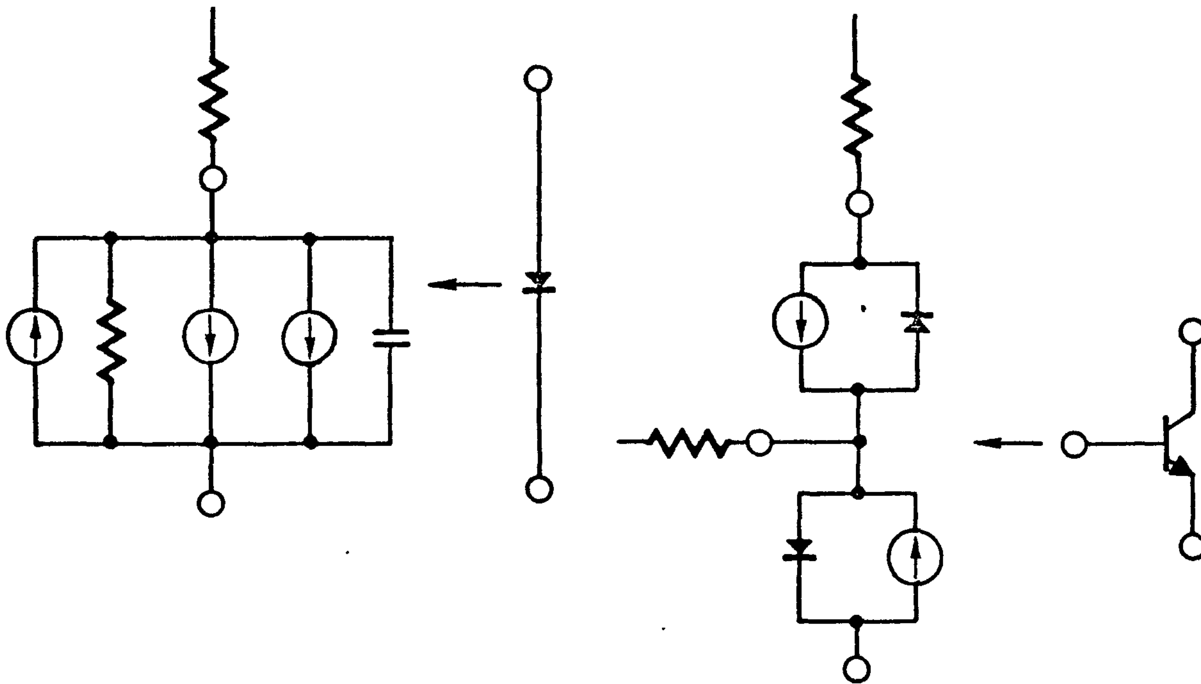

Figure 6. Active Elements (Includes Photocurrent Generators)

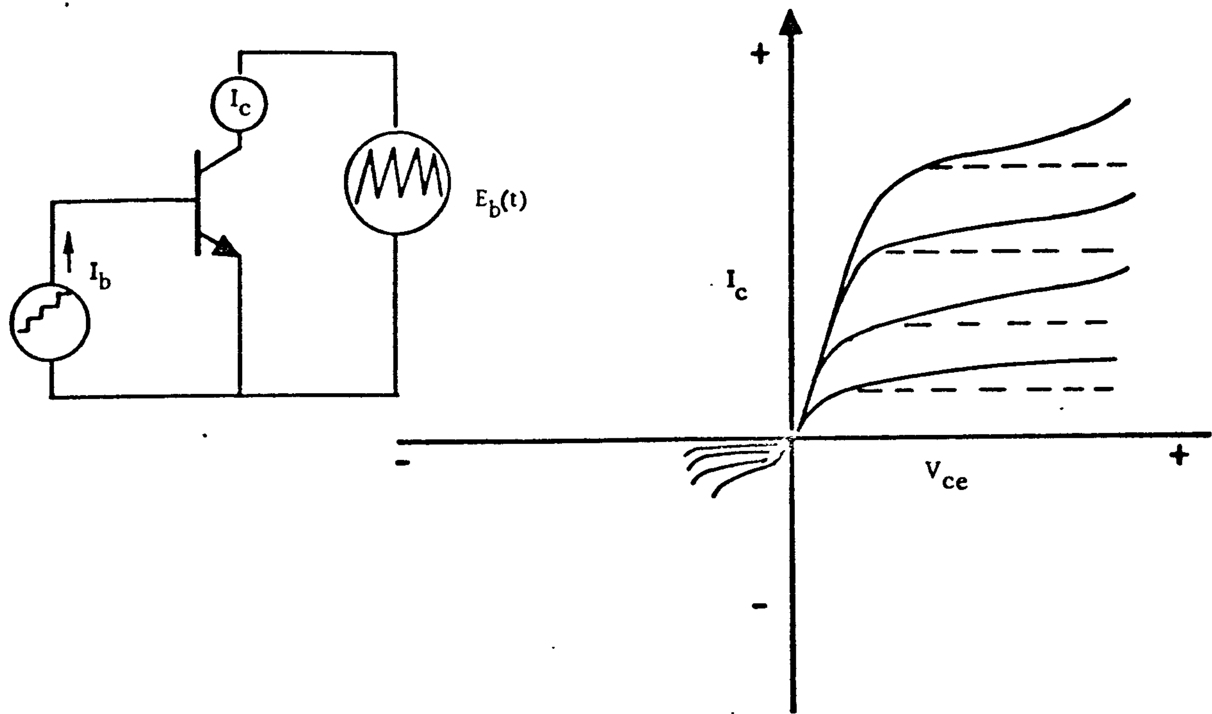

Figure 7. V_{ce}-I_c Curve Trace of Bi-polar Transistor Model

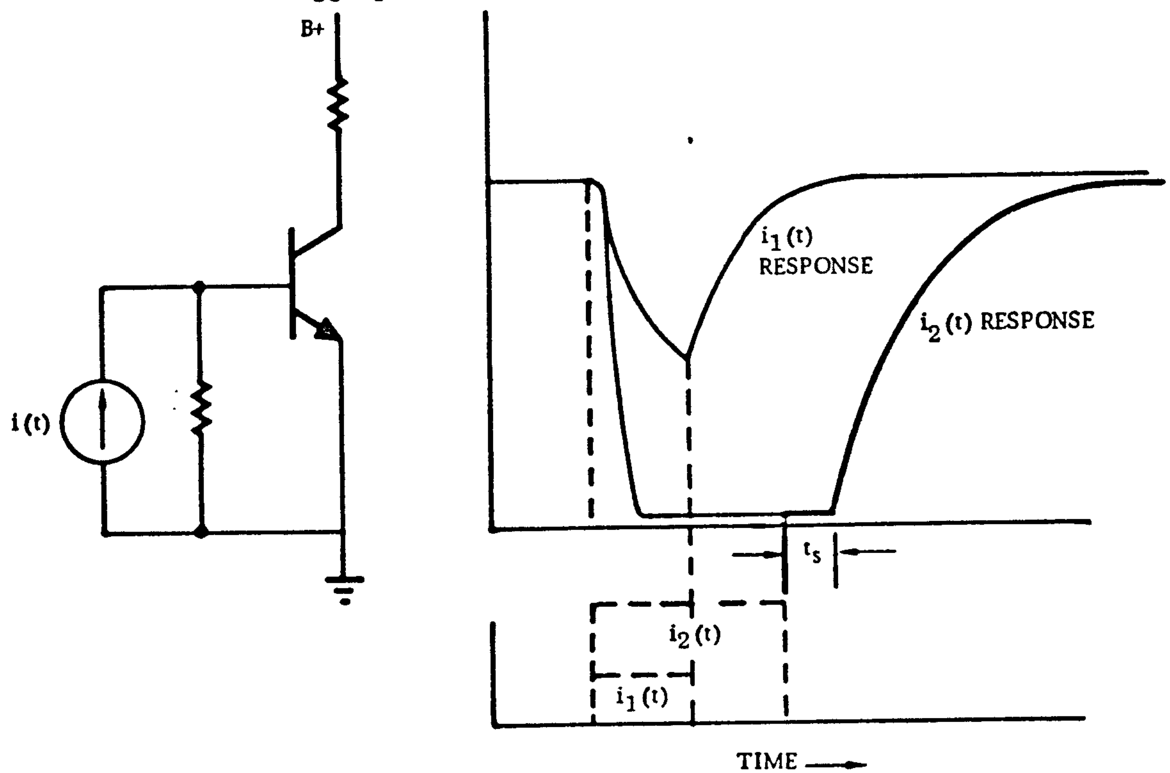

Figure 8. Electrical Storage time, t_s, Resulting from a Pulse of Base Current

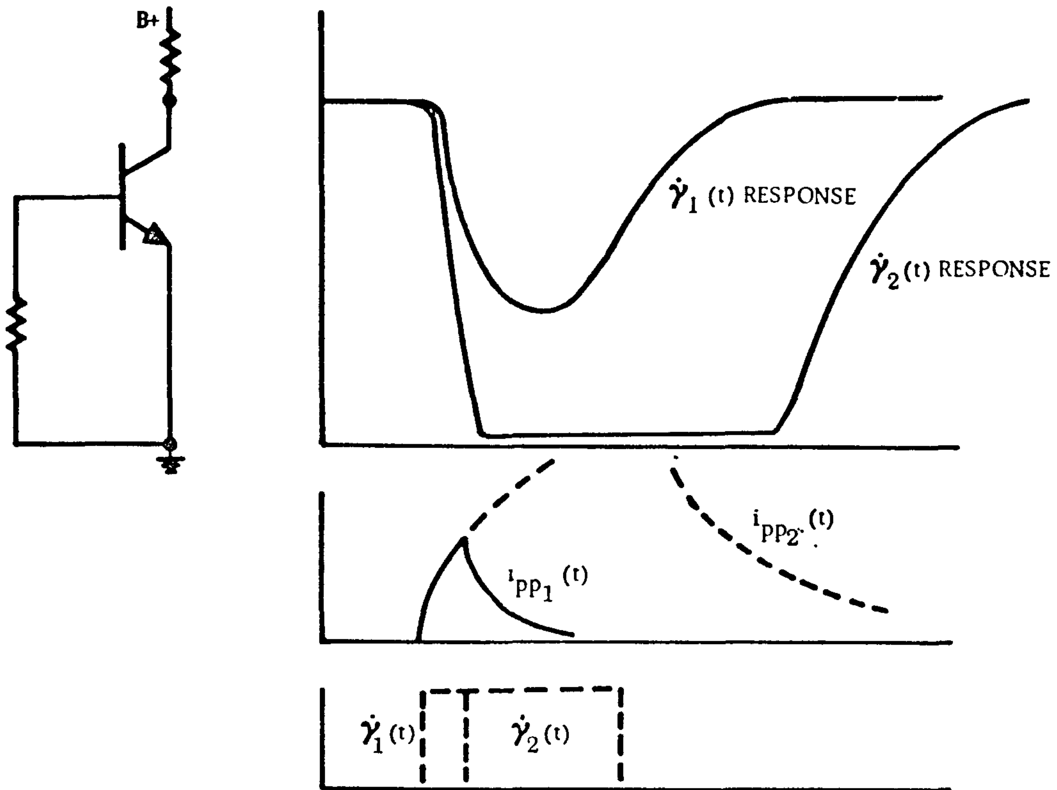

Figure 9. Radiation Storage Time, t_{sr}, Resulting from Ionizing Radiation

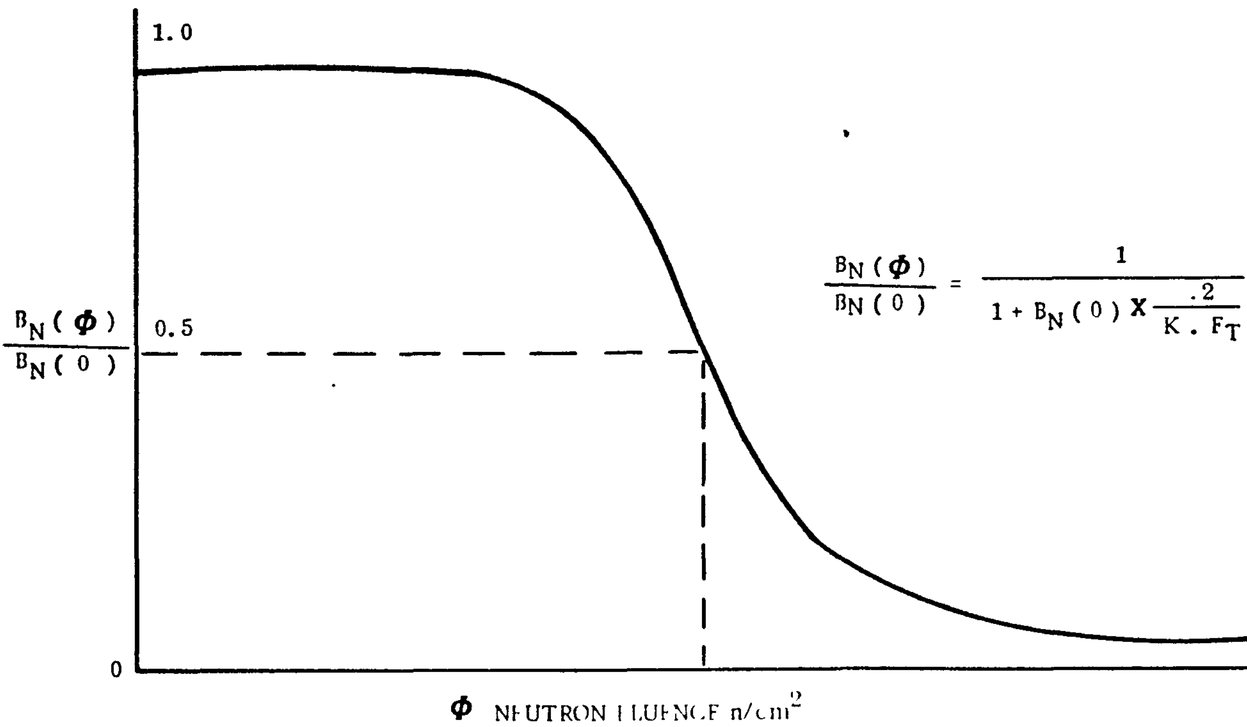

Figure 10. Neutron Degradation of Bn (Φ)/Bn (0)

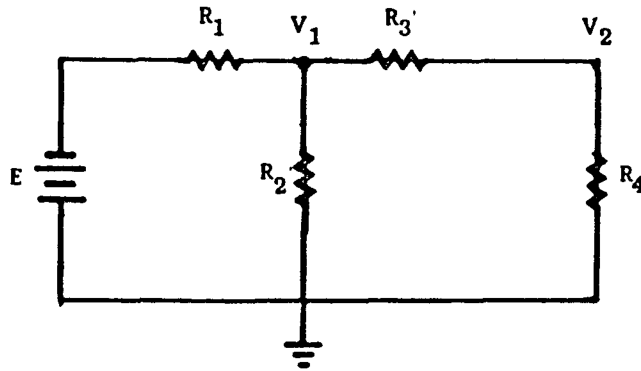

AROUND: V_1 :

$$\sum_{I=1}^{I=3} I = 0 = (V_1 - E)/R_1 + V_1/R_2 + (V_1 - V_2)/R_3$$

AROUND V_2 :

$$\sum_{I=1}^{I=2} I = 0 = (V_2 - V_1)/R_3 + V_2/R_4$$

Figure 11. Simple Resistor Network and Equations

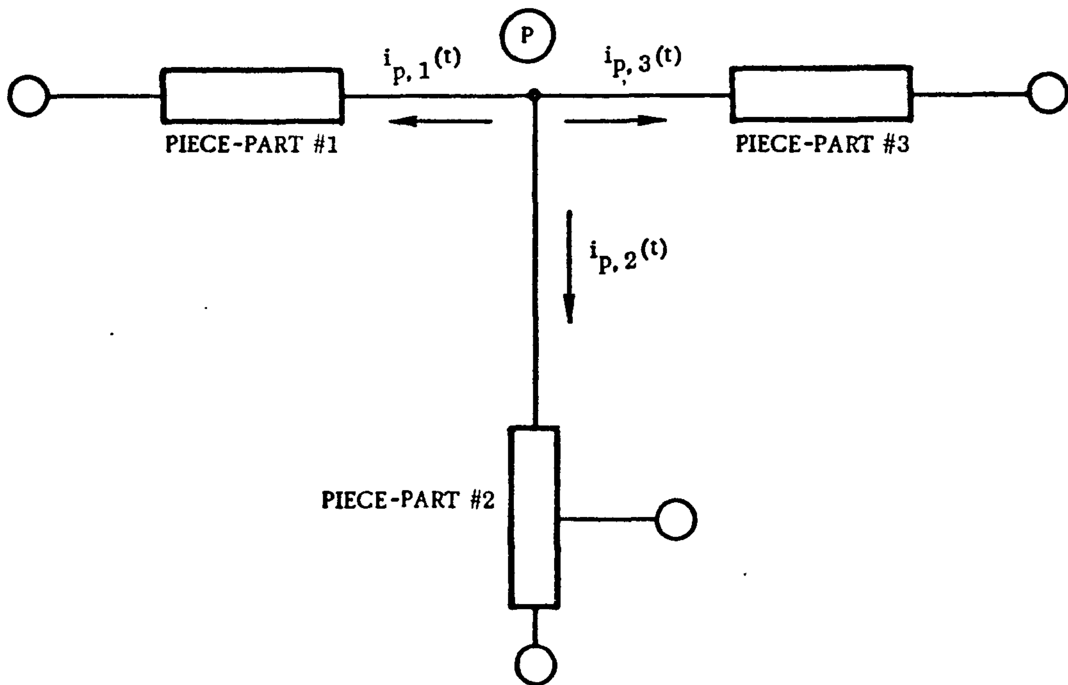

Figure 12. Generalized Nodal Model

Applying Kirchhoff's current law with respect to current leaving node P of Figure 12:

$$\sum_{K} i_{p,k}(t) = 0 \qquad (1)$$

The current, $i_{p,k}(t)$, will have a functional relationship to the dependent node voltages, v's, the piece-part parameter, p's, the grounded voltage sources, the current sources, and the auxiliary quantities and time.

$$i_{p,k}(t) = F_{p,k}\,(V's,\ p's,\ e_{vs}'s,\ i_{cs}'s,\ \mu's.\ t) \qquad (2)$$

V's	=	node voltages
p's	=	parameters
e_{vs}'s	=	grounded voltage sources
i_{cs}'s	=	current sources
μ's	=	other auxiliary quantities
t	=	time (also implies $t = \Delta t$)
Δt	=	time increment

The exact form of Equation (2) is dependent upon the piece-part model. The built-in models of the TRAC Program consist of difference equation representations of Equation (2). This difference equation is linear and of the form:

$$i_{p,k}(t_n) = [\Delta h_{p,q,k}(t_n) \quad V_q(t_n) - \Delta W_{p,k}(t_n)] \qquad (3)$$

where

p, q	=	dependent node number p and q
$\Delta h_{p,q,k}(t_n)$	=	K^{th} piece-part admittance contribution at time t_n
$V_q(t_n)$	=	voltage of dependent node Q at time t_n
$\Delta W_{p,k}(t_n)$	=	K^{th} piece-part "pseudo-current" contribution at t_n

The Δh and ΔW terms are known functions of quantities whose values are known prior to solving for $V_q(t_n)$ and $I_{p,k}(t_n)$. e.g., functions of past voltage, $V_q(t_{n-1})$, past current, $i_{p,k}(t_{n-1})$, and/or grounded voltage source. $e_{vs}(t_n)$.

Since the voltages at the independent nodes are already known at time, t_n, the only voltage values to be determined are those of the dependent nodes, $V_q(t_n)$. The dependent node voltages, $V_q(t_n)$, are determined by substituting Equation (3) into Equation (1) for each dependent node, P, and solve for each of the dependent nodes. This can be represented by a matrix of the form:

$$
\overbrace{\begin{vmatrix} \sum_K \Delta W_{1,k}(t_n) \\ \\ \cdot \\ \\ \sum_K \Delta W_{nv,k}(t_n) \end{vmatrix}}^{T} = \overbrace{\begin{vmatrix} \sum_K \Delta h_{1,1,k}(t_n) & \cdots & \sum_K \Delta h_{1,nv,k}(t_n) \\ & \cdot & \\ \sum_K \Delta h_{nv,1,k}(t_n) & \cdots & \sum_K \Delta h_{nv,nv,k}(t_n) \end{vmatrix}}^{H} \times \overbrace{\begin{vmatrix} V_1(t_n) \\ \\ \\ V_{nv}(t_n) \end{vmatrix}}^{V}
$$

where nv = number of dependent nodes (note for a 32-K word core memory, nv = 60 max), the H matrix is non-singular in most instances (where the circuit is realistic and main diagonal is occuped by non-zero terms). Equation (3) can be used to solve for $V_q(t_n)$ for Q = 1, 2, . . ., NV.

An example of a piece-part generally mechanized for TRAC is given as follows (see Figure 13):

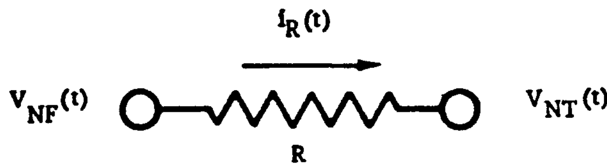

Figure 13. Resistor Piece-Part

The difference equation used in TRAC to mechanize this model equation is:

5. $i_r = (1/R)\ V_{nf}(t_n) = i_r(t_n)$

6. $i_{NF,k}(t_n) = i_R(t_n) = i_R(t_n)$

7. $\Delta h_{NF,NF,K}(t_n) = 1/R$

8. $\Delta h_{NF, NT, K}(t_n) = -1/R$

9. $\Delta h_{ND, Q, K}(t_n) = 0 \quad Q \neq NF, \ Q \neq NT, \ Q = 1, 2, \ldots, NV$

10. $\Delta W_{NF, K}(t_n) = 0$

Since $I_{NT, K}(t_n) = -i_{NF, K}(t_n)$, it follows that:

11. $\Delta h_{NT, NT, K}(t_n) = 1/R$

12. $\Delta h_{NT, NF, K}(t_n) = -1/R$

13. $\Delta h_{NT, Q, K}(t_n) = 0 \quad Q \neq NV, \ Q \neq NT, \ Q \neq 1, 2, \ldots, NV$

14. $\Delta W_{NT, K}(t_n) = 0$

Similar derivations for a capacitor, inductor, diode, and bipolar transistor can be obtained. These derivations are more tedious and are covered in detail in Reference 5.

Radiation effects and data are entered as an additional current generator, (i_{pp}), or as a change in parameters, e.g., h_{FE} (ϕ). The effects are included in the conventional model calculation procedure. Temperature and other effects can also be input with the result that combined effects are properly correlated through the solution of the H, T, and V matrix manipulation. The flow chart for solution is illustrated in Figure 14.

The solution proceeds are as follows:

1. Take last solution at $t = t_{n-1}$
2. Advance time to t_n; ($t_n = t_{n-1} + \Delta t$)
3. Generate H&T matrix components in the equation writer
4. Solve H * V = T for dependent node voltages
5. Perform convergence tests in non-linear solution subroutine
6. Accept or reject solution
7. Calculate auxiliary quantities
8. Recycle to the next time step.

Input/output is handled through punched card and tab printout.

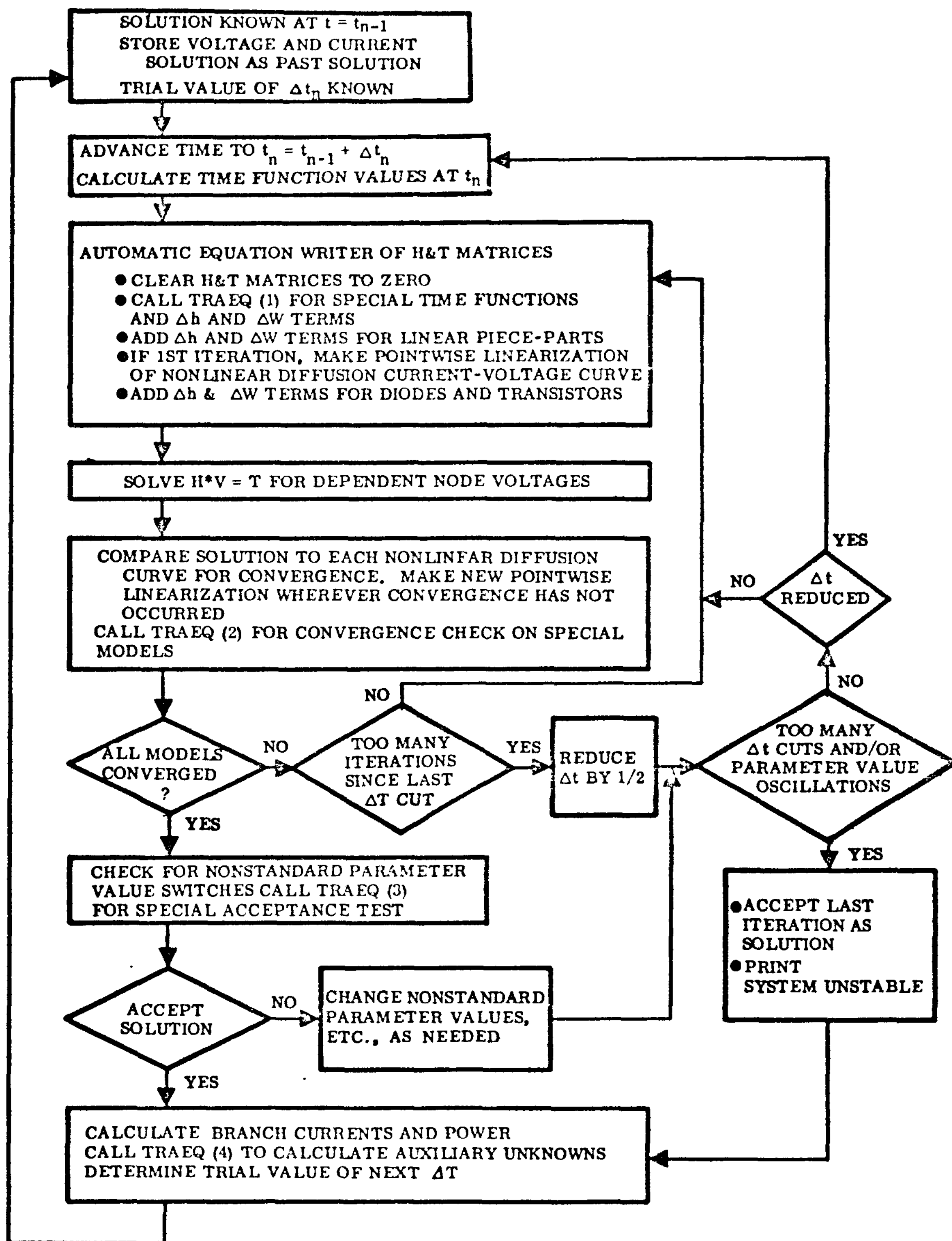

Figure 14. Flow Chart for Solution (TRAC)

The SCEPTRE and CIRCUS codes have a free format or partial free format input. TRAC and NET-R have fixed formal input which requires a precise set of sequential instructions which, if not in the correct order, will prohibit proper computer execution.

The output of all the programs is tabular, with options for print-plotting, or the use of peripheral plotting equipment. The example which follows illustrates the application of the TRAC code for circuit ionization (induced by gamma radiation) and neutron induced degradation.

EXAMPLES OF CIRCUITS ANALYZED BY A DIGITAL COMPUTER

The circuit to be considered is a simple unijunction oscillator. The equivalent circuit of the unijunction is illustrated in Figure 15, including the other components (R's and C's), which form the oscillator circuit. Normal circuit operation will be obtained first. This will be followed by a case where an ionization pulse is introduced. Faulty neutron damage effects are introduced.

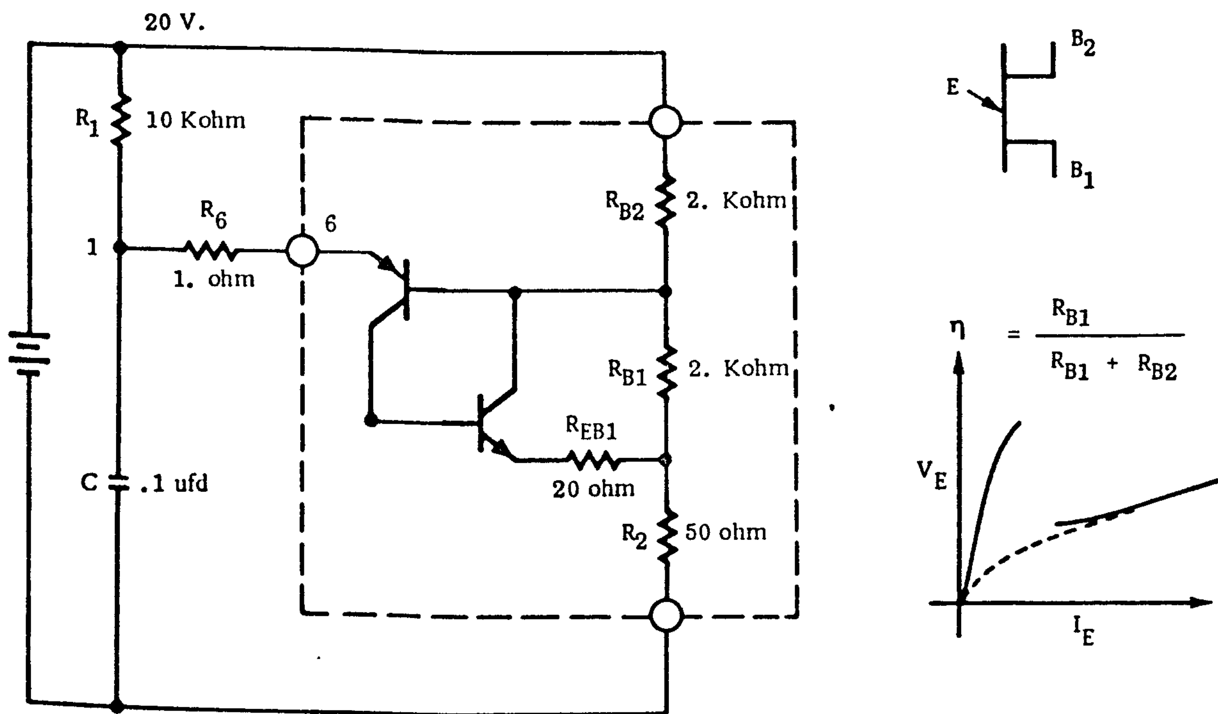

Figure 15. Unijunction Oscillator Circuit and Model for the Unijunction Transistor

The circuit is appropriately numbered from node 1 through node 6. An example of the computer coding is illustrated in Appendix A. Summarizing the results:

1. The ionization produced by gamma radiation causes a momentary discharge of the capacitor, and the oscillator circuit resumes normal operation.

2. The neutron damage effect causes an increase in frequency until the oscillator ceases operation.

Circuit simulation of this type can be extended to much larger circuits than the one shown in Figure 15. Circuits of up to 60 nodes, containing 100 elements (resistors, capacitors, inductors, diodes, and transistors), have been successfully simulated using the computer codes.

The results of these circuit analyses must be folded into an overall system evaluation. The next section discusses several methods for system analyses.

APPLICATION OF COMPUTER CODES FOR RADIATION EFFECTS AT THE SYSTEM LEVEL

System modeling for non-radiation effects has progressed to the point where several computer codes have been developed for the purpose. Two such programs will be discussed here. One program - Continuous System Modeling Program (CSMP)- provides a means of simulating system response by use of functional blocks.** A typical set of functional blocks is illustrated in Figure 16. The functional block representation can be used to represent an entire circuit or an electromechanical device. Modifications are generally required for the electronic block equivalents to represent loss of gain, d-c offset, and spurious transients. An example of this is illustrated in Figure 17. This procedure can be extended to complex systems. The difficulty with this approach for predicting system response to radiation effects requires that the complex interactions within electronic circuits be neglected with the added assumption that each block input impedance is infinite with a corresponding zero output impedance. It is necessary , therefore, to include actual circuits in conjunction with functional blocks. A computer code for this purpose has been recently developed[7] and is termed System Evaluation Code Under a Radiation Environment (SECURE). The following example illustrates the use of this program for determining a closed loop response to ionization and degradation effects. The system to be analyzed is illustrated in Figure 3.

A nominal test signal (to provide an electrically induced transient) is applied to establish the correspondence between a block equivalent of Figure 3 and an equivalent with detailed circuits. The comparison is illustrated in Figure 18. A detailed diagram of the servo loop, including all circuits, is illustrated in Figure 19.

The introduction of a 10 percent beta reduction due to neutron damage causes a loop transient due to the change in base current of Q1. The transient response is shown in Figure 20.

The addition of ionization will cause momentary saturation of the amplifiers, as depicted in Figure 21.

**Functional blocks receive inputs and present infinite input impedance to the inputs. The blocks deliver outputs (after proper mathematical operations) with zero output impedance.

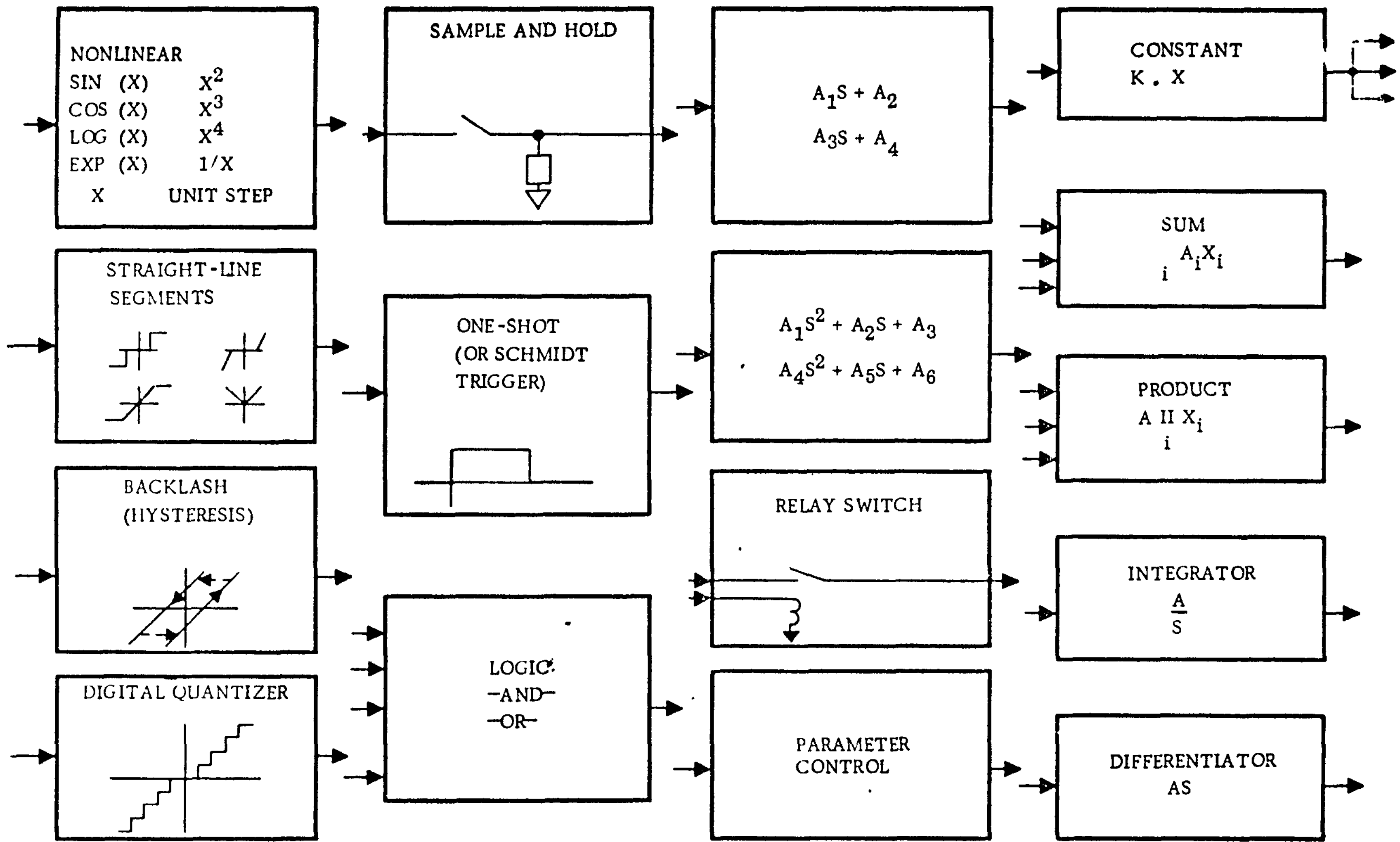

Figure 16. Functional Block Models

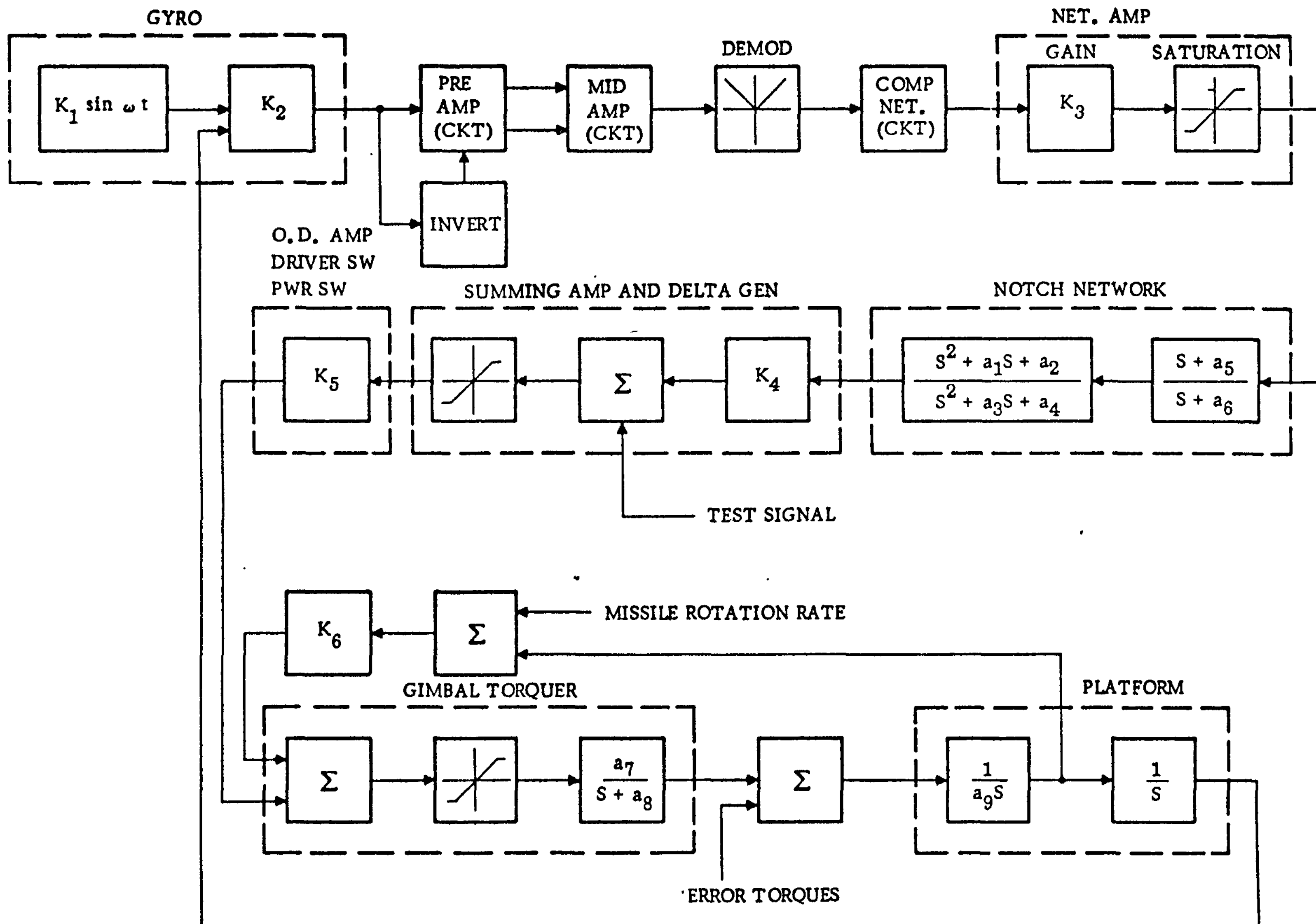

Figure 17. Functional Block Models Used to Represent a Platform (Gyro) Stabilization Loop

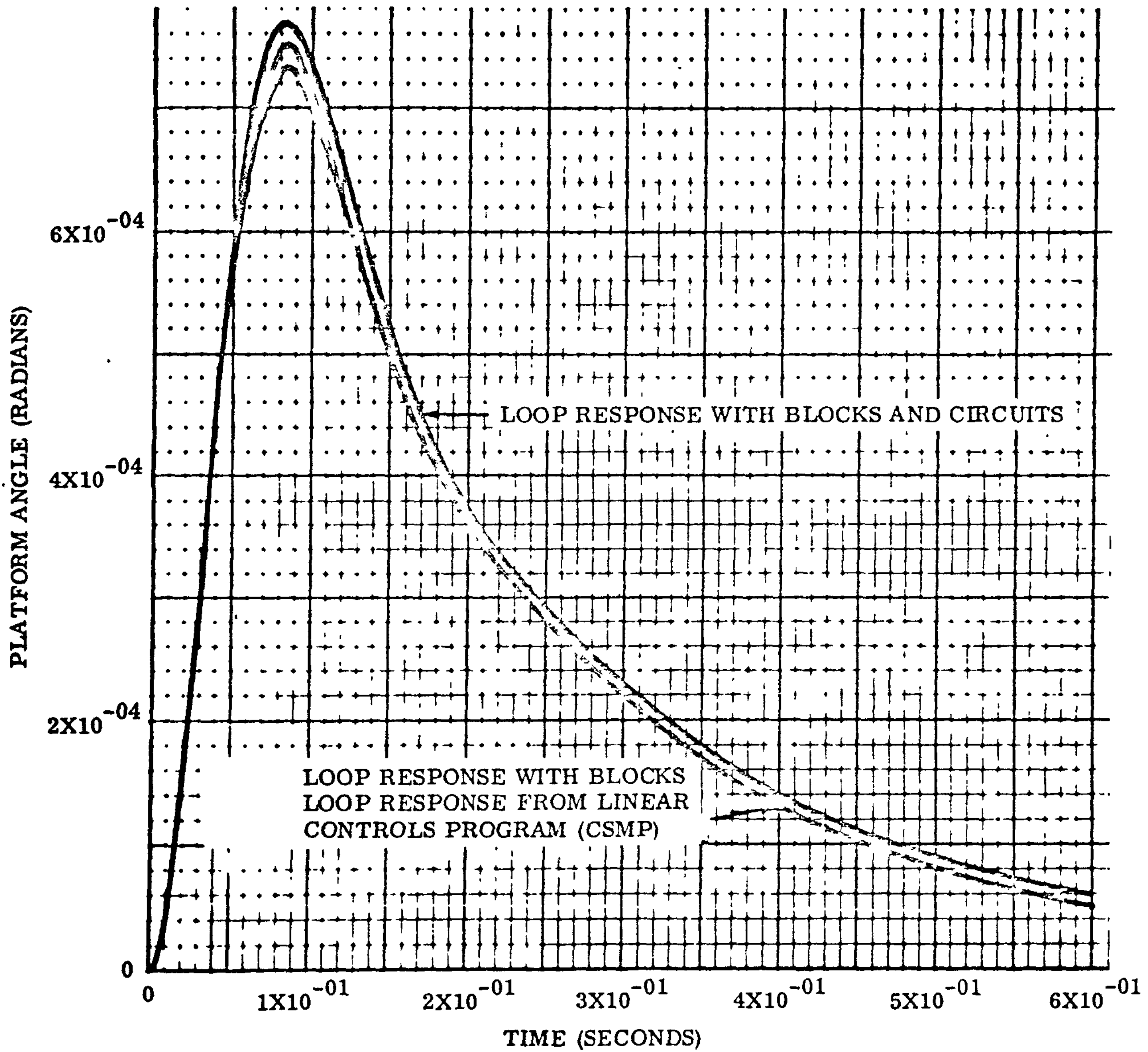

Figure 18. Comparison of Loop Response, θ p(t), to an Electrical Test Signal for (a) Functional Blocks and (b) Functional Blocks and Circuits

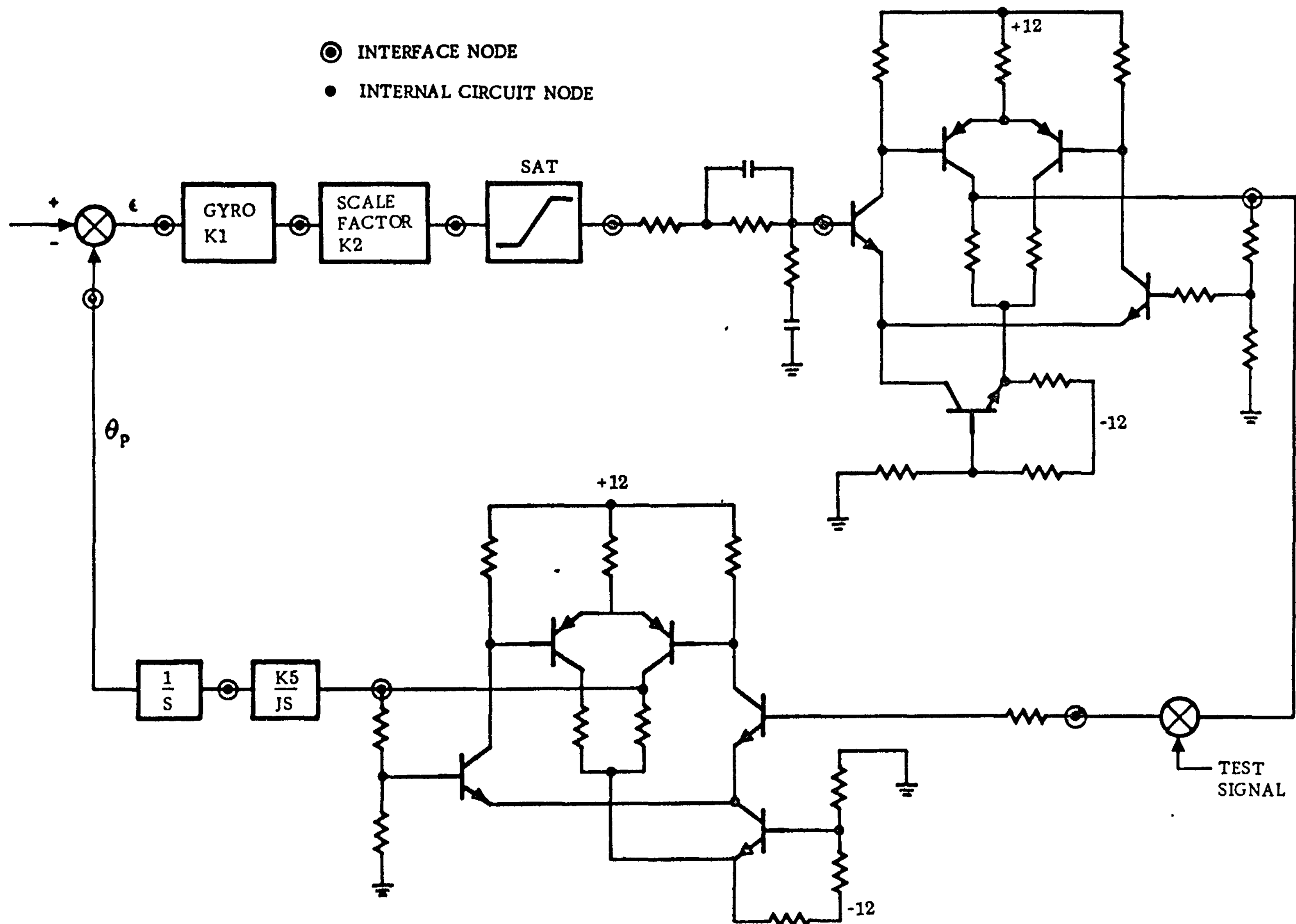

Figure 19. Detailed Diagram of Servo Loop for Secure Simulation (Functional Blocks and Circuits)

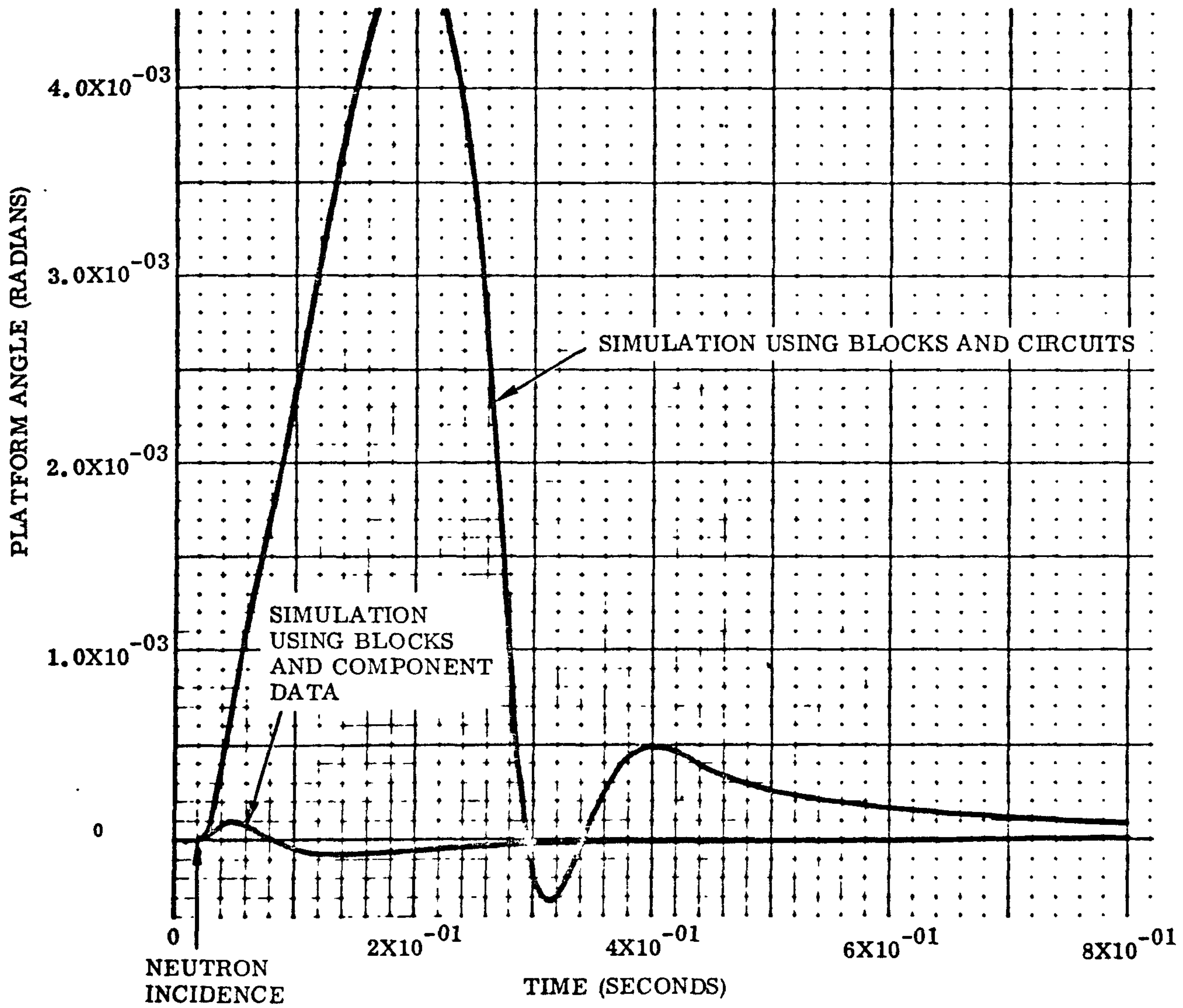

Figure 20. Loop Response for a 10 Percent Reduction in DC Current Gain (Beta) of Operational Amplifier Input Transistors

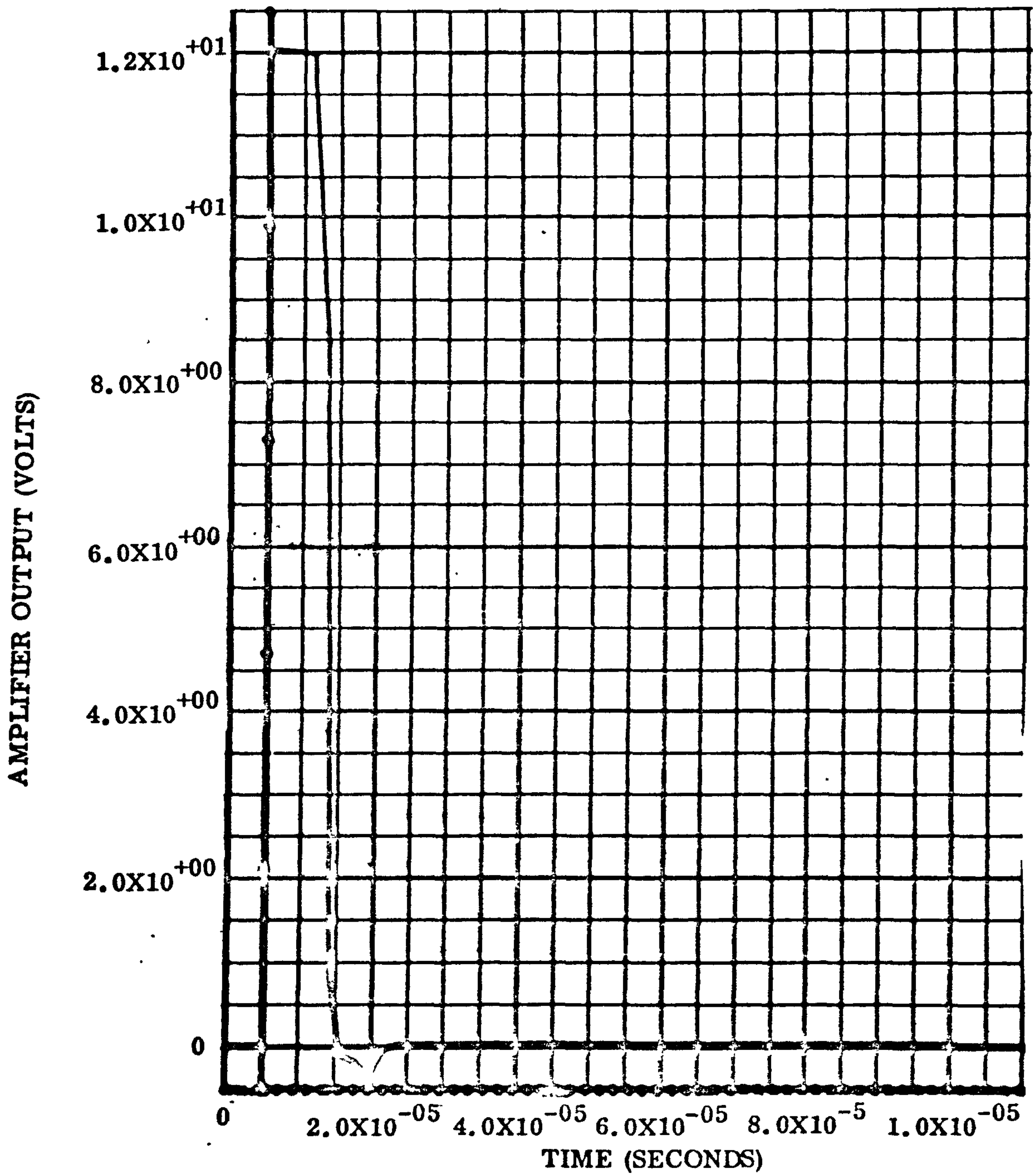

Figure 21. Introduction of 50/usec Ionization Pulse Causes Momentary Saturation of Operational Amplifier

SUMMARY

The preceding discussion has illustrated how radiation effects at the piece-part, circuit, and system levels can be performed with the aid of computers and the appropriate software. There are several accepted computer programs which are available to industry and the University for radiation effects analysis at the circuit or subsystem level. Two computer programs for system simulation (digital simulation) were discussed and an example of one of these (SECURE) was illustrated using a relatively simple servo-loop as an example.

The state-of-the-art in this field is advancing at a rapid pace. This advance is due to the following factors:

1. The rapid advancement of computer hardware--Larger memory and faster access time

2. Improvement in computer software and programming languages

3. Development of improved mathematical techniques for the solution of large sets of non-linear differential equations.

The present trend of development is directed toward digital simulation of large systems with the objective of obtaining an accurate system prediction model. These prediction models must, however, be verified by functional and radiation tests.

In addition, effort is underway to include statistical considerations in the system modeling effort in order to ascertain:

1. The sensitivity of system response to various radiation inputs

2. The relationship between piece-part behavior and system behavior

3. The probability of system survival as a function of various nuclear environments.

As a result of these developments, it appears that the time is not far off when the evaluation of systems for functional (non-radiation) response and for radiation effects becomes a matter of standard practice.

REFERENCES

1. "Simplified Engineering Techniques for Predicting Diode and Transistor Photocurrent" HDL 017-1 U.S. Army Materiel Command, Harry Diamond Laboratories and DASA (March 1968) by Hughes Aircraft Company, Fullerton, California.

2. "Analog Transient Radiation Response Analysis For Multiple-Circuit Systems"; June 64; WLTDR 64-41 Air Force Weapons Laboratory founded under DASA WEB No. 16,024; Hughes Aircraft Co., Fullerton, California.

3. NET-1 Network Analysis Program, Los Alamos Scientific Laboratory of the University of California, LA-3119, 8-10-64.

4. CIRCUS, A Digital Computer Program for Transient Analysis of Electronic Circuits, Users Guide: Report 346-1. Programmers Guide: Report 346-2. The Boeing Co., Seattle, Washington.

5. "Transient Radiation Analysis by Computer Program (TRAC)" Vol. I and Vol. II, Sponsored by U.S. Army Materiel Command, Harry Diamond Laboratories and DASA (June 1968) by Autonetics, a Division of North American Rockwell.

6. "Continuous System Modeling Program (360A-CX-16X) Users Manual" H20-0367-1 Available from IBM to users.

7. "Predicting Combined Neutron Degradation and Gamma Induced Effects on a Closed Loop System" Presented at IEEE Annual Conference on Nuclear and Space Radiation Effects at Missoula, Montana; 15-18 July 68; Autonetics Document X8-1514/501. To be published in IEEE Trans. on Nucl. Sc. Vol. NS-15, No. 6.

APPENDIX A

COMPUTER CODE SHEET AND LISTING FOR UNIJUNCTION OSCILLATOR CIRCUIT

FORTRAN CODE SHEET

DECK NO ______ PROGRAMMER ______ DATE ______ PAGE 1 of ______ JOB NO. ______

C FOR COMMENT / STATEMENT NUMBER		FORTRAN STATEMENT	IDENTIFICATION
		V(7)=(V(1)-V(6))/1.	
			00020000
		V(8)=V(6)-V(2)	
			00020010

FORM 114 C 15 REV 7 66

FORTRAN FIXED 10 DIGIT DECIMAL DATA

DECK NO. D PROGRAMMER xxx DATE xx/xx/xx PAGE 1 of ____ JOB NO. xxxx-xx

Col.	NUMBER	IDENTIFICATION (73–80)	DESCRIPTION DO NOT KEY PUNCH
1	0		Number of nonstandard parameters
13	6		Number of dependent node voltage unknowns
25	2		Number of auxiliary unknowns
37	0		Number of nonstandard parameter switches
49	− 1		Selection of initial conditions (-1 DC)
61	1	00050000	Number of time functions - i ground voltage sources
1	1		Ratio of calculated points to plotted points
13	1 5		(Unknown + Branch Current), Ratio Plotted to Printed
25	1		Phase plane plots desired
37	1		Initialization check (print error + continue)
49	0		Plots required
61	2	00050001	Number of item vs item plots (V_E, I_E)
1	1		NODE (1) VS TIME
13	2		NODE (2) VS TIME
25	3		NODE (3) VS TIME
37	4		NODE (4) VS TIME
49	5		NODE (5) VS TIME
61	6	00050010	NODE (6) VS TIME
1	7		AUXILIARY (7) I_E VS TIME
13	8		AUXILIARY (8) V_{E-B1} VS TIME
25			
37			
49			
61		00050011	

FORM 114 C-17 REV 7-58

FORTRAN FIXED 10 DIGIT DECIMAL DATA

DECK NO. D PROGRAMMER xxx DATE xx/xx/xx PAGE 2 of ___ JOB NO. XXXX-XX

	NUMBER	IDENTIFICATION	DESCRIPTION DO NOT KEY PUNCH
1	7		Auxiliary (7) I_E on X-AXIS
13	8		Auxiliary (8) V_{E-B1} ON Y-AXIS
25			
37			
49		73 80	
61		00050040	
1	.01 -03		Maximum value of Δt 1st region t=0 to t_1
13	2.5 -03		First time to change Δt
25			NO FURTHER TIME INSTRUCTIONS REQUIRED
37			
49		73 80	
61		00050100	
1			
13			
25			
37			
49		73 80	
61		00050101	
1			
13			
25			
37			
49		73 80	
61		00050102	↓ NEXT PAGE

FORM 114 C 17 REV 7 66

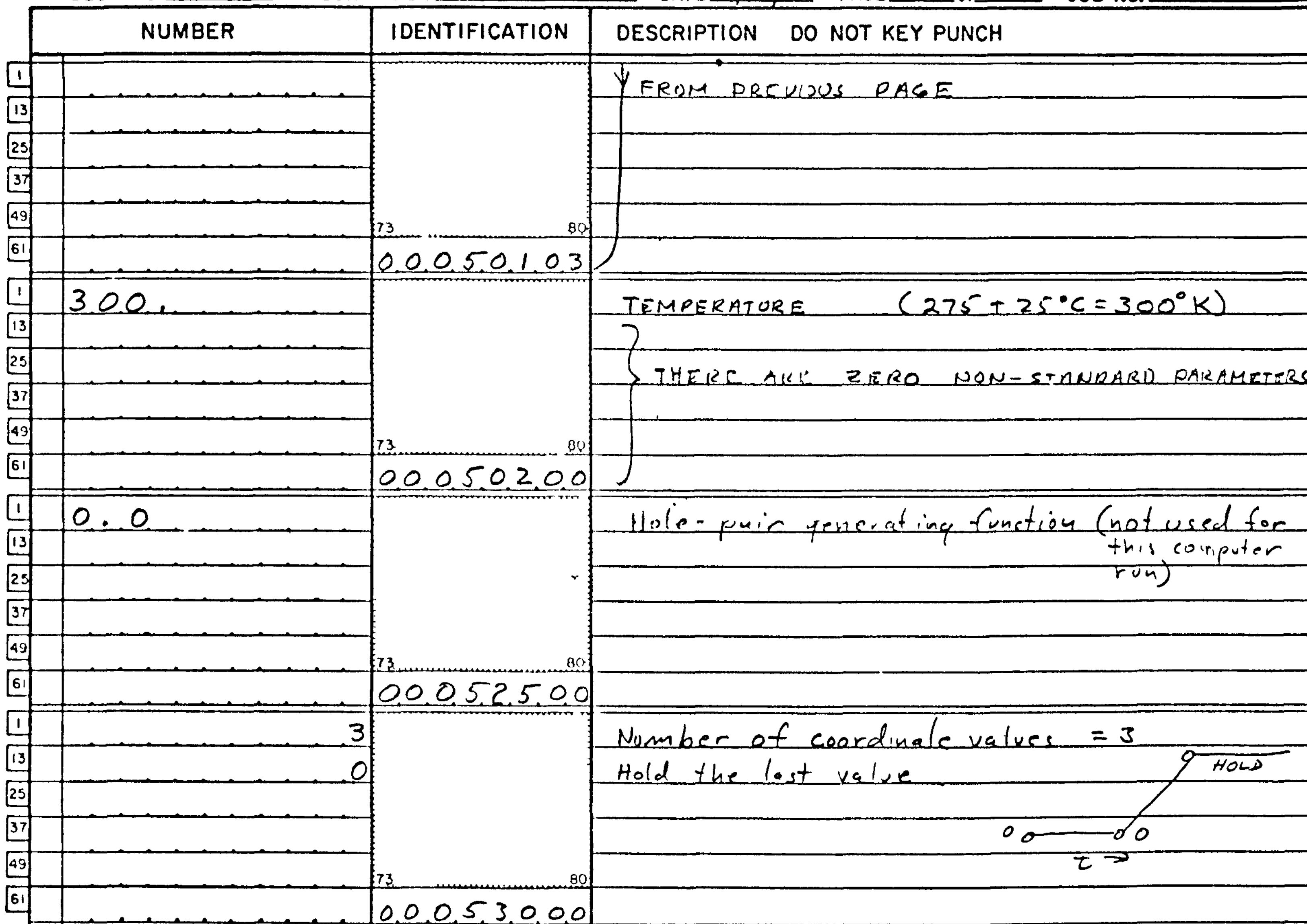

FORTRAN FIXED 10 DIGIT DECIMAL DATA

DECK NO. D PROGRAMMER XXX DATE XX/XX/XX PAGE 3 of ___ JOB NO. ___

NUMBER	IDENTIFICATION	DESCRIPTION DO NOT KEY PUNCH
	0.0.0.5.0.1.0.3	FROM PREVIOUS PAGE
300.	0.0.0.5.0.2.0.0	TEMPERATURE (275 + 25°C = 300°K) THERE ARE ZERO NON-STANDARD PARAMETERS
0.0	0.0.0.5.2.5.0.0	Hole-pair generating function (not used for this computer run)
3 0	0.0.0.5.3.0.0.0	Number of coordinate values = 3 Hold the last value

FORM 114 C 17 REV 7 88

FORTRAN FIXED 10 DIGIT DECIMAL DATA

DECK NO. D PROGRAMMER XXX DATE XX/XX/XX PAGE 4 of ___ JOB NO. XXXX

		NUMBER	IDENTIFICATION	DESCRIPTION DO NOT KEY PUNCH
1		0.0		Value of S_1 at $t = 0$
13				$t = 0$
25		0.0		value of S_1 at $t = .1$ Millisecond
37		0.1 -03		$t = .1 \times 10^{-3}$ sec
49		20.0	73 80	value of S_1 at $t = .2$ Millisecond (volts)
61		0.2 -03	00053001	$t = .2 \times 10^{-3}$ sec
1		0		
13				
25				
37				
49			73 80	
61			00054000	
1		6		Number of resistors
13				
25				
37				
49			73 80	
61			00055000	
1	S	1		R1 connected to S1
13		1		R1 connected to node (1)
25		10. +03		$R1 = 10 \times 10^3 = 10K$ ohm
37				
49			73 80	
61			00055010	

FORM 114 C 17 REV 7 68

FORTRAN FIXED 10 DIGIT DECIMAL DATA

DECK NO. ______ PROGRAMMER ______ DATE ______ PAGE 5 of ______ JOB NO. ______

Col.		NUMBER	IDENTIFICATION	DESCRIPTION DO NOT KEY PUNCH
1		2		Resistor R_2 connected to node 2
13	G			Resistor R_2 connected to ground
25		50.		R_2 = 50 ohms
37				
49			73 … 80	
61			00055020	
1	S	1		S1
13		5		node (5)
25		2. +03		R_3 = 2 Kohm
37				
49			73 … 80	
61			00055030	
1		5		NODE (5)
13		2		NODE (2)
25		2. +03		R_4 = 2 Kohms
37				
49			73 … 80	
61			00055040	
1		3		NODE (3)
13		2		NODE (2)
25		20.0		R_5 = 20 ohms
37				
49			73 … 80	
61			00055050	

FORM 114 C 17 REV 7 66

FORTRAN FIXED 10 DIGIT DECIMAL DATA

DECK NO. ______ PROGRAMMER ______ DATE ______ PAGE 6 of ______ JOB NO. ______

Col.	NUMBER	IDENTIFICATION (73–80)	DESCRIPTION DO NOT KEY PUNCH
1	1		NODE (1)
13	6		NODE (6)
25	1.		Rs - 1.0 ohm
37			
49			
61		00055060	
1	1		Number of Capacitors = 1
13			
25			
37			
49			
61		00056000	
1	1		CONNECTED TO NODE (1)
13	6		CONNECTED TO GROUND
25	.1 -06		C = .1 μfd
37	1.0		Rs = 1.0 ohm
49	0.0		Value of initial current = 0
61	10. +06	00056010	Value of shunt (leakage) resistance 10Mohm
1	0		There are no inductors in
13			this circuit
25			
37			
49			
61		00057000	

FORM 114 C 17 REV 7 60

FORTRAN FIXED 10 DIGIT DECIMAL DATA

DECK NO. ______ PROGRAMMER ______ DATE ______ PAGE 7 of ______ JOB NO. ______

Col.	NUMBER	IDENTIFICATION (73–80)	DESCRIPTION DO NOT KEY PUNCH
1	0		There are no diodes in this
13			circuit
25			
37			
49			
61		00058000	
1	2		There are two transistors in
13			the circuit
25			
37			
49			
61		00059000	
1	1		1 for PNP
13	5		Base connected to node (5)
25	4		Collector connected to node (4)
37	6		Emitter connected to node (6)
49			DATA NOT THE SAME AS PRECEEDING TRANSISTOR
61		00059010	
1	1.5		$h_{FEN} = 1.5$
13	.2		$h_{FEI} = .2$
25	1. -06		$T_N = 1. \times 10^{-6}$ sec
37	4. -06		$T_I = 4. \times 10^{-6}$ sec
49	0.1 -06		$I_{CS} = .1\ \mu A$
61	1.0	00059015	$M_C = 1.$

FORM 114 C 17 REV 7-66

FORTRAN FIXED 10 DIGIT DECIMAL DATA

DECK NO. ______ PROGRAMMER ______ DATE ______ PAGE 8 of ______ JOB NO. ______

Col.	NUMBER		IDENTIFICATION	DESCRIPTION DO NOT KEY PUNCH
1	5.	-12		C_{CO} = 5 pfd
13	.75			V_{CBI} = .75 volt
25	10.	+06		R_{CL} = 10 MΩ
37	.05	-06		I_{ES} = .05 μa
49	1.		73 80	M_E = 1
61	10.	-12	00059020	C_{EO} = 10 pfd
1	.75			V_{EBI} = .75 volt
13	10.	+06		I_{ppc} = 1 ma / 10^7 R/sec
25	1.0	-03		I_{ppe} = .1 ma / 10^7 R/sec
37	.1	-03		
49			73 80	
61			00059030	
1		0		0 for NPN
13		4		Base connected to node (4)
25		5		collector connected to node (5)
37		3		Emitter connected to node (6)
49		1	73 80	Data for NPN assumed same as PNP
61			00059040	
1				
13				
25				
37				
49			73 80	
61				

ORM 114 C-17 REV 7 58

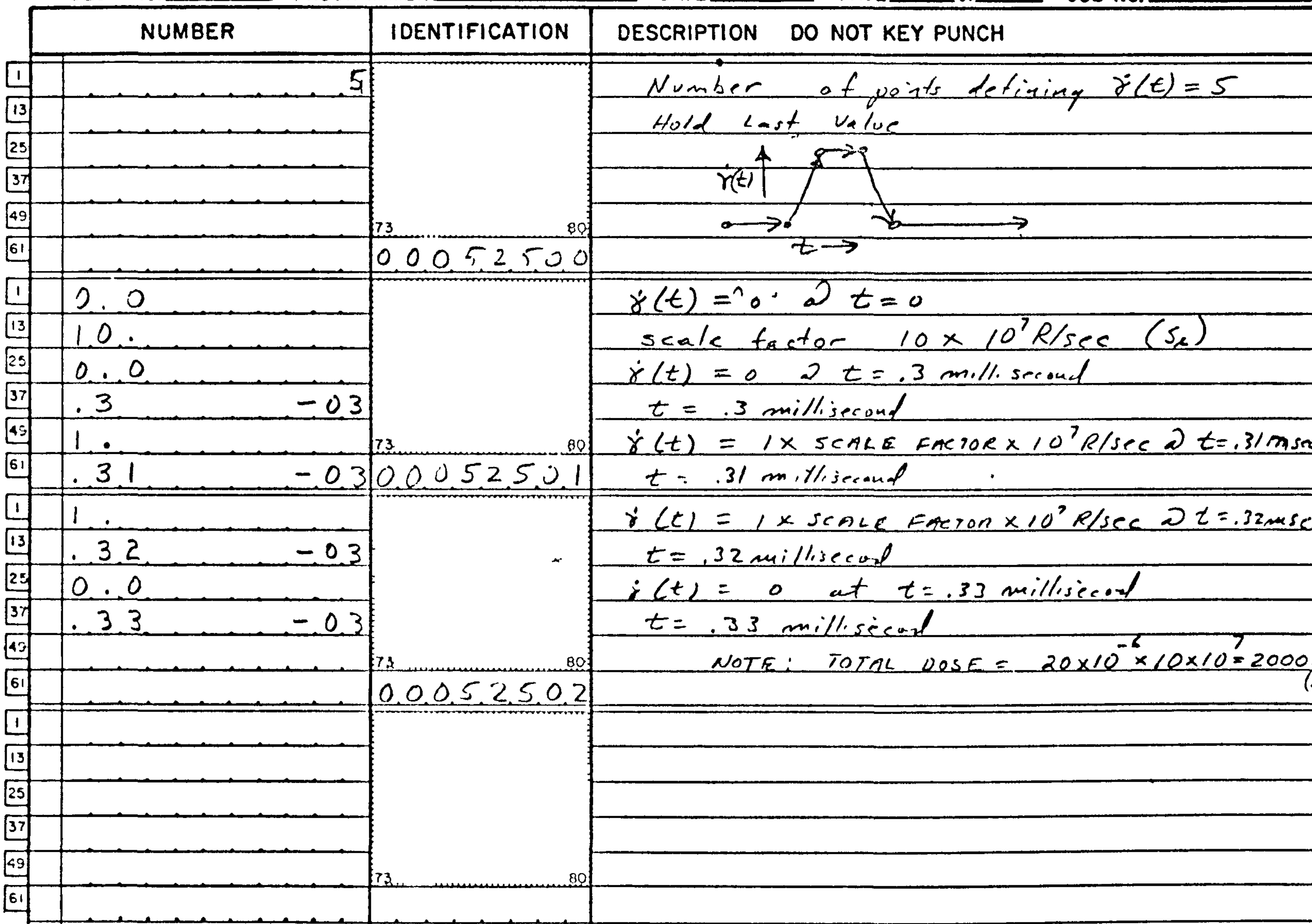

FORTRAN FIXED 10 DIGIT DECIMAL DATA

INSERT FOR IONIZATION

DECK NO. ____ PROGRAMMER ____ DATE ____ PAGE ___ of ___ JOB NO. ____

Col.	NUMBER	IDENTIFICATION (73–80)	DESCRIPTION DO NOT KEY PUNCH
1	5		Number of points defining $\dot{\gamma}(t) = 5$
13			Hold Last Value
25			
37			
49			
61		00052500	
1	0.0		$\dot{\gamma}(t) = 0$ @ $t=0$
13	10.		scale factor 10×10^7 R/sec (S_F)
25	0.0		$\dot{\gamma}(t) = 0$ @ $t = .3$ milli second
37	.3 -03		$t = .3$ millisecond
49	1.		$\dot{\gamma}(t) = 1 \times$ SCALE FACTOR $\times 10^7$ R/sec @ $t = .31$ msec
61	.31 -03	00052501	$t = .31$ millisecond
1	1.		$\dot{\gamma}(t) = 1 \times$ SCALE FACTOR $\times 10^7$ R/sec @ $t = .32$ msec
13	.32 -03		$t = .32$ millisecond
25	0.0		$\dot{\gamma}(t) = 0$ at $t = .33$ millisecond
37	.33 -03		$t = .33$ millisecond
49			NOTE: TOTAL DOSE $= 20 \times 10^{-6} \times 10 \times 10^{7} = 2000$ Rad (S_F)
61		00052502	
1			
13			
25			
37			
49			
61			

FORTRAN FIXED 10 DIGIT DECIMAL DATA *NEUTRON*

DECK NO. ______ PROGRAMMER ______ DATE ______ PAGE ___ of ___ JOB NO. ______

	NUMBER	IDENTIFICATION	DESCRIPTION DO NOT KEY PUNCH
1	3		
13	2		
25	50.		
37			
49		73 80	
61		00055050	
1	3		
13	2		
25	150.		
37			
49		73 80	
61		00055050	
1	3		
13	2		
25	250.		
37			
49		73 80	
61		00055050	
1	3		
13	2		
25	1500.		
37			
49		73 80	
61		00055050	

FORM 114 C 17 REV 7 60

```
TRAC D   PROGRAM        VERSION 7094                    C7/25/68


  0  NO. OF NONSTANCARD PARAMETERS
  6  NO. OF NODE UNKNOWNS
  2  NO. OF AUX. UNKNOWNS
  0  NO. OF PARAMETER SW.
 -1  INITIAL CCNDITICNS
     (-2=PRV, -1=DC, C=ZERO, 1=RD V,I, 2=RD V+I, 3=RD V-DC, 4=RD V,I-CALC)
  1  NO. OF TIME FUNCT. AND GRD. VOLT. SOURCES
  1  RATIO OF CALC. PTS. TO PLOTTED PTS.
  5  RATIO OF PLOTTED PTS. TO PRINTED PTS.
  1  1 FOR PHASE PLANE PLOTS
  1  PROGRAM I.C. CHECK
     (-1=I.C. CNLY, C=HALT FOR P.E., 1=CONTINUE FOR P.E.)


PLOTS OF ITEMS VS TIME
 NAME      NO.
             1
             2
             3
             4
             5
             6
             7
             8


PLOTS OF ITEM VS ITEM
ITEM X    ITEM Y
   7         8
```

NO.	MAXIMUM DELTA TIME	END TIME
1	0.1CCC0CE-C4	C.2500U0E-02
2	-0.	-C.
3	-0.	-C.
4	-0.	-C.
5	-0.	-C.
6	-C.	-C.
7	-0.	-C.
8	-0.	-C.
9	-C.	-C.
10	-0.	-C.

TEMPFRATURE= C.3CCCCE C3

NO.	MAXIMLM DELTA TIME	END TIME
1	0.1CCCOCE-C4	C.2500UUE-02
2	-0.	-C.
3	-0.	-C.
4	-0.	-C.
5	-0.	-C.
6	-C.	-C.
7	-0.	-C.
8	-0.	-C.
9	-0.	-C.
10	-0.	-C.

TEMPFRATURE= C.3CCCCE C3

```
TIME FN.(GRD. VOLT. SOURCE) NO.  1       LAST VALUE HELD
PT.NO.      VALUE          TIME
   1  -0.              -C.
   2  -0.               1.000000E-04
   3   0.2CCCOE 02     C.200000E-03
```

RESISTORS

PART NO.	NODE F	NODE T	BRANCH NO.	BRANCH CURRENT	RESISTANCE
1	S 1	1	1	C.	0.10000E 05
2	2	GROUND	2	C.	0.50000E 02
3	S 1	5	3	C.	0.20000E 04
4	5	2	4	C.	0.20000E 04
5	3	2	5	C.	0.20000E 02
6	1	6	6	C.	0.10000E 01

CAPACITORS

PART NO.	NODE F	NODE T	BRANCH NO.	BRANCH CURRENT	CAPACITANCE	SERIES RESISTANCE	SHUNT RESISTANCE
1	1	GROUND	7	0.	0.10000E-06	0.10000E 01	0.10000E 08

```
TRANSISTOR NO.  1    PNP  TYPE
NODE B  NODE C  NODE E                        BRANCH CURRENT NO.   8  IB=  0.
   5       4       6                                         NO.   9  IC=  0.
 HFE N 0.1500E 01  HFE I 0.2000E-00    T N 1.0000E-06    T I 0.4000E-05
   ICS 0.1000E-06      MC 0.1000E 01   CCO 0.5000E-11   VCBI 0.7500E 00    RCL 0.1000E 08
   IES 0.5000E-07      ME 0.1000E 01   CEO 0.1000E-10   VEBI 0.7500E 00    REL 0.1000E 08
  IPPC 1.0000E-03    IPPE 1.0000E-04

TRANSISTOR NO.  2    NPN  TYPE
NODE B  NODE C  NODE E                        BRANCH CURRENT NO.  10  IB=  0.
   4       5       3                                         NO.  11  IC=  0.
 HFE N 0.1500E 01  HFE I 0.2000E-00    T N 1.0000E-06    T I 0.4000E-05
   ICS 0.1000E-06      MC 0.1000E 01   CCO 0.5000E-11   VCBI 0.7500E 00    RCL 0.1000E 08
   IES 0.5000E-07      ME 0.1000E 01   CEO 0.1000E-10   VEBI 0.7500E 00    REL 0.1000E 08
  IPPC 1.0000E-03    IPPE 1.0000E-04
```

INITIAL CONDITIONS

```
TIME= 0.                DELTA TIME= 0.                         H-P GEN. FN.=  0.
TIME FNS. AND GRD. VOLT. SOURCES
  1 -0.
UNKNOWNS
  1  0.           2  0.           3  0.           4  0.           5  0.           6  0.
  7  0.           8  0.
BRANCH CURRENTS
  1 -0.           2  0.           3 -0.           4  0.           5  0.           6  0.
  7  0.           8  0.           9 -0.          10  0.          11 -0.

MAXIMUM DELTA TIME=   0.100000E-04     START TIME=   0.              END TIME=   0.250000E-02
```

```
TIME= 0.10C000E-C4     DELTA TIME= 0.100000E-04          H-P GEN. FN.=  0.
TIME FNS. AND GRD. VCLT. SOURCES
  1  0.
UNKNOWNS
  1  0.              2  C.             3  0.              4  0.             5  0.             6  0.
  7  0.              8  0.
BRANCH CURRENTS
  1  0.              2  0.             3  0.              4  0.             5  0.             6  0.
  7  0.              8  0.             9 -0.             10  0.            11 -0.

TIME= 0.50C000E-04     DELTA TIME= 0.100000E-04          H-P GEN. FN.=  0.
TIME FNS. AND GRD. VCLT. SOURCES
  1  0.
UNKNOWNS
  1  0.              2  0.             3  0.              4  0.             5  0.             6  C.
  7  0.              8  C.
BRANCH CURRENTS
  1  0.              2  0.             3  0.              4  0.             5  0.             6  0.
  7  0.              8  C.             9 -0.             10  0.            11 -0.

TIME= 1.00C000E-C4     DELTA TIME= 0.1C0000E-04          H-P GEN. FN.=  0.
TIME FNS. AND GRD. VCLT. SOURCES
  1  0.
UNKNOWNS
  1  0.              2  0.             3  0.              4  0.             5  0.             6  0.
  7  0.              8  0.
BRANCH CURRENTS
  1  0.              2  0.             3  0.              4  0.             5  0.             6  0.
  7  0.              8  0.             9 -0.             10  0.            11 -0.

TIME= 1.00C0C0E-C4     DELTA TIME= 0.100000E-04          H-P GEN. FN.=  0.
TIME FNS. AND GRD. VCLT. SOURCES
  1  0.
UNKNOWNS
  1  0.              2  0.             3  0.              4  0.             5  0.             6  0.
  7  0.              8  C.
BRANCH CURRENTS
  1  0.              2  0.             3  0.              4  0.             5  0.             6  C.
```

```
  7  0.              8  0.              9 -0.             10  0.             11 -0.

TIME= 0.150000E-03      DELTA TIME= 0.100000E-04           H-P GEN. FN.=  0.
TIME FNS. AND GRD. VOLT. SOURCES
  1  0.10000E 02
UNKNOWNS
  1  0.24709E-00     2  0.12351E-00     3  0.12357E-00     4  0.22997E-00     5  0.50580E 01     6  0.24709E-00
  7 -0.82888E-06     8  0.12358E-00
BRANCH CURRENTS
  1  0.97529E-03     2  0.24702E-02     3  0.24710E-02     4  0.24672E-02     5  0.29786E-05     6 -0.82888E-06
  7  0.97610E-03     8  0.14274E-05     9 -0.60149E-06    10  0.60149E-06    11  0.23771E-05

TIME= 0.200000E-03      DELTA TIME= 0.100000E-04           H-P GEN. FN.=  0.
TIME FNS. AND GRD. VOLT. SOURCES
  1  0.20000E 02
UNKNOWNS
  1  0.96992E 00     2  0.24702E-00     3  0.24712E-00     4  0.36863E-00     5  0.10117E 02     6  0.96992E 00
  7 -0.11623E-05     8  0.72290E 00
BRANCH CURRENTS
  1  0.19030E-02     2  0.49403E-02     3  0.49415E-02     4  0.49350E-02     5  0.53568E-05     6 -0.11623E-05
  7  0.19041E-02     8  0.22271E-05     9 -0.10787E-05    10  0.10787E-05    11  0.42780E-05

TIME= 0.200000E-03      DELTA TIME= 0.100000E-04           H-P GEN. FN.=  0.
TIME FNS. AND GRD. VOLT. SOURCES
  1  0.20000E 02
UNKNOWNS
  1  0.96992E 00     2  0.24702E-00     3  0.24712E-00     4  0.36863E-00     5  0.10117E 02     6  0.96992E 00
  7 -0.11623E-05     8  0.72290E 00
BRANCH CURRENTS
  1  0.19030E-02     2  0.49403E-02     3  0.49415E-02     4  0.49350E-02     5  0.53568E-05     6 -0.11623E-05
  7  0.19041E-02     8  0.22271E-05     9 -0.10787E-05    10  0.10787E-05    11  0.42780E-05

TIME= 0.250000E-03      DELTA TIME= 0.100000E-04           H-P GEN. FN.=  0.
TIME FNS. AND GRD. VOLT. SOURCES
  1  0.20000E 02
UNKNOWNS
  1  0.18983E 01     2  0.24702E-00     3  0.24713E-00     4  0.36826E-00     5  0.10117E 02     6  0.18983E 01
  7 -0.83447E-06     8  0.16513E 01
BRANCH CURRENTS
  1  0.18102E-02     2  0.49405E-02     3  0.49413E-02     4  0.49352E-02     5  0.52565E-05     6 -0.83447E-06
```

```
7 0.181C8E-C2   8 C.18565E-05   9 -0.10449E-05  10 0.10449E-C5  11 0.42115E-05

TIME= 0.30C000E-03     DELTA TIME= 0.100000E-04          H-P GEN. FN.=  0.
TIME FNS. AND GRD. VCLT. SOURCES
  1  0.2C0C0E C2
UNKNOWNS
  1  0.27814E 01   2  0.24703E-00   3  0.24713E-00   4  0.36826E-00   5  0.10118E 02   6  0.27814E 01
  7 -0.77486E-C6   8  0.25343E 01
BRANCH CURRENTS
  1  0.17219E-02   2  0.49405E-02   3  0.49412E-02   4  0.49353E-C2   5  0.52566E-05   6 -C.77486E-C6
  7  0.17224E-C2   8  0.17681E-05   9 -0.10449E-05  10  0.10449E-05  11  0.42115E-05

TIME= 0.35C000E-C3     DELTA TIME= 0.100000E-C4          H-P GEN. FN.=  0.
TIME FNS. AND GRD. VCLT. SOURCES
  1  0.2CCC0E C2
UNKNOWNS
  1  0.36213E C1   2  0.24703E-00   3  0.24713E-00   4  0.36826E-00   5  0.10118E 02   6  0.36213E 01
  7 -0.68545E-C6   8  0.33742E 01
BRANCH CURRENTS
  1  0.16379E-02   2  0.49406E-02   3  0.49412E-02   4  0.49353E-C2   5  0.52566E-05   6 -0.68545E-06
  7  0.16382E-C2   8  C.16840E-05   9 -0.10449E-05  10  0.10449E-C5  11  0.42116E-05

TIME= 0.40C0C0E-03     DELTA TIME= 0.100000E-04          H-P GEN. FN.=  0.
TIME FNS. AND GRD. VCLT. SOURCES
  1  0.2C0C0E C2
UNKNOWNS
  1  0.44201E C1   2  0.24703E-00   3  0.24713E-00   4  0.36827E-00   5  0.10118E 02   6  0.44201E 01
  7 -0.65565E-C6   8  0.41731E 01
BRANCH CURRENTS
  1  0.15580E-C2   2  0.49406E-02   3  0.49412E-02   4  0.49353E-C2   5  0.52568E-05   6 -0.65565E-06
  7  0.15582E-C2   8  C.16038E-05   9 -0.10449E-05  10  0.10449E-C5  11  0.42116E-05

TIME= 0.45C0CCE-C3     DELTA TIME= 0.100000E-04          H-P GEN. FN.=  0.
TIME FNS. AND GRD. VOLT. SOURCES
  1  0.2CCC0E C2
UNKNOWNS
  1  0.518C0E C1   2  0.24703E-00   3  0.24714E-00   4  0.36827E-00   5  0.10118E 02   6  0.51800E C1
  7 -0.59605E-C6   8  C.49329E 01
BRANCH CURRENTS
  1  0.14820E-02   2  0.49406E-02   3  0.49411E-02   4  0.49354E-02   5  0.52568E-05   6 -C.59605E-06
```

```
  7  0.14821E-C2   8  0.15273E-05   9 -0.10450E-05  10  0.10450E-05  11  0.42116E-05

TIME= 0.5CCC00E-C3     DELTA TIME= 0.100000E-04          H-P GEN. FN.=  0.
TIME FNS. AND GRD. VCLT. SOURCES
  1  0.2CCC0E C2
UNKNOWNS
  1  0.59027E C1   2  0.24703E-00   3  0.24714E-00   4  0.36827E-00   5  0.10118E 02   6  C.59027E 01
  7 -0.47684E-C6   8  C.56557E 01
BRANCH CURRENTS
  1  0.14057E-C2   2  0.49407E-02   3  0.49411E-02   4  0.49354E-C2   5  0.52568E-05   6 -0.47684E-C6
  7  0.14057E-C2   8  0.14543E-05   9 -0.10450E-05  10  0.10450E-C5  11  0.42117E-05

TIME= 0.55CCCCE-C3     DELTA TIME= 0.100000E-04          H-P GEN. FN.=  0.
TIME FNS. AND GRC. VCLT. SOURCES
  1  0.2C0C0E C2
UNKNOWNS
  1  0.659C1E C1   2  0.24703E-00   3  0.24714E-00   4  0.36827E-00   5  0.10118E 02   6  C.65901E 01
  7 -0.47684E-C6   8  0.63431E 01
BRANCH CURRENTS
  1  C.13410E-C2   2  0.49407E-02   3  0.49410E-02   4  0.49354E-02   5  0.52569E-05   6 -0.47684E-C6
  7  C.13409E-C2   8  C.13845E-05   9 -0.1045CE-05  10  0.10450E-C5  11  0.42117E-05

TIME= 0.6CCCCCE-C3     DELTA TIME= 0.100000E-04          H-P GEN. FN.=  0.
TIME FNS. AND GRD. VCLT. SOURCES
  1  0.2CCC0E C2
UNKNOWNS
  1  0.72440E C1   2  C.24704E-00   3  0.24714E-00   4  0.36827E-00   5  0.10118E 02   6  0.72440E 01
  7 -0.35763E-C6   8  C.69969E 01
BRANCH CURRENTS
  1  0.12756E-02   2  0.49407E-02   3  0.49410E-02   4  0.49355E-C2   5  0.52568E-05   6 -0.35763E-C6
  7  C.12754E-C2   8  0.13177E-05   9 -0.10450E-05  10  0.10450E-C5  11  0.42117E-05

TIME= 0.65CC0CE-C3     DELTA TIME= 0.1C0000E-04          H-P GEN. FN.=  0.
TIME FNS. AND GRD. VCLT. SOURCES
  1  0.20CC0E 02
UNKNOWNS
  1  0.78659E C1   2  0.24704E-00   3  0.24714E-00   4  0.36828E-00   5  0.10118E 02   6  C.78659E C1
  7 -0.23842E-C6   8  C.76188E 01
BRANCH CURRENTS
  1  C.12134E-C2   2  0.49406E-02   3  0.49410E-02   4  0.49355E-02   5  0.52568E-05   6 -0.23842E-C6
```

```
  1  0.
UNKNOWNS
  1  0.84574E 01    2  0.
  7 -0.23842E-06    8  0.82104E 01
BRANCH CURRENTS
  1  0.11543E-02    2  0.49408E-02    3  0.49409E-02
  7  0.11538E-02    8  0.11914E-05    9 -0.10450E-05   10  0.

TIME= 0.750000E-03     DELTA TIME= 0.100000E-04          H-P GEN. FN.=  0.
TIME FNS. AND GRD. VOLT. SOURCES
  1  0.20000E 02
UNKNOWNS
  1  0.90200E 01    2  0.24704E-00    3  0.24715E-00    4  0.36828E-00    5  0.10118E 02    6  0.90200E 01
  7 -0.23842E-06    8  0.87730E 01
BRANCH CURRENTS
  1  0.10980E-02    2  0.49408E-02    3  0.49409E-02    4  0.49356E-02    5  0.52569E-05    6 -0.23842E-06
  7  0.10974E-02    8  0.11309E-05    9 -0.10450E-05   10  0.10450E-05   11  0.42118E-05

TIME= 0.800000E-03     DELTA TIME= 0.100000E-04          H-P GEN. FN.=  0.
TIME FNS. AND GRD. VOLT. SOURCES
  1  0.20000E 02
UNKNOWNS
  1  0.95552E 01    2  0.24704E-00    3  0.24715E-00    4  0.36828E-00    5  0.10118E 02    6  0.95552E 01
  7 -0.23842E-06    8  0.93081E 01
BRANCH CURRENTS
  1  0.10445E-02    2  0.49409E-02    3  0.49409E-02    4  0.49356E-02    5  0.52569E-05    6 -0.23842E-06
  7  0.10438E-02    8  0.10707E-05    9 -0.10450E-05   10  0.10450E-05   11  0.42118E-05

TIME= 0.850000E-03     DELTA TIME= 0.100000E-04          H-P GEN. FN.=  0.
TIME FNS. AND GRD. VOLT. SOURCES
  1  0.20000E 02
UNKNOWNS
  1  0.10064E 02    2  0.24704E-00    3  0.24715E-00    4  0.36829E-00    5  0.10118E 02    6  0.10064E 02
  7  0.             8  0.98171E 01
BRANCH CURRENTS
  1  0.99359E-03    2  0.49409E-02    3  0.49408E-02    4  0.49356E-02    5  0.52577E-05    6  0.
```

```
  7  0.99277E-03    8  0.10072E-05    9 -0.10454E-05   10  0.10454E-05   11  0.42123E-05

TIME= 0.685000E-03     DELTA TIME= 0.500000E-05          H-P GEN. FN.=  0.
TIME FNS. AND GRD. VOLT. SOURCES
  1  0.20000E 02
UNKNOWNS
  1  0.10294E 02    2  0.40351E-00    3  0.46888E-00    4  0.75414E 00    5  0.10007E 02    6  0.10291E 02
  7  0.30736E-02    8  0.98872E 01
BRANCH CURRENTS
  1  0.97062E-03    2  0.80702E-02    3  0.49965E-02    4  0.48017E-02    5  0.32685E-02    6  0.30736E-02
  7 -0.21038E-02    8 -0.14897E-02    9 -0.15839E-02   10  0.15839E-02   11  0.16846E-02

TIME= 0.915000E-03     DELTA TIME= 0.500000E-05          H-P GEN. FN.=  0.
TIME FNS. AND GRD. VOLT. SOURCES
  1  0.20000E 02
UNKNOWNS
  1  0.14252E 01    2  0.72599E 00    3  0.10125E 01    4  0.13429E 01    5  0.11139E 01    6  0.14201E 01
  7  0.50768E-02    8  0.69408E 00
BRANCH CURRENTS
  1  0.18575E-02    2  0.14520E-01    3  0.94431E-02    4  0.19395E-03    5  0.14326E-01    6  0.50768E-02
  7 -0.32195E-02    8 -0.66894E-03    9 -0.44079E-02   10  0.44079E-02   11  0.99180E-02

TIME= 0.955000E-03     DELTA TIME= 0.100000E-04          H-P GEN. FN.=  0.
TIME FNS. AND GRD. VOLT. SOURCES
  1  0.20000E 02
UNKNOWNS
  1  0.20997E 01    2  0.24731E-00    3  0.24765E-00    4  0.40890E-00    5  0.10106E 02    6  0.20997E 01
  7 -0.80466E-06    8  0.18524E 01
BRANCH CURRENTS
  1  0.17900E-02    2  0.49462E-02    3  0.49470E-02    4  0.49293E-02    5  0.16901E-04    6 -0.80466E-06
  7  0.17907E-02    8  0.18439E-05    9 -0.10425E-05   10  0.10425E-05   11  0.15858E-04

TIME= 0.100500E-02     DELTA TIME= 0.100000E-04          H-P GEN. FN.=  0.
TIME FNS. AND GRD. VOLT. SOURCES
  1  0.20000E 02
UNKNOWNS
  1  0.29729E 01    2  0.24703E-00    3  0.24713E-00    4  0.36833E-00    5  0.10118E 02    6  0.29729E 01
  7 -0.74506E-06    8  0.27258E 01
BRANCH CURRENTS
  1  0.17027E-02    2  0.49405E-02    3  0.49412E-02    4  0.49353E-02    5  0.52650E-05    6 -0.74506E-06
```

```
   0.17032E-02   8  0.17490E-05   9 -0.10449E-05  10  0.10449E-05  11  0.42200E-05

TIME= 0.105500E-02     DELTA TIME= 0.100000E-04          H-P GEN. FN.=  0.
TIME FNS. AND GRD. VOLT. SOURCES
  1  0.20000E 02
UNKNOWNS
  1  0.38034E 01   2  0.24703E-00   3  0.24713E-00   4  0.36826E-00   5  0.10118E 02   6  0.38034E 01
  7 -0.68545E-06   8  0.35564E 01
BRANCH CURRENTS
  1  0.16197E-02   2  0.49406E-02   3  0.49412E-02   4  0.49353E-02   5  0.52566E-05   6 -0.68545E-06
  7  0.16200E-02   8  0.16657E-05   9 -0.10449E-05  10  0.10449E-05  11  0.42116E-05

TIME= 0.110500E-02     DELTA TIME= 0.100000E-04          H-P GEN. FN.=  0.
TIME FNS. AND GRD. VOLT. SOURCES
  1  0.20000E 02
UNKNOWNS
  1  0.45934E 01   2  0.24703E-00   3  0.24714E-00   4  0.36827E-00   5  0.10118E 02   6  0.45934E 01
  7 -0.65565E-06   8  0.43464E 01
BRANCH CURRENTS
  1  0.15407E-02   2  0.49406E-02   3  0.49411E-02   4  0.49353E-02   5  0.52567E-05   6 -0.65565E-06
  7  0.15409E-02   8  0.15864E-05   9 -0.10449E-05  10  0.10449E-05  11  0.42116E-05

TIME= 0.115500E-02     DELTA TIME= 0.100000E-04          H-P GEN. FN.=  0.
TIME FNS. AND GRD. VOLT. SOURCES
  1  0.20000E 02
UNKNOWNS
  1  0.53448E 01   2  0.24703E-00   3  0.24714E-00   4  0.36827E-00   5  0.10118E 02   6  0.53448E 01
  7 -0.53644E-06   8  0.50977E 01
BRANCH CURRENTS
  1  0.14655E-02   2  0.49406E-02   3  0.49411E-02   4  0.49354E-02   5  0.52567E-05   6 -0.53644E-06
  7  0.14656E-02   8  0.15107E-05   9 -0.10450E-05  10  0.10450E-05  11  0.42116E-05

TIME= 0.120500E-02     DELTA TIME= 0.100000E-04          H-P GEN. FN.=  0.
TIME FNS. AND GRD. VOLT. SOURCES
  1  0.20000E 02
UNKNOWNS
  1  0.60595E 01   2  0.24703E-00   3  0.24714E-00   4  0.36827E-00   5  0.10118E 02   6  0.60595E 01
  7 -0.41723E-06   8  0.58124E 01
BRANCH CURRENTS
  1  0.13941E-02   2  0.49407E-02   3  0.49411E-02   4  0.49354E-02   5  0.52568E-05   6 -0.41723E-06
```

```
  7  0.13940E-02   8  0.14364E-05   9 -0.10450E-05  10  0.10450E-05  11  0.42117E-05

TIME= 0.125500E-02      DELTA TIME= 0.100000E-04          H-P GEN. FN.=  0.
TIME FNS. AND GRD. VOLT. SOURCES
  1  0.20000E 02
UNKNOWNS
  1  0.67392E 01   2  0.24704E-00   3  0.24714E-00   4  0.36827E-00   5  0.10118E 02   6  0.67392E 01
  7 -0.35763E-06   8  0.64922E 01
BRANCH CURRENTS
  1  0.13261E-02   2  0.49407E-02   3  0.49410E-02   4  0.49355E-02   5  0.52568E-05   6 -0.35763E-06
  7  0.13259E-02   8  0.13693E-05   9 -0.10450E-05  10  0.10450E-05  11  0.42117E-05

TIME= 0.130500E-02      DELTA TIME= 0.100000E-04          H-P GEN. FN.=  0.
TIME FNS. AND GRD. VOLT. SOURCES
  1  0.20000E 02
UNKNOWNS
  1  0.73858E 01   2  0.24704E-00   3  0.24714E-00   4  0.36827E-00   5  0.10118E 02   6  0.73858E 01
  7 -0.29802E-06   8  0.71387E 01
BRANCH CURRENTS
  1  0.12614E-02   2  0.49407E-02   3  0.49410E-02   4  0.49355E-02   5  0.52569E-05   6 -0.29802E-06
  7  0.12611E-02   8  0.13031E-05   9 -0.10450E-05  10  0.10450E-05  11  0.42117E-05

TIME= 0.135500E-02      DELTA TIME= 0.100000E-04          H-P GEN. FN.=  0.
TIME FNS. AND GRD. VOLT. SOURCES
  1  0.20000E 02
UNKNOWNS
  1  0.80008E 01   2  0.24704E-00   3  0.24714E-00   4  0.36828E-00   5  0.10118E 02   6  0.80008E 01
  7 -0.35763E-06   8  0.77537E 01
BRANCH CURRENTS
  1  0.11999E-02   2  0.49408E-02   3  0.49410E-02   4  0.49355E-02   5  0.52569E-05   6 -0.35763E-06
  7  0.11996E-02   8  0.12394E-05   9 -0.10450E-05  10  0.10450E-05  11  0.42117E-05

TIME= 0.140500E-02      DELTA TIME= 0.100000E-04          H-P GEN. FN.=  0.
TIME FNS. AND GRD. VOLT. SOURCES
  1  0.20000E 02
UNKNOWNS
  1  0.85857E 01   2  0.24704E-00   3  0.24715E-00   4  0.36828E-00   5  0.10118E 02   6  0.85857E 01
  7 -0.23842E-06   8  0.83387E 01
BRANCH CURRENTS
  1  0.11414E-02   2  0.49408E-02   3  0.49409E-02   4  0.49355E-02   5  0.52569E-05   6 -0.23842E-06
```

```
   0.11409E-02   8  0.11776E-05   9 -0.10450E-05  10  0.10450E-05  11  0.42118E-05

TIME= 0.145500E-02     DELTA TIME= 0.100000E-04          H-P GEN. FN.=  0.
TIME FNS. AND GRD. VOLT. SOURCES
  1  0.20000E 02
UNKNOWNS
  1  0.91421E 01   2  0.24704E-00   3  0.24715E-00   4  0.36828E-00   5  0.10118E 02   6  0.91421E 01
  7 -0.23842E-06   8  0.88950E 01
BRANCH CURRENTS
  1  0.10858E-02   2  0.49408E-02   3  0.49409E-02   4  0.49356E-02   5  0.52569E-05   6 -0.23842E-06
  7  0.10852E-02   8  0.11175E-05   9 -0.10450E-05  10  0.10450E-05  11  0.42118E-05

TIME= 0.150500E-02     DELTA TIME= 0.100000E-04          H-P GEN. FN.=  0.
TIME FNS. AND GRD. VOLT. SOURCES
  1  0.20000E 02
UNKNOWNS
  1  0.96712E 01   2  0.24704E-00   3  0.24715E-00   4  0.36828E-00   5  0.10118E 02   6  0.96712E 01
  7 -0.11921E-06   8  0.94242E 01
BRANCH CURRENTS
  1  0.10329E-02   2  0.49409E-02   3  0.49409E-02   4  0.49356E-02   5  0.52570E-05   6 -0.11921E-06
  7  0.10322E-02   8  0.10570E-05   9 -0.10450E-05  10  0.10450E-05  11  0.42118E-05

TIME= 0.155500E-02     DELTA TIME= 0.100000E-04          H-P GEN. FN.=  0.
TIME FNS. AND GRD. VOLT. SOURCES
  1  0.20000E 02
UNKNOWNS
  1  0.10175E 02   2  0.24707E-00   3  0.24719E-00   4  0.37087E-00   5  0.10118E 02   6  0.10175E 02
  7  0.47684E-06   8  0.99275E 01
BRANCH CURRENTS
  1  0.98255E-03   2  0.49414E-02   3  0.49409E-02   4  0.49356E-02   5  0.58280E-05   6  0.47684E-06
  7  0.98123E-03   8  0.81193E-06   9 -0.13051E-05  10  0.13051E-05  11  0.45228E-05

TIME= 0.158500E-02     DELTA TIME= 0.500000E-05          H-P GEN. FN.=  0.
TIME FNS. AND GRD. VOLT. SOURCES
  1  0.20000E 02
UNKNOWNS
  1  0.94749E 01   2  0.16338E 01   3  0.22126E 01   4  0.25536E 01   5  0.91082E 01   6  0.94476E 01
  7  0.27230E-01   8  0.78138E 01
BRANCH CURRENTS
  1  0.10525E-02   2  0.32677E-01   3  0.54459E-02   4  0.37372E-02   5  0.28939E-01   6  0.27230E-01
```

```
  7 -0.26179E-01   8 -0.13201E-01   9 -0.14030E-01  10  0.14030E-01  11  0.14909E-01

TIME= 0.161500E-02     DELTA TIME= 0.500000E-05          H-P GEN. FN.=  0.
TIME FNS. AND GRD. VOLT. SOURCES
  1  0.20000E 02
UNKNOWNS
  1  0.14197E 01   2  0.33979E-00   3  0.43974E-00   4  0.74724E 00   5  0.39361E 01   6  0.14209E 01
  7 -0.12362E-02   8  0.10811E 01
BRANCH CURRENTS
  1  0.18580E-02   2  0.67958E-02   3  0.80319E-02   4  0.17982E-02   5  0.49976E-02   6 -0.12362E-02
  7  0.30941E-02   8  0.16800E-02   9 -0.44387E-03  10  0.44387E-03  11  0.45537E-02

TIME= 0.166000E-02     DELTA TIME= 0.100000E-04          H-P GEN. FN.=  0.
TIME FNS. AND GRD. VOLT. SOURCES
  1  0.20000E 02
UNKNOWNS
  1  0.22662E 01   2  0.24708E-00   3  0.24723E-00   4  0.38201E-00   5  0.10115E 02   6  0.22662E 01
  7 -0.80466E-06   8  0.20191E 01
BRANCH CURRENTS
  1  0.17734E-02   2  0.49416E-02   3  0.49423E-02   4  0.49341E-02   5  0.74424E-05   6 -0.80466E-06
  7  0.17740E-02   8  0.18211E-05   9 -0.10445E-05  10  0.10445E-05  11  0.63979E-05

TIME= 0.171000E-02     DELTA TIME= 0.100000E-04          H-P GEN. FN.=  0.
TIME FNS. AND GRD. VOLT. SOURCES
  1  0.20000E 02
UNKNOWNS
  1  0.31313E 01   2  0.24703E-00   3  0.24713E-00   4  0.36827E-00   5  0.10118E 02   6  0.31313E 01
  7 -0.68545E-06   8  0.28843E 01
BRANCH CURRENTS
  1  0.16869E-02   2  0.49405E-02   3  0.49412E-02   4  0.49353E-02   5  0.52582E-05   6 -0.68545E-06
  7  0.16873E-02   8  0.17331E-05   9 -0.10449E-05  10  0.10449E-05  11  0.42131E-05

TIME= 0.176000E-02     DELTA TIME= 0.100000E-04          H-P GEN. FN.=  0.
TIME FNS. AND GRD. VOLT. SOURCES
  1  0.20000E 02
UNKNOWNS
  1  0.39541E 01   2  0.24703E-00   3  0.24713E-00   4  0.36826E-00   5  0.10118E 02   6  0.39541E 01
  7 -0.62585E-06   8  0.37071E 01
BRANCH CURRENTS
  1  0.16046E-02   2  0.49406E-02   3  0.49412E-02   4  0.49353E-02   5  0.52566E-05   6 -0.62585E-06
```

```
  7  0.16049E-C2    E  C.16506E-05    9 -0.10449E-05  10  0.10449E-C5  11  0.42116E-05

TIME= 0.18100CE-02      DELTA TIME= 0.100000E-04          H-P GEN. FN.=  0.
TIME FNS. AND GRD. VOLT. SOURCES
  1  0.200C0E 02
UNKNOWNS
  1  0.47367E C1    2  0.24703E-00    3  0.24714E-00    4  0.36827E-00    5  0.10118E 02    6  0.47367E 01
  7 -0.53644E-C6    8  C.44897E 01
BRANCH CURRENTS
  1  0.15263E-02    2  0.49406E-02    3  0.49411E-02    4  0.49354E-02    5  0.52567E-05    6 -0.53644E-C6
  7  0.15265E-02    E  C.15719E-05    9 -0.10449E-05  10  0.10449E-05  11  0.42116E-05

TIME= 0.18600CE-C2      DELTA TIME= 0.100000E-04          H-P GEN. FN.=  0.
TIME FNS. AND GRD. VOLT. SOURCES
  1  0.200C0E C2
UNKNOWNS
  1  0.54811E 01    2  0.24703E-00    3  0.24714E-00    4  0.36827E-C0    5  0.10118E 02    6  0.54811E C1
  7 -0.53644E-C6    E  0.52340E 01
BRANCH CURRENTS
  1  0.14519E-02    2  0.49406E-02    3  0.49411E-02    4  0.49354E-C2    5  0.52568E-05    6 -0.53644E-C6
  7  0.14519E-C2    E  C.14969E-05    9 -0.10450E-05  10  0.10450E-C5  11  0.42116E-05

TIME= 0.191C00E-C2      DELTA TIME= 0.100000E-04          H-P GEN. FN.=  0.
TIME FNS. AND GRD. VCLT. SOURCES
  1  C.20C00E 02
UNKNOWNS
  1  0.61891E 01    2  0.24703E-00    3  0.24714E-00    4  0.36827E-00    5  0.10118E 02    6  0.61891E 01
  7 -0.47684E-C6    E  C.59421E 01
BRANCH CURRENTS
  1  0.13811E-02    2  0.49407E-02    3  0.49411E-02    4  0.49354E-C2    5  0.52568E-05    6 -0.47684E-C6
  7  0.13810E-C2    E  0.14253E-05    9 -0.10450E-05  10  0.10450E-C5  11  0.42117E-05

TIME= 0.19600CE-C2      DELTA TIME= 0.1C0000E-04          H-P GEN. FN.=  0.
TIME FNS. AND GRD. VOLT. SOURCES
  1  0.200C0E C2
UNKNOWNS
  1  0.68625E C1    2  0.24704E-00    3  0.24714E-00    4  0.36827E-00    5  0.10118E 02    6  C.68625E C1
  7 -0.35763E-06    E  C.66155E 01
BRANCH CURRENTS
  1  0.13137E-02    2  0.49407E-02    3  0.49410E-02    4  0.49355E-C2    5  0.52568E-05    6 -0.35763E-C6
```

```
  7  0.13136E-02   8  C.13567E-05   9 -0.10450E-05  10  0.10450E-C5  11  0.42117E-05

TIME= 0.201000E-02     DELTA TIME= 0.100000E-04          H-P GEN. FN.=  0.
TIME FNS. AND GRD. VOLT. SOURCES
  1  0.2C0C0E C2
UNKNOWNS
  1  0.75031E C1    2  0.24704E-00    3  0.24714E-00    4  0.36827E-00    5  0.10118E 02    6  C.75031E C1
  7 -0.298C2E-06    8  C.72560E 01
BRANCH CURRENTS
  1  0.12497E-C2    2  0.49407E-02    3  0.49410E-02    4  0.49355E-C2    5  0.52568E-05    6 -0.29802E-06
  7  0.12494E-C2    8  C.12910E-05    9 -0.10450E-05   10  0.10450E-C5   11  0.42117E-05

TIME= 0.2060C0E-C2     DELTA TIME= 0.100000E-04          H-P GEN. FN.=  0.
TIME FNS. AND GRD. VOLT. SOURCES
  1  0.200C0E C2
UNKNOWNS
  1  0.81123E C1    2  0.24704E-00    3  0.24714E-00    4  0.36828E-00    5  0.10118E 02    6  0.81123E 01
  7 -0.35763E-C6    8  0.78653E 01
BRANCH CURRENTS
  1  0.11888E-C2    2  0.49408E-02    3  0.49410E-02    4  0.49355E-C2    5  0.52569E-05    6 -0.35763E-06
  7  0.11883E-C2    8  0.12277E-05    9 -0.10450E-05   10  0.10450E-C5   11  0.42118E-05

TIME= 0.211000E-02     DELTA TIME= 0.100000E-04          H-P GEN. FN.=  0.
TIME FNS. AND GRD. VOLT. SOURCES
  1  0.2C0C0E C2
UNKNOWNS
  1  0.86918E C1    2  0.24704E-00    3  0.24715E-00    4  0.36828E-00    5  0.10118E 02    6  C.86918E 01
  7 -0.35763E-C6    8  C.84448E 01
BRANCH CURRENTS
  1  0.11308E-C2    2  0.49408E-02    3  0.49409E-02    4  0.49356E-02    5  0.52569E-05    6 -0.35763E-06
  7  0.11303E-C2    8  0.11664E-05    9 -0.10450E-05   10  0.10450E-C5   11  0.42118E-05

TIME= 0.2160C0E-02     DELTA TIME= 0.100000E-04          H-P GEN. FN.=  0.
TIME FNS. AND GRD. VOLT. SOURCES
  1  0.2C000E C2
UNKNOWNS
  1  0.92430E 01    2  0.24704E-00    3  0.24715E-00    4  0.36828E-00    5  0.10118E 02    6  0.92430E C1
  7 -0.23842E-C6    8  0.89959E 01
BRANCH CURRENTS
  1  0.10757E-C2    2  0.49408E-02    3  0.49409E-02    4  0.49356E-C2    5  0.52569E-05    6 -0.23842E-06
```

```
  7  0.1C751E-C2   E  C.11062E-05   S -0.10450E-05  10  0.10450E-C5  11  0.42118E-05

TIME= 0.2210C0E-02     DELTA TIME= 0.100000E-04          H-P GEN. FN.=  0.
TIME FNS. AND GRD. VOLT. SOURCES
  1  0.2C0C0E C2
UNKNOWNS
  1  0.97672E C1   2  0.24704E-00   3  0.24715E-00   4  0.36828E-00   5  0.10118E 02   6  0.S7672E C1
  7 -0.11921E-C6   E  C.95202E 01
BRANCH CURRENTS
  1  0.10233E-02   2  0.49409E-02   3  0.49409E-02   4  0.49356E-02   5  0.52569E-05   6 -0.11921E-C6
  7  0.10225E-02   E  C.10454E-05   9 -0.10450E-05  10  0.10450E-C5  11  0.42118E-05

TIME= 0.2260C0E-02     DELTA TIME= 0.100000E-C4          H-P GEN. FN.=  0.
TIME FNS. AND GRD. VCLT. SOURCES
  1  0.200C0E C2
UNKNOWNS
  1  0.10265E C2   2  0.24794E-00   3  0.24844E-00   4  0.40889E-00   5  0.10115E 02   6  0.10265E 02
  7  0.16212E-04   E  0.10017E 02
BRANCH CURRENTS
  1  0.97350E-C3   2  0.49587E-02   3  0.49423E-02   4  0.49337E-02   5  0.25000E-04   6  0.16212E-04
  7  0.95639E-C3   E -C.63833E-05   S -0.10006E-04  10  0.10006E-C4  11  0.14994E-04

TIME= C.226500E-02     DELTA TIME= 0.5C0000E-05          H-P GEN. FN.=  0.
TIME FNS. AND GRD. VCLT. SOURCES
  1  0.2CCC0E C2
UNKNOWNS
  1  C.70030E C1   2  0.45731E 01   3  0.63825E 01   4  0.67549E 01   5  0.65476E 01   6  0.69183E 01
  7  0.84735E-C1   E  C.23452E 01
BRANCH CURRENTS
  1  0.12957E-C2   2  0.91461E-01   3  0.67262E-02   4  0.98729E-03   5  0.90474E-01   6  C.84735E-01
  7 -0.83436E-C1   E -0.40991E-01   S -0.43744E-01  10  0.43744E-C1  11  0.46730E-01

TIME= 0.231500E-C2     DELTA TIME= 0.500000E-05          H-P GEN. FN.=  0.
TIME FNS. AND GRD. VCLT. SOURCES
  1  0.200C0E C2
UNKNOWNS
  1  0.15482E 01   2  0.28302E-00   3  0.31237E-00   4  0.59305E 00   5  0.86686E 01   6  0.15482E C1
  7 -0.52899E-C5   E  C.12652E 01
BRANCH CURRENTS
  1  0.18452E-02   2  0.56604E-02   3  0.56657E-02   4  0.41928E-02   5  0.14676E-02   6 -0.52899E-C5
```

```
  7  0.18503E-02   8  0.67767E-05   9 -0.15061E-05  10  0.15065E-05  11  0.14661E-02

TIME= 0.236500E-02     DELTA TIME= 0.100000E-04          H-P GEN. FN.=  0.
TIME FNS. AND GRD. VOLT. SOURCES
  1  0.20000E 02
UNKNOWNS
  1  0.24486E 01   2  0.24704E-00   3  0.24715E-00   4  0.37381E-00   5  0.10117E 02   6  0.24486E 01
  7 -0.77486E-06   8  0.22016E 01
BRANCH CURRENTS
  1  0.17551E-02   2  0.49407E-02   3  0.49415E-02   4  0.49350E-02   5  0.57219E-05   6 -0.77486E-06
  7  0.17557E-02   8  0.18016E-05   9 -0.10447E-05  10  0.10447E-05  11  0.46770E-05

TIME= 0.241500E-02     DELTA TIME= 0.100000E-04          H-P GEN. FN.=  0.
TIME FNS. AND GRD. VOLT. SOURCES
  1  0.20000E 02
UNKNOWNS
  1  0.33048E 01   2  0.24703E-00   3  0.24713E-00   4  0.36827E-00   5  0.10118E 02   6  0.33048E 01
  7 -0.68545E-06   8  0.30577E 01
BRANCH CURRENTS
  1  0.16695E-02   2  0.49405E-02   3  0.49412E-02   4  0.49353E-02   5  0.52569E-05   6 -0.68545E-06
  7  0.16699E-02   8  0.17157E-05   9 -0.10449E-05  10  0.10449E-05  11  0.42119E-05

TIME= 0.246500E-02     DELTA TIME= 0.100000E-04          H-P GEN. FN.=  0.
TIME FNS. AND GRD. VOLT. SOURCES
  1  0.20000E 02
UNKNOWNS
  1  0.41191E 01   2  0.24703E-00   3  0.24713E-00   4  0.36826E-00   5  0.10118E 02   6  0.41191E 01
  7 -0.65565E-06   8  0.38721E 01
BRANCH CURRENTS
  1  0.15881E-02   2  0.49406E-02   3  0.49412E-02   4  0.49353E-02   5  0.52567E-05   6 -0.65565E-06
  7  0.15884E-02   8  0.16340E-05   9 -0.10449E-05  10  0.10449E-05  11  0.42116E-05

TIME= 0.250000E-02     DELTA TIME= 0.500205E-05          H-P GEN. FN.=  0.
TIME FNS. AND GRD. VOLT. SOURCES
  1  0.20000E 02
UNKNOWNS
  1  0.46654E 01   2  0.24703E-00   3  0.24714E-00   4  0.36827E-00   5  0.10118E 02   6  0.46654E 01
  7 -0.59605E-06   8  0.44184E 01
BRANCH CURRENTS
  1  0.15335E-02   2  0.49406E-02   3  0.49411E-02   4  0.49353E-02   5  0.52566E-05   6 -0.59605E-06
```

7 0.15337E-C2 E C.15790E-05 9 -0.10449E-05 10 0.10449E-C5 11 0.42116E-05

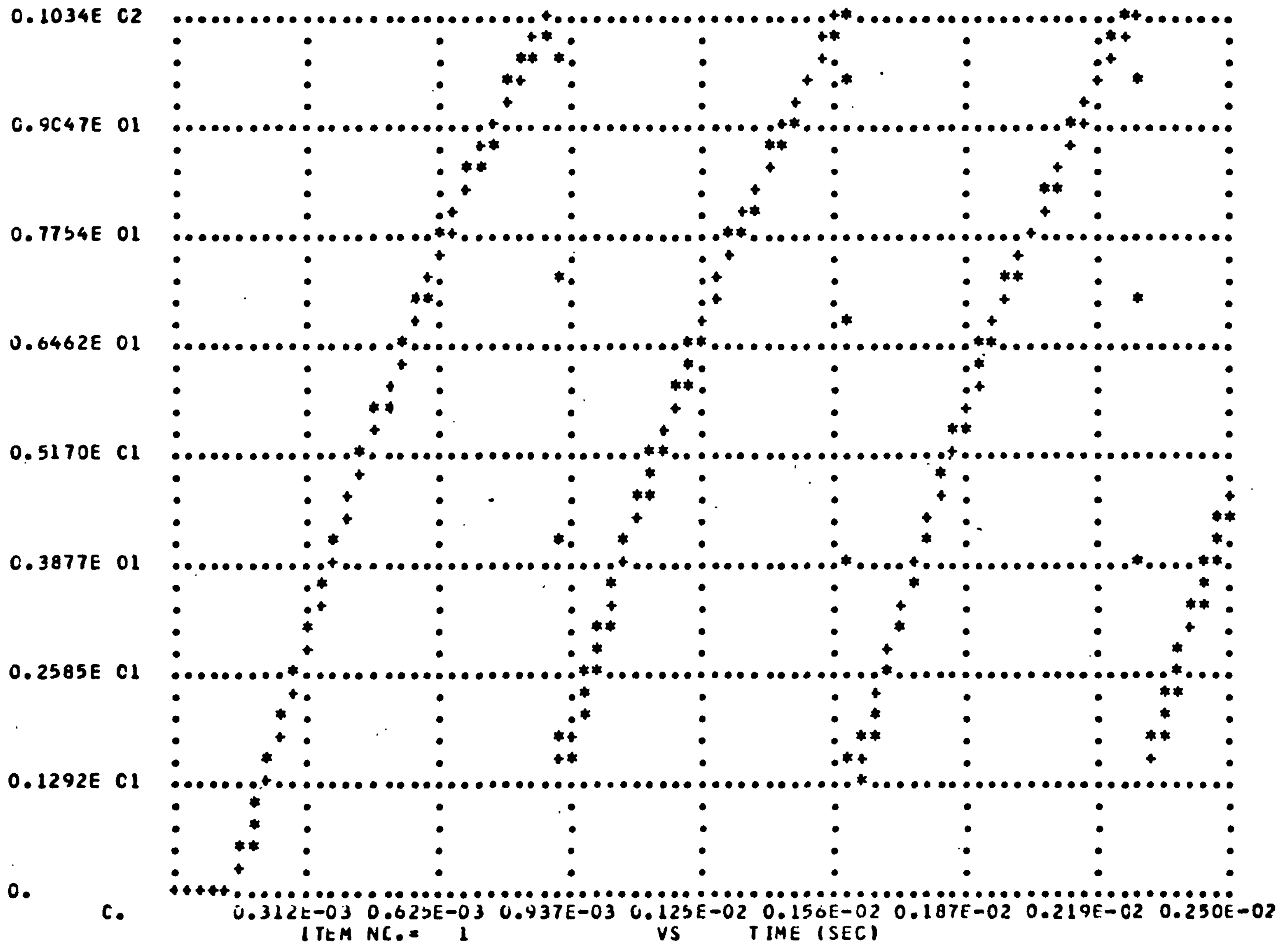
0.1034E 02
0.9047E 01
0.7754E 01
0.6462E 01
0.5170E 01
0.3877E 01
0.2585E 01
0.1292E 01
0.
0.
0.312E-03 0.625E-03 0.937E-03 0.125E-02 0.156E-02 0.187E-02 0.219E-02 0.250E-02
ITEM NO.= 1 VS TIME (SEC)

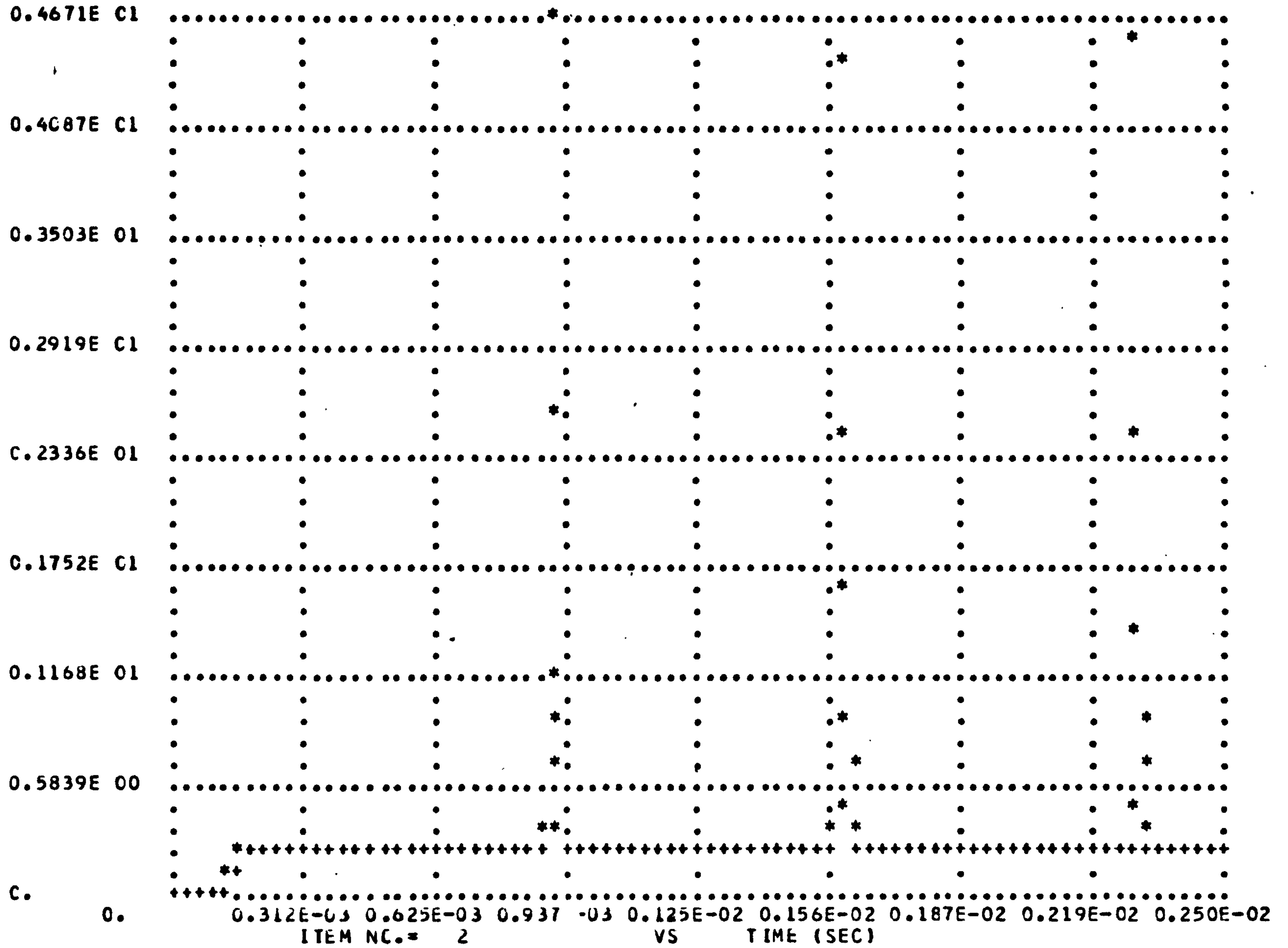
0.4671E C1
0.4C87E C1
0.3503E 01
0.2919E C1
C.2336E 01
0.1752E C1
0.1168E 01
0.5839E 00
C.
0.
0.312E-03 0.625E-03 0.937 -03 0.125E-02 0.156E-02 0.187E-02 0.219E-02 0.250E-02
ITEM NC.= 2 VS TIME (SEC)

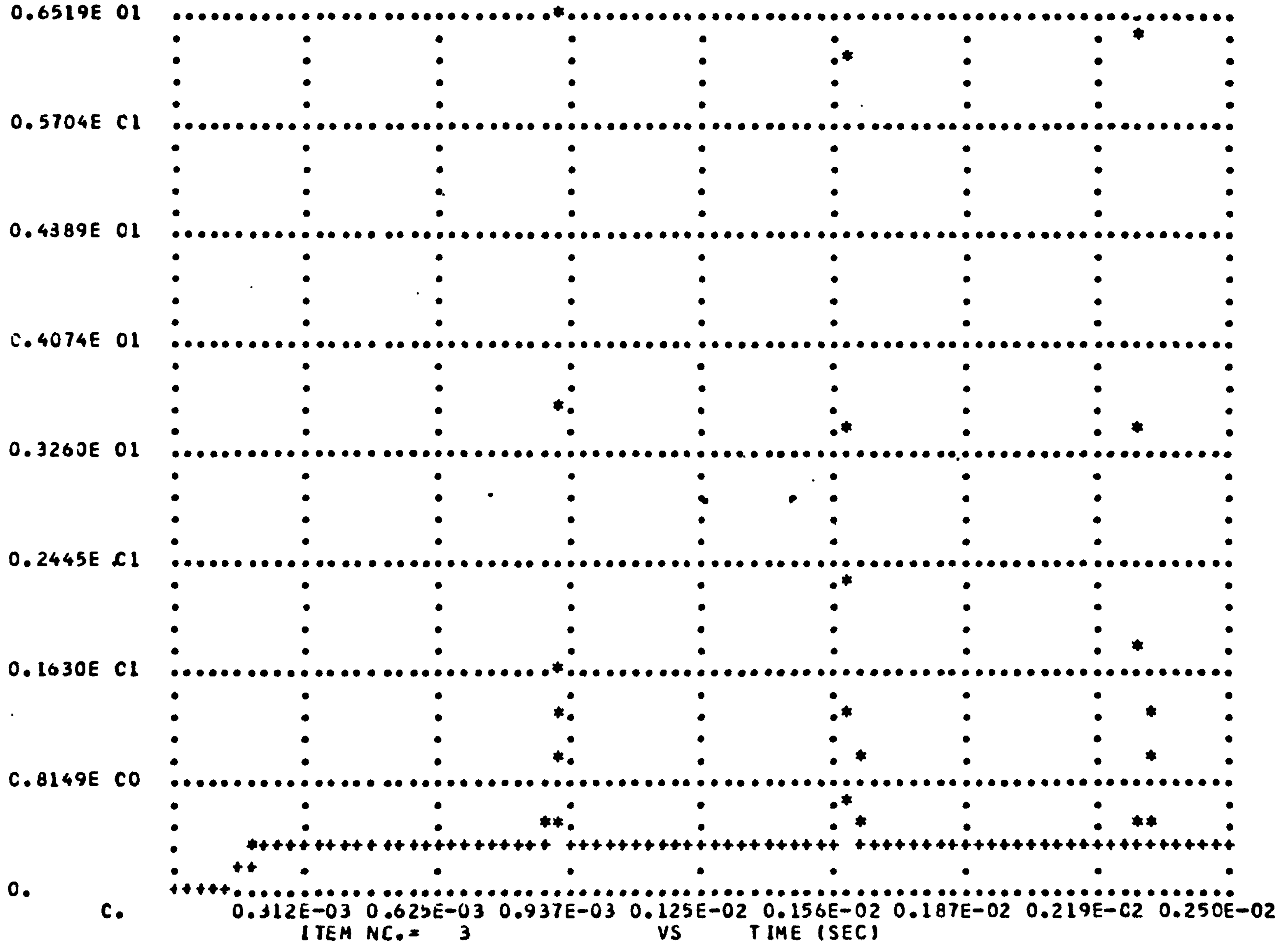

0.6519E 01
0.5704E C1
0.4389E 01
C.4074E 01
0.3260E 01
0.2445E C1
0.1630E C1
C.8149E C0
0.
C.
0.312E-03 0.625E-03 0.937E-03 0.125E-02 0.156E-02 0.187E-02 0.219E-C2 0.250E-02
ITEM NC.= 3 VS TIME (SEC)

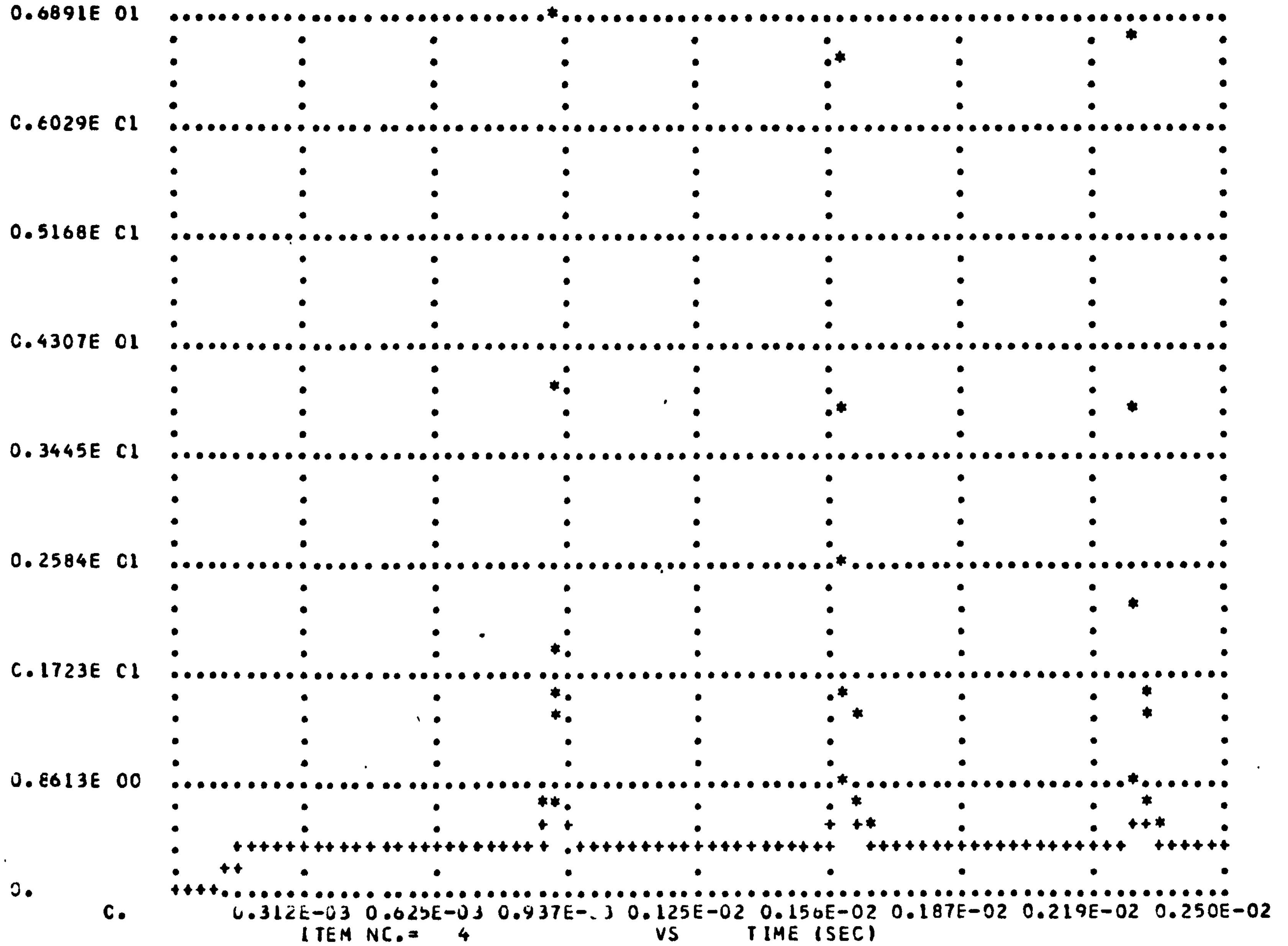
0.6891E 01
C.6029E C1
0.5168E C1
C.4307E 01
0.3445E C1
0.2584E C1
C.1723E C1
0.8613E 00
0.
C.
0.312E-03 0.625E-03 0.937E-03 0.125E-02 0.156E-02 0.187E-02 0.219E-02 0.250E-02
ITEM NC.= 4 VS TIME (SEC)

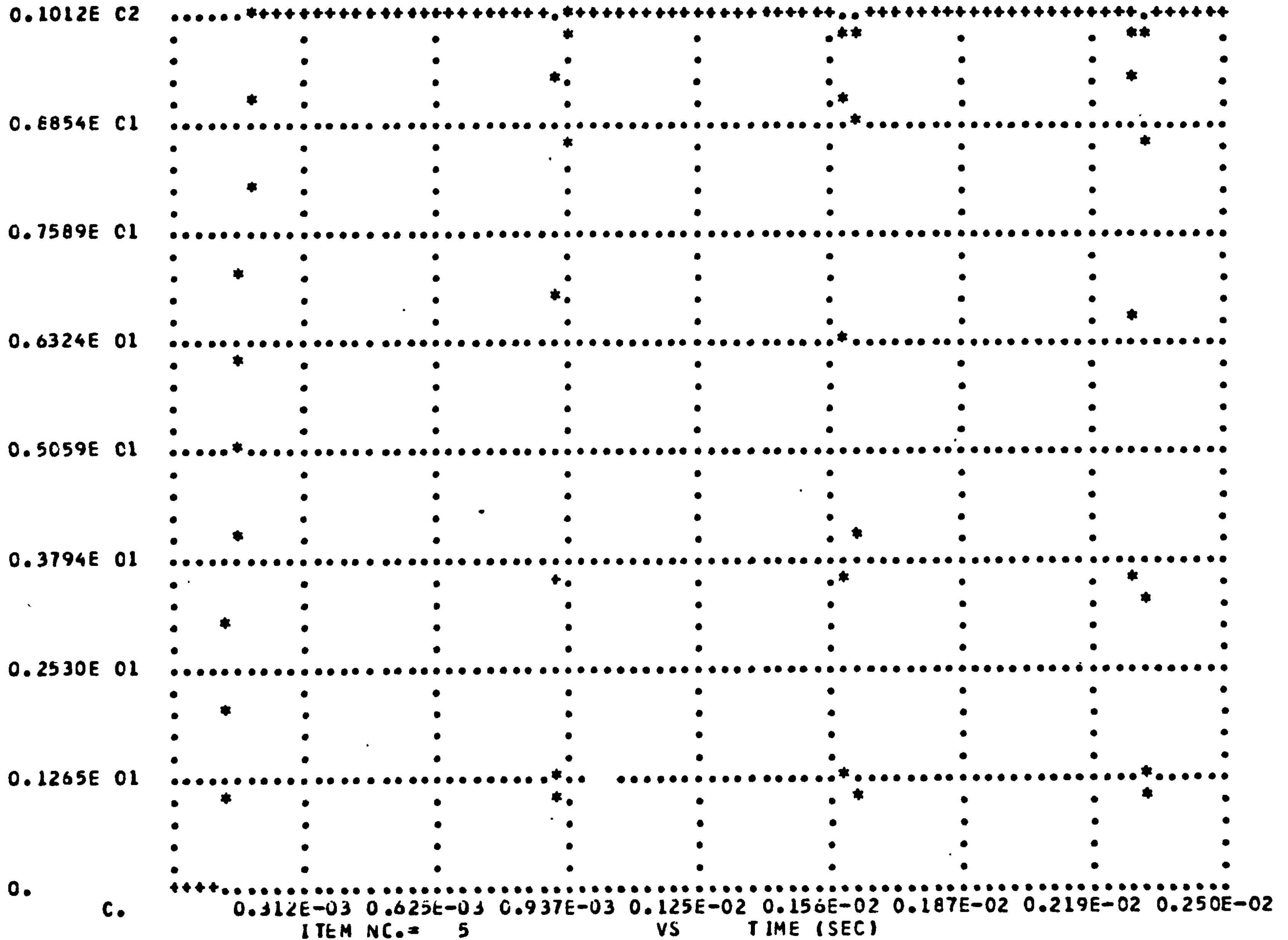
0.1012E C2
0.8854E C1
0.7589E C1
0.6324E 01
0.5059E C1
0.3794E 01
0.2530E 01
0.1265E 01
0.
C.
0.312E-03 0.625E-03 0.937E-03 0.125E-02 0.156E-02 0.187E-02 0.219E-02 0.250E-02
ITEM NC.= 5 VS TIME (SEC)

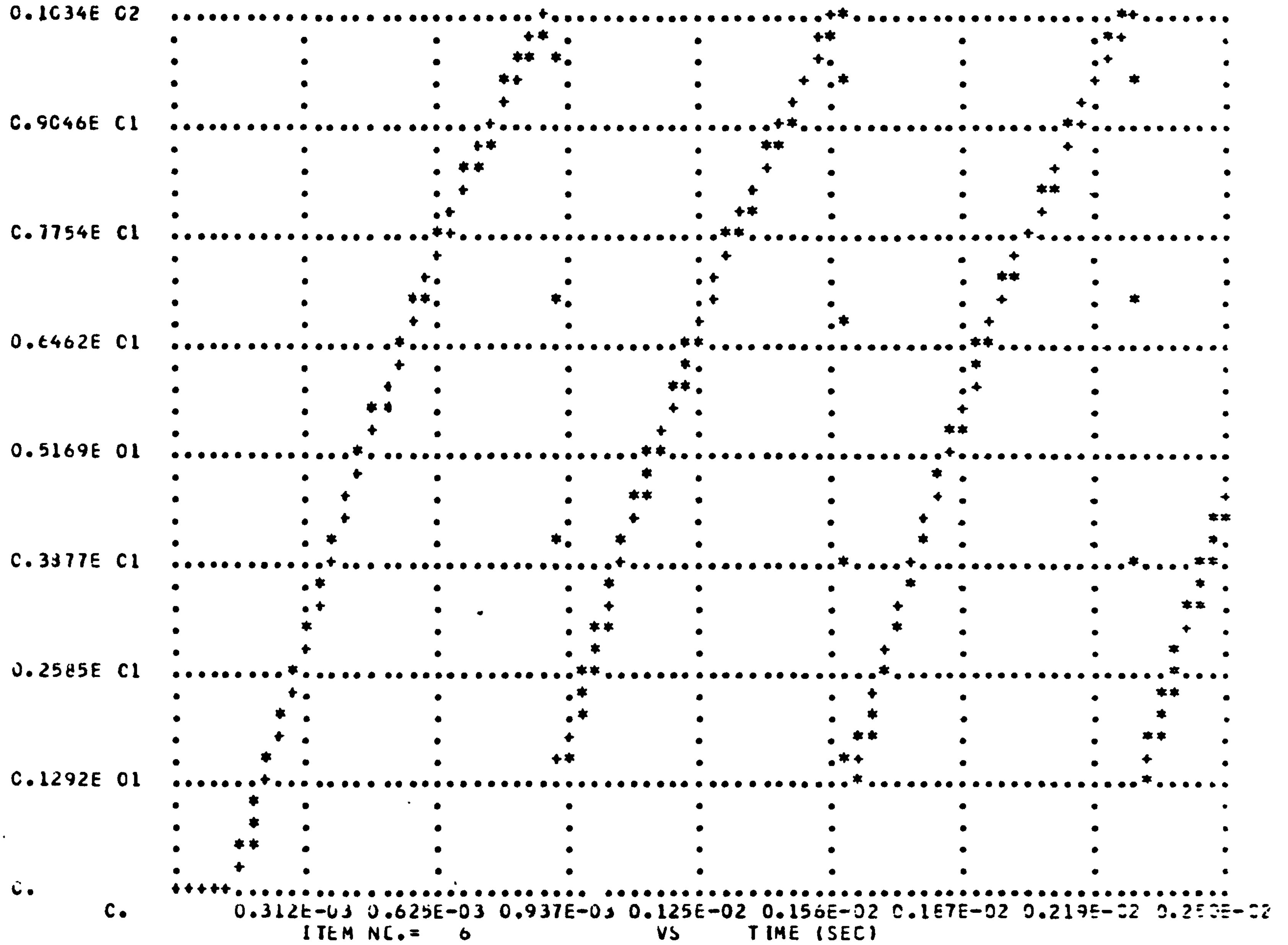
0.1034E 02
0.9046E 01
0.7754E 01
0.6462E 01
0.5169E 01
0.3377E 01
0.2585E 01
0.1292E 01
0.
0.
0.312E-03 0.625E-03 0.937E-03 0.125E-02 0.156E-02 0.187E-02 0.219E-02 0.250E-02
ITEM NO.= 6
VS
TIME (SEC)

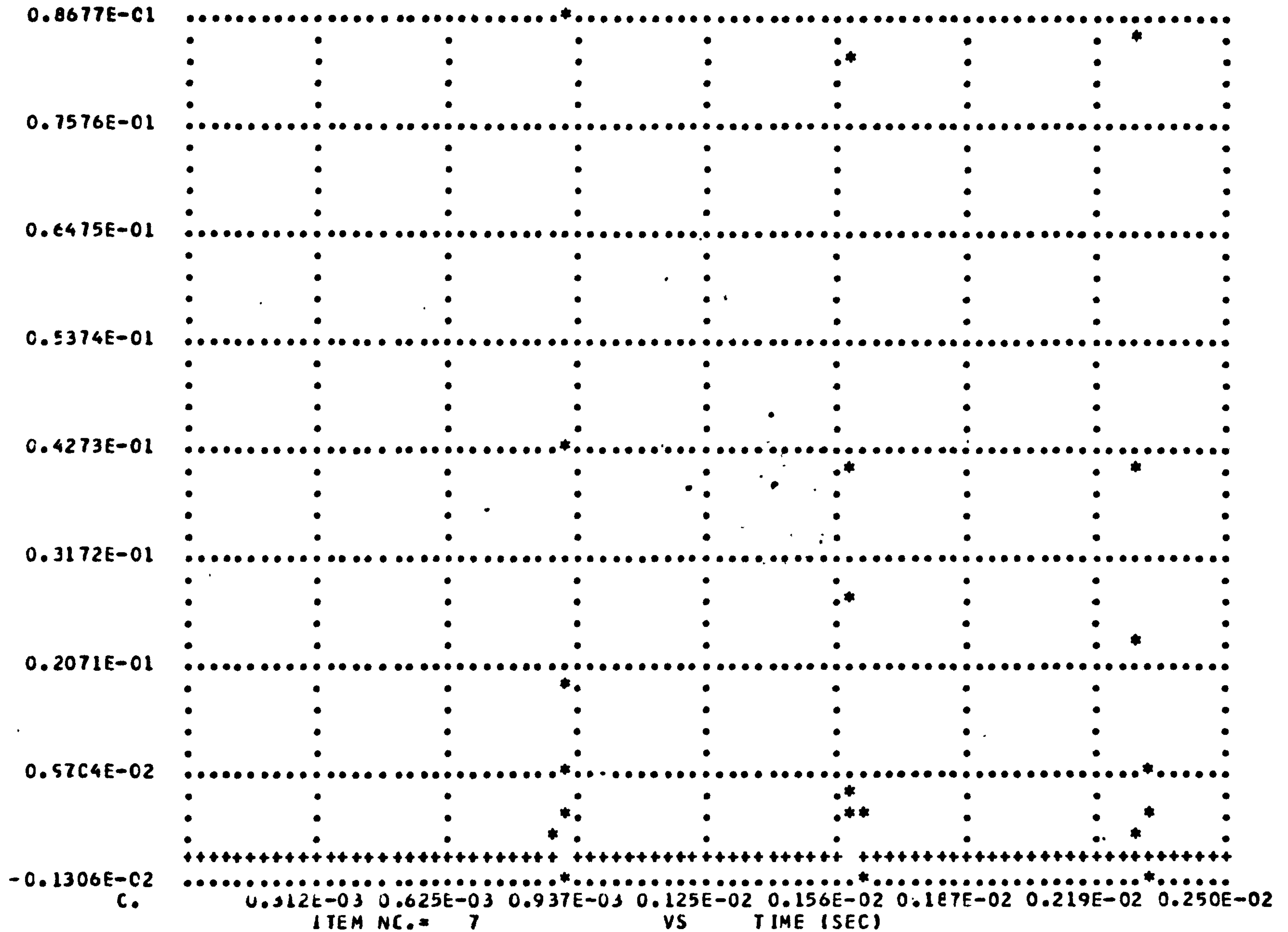

0.8677E-01
0.7576E-01
0.6475E-01
0.5374E-01
0.4273E-01
0.3172E-01
0.2071E-01
0.9704E-02
-0.1306E-02
0.
0.312E-03 0.625E-03 0.937E-03 0.125E-02 0.156E-02 0.187E-02 0.219E-02 0.250E-02
ITEM NO.= 7 VS TIME (SEC)

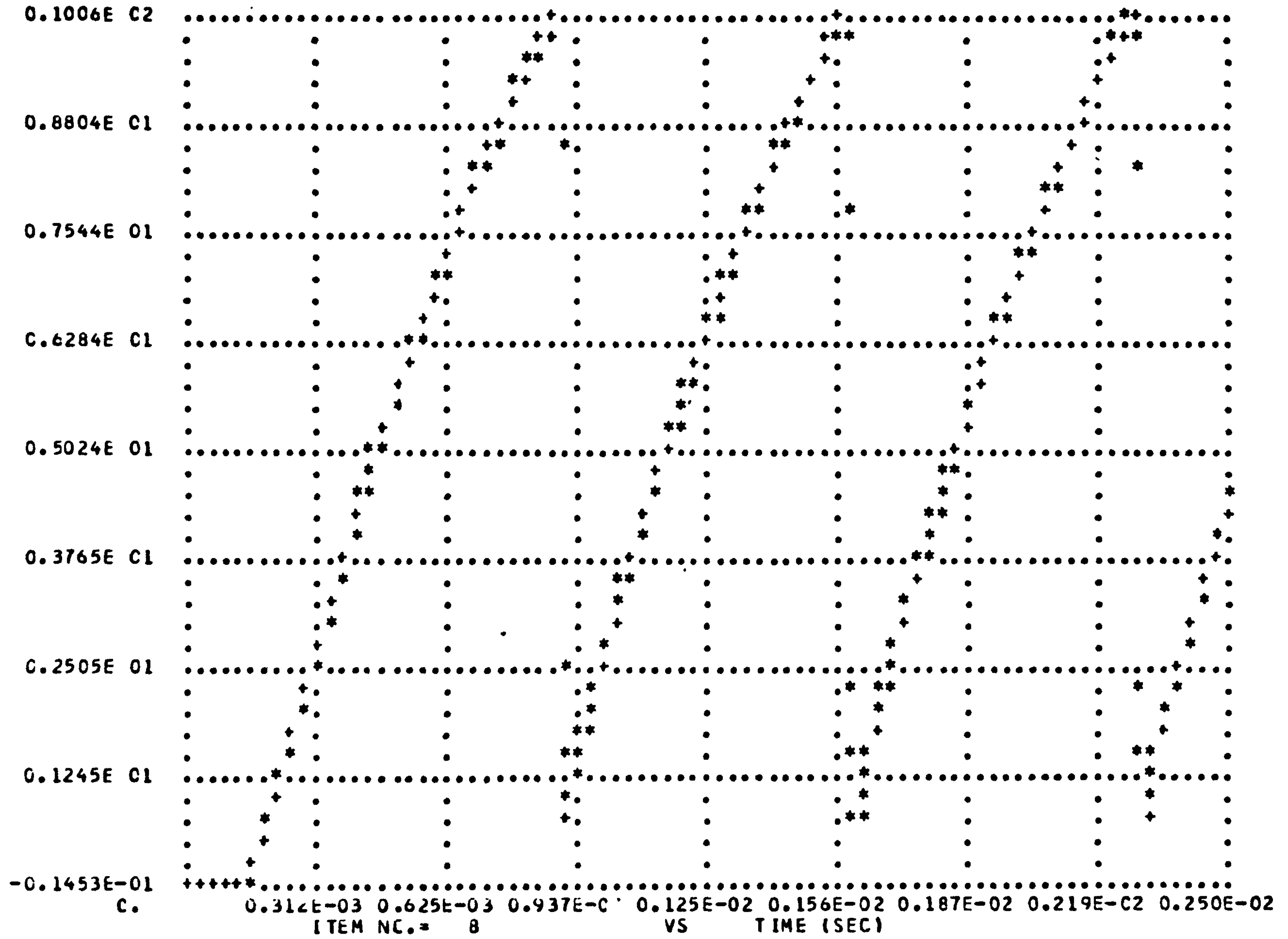
0.1006E C2
0.8804E C1
0.7544E 01
C.6284E C1
0.5024E 01
0.3765E C1
C.2505E 01
0.1245E C1
-0.1453E-01
C.
0.312E-03 0.625E-03 0.937E-C 0.125E-02 0.156E-02 0.187E-02 0.219E-C2 0.250E-02
ITEM NC.= 8 VS TIME (SEC)

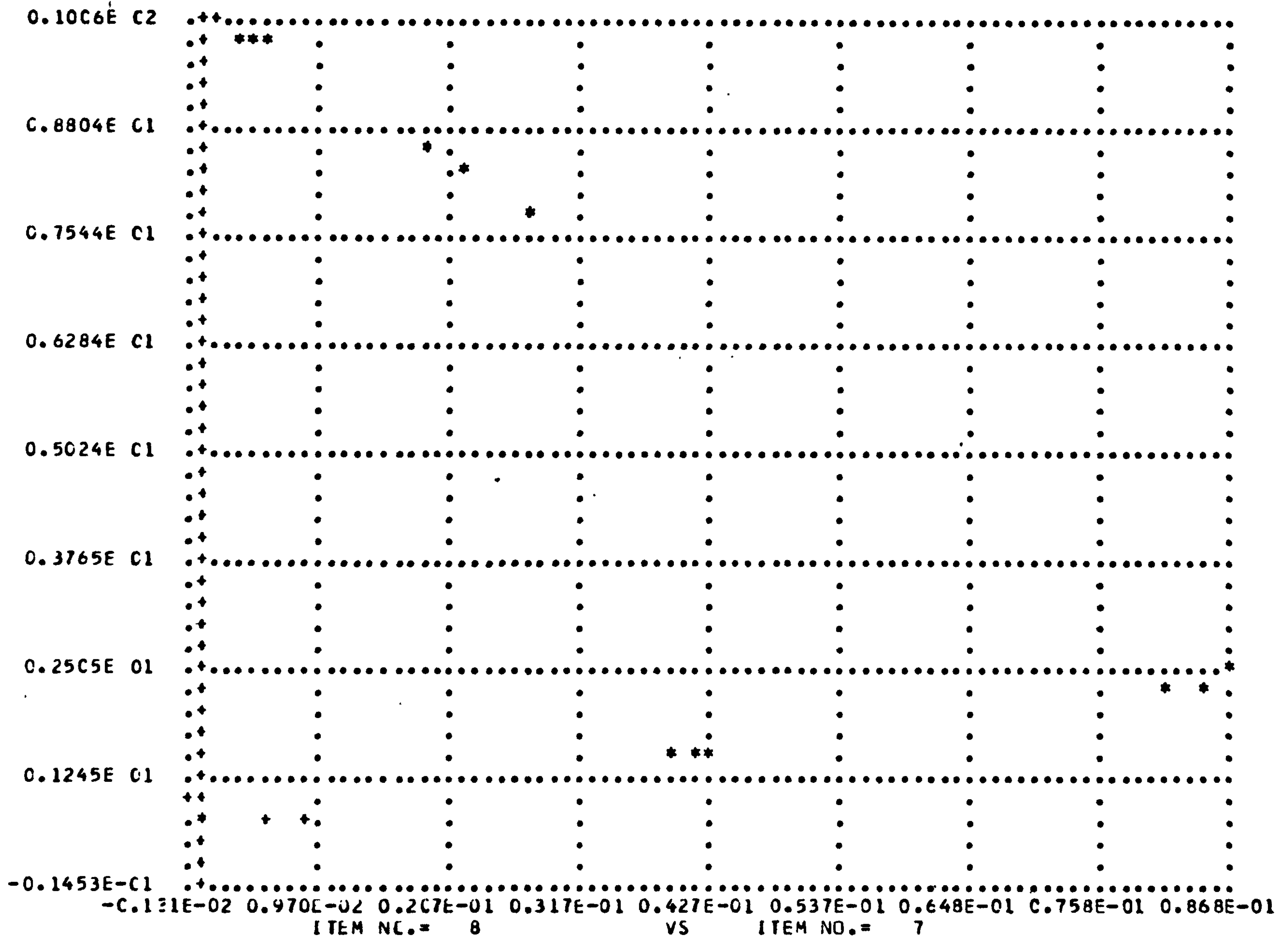
0.1006E 02
0.8804E 01
0.7544E 01
0.6284E 01
0.5024E 01
0.3765E 01
0.2505E 01
0.1245E 01
-0.1453E-01
-0.131E-02 0.970E-02 0.207E-01 0.317E-01 0.427E-01 0.537E-01 0.648E-01 0.758E-01 0.868E-01
ITEM NO.= 8 VS ITEM NO.= 7

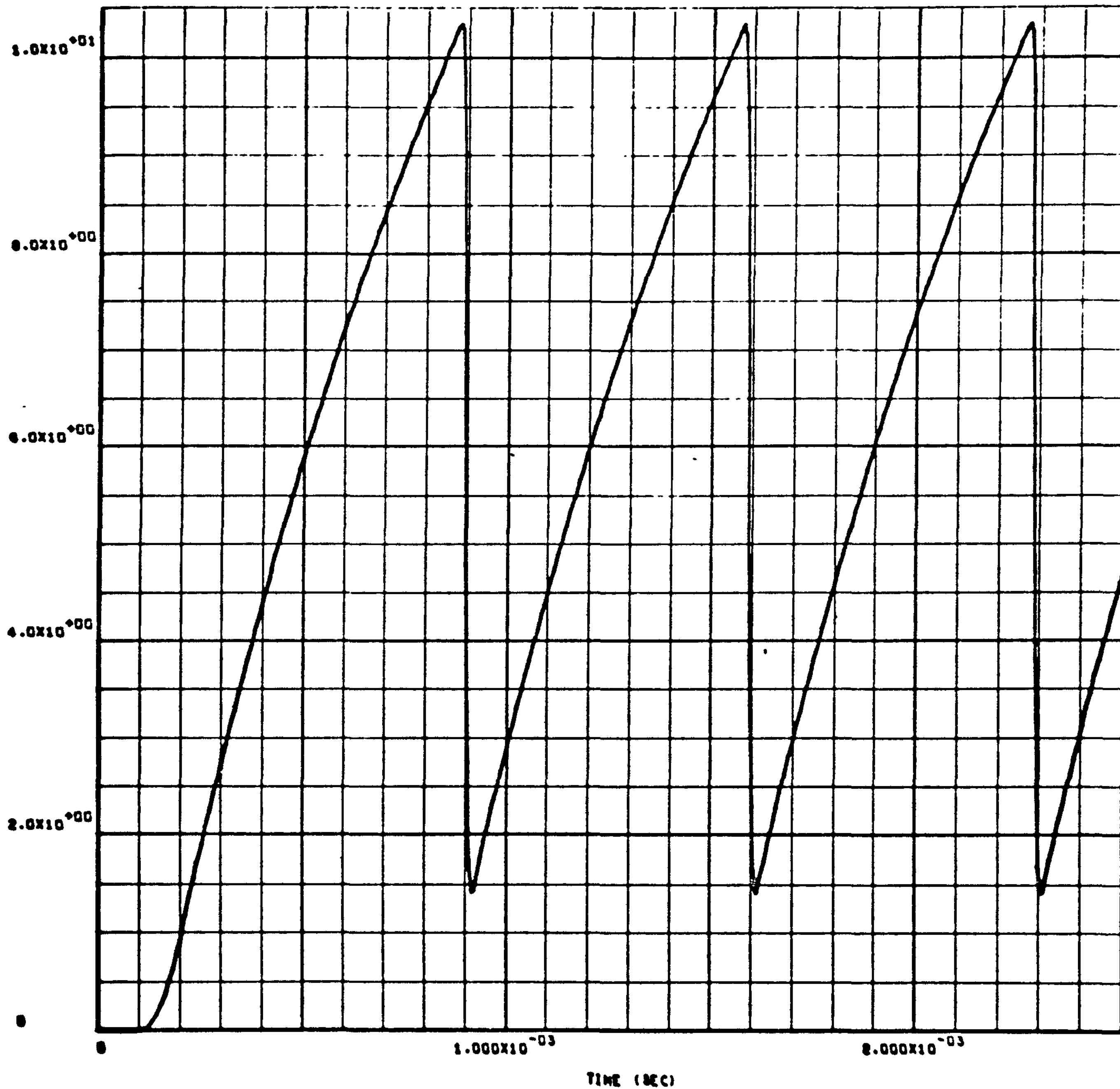

Capacitor Charge - Discharge Waveform (Normal Operation)

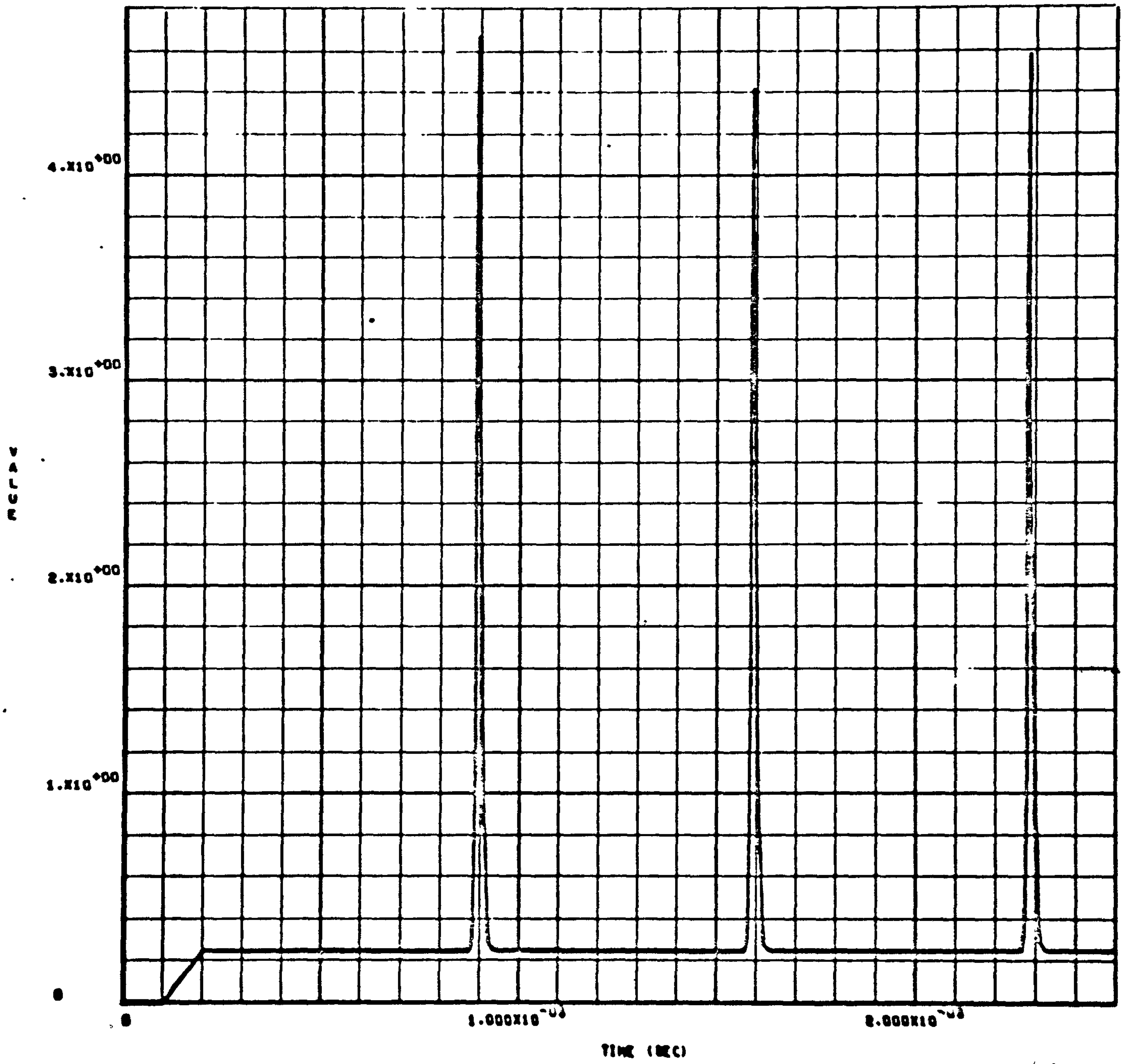

Output Pulse-Train vs Time (Normal Operation)

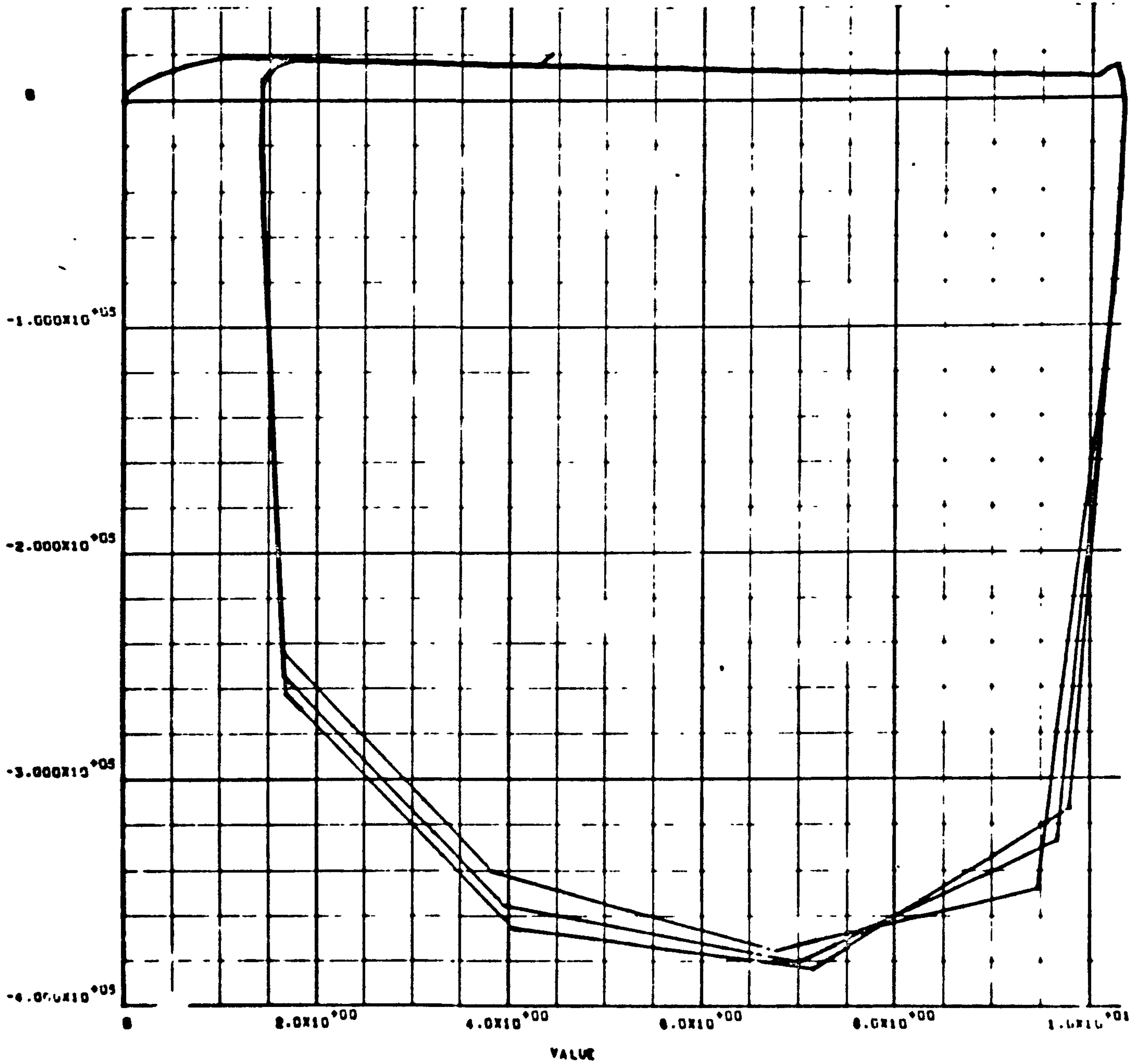

Capacitor Voltage Rate, $\frac{dv}{dt}$, vs Capacitor Voltage
(Phase Plane Plot)

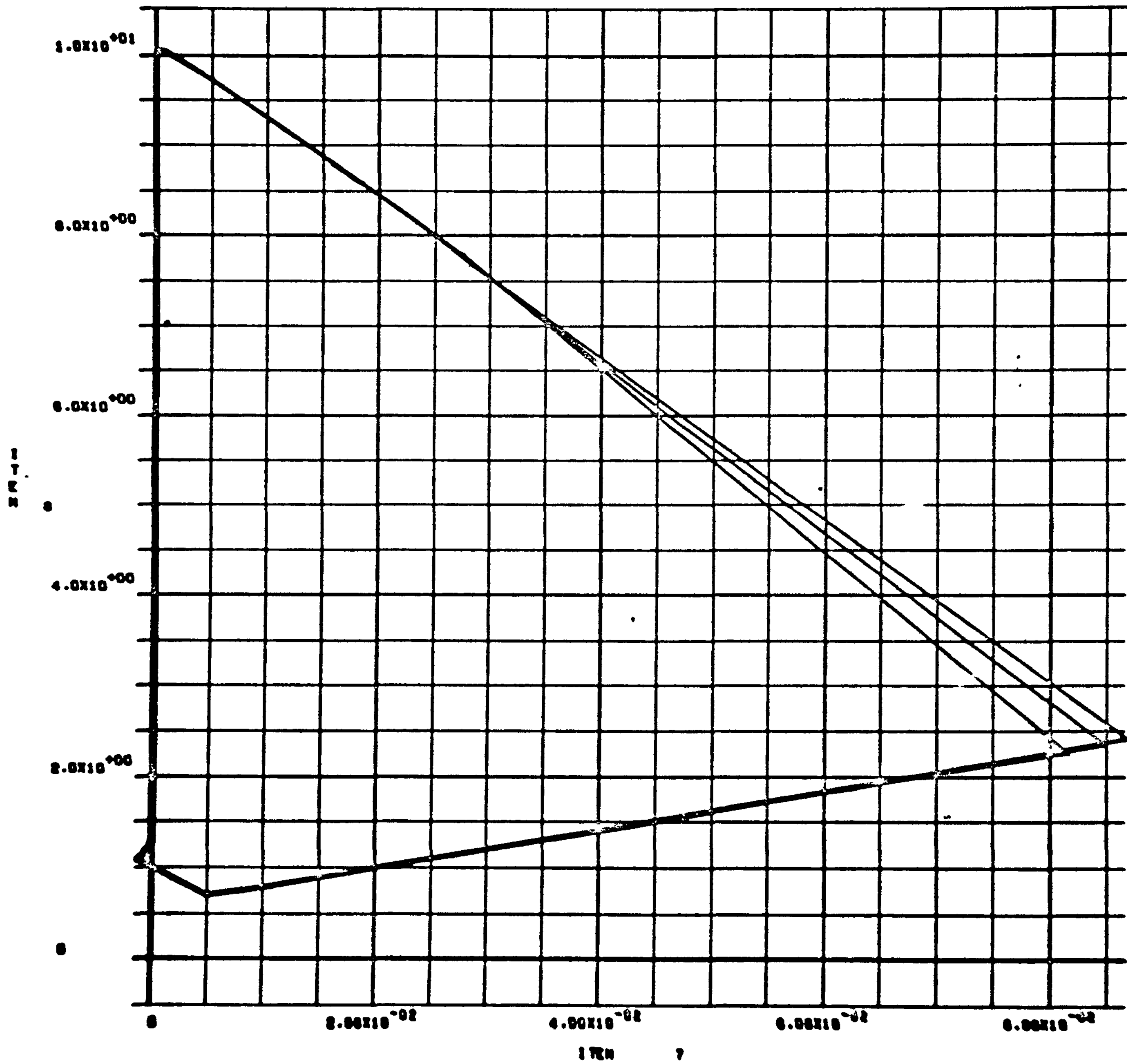

V_E vs I_E Normal Operation

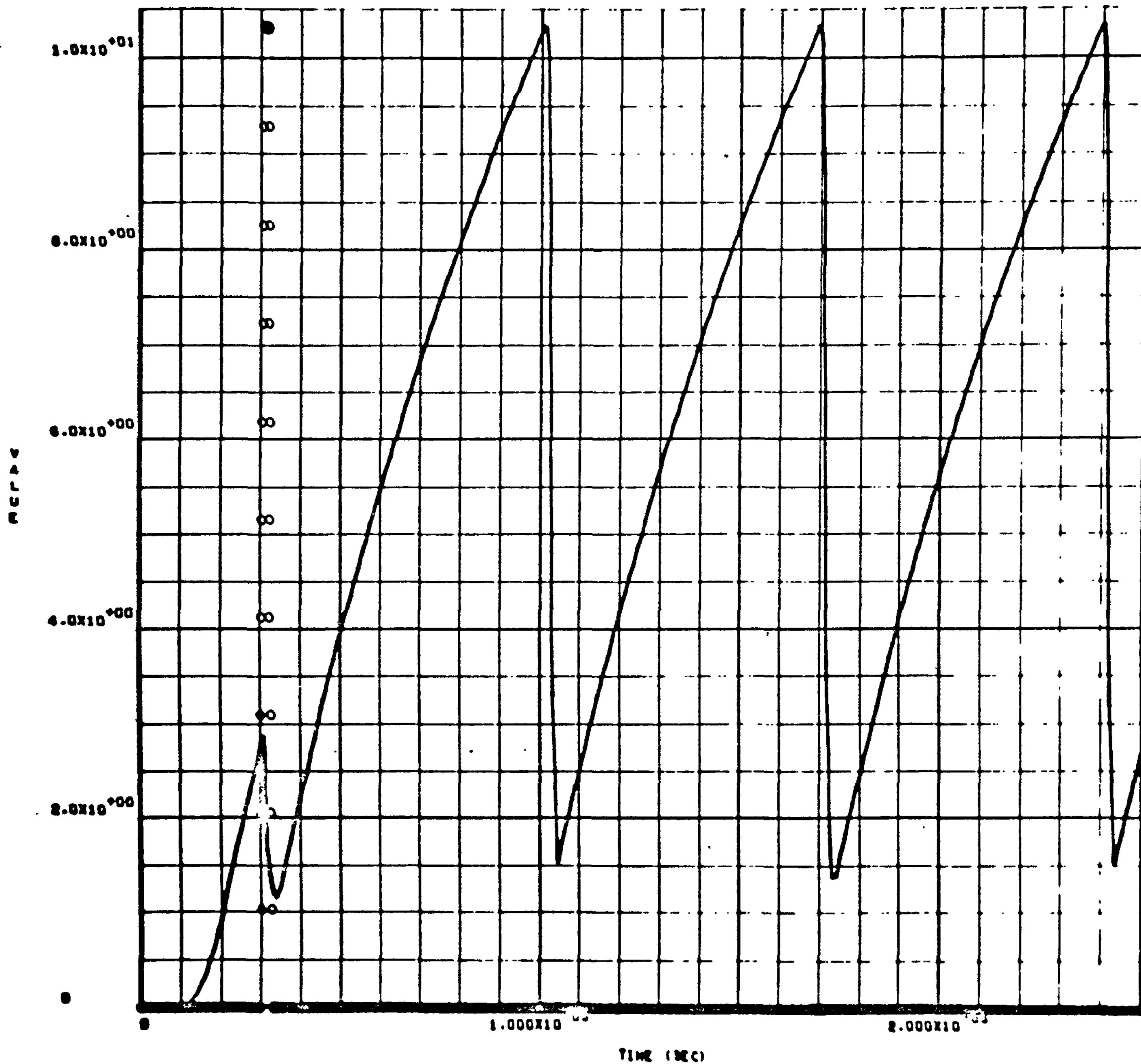

Capacitor Charge-Discharge Voltage vs Time for Ionizing Dose Rate of

10^8 R/sec (tp = 20 μsec)

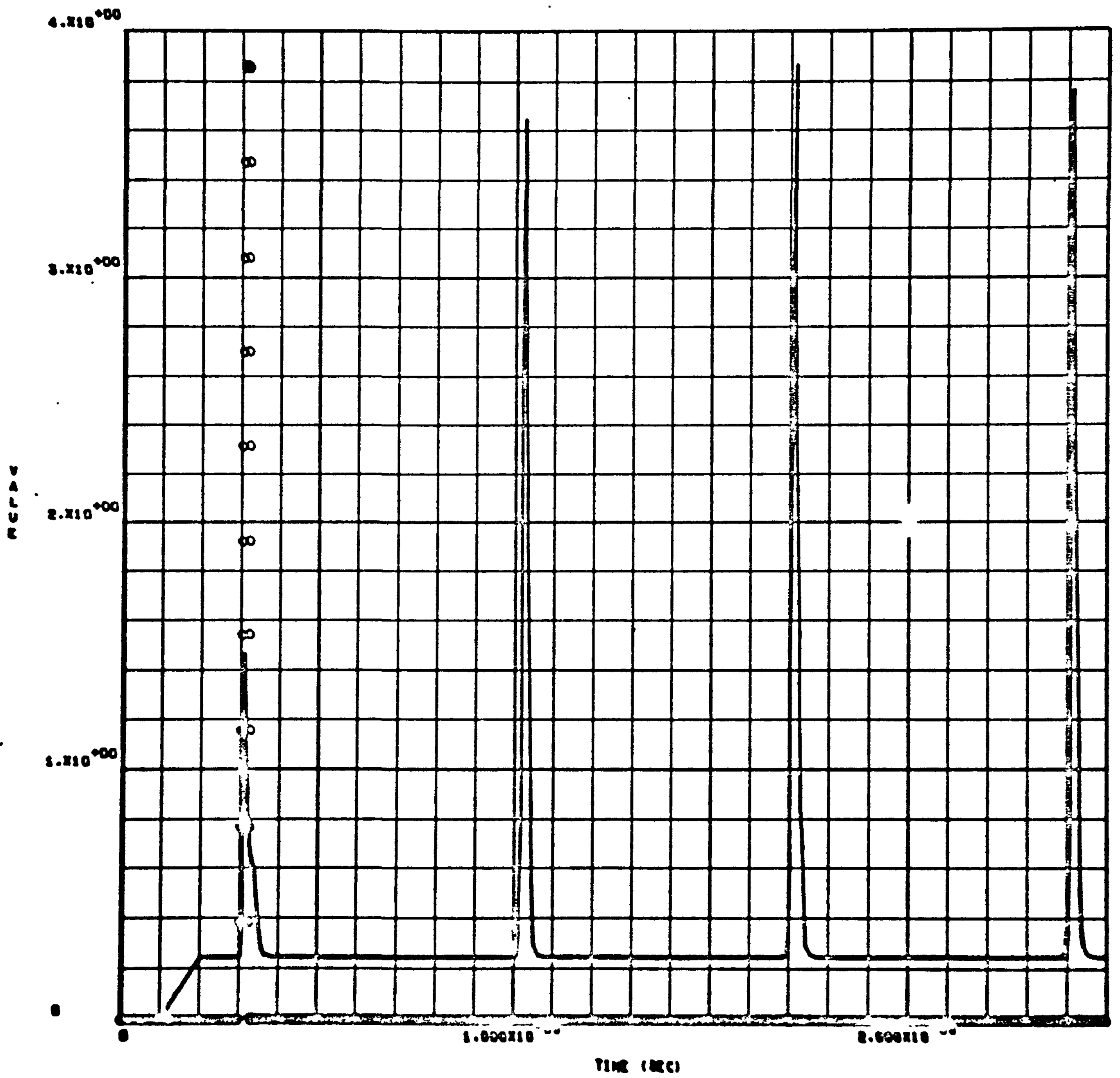

Output Pulse-Train with 10^8 R/sec Pulse (20 μsec tp) R = 20 Ω

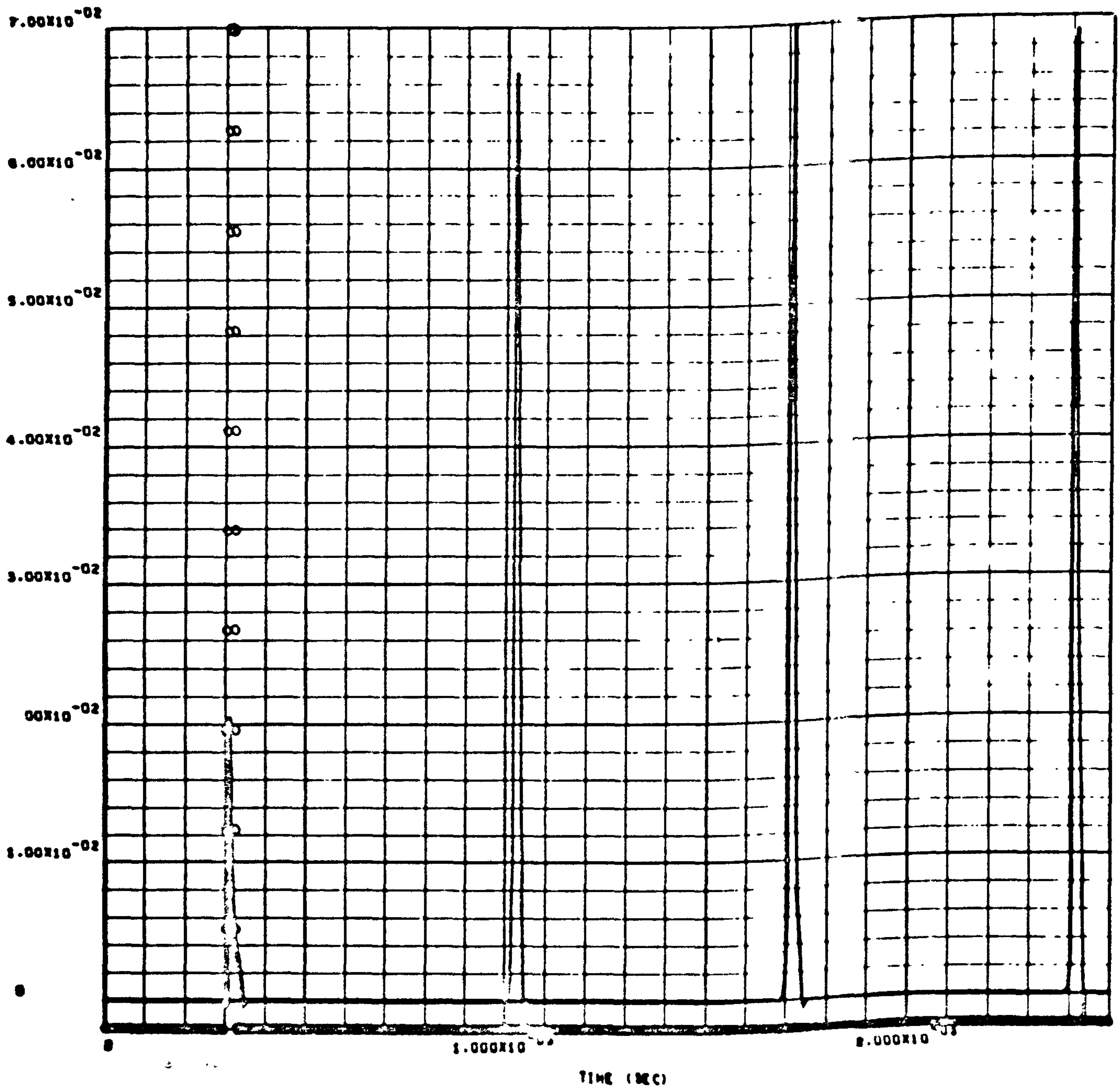

I_E vs Time with 10^8 R/sec 20 μsec Ionizing Pulse

R = 20 Ω

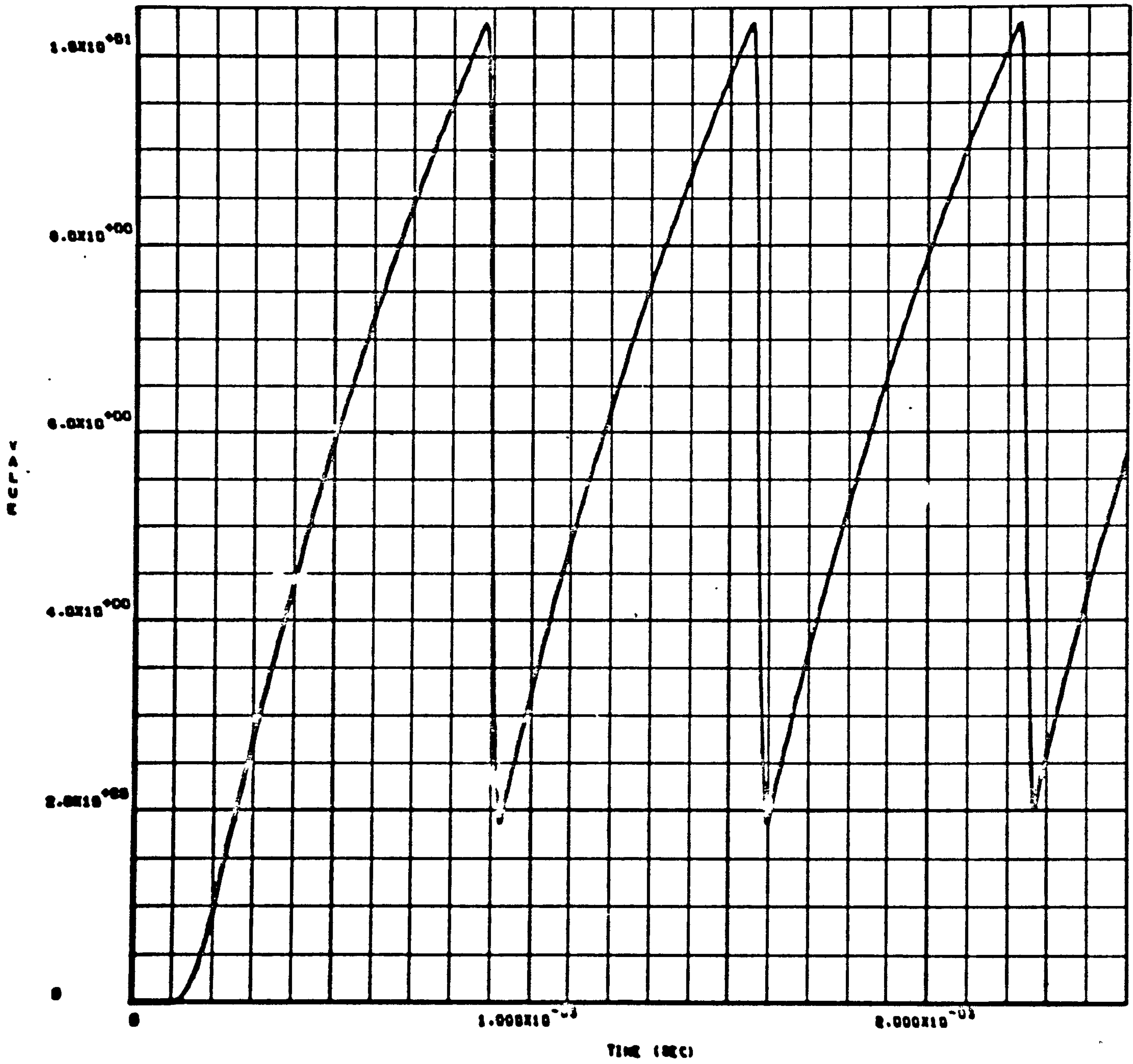

Capacitor Charge-Discharge Voltage vs Time

$R = 50\Omega$

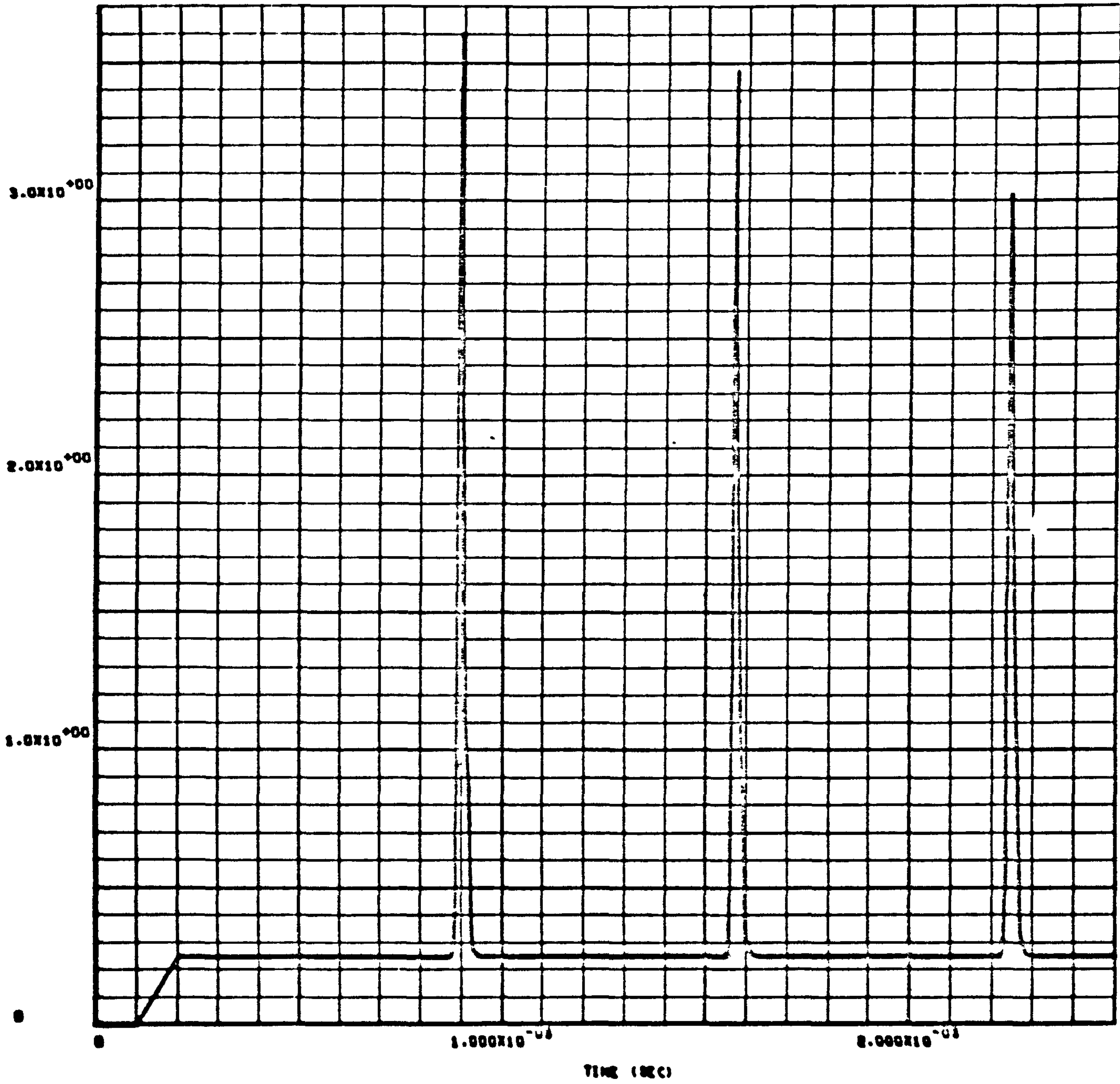

Output Pulse Train (V2) vs Time
R = 50Ω

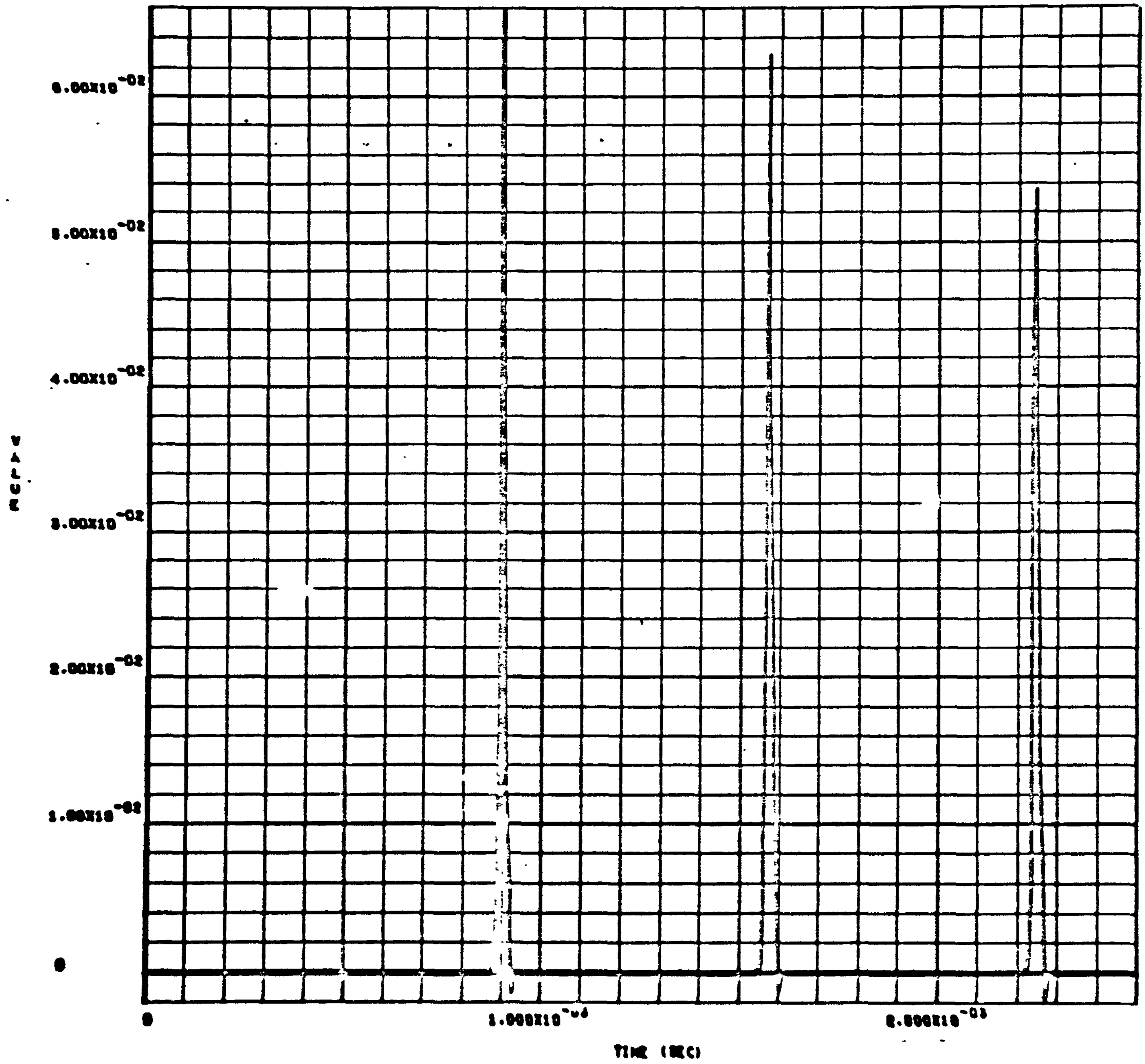

I_E (Item 7) vs Time for R = 50Ω

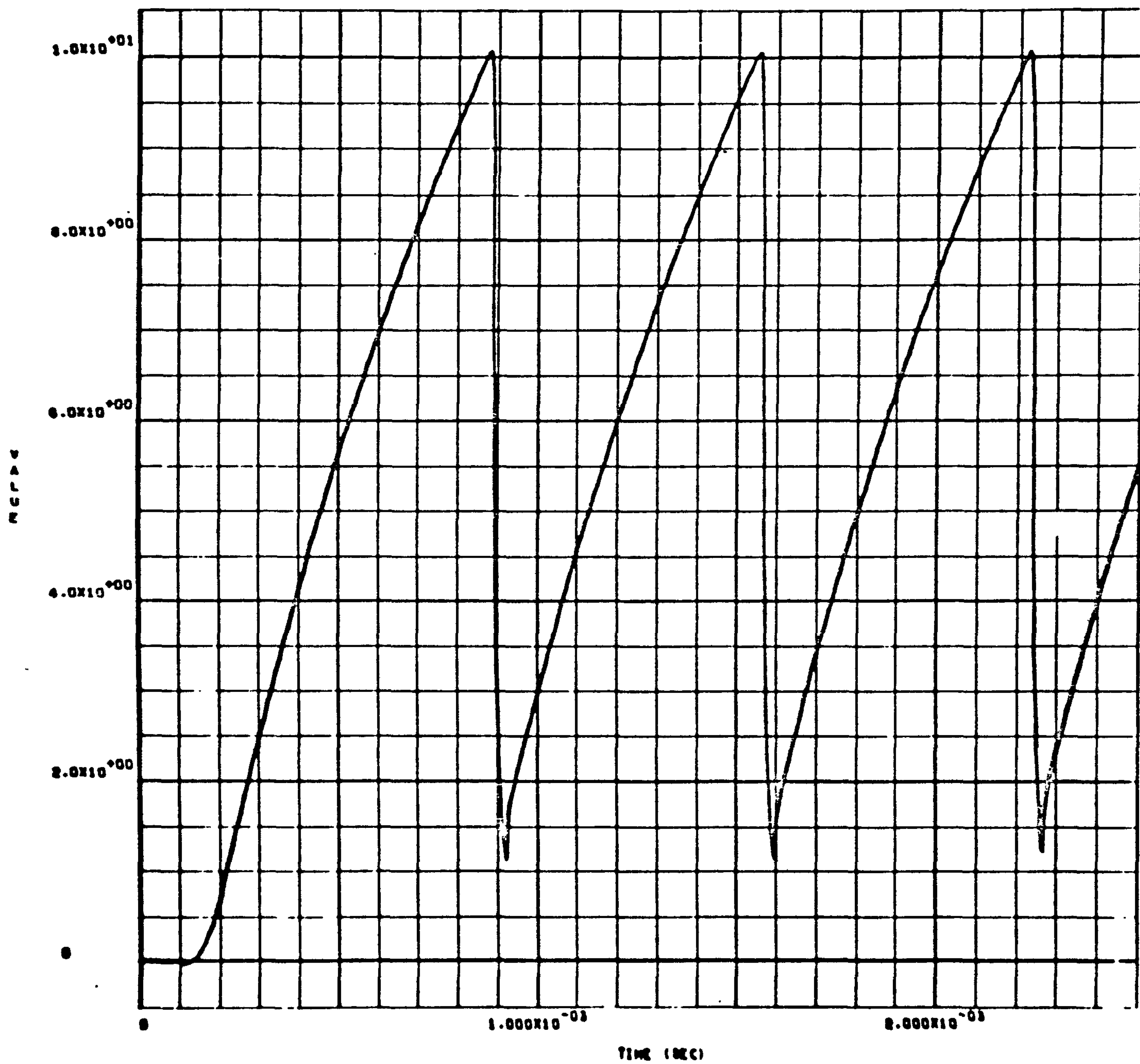

V_E (Item 8) vs Time for R = 50Ω

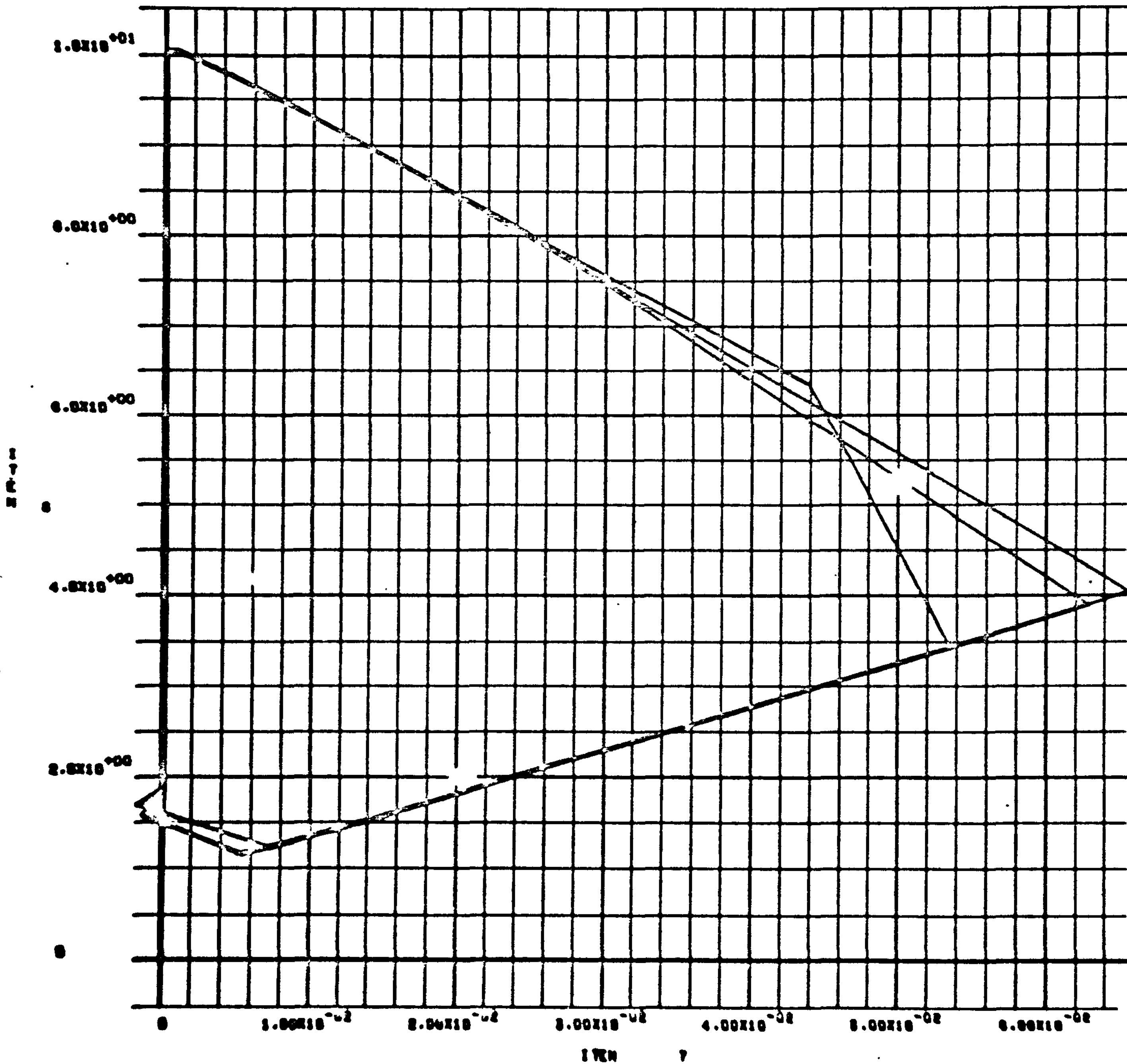

V_E vs I_E for $R = 50\,\Omega$

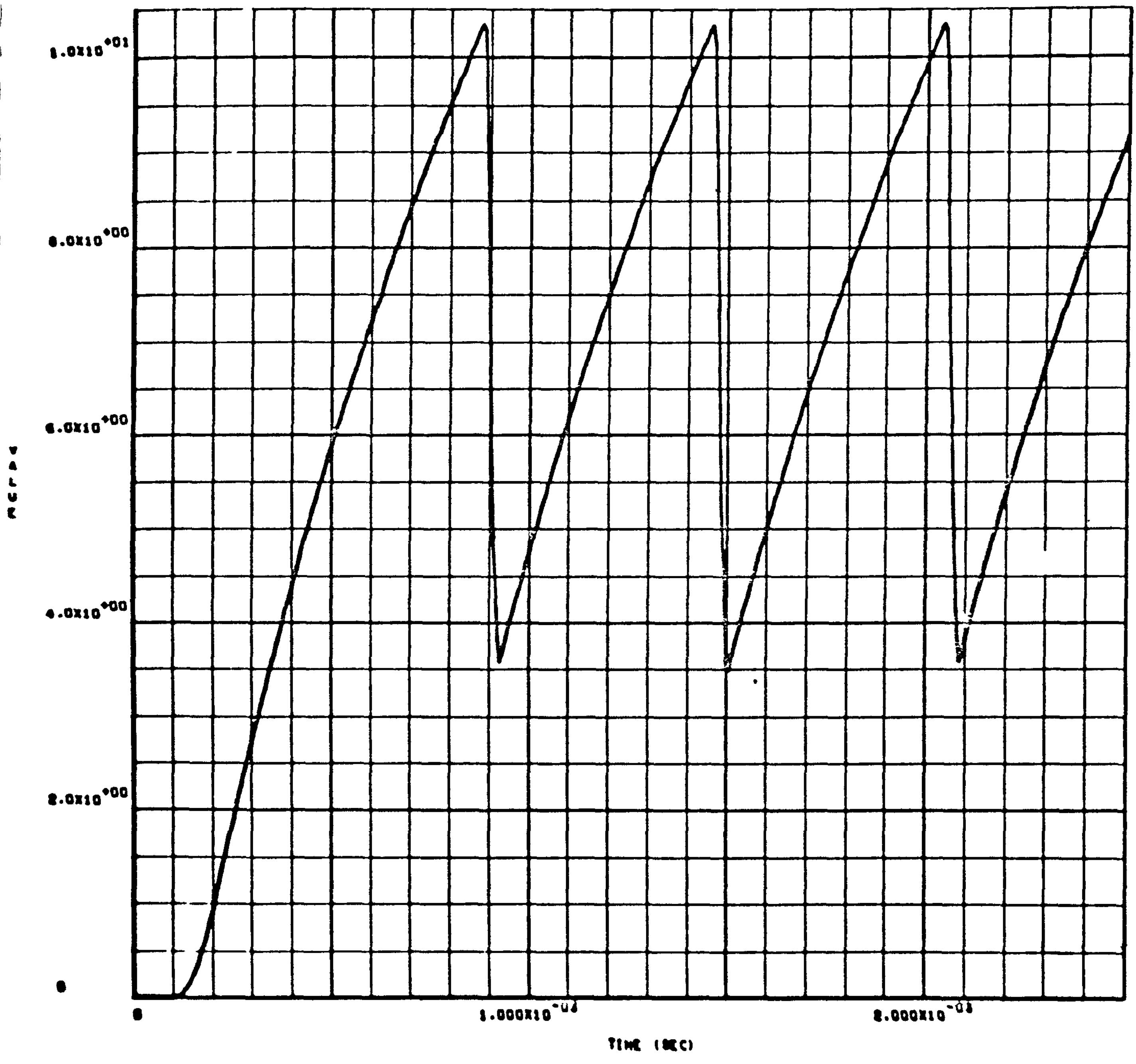

Capacitor Charge-Discharge R = 150Ω

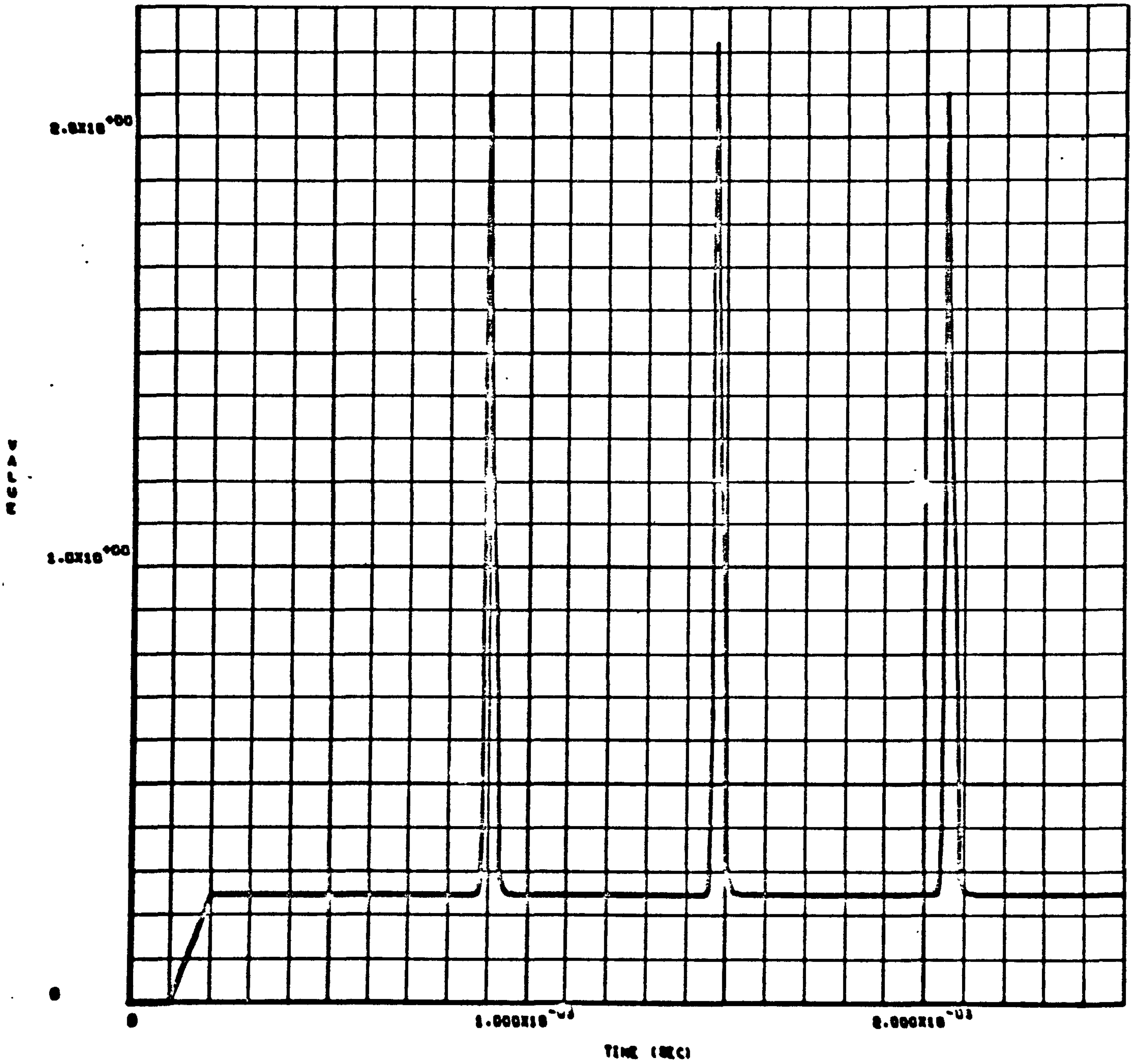

Output Pulse Train R = 150Ω

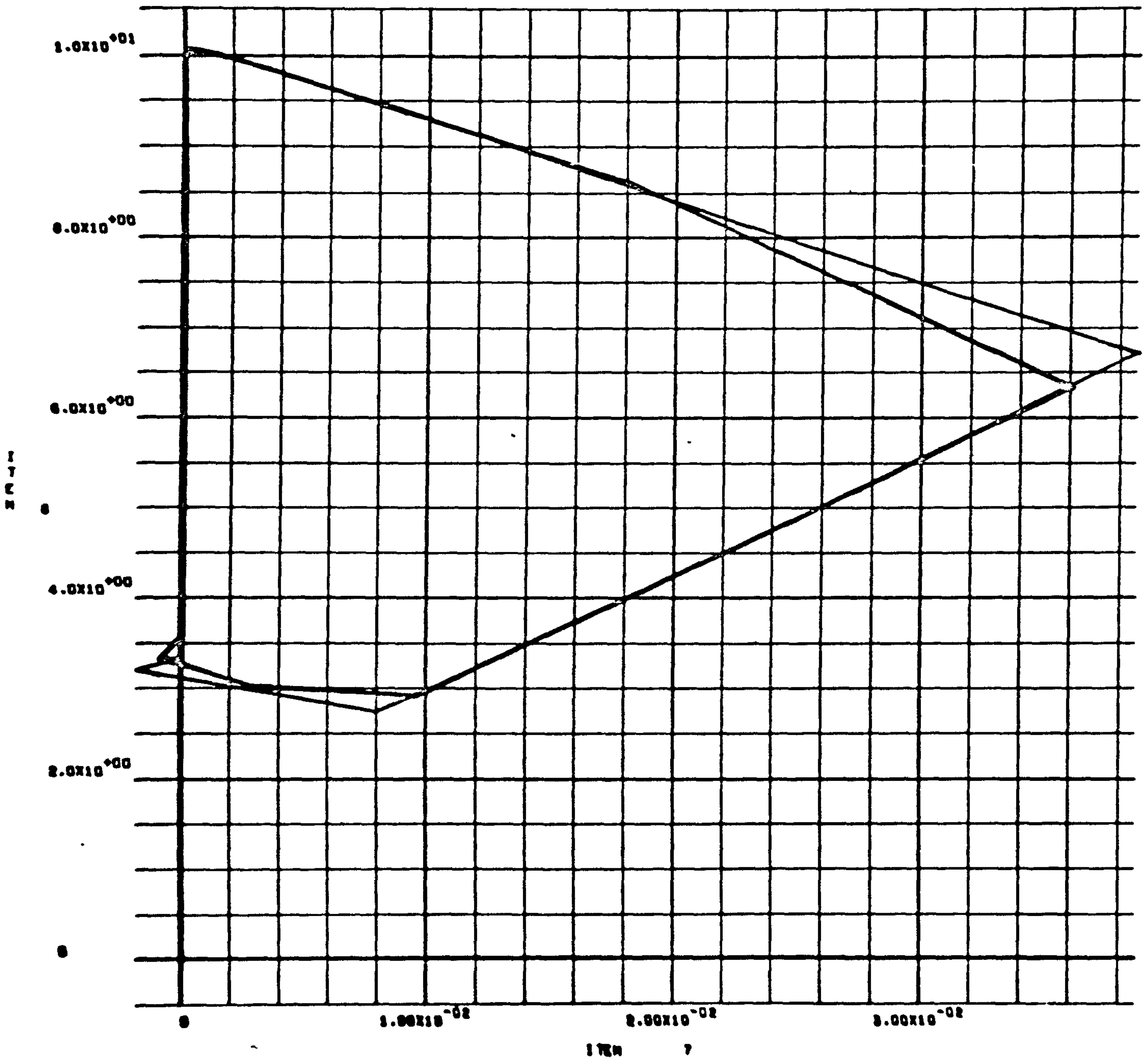

V_E - I_E Plot for R = 150 Ω

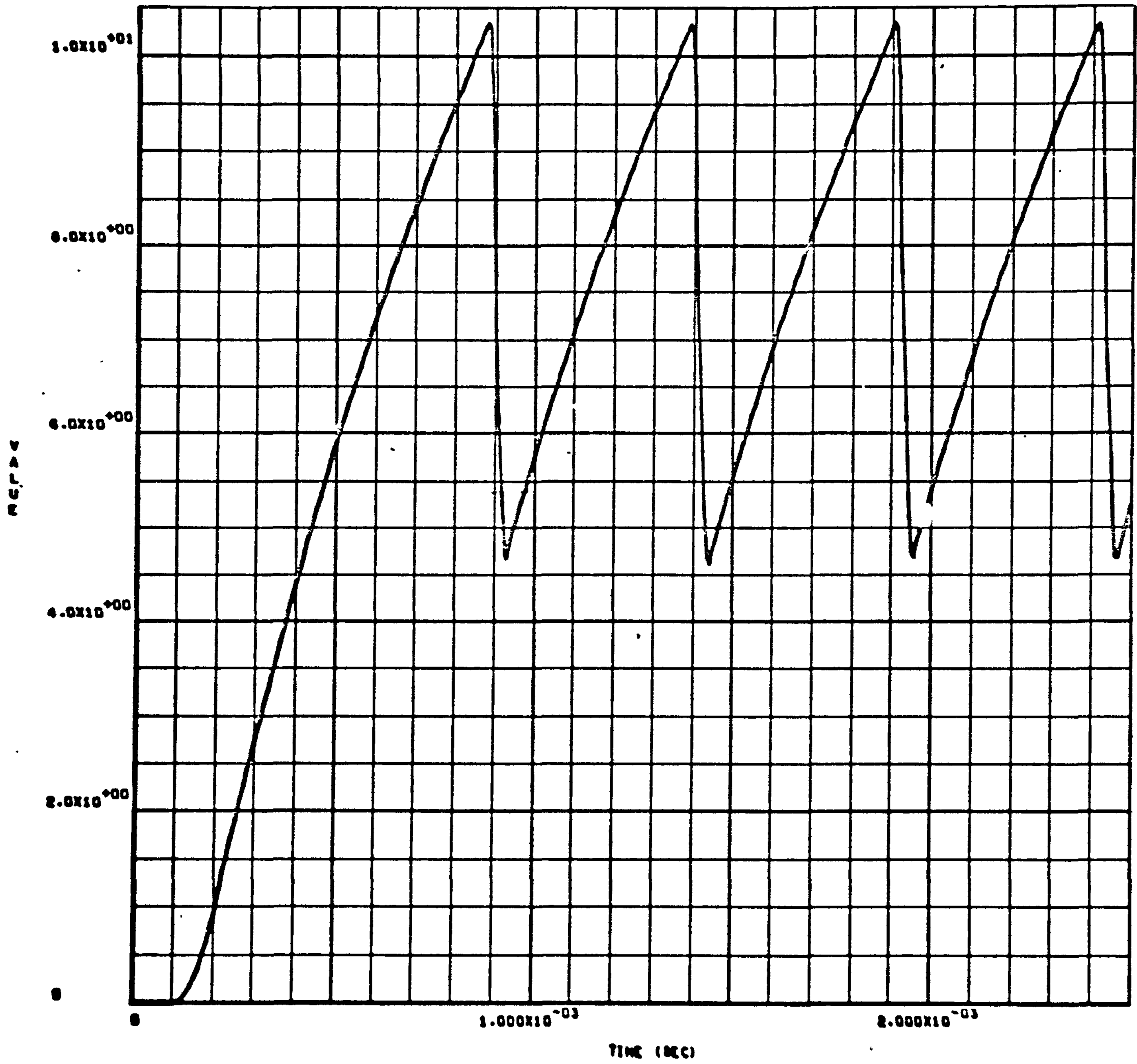

Capacitor Charge – Discharge Waveform R = 250 Ω

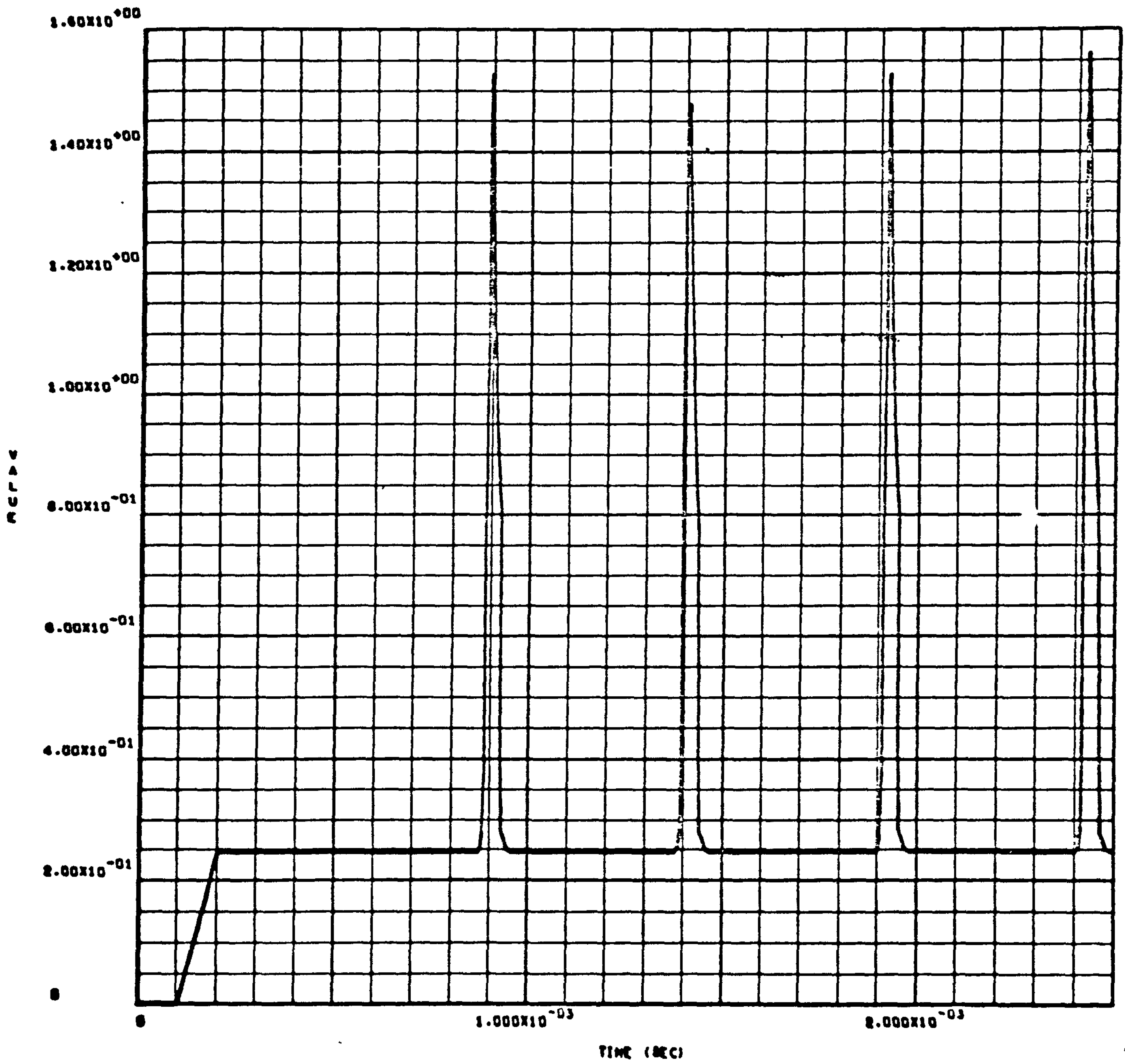

Output Pulse Train $R = 250\Omega$

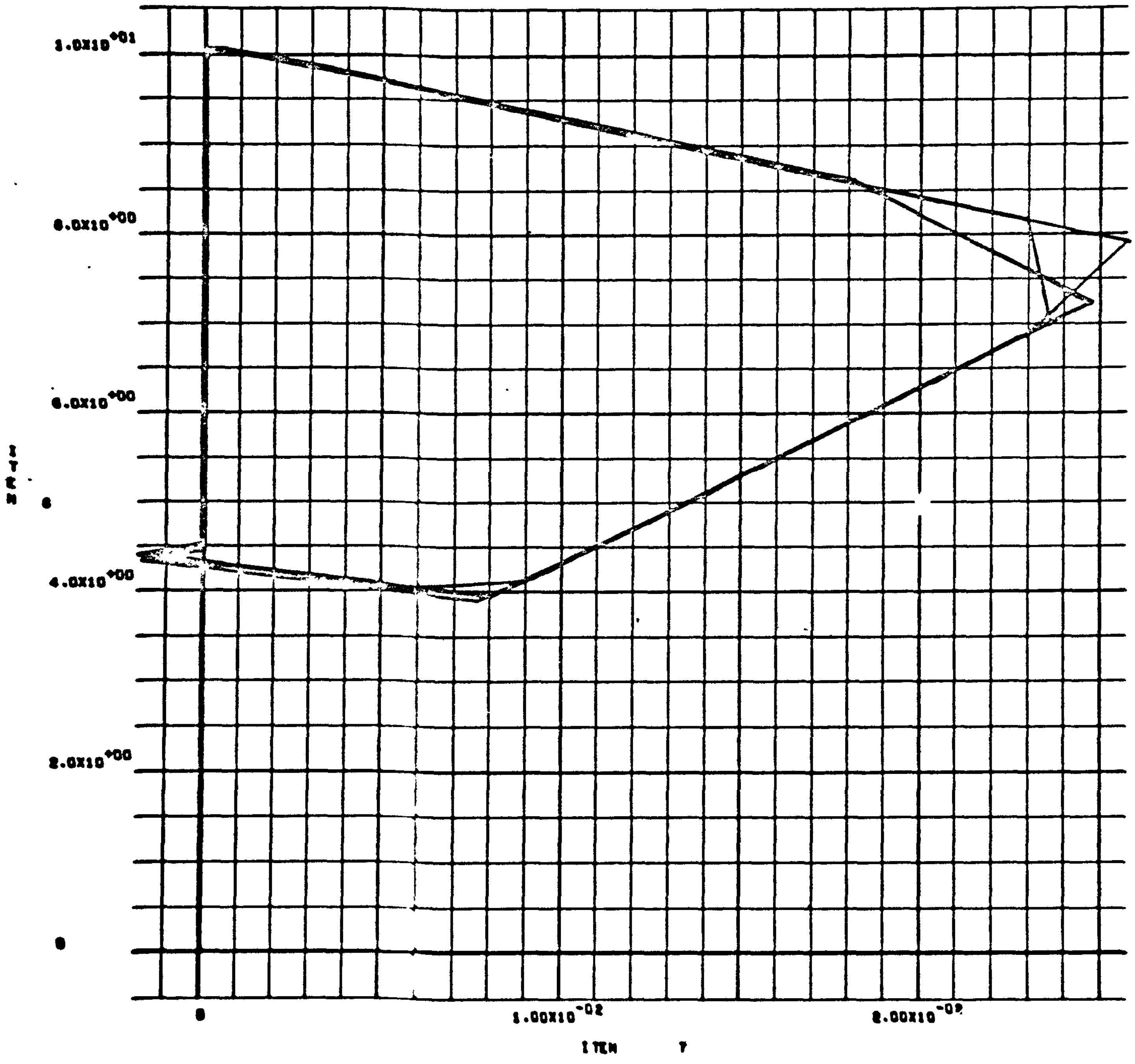

V_E vs I_E R = 250Ω

200 μSEC/DIV

(a) Φ = 0 N/CM^2
t = 0 MIN REACTOR TIME

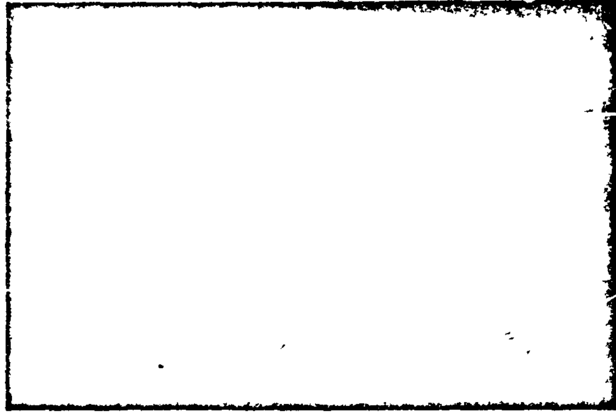

200 μSEC/DIV

(b) Φ =
t = 3 MIN REACTOR TIME

200 μSEC/DIV

(c) t = 22 MINUTES

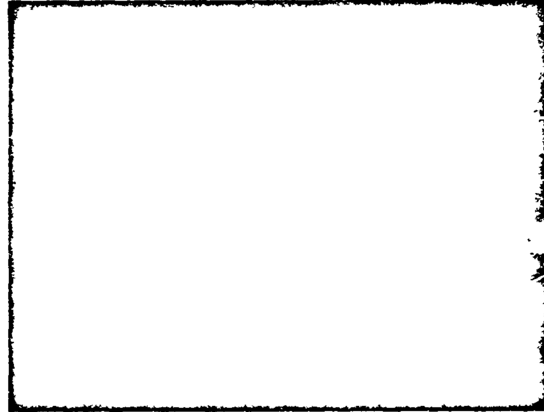

(d) t = 32 MINUTES

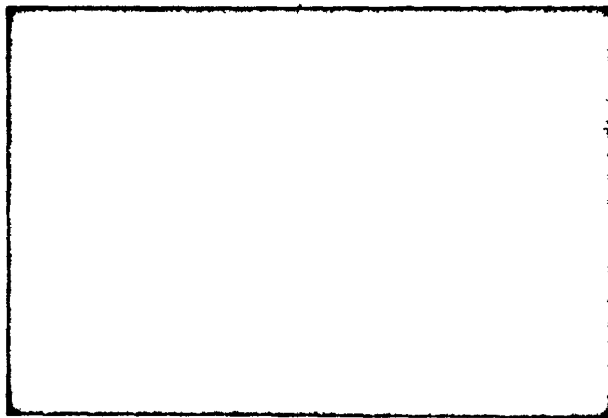

(e) t = 42 MINUTES

Neutron Test Results on Unijunction Oscillator